Dissertation

Aspects of dispersion interactions and of the full-potential Korringa-Kohn-Rostoker (KKR) method for semi-infinite systems

ausgeführt zum Zwecke der Erlangung des akademischen Grades eines
Doktors der technischen Wissenschaften
unter der Leitung von

Univ.-Prof. Dr. Peter Weinberger
Institutsnummer: E 134
Institut für Allgemeine Physik

eingereicht an der Technischen Universität Wien
Technisch-Naturwissenschaftliche Fakultät

von

Dipl.-Ing. Robert Hammerling
Matrikelnummer: 9325050
A-1170 Wien, Hormayrg. 52/8

Wien, am 29. September 2003

Kurzfassung

Die vorliegende Arbeit ist in 3 nahezu unabhängige Teile gegliedert.

Der ersteTeil befasst sich mit Aspekten der Dispersionswechselwirkung, auch als Van der Waals Wechselwirkung bekannt. Dabei werden nach einer "unkonventionellen" Erklärung des Problems der Van der Waals Wechselwirkung zwei Arbeiten präsentiert. Die erste Arbeit behandelt Korrekturen zur Hamaker Formel mit Hilfe der Lifshitz Gleichung und der Clausius Mossotti Formel für das lokale Feld. Die zweite die Dispersionswechselwirkung in kristallinen Polymeren, wo schon ein einfaches Hamaker Modell viele wesentlichen Eigenschaften dieser anisotropen Materialien erklären kann.

Der zweite Teil widmet sich der Theorie der KKR Methode für sogenannte volle Potentiale. Vor allem ein numerisch effizientes Verfahren zur Berechnung des elektrostatischen Potentials solcher Ladungsverteilungen, das notwendig ist innerhalb der Dichtefunktionaltheorie, wurde entwickelt und programmiert. Besonders für Systeme mit Fremdatomen, Oberflächen oder andere ausgedehnte Störungen stellt dies eine wichtige Verbesserung der ASA Näherung da. In der Arbeit wird auch auf niedrigdimensionale Modellsysteme eingegangen, um Analogien zu den wesentlichen Begriffen zu finden.

Schlussendlich werden im dritten Teil einige Rechnungen mit der KKR-ASA Methode, die im Zeitraum der Dissertation durchgeführt wurden, präsentiert. Dies betrifft 3 typische Oberflächensysteme, nämlich:

$Cu(111)/Co/Vac$, bei dem die Magnetische Anisotropie Energie (MAE) berechnet wurde,

$Cu(100)/Ni/Cu/Ni/Cu/Vac$, als Prototyp eines Trilayer Systems, bei dem sowohl MAE als auch die Zwischenlagenaustauschkopplung berechnet wurde, und

$Cu(100)/Ni/H/Vac$, hier wurde die Änderung in den magnetischen Eigenschaften durch die H Adsorption untersucht.

Abstract

This thesis contains three more or less independent parts:

The first part deals with aspects of the dispersion interactions, also known as Van der Waals interactions. In there, after an 'unconventional' approach to explain Van der Waals interactions is given, there are two contributions presented. The first one deals with corrections to the Hamaker formula for two interacting slabs by means of the Lifshitz formula and the Clausius Mossotti local field correction. The second one studies the properties of crystalline organic polymers, for which a simple model system is already able to explain characteristic properties of these anisotropic media.

The second main part deals with aspects of the theory of the KKR method using full potentials. A numerical efficient way to solve the electrostatic problem, necessary to be solved with the Density Functional Theory (DFT) approach, is developed, programmed and presented in this work. Especially for systems with impurities, surfaces or other extended defects a full potential treatment is a major improvement to the ASA approximation. Also comparisons to lower dimensional model systems are given to clarify the main aspects.

In the third part typical calculations with the KKR ASA method, which have been performed during the doctoral work, are presented. These are three typical surface systems:

$Cu(111)/Co/Vac$, where the magnetic anisotropy energy (MAE) was studied,

$Cu(100)/Ni/Cu/Ni/Cu/Vac$, as a prototype trilayer system, where the MAE as well as the interlayer exchange coupling (IEC) was calculated,

$Cu(100)/Ni/H/Vac$, for which the change in the magnetic properties with the adsorption of Hydrogen was studied.

Contents

---

[1] The results of these calculation are published in an article [17]

---

[2] The results of these calculation are published in an article [19]

[3] The results of these calculation are published in an article [18]

Chapter 1

Overview

This doctor thesis contains three parts, the first one resulted from an investigation of certain properties of dispersion forces and was carried out under the guidance of Prof. W. Kohn at the University of California, Santa Barbara (UCSB) during the months October 2000 - March 2001.

The second part is devoted to the KKR method. In particular to the problem of using a full-potential multiple scattering approach for semi-infinite systems. Since this kind of electronic structure calculation is based on Kohn's density functional theory [26], the condition of selfconsistency within DFT automatically leads to the problem of solving the Poisson equation in the most general context. In this part of the thesis the necessary mathematical tools and relations for that purpose are summarized, which in turn served as the basis for corresponding computer codes.

The third part of the thesis is devoted to the problem of interlayer exchange coupling and magnetic properties in magnetic multilayer systems. It should be noted that this part of the thesis not only was directed to the actual physical properties, but also served the purpose of getting familiar with the screened KKR-code in order to be able to supply matching routines for the numerical procedures developed in part 2.

I performed this thesis as a collegiate of the Science College 'Computational Material Science', (FWF W004), which facilitated also partially my stay at the UCSB with Prof. W. Kohn.

Part I

Dispersion forces

Chapter 2

An unconventional approach to Van der Waals Interactions

This part was mainly done at the Department for Physics, UCSB, Santa Barbara under the supervision of Prof. Dr. Walter Kohn.

2.1 An easy example

An He atom is a closed shell atom because its two $1s$ electrons have different spins. If we ignore the spin degree of freedom of the electron a hydrogen atom with one electron would be a real gas atom. Consider 2 such H atoms, then we have a 4 particle problem, namely 2 nuclei (here just protons) and 2 electrons $(2p^+, 2e^-)$. Using the Born-Oppenheimer approximation for the positions of the nuclei $\mathbf{R}_1, \mathbf{R}_2$ the 2 electron problem is mathematically described in the Hilbert space $\mathcal{H}_{2,-} = (h \otimes h)_-$ with $h = L_2(\mathbb{R}^3)$. The Van der Waals interaction is not a result of the Born Oppenheimer approximation. The Hamilton operator in the 2 particle space is given by

$$\begin{aligned} \widehat{H} &= \widehat{T}_{(e)} + \widehat{V}_{(pe)} + \widehat{V}_{(pp)} + \widehat{V}_{(ee)} = \\ &= \frac{1}{2m}\left(\widehat{p}_1^2 + \widehat{p}_2^2\right) - \frac{e^2}{|\mathbf{x}_1 - \mathbf{R}_1|} - \frac{e^2}{|\mathbf{x}_1 - \mathbf{R}_2|} - \frac{e^2}{|\mathbf{x}_2 - \mathbf{R}_1|} - \frac{e^2}{|\mathbf{x}_2 - \mathbf{R}_2|} + \frac{e^2}{|\mathbf{R}_1 - \mathbf{R}_2|} + \frac{e^2}{|\mathbf{x}_1 - \mathbf{x}_2|} \end{aligned}$$

$\widehat{H}$ is a self adjoint Schroedinger operator in the Hilbert space $\mathcal{H}_{2,-}$. It only contains electrostatic interactions. We consider $R = |\mathbf{R}_1 - \mathbf{R}_2|$ only as a parameter and study the solutions of the eigenvalue problem (EVP)

$$\widehat{H}(R)\,\Phi = E\Phi, \quad \text{in the Hilbert space } \mathcal{H}_{2,-} \quad ,$$

Qualitatively the spectrum $\sigma\left(\widehat{H}\right)$ has the following form (see Fig. 2.1):

$$\sigma\left(\widehat{H}\right) = \sigma_p\left(\widehat{H}\right) \cup \sigma_p\left(\widehat{H}\right) \quad ,$$

i.e. we have a point spectrum, representing bound states of the system and a continuous spectrum. Notice that the point spectrum and the continuous spectrum are not disjunct because there are

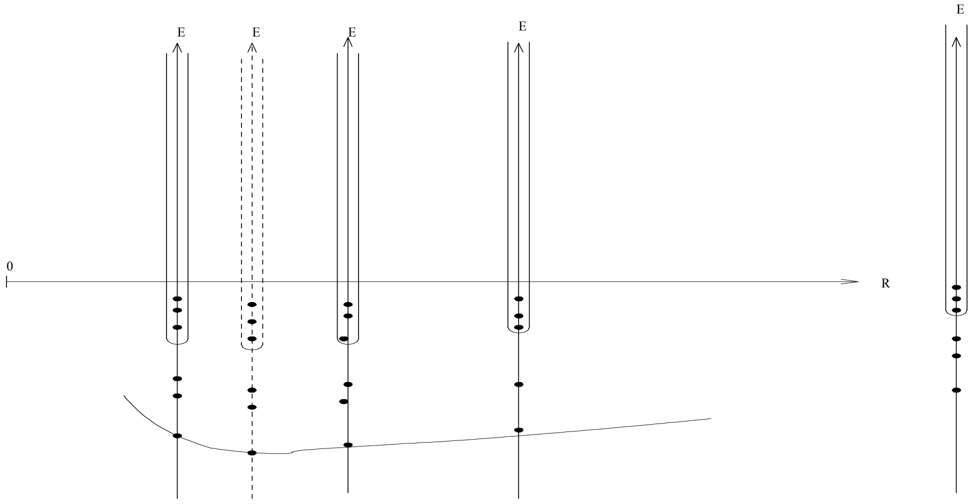

Figure 2.1: Qualitative form of $\sigma\left(\widehat{H}\right)$: there is an equilibrium distance where $E_o\left(R\right)$ has a minimum; for smaller R there is repulsion, for larger R attraction.

also bound states with energies higher then the first ionization energy. The groundstate $\Phi_0\left(R\right)$ with energy $E_0\left(R\right)$ is not degenerated and $E=0$ refers to the energy of four free particles (without kinetic energy). We define the Van der Waals energy as the molecular binding energy

$$E_{VdW}(R)=\left\langle \Phi_0\left(R\right)\left|\widehat{H}\left(R\right)\right|\Phi_0\left(R\right)\right\rangle-\lim_{R\to\infty}E_0\left(R\right)=E\left(R\right)-E\left(\infty\right).$$

Without further notice in the following we will use 3 different coordinate systems (see Fig. 2.2), each one translated by a given vector from the other one. Strictly speaking the coordinates of $\mathbf{x}$ in these coordinate systems should be denoted by

$${}_i^k x_j,\text{ with }k\in\left\{1,2\right\},i\in\left\{p_1^+,cm,p_2^+\right\},j\in\left\{1,2,3\right\}\ ,$$

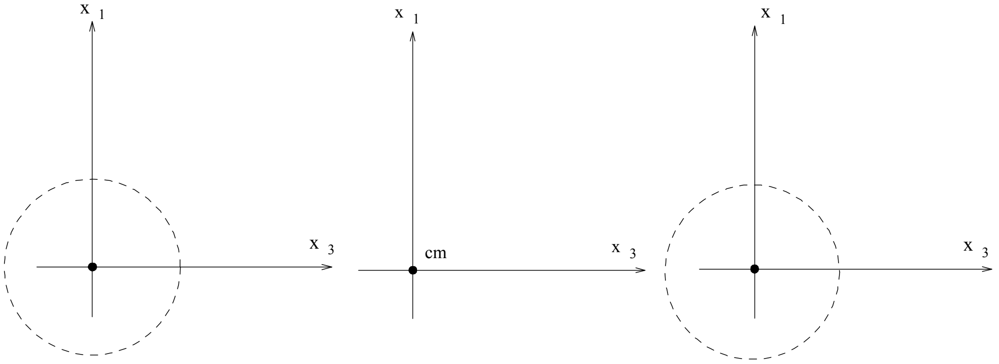

Figure 2.2: Coordinate systems at the left nucleus, center of mass (cm) and right nucleus. They only differ by a translation vector.

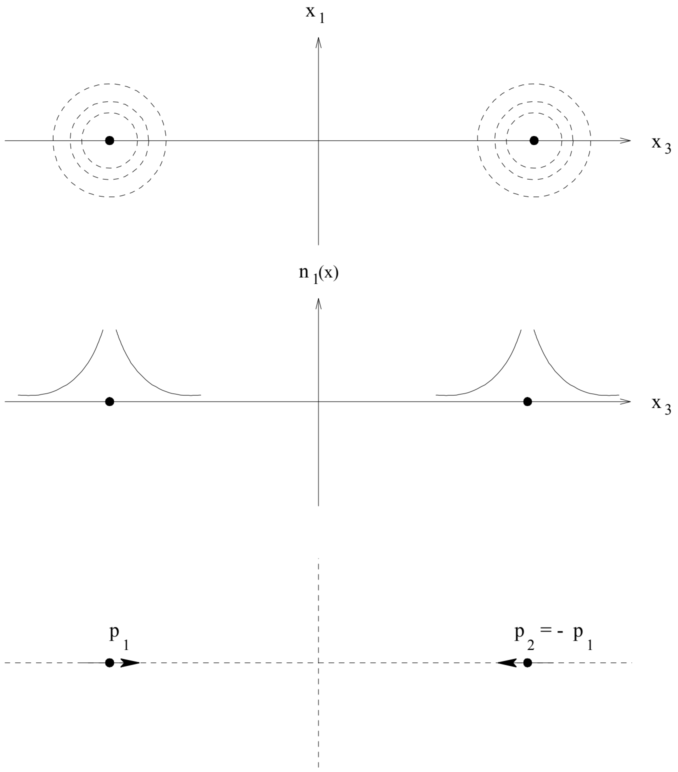

Figure 2.3: Qualitative form of the one particle density $n_1(\mathbf{x})$ in the ground state. Because of the mirror symmetry of $n_1(\mathbf{x})$, the resulting electric dipole moments are in a repulsive configuration, but the dipole moment is exponentially small with increasing R.

where k specifies the electron, i the coordinate system and j is one of the 3 Cartesian coordinates. The exact groundstate wavefunction shall be denoted by

$$\Phi_0(\mathbf{x}_1, \mathbf{x}_2; R) \ ,$$

it exists but there is no closed form solution. The time evolution of the groundstate is given by

$$\Phi_0(t) = e^{-i\frac{E_0(R)}{\hbar}t}\Phi_0$$

and the 1- and 2-particle densities are given by

$$\begin{aligned} n_2(\mathbf{x}_1, \mathbf{x}_2; R) &= |\Phi_0(\mathbf{x}_1, \mathbf{x}_2; R)|^2 \ , \\ n_1(\mathbf{x}; R) &= \int d^3x_2 \, n_2(\mathbf{x}, \mathbf{x}_2; R) \ , \end{aligned}$$

both are time independent. If we choose $\mathbf{R}_2 - \mathbf{R}_1 = R\mathbf{e}_3$, a sketch of n_1 would have the form as shown in (Fig. 2.3).We have two small static electric dipole moments,

$$\mathbf{p}_1 = -e\int_{x_3<0} (n_1(\mathbf{x})\,\mathbf{x})\, d^3x \text{ and } \mathbf{p}_2 = -e\int_{x_3>0} (n_2(\mathbf{x})\,\mathbf{x})\, d^3x \ ,$$

leading to repulsion. Because of the mirror symmetry of the problem the groundstate one electron density has a mirror symmetry and therefore the dipole moments are in a repulsive configuration, but the magnitude of the dipole moment $|\mathbf{p}_1|$ vanishes exponentially with increasing R.

Another main aspect is the overlap between the two electron wavefunctions: around the equilibrium distance there is significant overlap and repulsive force, but we limit ourselves to the attractive part only, which is the dominant one for large separations. In this regime the overlap is negligible and the antisymmetrization of the electron WF not necessary. Attractive dispersion interactions are not a result of the fermionic nature of electrons (antisymmetrization of WF, indistinguishability).

2.1.1 Correlation

To be able to explain the reason for the attractive interaction we take a look at

$$n_2\left(\mathbf{x}_1, \mathbf{x}_2; R\right) = n_2\left(x_{11}, x_{12}, x_{13}, x_{21} x_{22} x_{23}; R\right) \ ,$$

namely the 2 particle density. Although it is problematic to visualize this function the sketch in (Fig. 2.4) serves as a qualitative explanation. All these configurations sketched there are present at the same time if we follow the standard interpretation of time in quantum mechanics. However,

$$\begin{gathered} n_2\left(\mathbf{x}_1, \mathbf{x}_2\right) \overset{\int d^3x_2}{\rightarrow} n_1\left(\mathbf{x}\right) = \int d^3x_2 \; n_2\left(\mathbf{x}_1, \mathbf{x}_2\right) \\ n_2\left(\mathbf{x}_1, \mathbf{x}_2\right) \neq n_1\left(\mathbf{x}_1\right) \; n_1\left(\mathbf{x}_2\right) \ , \end{gathered}$$

which means that the two electrons are correlated:

1. There is no exchange present in this situation, therefore the word correlation is used in physics and mathematics in the same way.
2. The Hohenberg-Kohn-Sham theorem claims that '$n_1\left(\mathbf{x}\right)$ contains all information'
3. If we take a single determinant HF trial function (or here Hartree) $\Phi\left(\mathbf{x}_1, \mathbf{x}_2\right) = \left[\varphi_1\left(\mathbf{x}_1\right), \varphi_2\left(\mathbf{x}_2\right)\right]$, we always have $n_2\left(\mathbf{x}_1, \mathbf{x}_2\right) = n_1\left(\mathbf{x}_1\right) \; n_1\left(\mathbf{x}_2\right)$ and therefore miss the effect completely
4. A classical (not QM) model could get the effect somehow, but the role of time is essentially different.

2.2 Quantitative treatment

1. The standard quantitative treatment is always limited to the case of *2 objects, which are small compared to their separation distance.* It is based on the well known multipole expansion

   $$\frac{1}{|\mathbf{R}-\mathbf{x}|} \overset{|\frac{\mathbf{x}}{\mathbf{R}}| \ll 1}{\approx} \frac{1}{|\mathbf{R}|} - \frac{\mathbf{x}\cdot\mathbf{R}}{|\mathbf{R}|^3} - \frac{\mathbf{R}\cdot\mathbf{R}\,\mathbf{x}\cdot\mathbf{x} - 3\mathbf{x}\cdot\mathbf{R}\,\mathbf{x}\cdot\mathbf{R}}{|\mathbf{R}|^5} + \ldots \ . \tag{2.1}$$

   We consider first 2 H atoms and briefly sketch afterwards (see subsection 2.2.2) the changes for a multielectron atom or molecule.

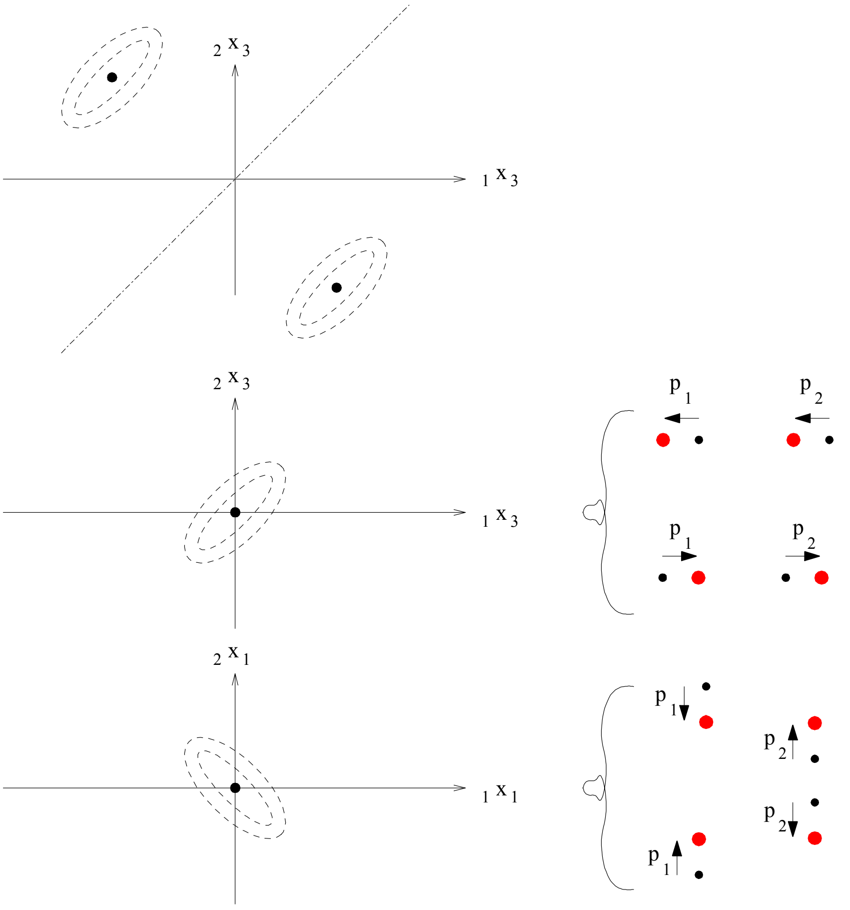

Figure 2.4: Qualitative sketch of the two particle density $n_2\,(\mathbf{x}_1, \mathbf{x}_2; R)$ for a given R in certain coordinate planes. The ellipses represent points of constant value.

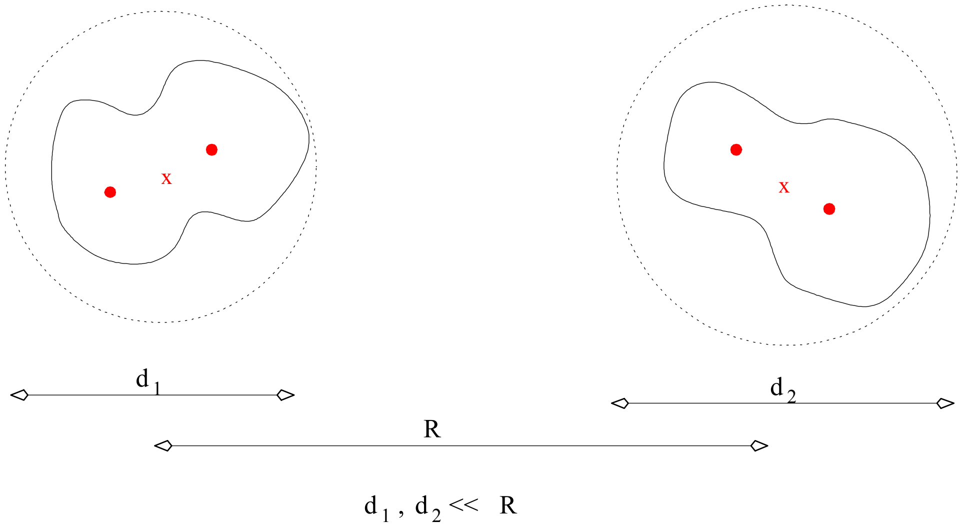

Figure 2.5: Conditions of small, compact systems for the multipole expansion.

2.2.1 Two H atoms

For 2 H atoms the Hamiltonian can be split into an unperturbed Hamiltonian $\widehat{H}_0$ of two independent H atoms and a perturbation $\widehat{H}_I(R)$ in the following way.

$$\begin{aligned}
\widehat{H} &= \left(\frac{1}{2m}\widehat{p}_1^2 - \frac{e^2}{|\mathbf{x}_{11}|}\right) + \left(\frac{1}{2m}\widehat{p}_2^2 - \frac{e^2}{|\mathbf{x}_{22}|}\right) + \\
&\quad + \left(\frac{e^2}{R} - \frac{e^2}{|\mathbf{R}+\mathbf{x}_2|} - \frac{e^2}{|\mathbf{R}-\mathbf{x}_1|} + \frac{e^2}{|\mathbf{R}+\mathbf{x}_2-\mathbf{x}_1|}\right) \\
&= \widehat{H}_0 + \widehat{H}_I(R) \ .
\end{aligned}$$

An expansion of the operator $\widehat{H}_I(R)$ in powers of R^{-1} leads to

$$\widehat{H}_I(R) = R^{-1}\widehat{A}_1 + R^{-2}\widehat{A}_2 + R^{-3}\widehat{A}_3 + R^{-4}\widehat{A}_4 + \ldots \ ,$$

where the first terms are given by

$$\begin{array}{cc}
\widehat{A}_1 \neq 0 & \text{only if } (N_1 - Z_1) * (N_2 - Z_2) \neq 0 \text{ mon.-mon.} \\
\widehat{A}_2 \neq 0 & \text{only if } (N_1 - Z_1) \neq 0 \vee (N_2 - Z_2) \neq 0 \text{ mon.-dip.} \\
\widehat{A}_3 = \frac{e^2}{R^3}\left(\widehat{x}_{11}\widehat{x}_{21} + \widehat{x}_{12}\widehat{x}_{22} - 2\widehat{x}_{13}\widehat{x}_{23}\right) & \text{dip.-dip.} \\
\widehat{A}_4 = \ldots & \text{higher order multipoles .}
\end{array}$$

The perturbation series for $\widehat{H}_0 + \widehat{H}_I(R)$ for the groundstate gives the result (we write $\sum\int d\mu(n)$ for the summation over the discrete and integration over the continuous spectrum, similar to the notation used in mathematical measure theory)

$$\begin{aligned}
\widehat{H}_0\Phi_n &= E_n^{(0)}\Phi_n \qquad (2.2)\\
\Phi &= \Phi_0 + \sum\int d\mu(n)\,\frac{\left\langle \Phi_n \middle| \widehat{H}_I \middle| \Phi_0 \right\rangle}{E_n^{(0)} - E_0^{(0)}} + \ldots \\
E &= E_0 + \underbrace{\left\langle \Phi_0 \middle| \widehat{H}_I \middle| \Phi_0 \right\rangle}_{V_1(R)} + \underbrace{\sum\int d\mu(n)\,\frac{\left|\left\langle \Phi_n \middle| \widehat{H}_I \middle| \Phi_0 \right\rangle\right|^2}{E_0^{(0)} - E_n^{(0)}}}_{V_2(R)} + \ldots
\end{aligned}$$

One of the problems in (2.2) is that we have to take the whole excitation spectrum of the unperturbed Hamiltonian into account, also $\sigma_c\left(\widehat{H}_0\right)$.

First order in Energy

In first order the integrals vanish:

$$\begin{aligned} \Phi_0 &\rightarrow \rho_{el} = 2en_1 = \rho_{el,1} + \rho_{el,2} \\ \rho &= \rho_p + \rho_{el} = \left(\rho_{p,1} + \rho_{el,1}\right) + \left(\rho_{p,2} + \rho_{el,2}\right) \\ V_1\left(R\right) &= \left\langle \Phi_0 \left| \widehat{H}_I \right| \Phi_0 \right\rangle = \int_{\mathcal{V}_1} \int_{\mathcal{V}_2} d^3x d^3x' \frac{\rho_1\left(\mathbf{x}\right) \rho_2\left(\mathbf{x}'\right)}{\left|\mathbf{x} - \mathbf{x}'\right|} \underbrace{\approx}_{(=\ldots\textbf{no overlap})} 0 \end{aligned}$$

Second order in Energy

In second order with $\Phi_0 = \{\varphi_0, \varphi_0\}\ldots$,both in the groundstate, we get

$$V_2\left(R\right) = -\frac{6e^4}{R^6} \sum \int d\mu\left(m\right) d\mu\left(n\right) \frac{\left\langle \varphi_0 \left| \widehat{x}_3^2 \right| \varphi_m \right\rangle \left\langle \varphi_0 \left| \widehat{x}_3^2 \right| \varphi_n \right\rangle}{\left(\epsilon_0 - \epsilon_m\right) + \left(\epsilon_0 - \epsilon_n\right)} \; .$$

For the evaluation of the integral one needs to take into account all parts of the spectrum of the unperturbed Hamiltonian - also the continuous spectrum plays a significant role.

2.2.2 Two molecules - oscillator strength

To generalize the above ideas to the case of two small molecules (fulfilling Fig. 2.5) instead of Hydrogen atoms, we denote the unperturbed eigenstates of the N electron molecule by Φ_n which satisfy $\widehat{H}_0 \Phi_n = E_n \Phi_n$. The oscillator strengths (for polarization in z-direction) are given by:

$$f_{nl} = \frac{2m}{\hbar^2} \left(E_l - E_n\right) \left| \left\langle \Phi_n \left| \widehat{X}_3 \right| \Phi_l \right\rangle \right|^2$$

and satisfy the important sum rule

$$\sum \int f_{nl} \; d\mu\left(n\right) = N$$

for one given state, i.e., the groundstate, f is a generalized function of the energy $\triangle E$, with $E = \hbar\omega$. We can consider f also as a function of the excitation frequency. Via the oscillator strength the VdW energy can by written as

$$V\left(R\right) = -\frac{3e^4\hbar}{2m^2R^6} \int d\omega_1 \int d\omega_2 \frac{f_1\left(\omega_1\right) f_2\left(\omega_2\right)}{\omega_1\omega_2\left(\omega_1 + \omega_2\right)}. \tag{2.3}$$

2.2.3 Dynamic atomic polarizability in the harmonic oscillator model of an atom

We consider one atom with $N \geq 1$ electrons (without spin degrees of freedom) and an infinitely heavy nucleus without any other properties except an electric charge Z. The Hilbert space for the electronic problem is given by

$$\mathcal{H}_N = \bigotimes_{i=1}^{N} \mathcal{H}_1 = \bigotimes_{i=1}^{N} \bigotimes_{j=1}^{3} h \; ,$$

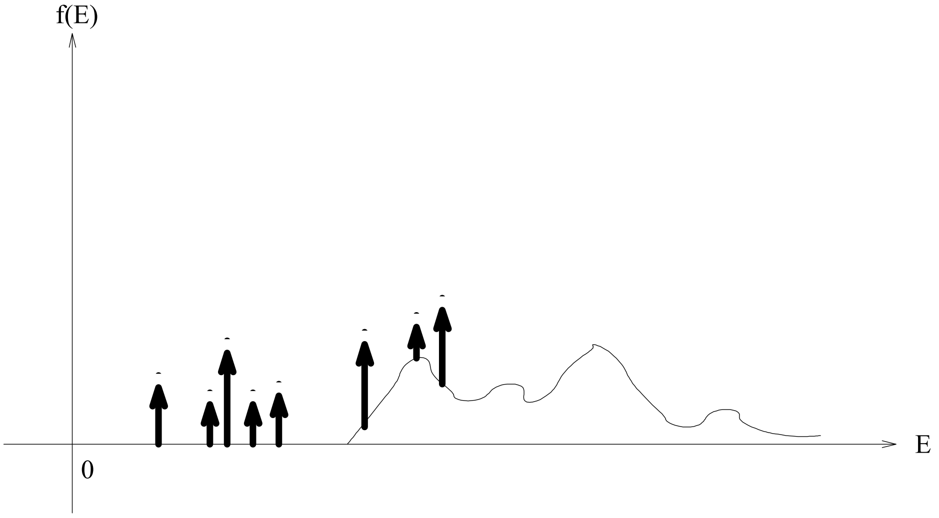

Figure 2.6: Plot of a typical oscillator strength $f\left(\omega\right)$ with point weights and a continuous density. The first arrow is at the lowest excitation frequency.

where each Hilbert space of a single degree of freedom is (isomorphic to)

$$h = L_2\left(\mathbb{R}\right) \ .$$

The electrons should interact with the nucleus over a sum of harmonic oscillator potentials which are given in real space representation as

$$\widehat{h} = -\frac{1}{2m}\widehat{p}^2 + \frac{m\omega^2}{2}\widehat{x}^2$$

and are of the form

$$\widehat{H} = \sum_{i=1}^{N}\sum_{j=1}^{3}\widehat{H}_{ij} \ , \tag{2.4}$$

where each $\widehat{H}_{ij}$ is one harmonic oscillator with frequency ω_{ij} (and the identity in the other spaces). Because no explicit electron-electron interaction is taken into account, the spectral problem of (2.4) is explicitly solvable. The spectrum of $\widehat{H}$ is a pure point spectrum and is given by

$$\begin{aligned}\sigma\left(\widehat{H}\right) &= \sigma_p\left(\widehat{H}\right) = \Big\{E_n = E_{n_1,\ldots,n_N} = E_{(n_{11},n_{12},n_{13}),\ldots,(n_{N1},n_{N2},n_{N3})} = \\ &= \frac{\hbar}{2}\sum_{i=1}^{N}\sum_{j=1}^{3}\omega_{ij}\left(1+2n_{ij}\right), \text{ with } n_{ij}\in\mathbb{N}_0\Big\} ,\end{aligned}$$

and a general eigenstate is denoted by

$$\Phi_n = \Phi_{n_1,\ldots,n_N} = \Phi_{(n_{11},n_{12},n_{13}),\ldots,(n_{N1},n_{N2},n_{N3})} = \left(\phi_{n_{11}},\phi_{n_{12}},\phi_{n_{13}}\right)\otimes\ldots\otimes\left(\phi_{n_{N1}},\phi_{n_{N2}},\phi_{n_{N3}}\right) \ ,$$

where n is a $3N$ multiindex, $n \in \mathbb{N}_0^{3N}$. The (3 Cartesian) electric dipole moment operator are given by

$$\widehat{D_j} = -e\widehat{X_j} = -e\sum_{i=1}^{N}\widehat{X_{ij}}, j \in \{1,2,3\} \ .$$

Therefore the only excited states which are connected via an electric single photon dipole transition are of the type

$$(0,0,0) \otimes \ldots \otimes (0,0,1) \otimes \ldots \otimes (0,0,0)$$

with one excited state at position $(i,j), i \in \{1,\ldots,N\}$. The oscillator strengths (of the groundstate) are given by

$$f_n = \frac{2m}{\hbar^2 e^2} E_n - E_0 \left|\left\langle \Phi_n \left| \widehat{D} \right| \Phi_0 \right\rangle\right|^2 , \quad \sum_{n=0}^{\infty} f_n = N \ .$$

The (complex) dynamic polarizability of an atom (in electric dipole approximation) is given by

$$\alpha : \begin{array}{ccc} \mathbb{C} & \rightarrow & \mathbb{C} \\ \omega & \mapsto & \frac{e^2}{m}\sum_n \frac{f_n}{\omega_n^2 - \omega} \end{array} ,$$

where in general the sum has to be viewed as a sum over the point spectrum and an integration over the continuous one. For our system the dynamic polarizability reduces to

$$\alpha(\omega) = \frac{e^2}{3m}\sum_{i,j}\frac{1}{\omega_{ij}^2 - \omega^2} ,$$

where $N, e, m, \omega_{ij} \in \mathbb{R}^+$ are all real positive parameters. For the special case that all frequencies are the same ω_0 (isotropic oscillator) one gets

$$\alpha(\omega) = \frac{Ne^2}{m}\frac{1}{\omega_0^2 - \omega^2} \ .$$

The important mathematical features of $\alpha(\omega)$ are

1. $\forall \omega \in \mathbb{C} \ \ (\alpha(-\omega) = \alpha(\omega))$
2. $\alpha(\omega)$ is a meromorphic function everywhere in $\mathbb{C}$ with a finite number of poles of first order at the frequencies $\omega = \pm\omega_{ij}$ on the real axis
3. on the imaginary axis the function is smooth and monotonically decreasing from $\alpha(0)$ to 0 for ω varying from 0 to $+i\infty$.

This form of α, resulting from this harmonic oscillator model is of course only a rough approximation for the dynamic atomic polarizability in a real atom.

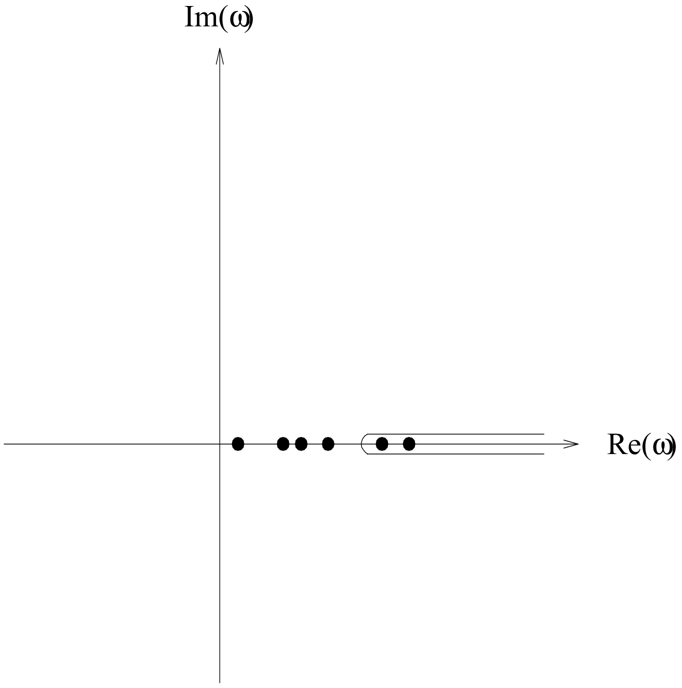

Figure 2.7: Domain in $\mathbb{C}$ for the dynamic polarisability $\alpha(\omega)$.

2.2.4 Dynamic polarizability and practical approximations

If we apply a harmonic electric field on a molecule we get an electric polarization

$$\mathbf{p}(t) = p(\omega)\,\mathbf{n}_0 e^{i\omega t} = \alpha(\omega)\left(\mathbf{E}_0 e^{i\omega t}\right) \ .$$

In first order time-dependent perturbation theory for a harmonic electric field in dipole approximation we get the result [6]

$$\alpha : \left\{ \begin{array}{ccc} \mathbb{C} \setminus P & \rightarrow & \mathbb{C} \\ \omega & \mapsto & \alpha(\omega) = -\frac{e^2}{m}\int_{\mathbb{R}} d\omega' \frac{f(\omega')}{\omega^2 - \omega'^2} . \end{array} \right.$$

The dynamic polarizability is defined everywhere in $\mathbb{C}$ except at some poles P (see Fig. 2.7), a direct physical interpretation, however, is only possible at real frequencies ω. With the help of the purely mathematical integral relation

$$\frac{2}{\pi}\int_0^\infty dx \frac{1}{(x^2+a^2)(x^2+b^2)} = \frac{1}{ab(a+b)} \text{ for } a, b > 0 \ ,$$

we can change (2.3) to

$$V(R) = -\frac{3\hbar}{\pi R^6}\int_0^\infty \alpha_1(i\omega)\,\alpha_2(i\omega)\,d\omega = -\frac{C}{R^6} \ , \tag{2.5}$$

with dynamic polarizabilities at imaginary frequencies

$$\alpha(i\omega) = \frac{e^2}{m}\int_{\mathbb{R}} d\omega' \frac{f(\omega')}{\omega^2 + \omega'^2} \ ,$$

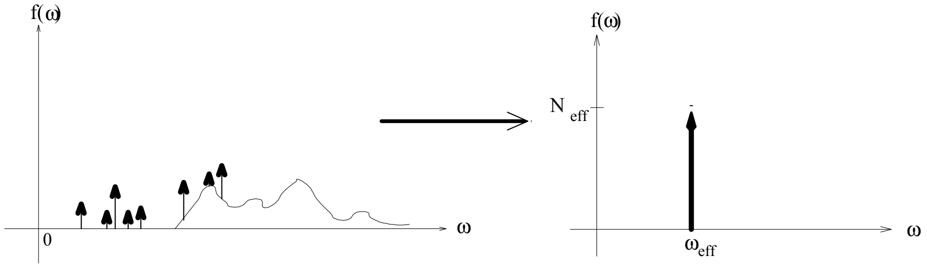

Figure 2.8: A model of an effective oscillator strength with only one possible transition at ω_{eff} with weight N_{eff}.

which have the following properties

$$0 < \alpha\left(i\omega\right) \leq \alpha\left(0\right) \ ,$$

$$\omega_2 > \omega_1 \Rightarrow \alpha\left(i\omega_2\right) < \alpha\left(i\omega_1\right) \ ,$$

$$\alpha\left(i\omega\right) \underset{\omega\rightarrow\infty}{\rightarrow} \frac{Ne^2}{m}\frac{1}{\omega^2} \ .$$

Approximations for $\alpha\left(\omega\right)$

There are various approximations in use. A common one is to replace the rich structure of $f\left(\omega\right)$ by a finite number of strong interactions, even the approximation

$$f\left(\omega\right) = N_{eff}\delta\left(\omega - \omega_{eff}\right)$$

is possible (see Fig. 2.8). Here we have the problem that the sum rule would lead to $N_{eff} = N$. It is much better to take

$$N_{eff} \approx N_{val} < N, \omega \approx \omega_{eff} \ ,$$

which is related to the fact that

1. in $f\left(\omega\right)$ all ω are of equal importance,

$$\int d\omega f\left(\omega\right) = \int d\omega f_p\left(\omega\right) + \int d\omega f_c\left(\omega\right) = N = N_p + N_c$$

2. since in $\alpha\left(i\omega\right)$ the transitions are weighted with

$$\int_{\mathbb{R}} d\omega' \frac{1}{\omega^2 + \omega'^2}$$

   and high frequencies (i.e., σ_c) have lower weights and therefore are not so important

3. $\alpha\left(\omega\right)$ is measurable in experiment but not needed; $\alpha\left(i\omega\right)$ is not observable, only the static value $\alpha\left(0\right)$ is available from experiment.

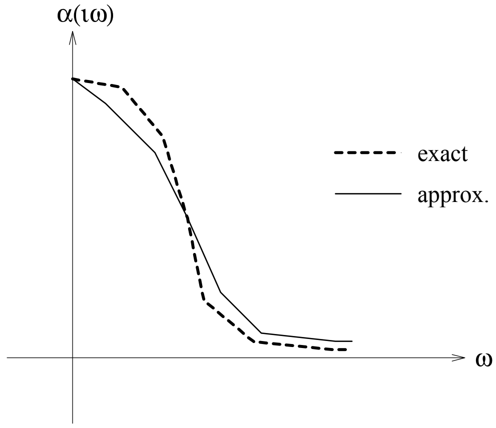

Figure 2.9: Approximation of thedynamical polarizability resulting from the effective oscillator strength model.

With the above mentioned method of just one frequency ω with weight N we evaluate the C_6 coefficient as

$$\begin{aligned} C_6^{X-Y} &= \frac{3\hbar}{\pi}\int_0^\infty \alpha_X\left(i\omega\right)\alpha_Y\left(i\omega\right)d\omega = \\ &= \frac{3\hbar e^4}{2m^2}\frac{N_X N_Y}{\omega_X\omega_Y(\omega_X+\omega_Y)} = \frac{3\hbar}{2}\frac{\omega_X\omega_Y}{\omega_X+\omega_Y}\alpha_X(0)\alpha_Y(0)\ , \end{aligned}$$

which is in the case of two identical atoms equal to $\left(C_6^{X-Y}\rightarrow C_{12}\right)$, and

$$C_{11} = \frac{3\hbar e^4}{4m^2}\frac{N_1^2}{\omega_1^3} = \frac{3}{4}\hbar\omega_1(\alpha_1(0))^2, \alpha_1\left(0\right) = \frac{Ne^2}{m\omega_1^2}\ . \tag{2.6}$$

A practical method in using (2.6) is to choose ω_1, N_1 in order to reproduce the experimental observables $\alpha_1\left(0\right), C_{11}$, which in turn leads to

$$\begin{aligned} \omega_1 &= \frac{4}{3\hbar}\frac{C_{11}}{\left(\alpha_1\left(0\right)\right)^2}\ , \\ N_1 &= \frac{16m}{9\hbar^2 e}\frac{\left(C_{11}\right)^2}{\left(\alpha_1\left(0\right)\right)^3}\ . \end{aligned}$$

The VdW coefficient C_{12} for two different atoms can be expressed as a function of the VdW coefficients C_{11}, C_{22} between two equal atoms as

$$C_{12} = 2\frac{C_{11}C_{22}}{\frac{\alpha_2(0)}{\alpha_1(0)}C_{11}+\frac{\alpha_1(0)}{\alpha_2(0)}C_{22}} \tag{2.7}$$

$$= 2\frac{C_{11}C_{22}}{\alpha_2(0)^2C_{11}+\alpha_1(0)^2C_{22}}\alpha_1(0)\alpha_2(0)\ . \tag{2.8}$$

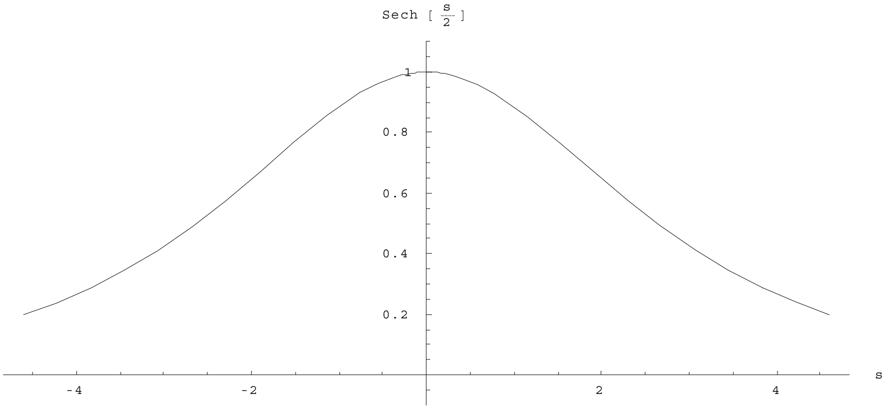

Figure 2.10: One can see that the geometric mean is only a good approximation for $\omega_1 \approx \omega_2$ otherwise $F\left(\frac{\omega_1}{\omega_2}\right)$ is better suited.

From this equation we easily arrive at the important Cross-term formula

$$C_{12} = \frac{2}{\left(\frac{\omega_1}{\omega_2}\right)^{\frac{1}{2}} + \left(\frac{\omega_1}{\omega_2}\right)^{-\frac{1}{2}}} \sqrt{C_{11}C_{22}} = F\left(\frac{\omega_1}{\omega_2}\right) \sqrt{C_{11}C_{22}} \; .$$

If we set $\gamma = \ln\left(\frac{\omega_1}{\omega_2}\right)$ we get (see Fig. 2.10)

$$\begin{aligned} C_{12} &= \frac{2}{e^{\frac{1}{2}\gamma} + e^{-\frac{1}{2}\gamma}} \sqrt{C_{11}C_{22}} = \left(\cosh\left(\frac{\gamma}{2}\right)\right)^{-1} \sqrt{C_{11}C_{22}} = &(2.9)\\ &= \operatorname{sech}\left(\frac{\gamma}{2}\right) \sqrt{C_{11}C_{22}} \; . &(2.10)\end{aligned}$$

We see that only for $\frac{\omega_1}{\omega_2} \approx 1$ the geometric mean $C_{12} = \sqrt{C_{11}C_{22}}$ is a good approximation, otherwise (2.9) is an improvement to the geometric mean.

2.2.5 Limits of the method

Here we want to summarize all the limits of the above method again:

1. the geometrical dimensions of the systems are small as compared to their distance, 'compact system' (see Fig. (2.5)).
2. the dipole approximation in first order time dependent perturbation theory for the dynamic electric polarizability $\alpha(\omega)$
3. multipole expansion of electrostatic interaction Hamiltonian up to the dipole moments
4. for each single molecule one needs the oscillator strengths for the whole spectrum, also the continuous one
5. it is only a theory for the attractive part of the intermolecular interaction and takes no account of repulsion as a consequence of overlap for smaller R

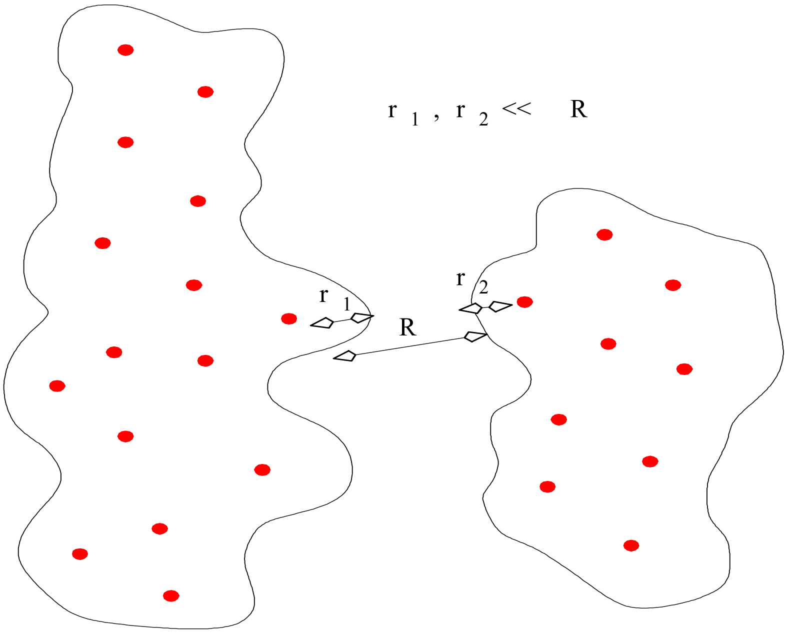

Figure 2.11: Two extended systems which are not small as compared to their distance, but do not have significant overlap.

2.3 Methods for extended geometries

The main limitation above is the small size of the systems as compared to their separation, $d_1, d_2 \ll R$, while the physical situation only demands that there is no overlap $r_1, r_2 \ll R$ (see Fig. 2.11)

2.3.1 Kohn-Mair formalism with a time dependent response function

For such extended systems without permanent dipole moments the VdW interaction is still the leading term. A new formalism via dynamic response functions in the time domain was developed by [24] and represents a conceptually new formalism with many computational advantages.

2.3.2 Pairwise summation technique (Hamaker method)

This simple method can yield approximate ideas about the Van der Waals interaction between two extended systems. We define the Hamaker interaction energy between two rigid systems as (see Fig. 2.12)

$$V^{(1,2)} = \sum_{i \in I_1} \sum_{j \in I_2} v\left(1i; 2j\right) \ ,$$

which treats the Van der Waals interaction as a sum of the interactions between the respective constituents; it also ignores the fact that the dispersion forces are not strictly additive (Axilrod -Teller) and the changed dispersion properties of the atoms depend on their bonding situation.

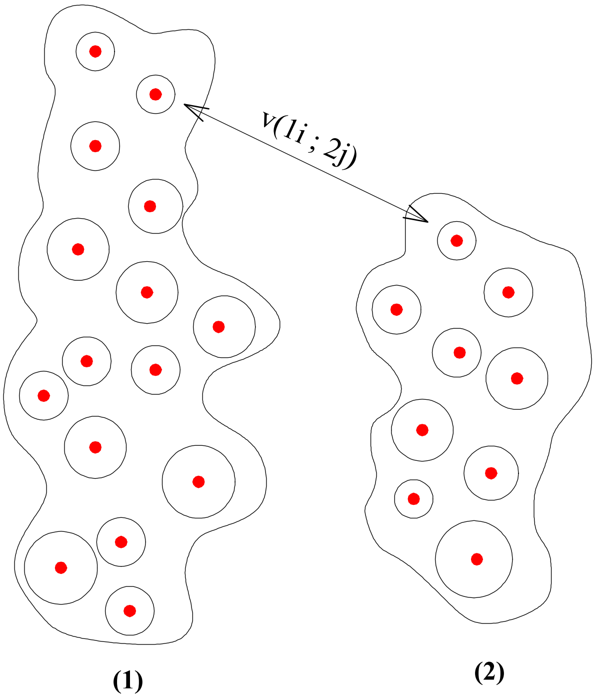

Figure 2.12: Hamaker method of pairwise summation: it treats the subsystem (1) just as the sum of its constituent molecules.

Chapter 3

Corrections to the Hamaker formula for dispersion interactions via Clausius-Mossotti formula

This part was mainly done at the Department for Physics, UCSB, Santa Barbara under the supervision of Prof. Dr. Walter Kohn. It presents a summary of results of a project dealing with dispersion forces between macroscopic bodies consisting of polarizable atoms.
The main aim was to see the leading corrections to the results obtained with the 'Hamaker method of pairwise summation' for media which are not highly diluted.
Here different geometries of the bodies are studied and the corrections are essentially different in character, while the condition for the applicability of the Hamaker method can always be expressed as $(\rho\alpha(0)) << 1$ for all systems. This approach can be extended to other geometries (e.g. cylinders) and later on to inhomogenous bodies with nonuniform density. Furthermore a discrete model of local field corrections in a finite cluster can be given.

3.1 Geometries of model systems

In the following sections the dispersion interaction between two macroscopic bodies are calculated with the help of the pairwise summation technique. In this chapter all the geometries considered are summarized.

3.1.1 Two semi-infinite half spaces

We consider 2 macroscopic bodies, each of them with a plane surface, which are aligned parallel to each other at a normal distance l. The linear dimensions of the 2 flat surface areas $L = A^{1/2}$ should be large enough as compared to the distance between the two bodies. On the other side the distance l should be large enough as compared to the intermolecular distances a of the constituent atoms of the bodies,

$$a << l << L \; . \tag{3.1}$$

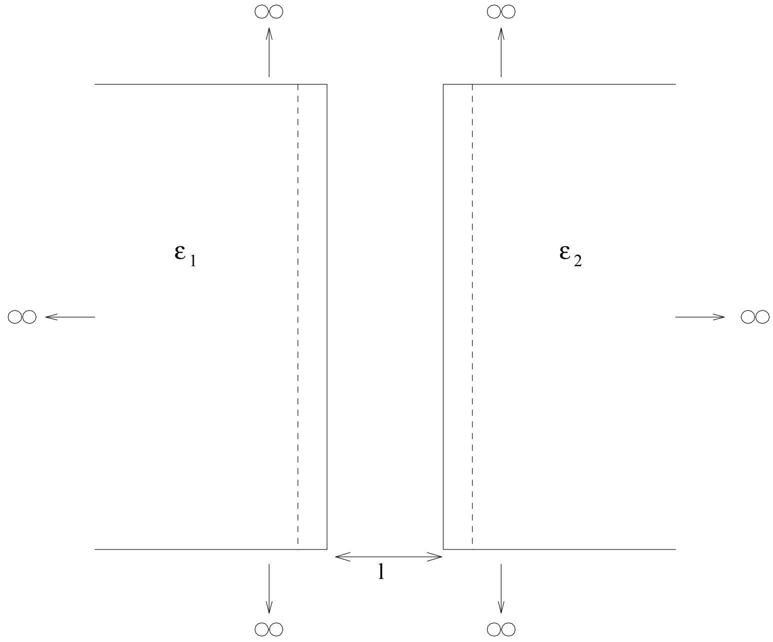

Figure 3.1: 2 half spaces (thick slabs) with given dielectric constants ϵ_1, ϵ_2 at a distance d. The dashed line shows the surface region of the slabs, where the dielectric properties are likely to be different.

If these conditions are fulfilled one can in good approximation consider the two bodies to be infinitely extended slabs separated by distance l. The total attractive dispersion energy will therefore be infinite and one can only calculate the interaction energy per unit area for this system.
More precisely the length a is given by the depth from the surface where the local electric field is already bulk like and is considered to be of the order of some interatomic distances. (Dashed line in Fig 3.1) Validity:
The form of the real macroscopic bodies has to be regular enough that this approximation with two slabs is valid, especially the surface should not be too rough or facetted.
An application is the adhesion of two macroscopic bodies to each other

3.1.2 Point-particle and semi-infinite slab

We consider one macroscopic body in the idealized form of a semi-infinite slab and a point-particle at a normal distance l from the surface. The linear dimension $L = A^{1/2}$ of the plane surface part of the condensed body should be large with respect to l such that this model becomes justified. On the other side the distance l should be large enough as compared to the intermolecular distances a of the constituent atoms of the bodies:

$$a < l < L \tag{3.2}$$

Again the length a is given by the depth from the surface where the matter is already bulk like and is known to be of the order of some interatomic distances. Application: This situation should be a good a proximation to the real situation of an atom adsorbed loosely (physisorption) to a condensed body with such a plain surface. Validity: The form of the real macroscopic body has to be regular enough such that an approximation with a slab is valid, especially the surface of the condensed body should not be too rough or facetted.

3.1.3 Two convex bodies

We consider two macroscopic bodies in the form of enclosed, convex, not touching regions in $\mathbb{R}^3$. Then there exist 2 points $\mathbf{x}_0 \in \delta B_1, \mathbf{y}_0 \in \delta B_2$ on the boundary of the bodies with minimal distance l such that

$$l^2 = (\mathbf{x}_0 - \mathbf{y}_0) \cdot (\mathbf{x}_0 - \mathbf{y}_0) = \min_{\mathbf{x} \in \delta B_1, \mathbf{y} \in \delta B_2} ((\mathbf{x} - \mathbf{y}) \cdot (\mathbf{x} - \mathbf{y})) \ .$$

Except for the case when the corresponding curvatures of the boundary at $\mathbf{x}_0, \mathbf{y}_0$ are zero, these points are uniquely determined. Through a translation and rotation of the coordinate system one can take the origin at one of these points, say at $\mathbf{x}_0$, the closest point of B_1 , and let the z-axis go through $\mathbf{y}_0 = (0, 0, y_{0z}) \in B_2$. Then there exists a local parametrization of the boundaries B_1, B_2 of the form

$$f_1 : \begin{array}{ccc} U & \to & \mathbb{R}^3 \\ (x, y) & \mapsto & (x, y, f_1(x, y)) \end{array} \qquad f_2 : \begin{array}{ccc} U & \to & \mathbb{R}^3 \\ (x, y) & \mapsto & (x, y, f_2(x, y)) \end{array} \ .$$

Because both bodies are assumed to be convex the second differentials of f_1 and f_2 are positive semi-definite and negative semi-definite quadratic forms, respectively. As Hesse matrices they are symmetric as well, and therefore are orthogonal similar to diagonal matrices. By choosing the x, y axis of the coordinate system to make the first form diagonal one gets two curvature radii κ_1, κ_2, the second one can be characterized by 2 other curvatures and one angle α between two main axes. By replacing the actual form of the two macroscopic bodies by the two (non necessarily rotational invariant) paraboloids one has a model geometry specified by 6 parameters, e.g., $l, \kappa_1, \kappa_2, \kappa_1', \kappa_2', \alpha$. This is a general model of two macroscopic bodies in long-range interaction with each other, which contains as special case the system of two slabs for which the curvature radii go to infinity. Validity of the approximation:

1. The real form of the condensed bodies should be close to paraboloids, especially there should not be more than one point at which these bodies come close to each other (e.g. no 'double tips in STM')

2. the intersection of the surface region with the VdW interaction region is small as compared to VdW interaction region.

Typical situations are Scanning Tunnelling Microscopy for far away tips, Atomic Force Microscopy in non-contact mode

3.1.4 Two cylindrical bodies

We consider two macroscopic bodies in the form of rotational cylinders with circular cross-sections, not touching each other. Then there exist 2 points $\mathbf{x}_0 \in \delta B_1, \mathbf{y}_0 \in \delta B_2$ on the boundary of the bodies with minimal distance l such that

$$l^2 = (\mathbf{x}_0 - \mathbf{y}_0) \cdot (\mathbf{x}_0 - \mathbf{y}_0) = \min_{x \in B_1, y \in B_2} ((\mathbf{x} - \mathbf{y}) \cdot (\mathbf{x} - \mathbf{y})) \ . \tag{3.3}$$

Except for the case when the two cylinders are parallel to each other these points are uniquely determined. Through a translation and rotation of the coordinate system one can shift the origin to one of these points, say at $\mathbf{x}_0$ the closest point of B_1, and let the z-axis go through $\mathbf{y}_0 = (0, 0, y_{0_z}) \in B_2$. By replacing the actual form of the two macroscopic bodies by the two cylinders one has a model geometry specified by 2 parameters, e.g.

$$l, \alpha \quad , \tag{3.4}$$

where $l \in [0, \infty[$ is the normal distance between the two wires and $\alpha \in [0, \frac{\pi}{2}]$ is the angle in the (x, y) plane by which one is rotated against the other. The case with $\alpha = 0$ where the two wires are parallel to each other is obviously a special case in the sense that the total interaction energy becomes infinite and only the interaction energy per unit length assumes a well defined value. Validity of approximation:

1. The real form of condensed matter chains should be close to long linear cylinders. There should not be any covalent bonding between the chains, the cylinders must be long as compared to their thickness (e.g., long linear carbon chains C_n with $n \geq 10$)
2. here the surface region of the chain and the VdW interaction region are almost identical

Applications: Interaction energy between chains in condensed polymer chains

3.2 Definitions for the VdW interaction between two atoms

The VdW dispersion interaction between 2 atoms (or isotropic small molecules) is given by

$$W(R) = -\frac{\Lambda_{12}}{R^6} = -\frac{C_{12}}{R^6} \ , \tag{3.5}$$

where the constant C_{12} has the dimension $[C_{12}] = energy * length^6$ and is given by

$$C_{12} = \frac{3\hbar}{\pi} \int_0^\infty \alpha_1(i\zeta)\alpha_2(i\zeta) d\zeta = \frac{3\hbar}{2\pi} \int_{-\infty}^\infty \alpha_1(i\zeta)\alpha_2(i\zeta) d\zeta \quad , \tag{3.6}$$

with α being the dynamic polarizability evaluated at the imaginary axis. With the previously defined oscillator strength one can write

$$C_{12} = \frac{3\hbar e^4}{2m^2} \sum_{m,n} \frac{f_{0m}^{(1)} f_{0n}^{(2)}}{\omega_{0n}^{(2)} \omega_{0m}^{(1)} (\omega_{0n}^{(2)} + \omega_{0m}^{(1)})} \ . \tag{3.7}$$

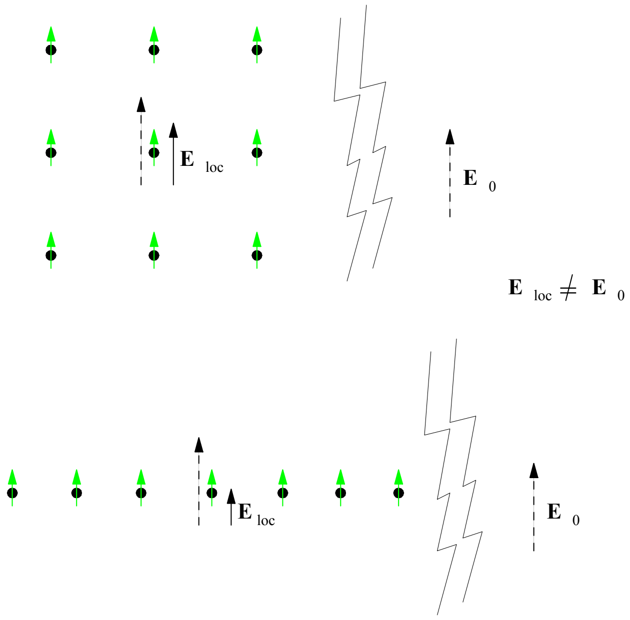

Figure 3.2: Local field corrections for different geometries. The local field corrections depend on the geometrical form of the system, e.g., 'bulk like' $\neq$ '1dimensional chain'

For two isotropic oscillators with just one frequency respectively, this can be simplified to

$$C_{12} = \frac{3\hbar e^4}{2m^2} \frac{N_1 N_2}{\omega_1 \omega_2 (\omega_1 + \omega_2)} = \frac{3}{2} \hbar \frac{\omega_1 \omega_2}{\omega_1 + \omega_2} \alpha_1(0) \alpha_2(0) \ , \tag{3.8}$$

which in the case of two identical atoms reduces to

$$C = \frac{3\hbar e^4}{4m^2} \frac{N^2}{\omega_0^3} = \frac{3}{4} \hbar \omega_0 (\alpha(0))^2 \ . \tag{3.9}$$

3.3 The Clausius-Mosotti local field correction

For the electric field in a bulk dielectric medium one has to distinguish between various fields:

$$E_{loc}, E = E_{av}, D, P \tag{3.10}$$

The local field corrections are known as the Clausius-Mosotti formula: for either cubic symmetric crystals or completely randomly amorphous condensed media it implies the following results:

$$E_{loc} = \frac{3}{3 + 8\pi\rho\alpha} D = \frac{3}{3 - 4\pi\rho\alpha} E \ , \tag{3.11}$$

$$E = \frac{3 - 4\pi\rho\alpha}{3 + 8\pi\rho\alpha} D \ , \tag{3.12}$$

$$P = \frac{3\rho\alpha}{3 + 8\pi\rho\alpha} D = \frac{3\rho\alpha}{3 - 4\pi\rho\alpha} E \ . \tag{3.13}$$

The dielectric constant is therefore related to the atomic polarizability by

$$\epsilon = \frac{3 + 8\pi\rho\alpha}{3 - 4\pi\rho\alpha} \; , \tag{3.14}$$

where the critical value $\rho\alpha = \frac{3}{4\pi}$ leads to an infinite dielectric constant, but this is of no importance in the following. The atomic polarizability of the oscillator model,

$$\alpha(\omega) = \frac{Ne^2}{m} \frac{1}{\omega_0^2 - \omega^2} \; ,$$

leads to the dielectric constant

$$\epsilon(\omega) = \frac{\omega^2 - (\omega_0^2 + 4a^2)}{\omega^2 - (\omega_0^2 - 2a^2)}, \quad a^2 = \frac{2\pi}{3}\frac{Ne^2\rho}{m} \; . \tag{3.15}$$

An important function related to the dielectric constant is

$$d(\omega) = \frac{\epsilon(\omega) - 1}{\epsilon(\omega) + 1} = \frac{6\pi\rho\alpha}{3 + 2\pi\rho\alpha} = -\frac{3a^2}{(\omega_0^2 + a^2) - \omega^2} \; . \tag{3.16}$$

Notes:

1. The Clausius-Mosotti formula was derived for static electric fields, but was applied in this context to electric fields which are spatially homogeneously but harmonically varying in time.

2. The form of $d(\omega)$ has essentially the same properties as the atomic polarizability of a single atom, except that the frequency of the pole is always shifted to higher frequencies, $\omega_0^2 \to \omega_0^2 + a^2$, remaining, however, on the real axis for all values of ρ.

3.4 Results for the 2-slabs model

3.4.1 The Hamaker result

The result of applying a pairwise summation (replaced by integration in the continuum limit) to the dispersion energy between two half spaces leads to the Hamaker result,

$$\frac{W(l)}{A} = -\frac{1}{l^2}\frac{\pi}{12}\rho_1\rho_2 C_{12} \; , \tag{3.17}$$

where the form of the atomic polarizabilities is only contained in C_{12}. For two isotropic oscillators this leads to

$$\frac{W(l)}{A} = -\frac{1}{l^2}\frac{\hbar e^4\pi}{8m^2}\frac{N_1\rho_1 N_2\rho_2}{\omega_1\omega_2(\omega_1 + \omega_2)} = -\frac{1}{l^2}\frac{\pi\hbar}{8}(\alpha_1(0)\rho_1)(\alpha_2(0)\rho_2)\frac{\omega_1\omega_2}{\omega_1 + \omega_2} \; , \tag{3.18}$$

which can be simplified for two identical slabs ($C_{12} = C_{11} = C_{22} = C$) to

$$W(l)/A = -\frac{1}{l^2}\frac{\pi\hbar\omega_0}{16}(\alpha(0)\rho)^2 = -\frac{1}{l^2}\frac{\pi}{12}\rho^2 C \; . \tag{3.19}$$

3.4.2 The Lifshitz-formula

The basic formula for the non-retarted regime as given by [8] and others for the interaction energy per unit surface for two parallel semi-infinite slabs separated by a distance l is

$$\begin{aligned}\frac{W(l)}{A} &= \frac{-1}{l^2}\frac{\hbar}{16\pi^2}\int_0^\infty \sum_{n=1}^\infty \frac{1}{n^3}\left(d_1\left(\imath\zeta\right)d_2\left(i\zeta\right)\right)^n = && (3.20)\\ &= -\frac{1}{l^2}\frac{\hbar}{16\pi^2}\int_0^\infty \sum_{n=1}^\infty \frac{1}{n^3}\left(\frac{\epsilon_1\left(i\zeta\right)-1}{\epsilon_1\left(i\zeta\right)+1}\frac{\epsilon_2\left(i\zeta\right)-1}{\epsilon_2\left(i\zeta\right)+1}\right)^n && (3.21)\end{aligned}$$

The above formula is equivalent to a formula with a double integral also given by Lifshitz. The convergence of the sum can be seen from the quotient criterion, because $\forall\zeta\in\mathbb{R}\left(d_1\left(i\zeta\right),d_2\left(i\zeta\right)<1\right)$, for all imaginary frequencies.

The leading term, $n = 1$

Following Lifshitz we first consider the leading term in the formula (3.20). With the help of the integral identity

$$\int_{\mathbb{R}}\left(\frac{1}{x^2+b_1^2}\right)\left(\frac{1}{x^2+b_2^2}\right)dx = \frac{\pi}{b_1b_2\left(b_1+b_2\right)} \tag{3.22}$$

one gets the result

$$\begin{aligned}\frac{W(l)}{A} &= -\frac{1}{l^2}\frac{9\hbar}{32\pi}\frac{a_1^2a_2^2}{b_1b_2(b_1+b_2)} = && (3.23)\\ &= -\frac{1}{l^2}\frac{9\hbar}{32\pi}\frac{a_1^2a_2^2}{(a_1^2+\omega_1^2)^{1/2}(a_2^2+\omega_2^2)^{1/2}((a_1^2+\omega_1^2)^{1/2}+(a_2^2+\omega_2^2)^{1/2})} && (3.24)\end{aligned}$$

where

$$\begin{array}{cc} a_1^2=\frac{2\pi}{3}\frac{N_1e^2\rho_1}{m} & a_2^2=\frac{2\pi}{3}\frac{N_2e^2\rho_2}{m}\\ b_1^2=a_1^2+\omega_1^2 & b_2^2=a_2^2+\omega_2^2\\ \frac{a_1^2}{\omega_1^2}=\frac{2\pi}{3}\rho_1\alpha_1(0) & \frac{a_2^2}{\omega_2^2}=\frac{2\pi}{3}\rho_2\alpha_2(0)\end{array}$$

Expressed in these parameters the result is

$$\begin{aligned}\frac{W(l)}{A} &= -\frac{1}{l^2}\frac{\hbar\pi}{8}\frac{\rho_1\alpha_1(0)}{(1+\frac{2\pi}{3}\rho_1\alpha_1(0))^{1/2}}\frac{\rho_2\alpha_2(0)}{(1+\frac{2\pi}{3}\rho_2\alpha_2(0))^{1/2}} && (3.25)\\ &\quad\frac{\omega_1\omega_2}{\omega_1(1+\frac{2\pi}{3}\rho_1\alpha_1(0))^{1/2}+\omega_2(1+\frac{2\pi}{3}\rho_2\alpha_2(0))^{1/2}} = && (3.26)\\ &= -\frac{1}{l^2}\frac{\pi}{6}\frac{\rho_1\alpha_1(0)}{(1+\frac{2\pi}{3}\rho_1\alpha_1(0))^{1/2}}\frac{\rho_2\alpha_2(0)}{(1+\frac{2\pi}{3}\rho_2\alpha_2(0))^{1/2}} && (3.27)\\ &\quad\frac{C_{11}C_{22}}{C_{11}\alpha_2^2(1+\frac{2\pi}{3}\rho_1\alpha_1(0))^{1/2}+C_{22}(1+\frac{2\pi}{3}\rho_2\alpha_2(0))^{1/2}}\ , && (3.28)\end{aligned}$$

which reduces for two identical slabs to

$$\frac{W(l)}{A} = -\frac{1}{l^2}\frac{\pi}{16}\hbar\omega_0\frac{(\rho\alpha(0))^2}{(1+\frac{2\pi}{3}\rho\alpha(0))^{3/2}} = -\frac{1}{l^2}\frac{\pi}{12}\frac{\rho^2 C}{(1+\frac{2\pi}{3}\rho\alpha(0))^{3/2}} \ . \tag{3.29}$$

For two identical slabs one can easily see the asymptotic forms for large and small densities:

$$\begin{array}{lll} \rho\alpha \to 0 & \frac{W(l)}{A} \to & -\frac{1}{l^2}\hbar\omega_0\frac{\pi}{16}(\rho\alpha(0))^2 = -\frac{1}{l^2}\frac{\pi}{12}\rho^2 C \ , \\ \rho\alpha \to \infty & \frac{W(l)}{A} \to & -\frac{1}{l^2}\hbar\omega_0\frac{\pi}{16}(\frac{3}{2\pi})^{3/2}(\rho\alpha(0))^{1/2} = -\frac{1}{l^2}\frac{\sqrt{3}}{8\sqrt{2\pi}}\frac{\rho^{1/2}C}{\alpha(0)^{3/2}} \ . \end{array}$$

For the case of different materials in the two slabs one has to compare all oscillator frequencies with the frequencies a_1, a_2 to determine the asymptotic behavior.

3.4.3 The comparison between Hamaker and Lifshitz results

When both systems are dilute

$$(\rho_1\alpha_1)\,,(\rho_2\alpha_2) \to 0 \qquad \Rightarrow \qquad \frac{W(l)}{A} \to \ -\frac{1}{l^2}\frac{\pi}{8}(\rho_1\alpha_1(0)\rho_2\alpha_2(0))\hbar\frac{\omega_1\omega_2}{\omega_1+\omega_2} = \tag{3.30}$$

$$= -\frac{1}{l^2}\frac{\pi}{6}\frac{\rho_1\alpha_1\rho_2\alpha_2 C_{11}C_{22}}{C_{11}\alpha_2(0)^2 + C_{22}\alpha_1(0)^2} = -\frac{1}{l^2}\frac{\pi}{6}\rho_1\rho_2 C_{12} \tag{3.31}$$

the Lifshitz result reduces to the Hamaker result. In general the attraction energy is reduced by the local field correction which can be interpreted as a partial shielding of the dipole moments in the condensed medium by the other dipole moments.

3.5 Dispersion forces between one atom and a slab

3.5.1 The Hamaker result

In its leading power in l for $l \to \infty$ the Hamaker result for this geometry is

$$W(l) = -\frac{1}{l^3}\frac{\pi}{6}\rho_1 C_{12} \ , \tag{3.32}$$

where the form of the atomic polarizabilities enters C_{12}. For isotropic oscillator models for the dynamic polarizability of the atoms in each system this leads to

$$W(l) = -\frac{1}{l^3}\frac{\pi}{4}(\alpha_1(0)\rho_1)\alpha_2(0)\hbar\frac{\omega_1\omega_2}{\omega_1+\omega_2} \ , \tag{3.33}$$

which can be simplified for two identical atoms to

$$W(l) = -\frac{1}{l^3}\frac{\pi}{6}\rho_1 C = -\frac{1}{l^3}\frac{\pi\hbar\omega_0}{8}\alpha(0)^2\rho \ . \tag{3.34}$$

3.5.2 The Clausius-Mossotti correction

The basic formula for the non-retarted regime given by [10] and others for the interaction energy for one atom separated by a distance l from a semi-infinite slab is given by

$$W(l) = -\frac{1}{l^3}\frac{\hbar}{4\pi}\int_0^\infty d\zeta \left(\alpha(i\zeta)\frac{\epsilon(i\zeta)-1}{\epsilon(i\zeta)+1}\right) \ . \tag{3.35}$$

For a more detailed analysis one has to specify the origin of the z coordinate with respect to the surface plane. With the help of the integral identity,

$$\int_{\mathbb{R}} \left(\frac{1}{x^2+b_1^2}\right)\left(\frac{1}{x^2+b_2^2}\right) dx = \frac{\pi}{b_1 b_2 \left(b_1+b_2\right)} \ , \tag{3.36}$$

one gets the result

$$W(l) = -\frac{1}{l^3}\frac{3\hbar N_1 e^2}{8m}\frac{a_2^2}{\omega_1 b_2(\omega_1+b_2)} \ , \tag{3.37}$$

where

$$a_2^2 = \tfrac{2\pi}{3}\tfrac{N_2 e^2 \rho_2}{m} \quad b_2^2 = a_2^2 + \omega_2^2 \quad \tfrac{a_2^2}{\omega_2^2} = \tfrac{2\pi}{3}\rho_2\alpha_2(0) \ .$$

Expressed in these parameters the result is

$$\begin{aligned} W(l) &= -\frac{1}{l^3}\alpha_1(0)\frac{\pi}{4}\frac{\rho_2\alpha_2(0)}{(1+\frac{2\pi}{3}\rho_2\alpha_2(0))^{1/2}}\hbar\frac{\omega_1\omega_2}{\omega_1+\omega_2(1+\frac{2\pi}{3}\rho_2\alpha_2(0))^{1/2}} = &(3.38)\\ &= -\frac{1}{l^3}\alpha_1(0)\frac{\pi}{3}\frac{\rho_2\alpha_2(0)}{(1+\frac{2\pi}{3}\rho_2\alpha_2(0))^{1/2}}\frac{C_{11}C_{22}}{C_{11}\alpha_2^2(0)+C_{22}\alpha_1^2(0)(1+\frac{2\pi}{3}\rho_2\alpha_2(0))^{1/2}} \ . &(3.39)\end{aligned}$$

which reduces for two identical atoms to

$$\begin{aligned} W(l) &= -\frac{1}{l^3}\alpha(0)\frac{\pi}{4}\frac{\rho_2\alpha(0)}{(1+\frac{2\pi}{3}\rho_2\alpha(0))^{1/2}}\hbar\frac{\omega_0}{1+(1+\frac{2\pi}{3}\rho_2\alpha(0))^{1/2}} = &(3.40)\\ &= -\frac{1}{l^3}\frac{\pi}{3}\frac{\rho C}{(1+\frac{2\pi}{3}\rho_2\alpha(0))^{1/2}(1+(1+\frac{2\pi}{3}\rho\alpha(0))^{1/2})} \ . &(3.41)\end{aligned}$$

3.5.3 Comparison of the Hamaker result with the Clausius-Mossotti correction

This can be seen at the asymptotic forms for large and small densities:

$$\begin{aligned} (\rho\alpha)\to 0 \qquad W(l) &\to -\frac{1}{l^3}\frac{\hbar\pi e^4}{4m^2}\frac{N_1 N_2 \rho_2}{\omega_1\omega_2(\omega_1+\omega_2)} = &(3.42)\\ &= -\frac{1}{l^3}\alpha_1(0)\rho_2\alpha_2(0)\frac{\hbar\pi}{4}\frac{\omega_1\omega_2}{\omega_1+\omega_2} = -\frac{1}{l^3}\frac{\pi}{6}\rho_1 C_{12} &(3.43)\\ (\rho\alpha)\to\infty \qquad W(l) &\to -\frac{1}{l^3}\frac{3\hbar N_1 e^2}{8\pi m\omega_1} = -\frac{1}{l^3}\alpha_1(0)\frac{3}{8}\hbar\omega_1 = &(3.44)\\ &= -\frac{1}{l^3}\frac{C_{11}}{2\alpha_1(0)} &(3.45)\end{aligned}$$

An interesting feature is that for large densities in the condensed medium the result is independent of the density and the atomic properties of the condensed medium.

The result for small densities is the same as the one obtained by the Hamaker method of using a pairwise summation. Equivalent to the slab-slab model system the slab-atom model system shows that the local field correction via the Clausius-Mossotti correction always decreases the attractive dispersion energy between the systems.

Chapter 4

Universal Model of Crystalline Polymers

4.1 Introduction

This chapter presents a model of crystalline linear polymers. The main aim was to describe the interchain dispersion interactions and the physical properties resulting from these interactions.

4.1.1 Organic polymers

We consider long, unbranched organic molecules. One such polymer is held together by typical covalent bonds between $C, H, ..$ atoms. The easiest (somehow really existing) example is polyyne (Fig. 4.1). The next difficult polymer is polyacetylene (Fig. 4.2), which is a periodic arrangement of C_2H_2 units.

The simplest saturated polymer is polyethylene (Fig. 4.3).

We will replace one polymer by a long, linear chain, where each unit (e.g. C_2H_4) is replaced by a so called bead, which should be located at the center of the replaced unit and its properties should mimic the replaced unit (e.g. $M_{bead} = \sum_{j \in unit} M_j$). One such chain we will also call a wire and consider as rigid in our model.

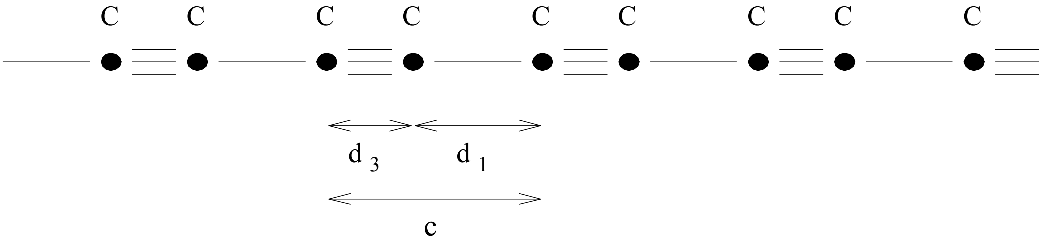

Figure 4.1: A polyyne polymer consists just of Carbon atoms which are arranged in a linear molecule. The bond length are unequal and alternate between single and triple bonds.

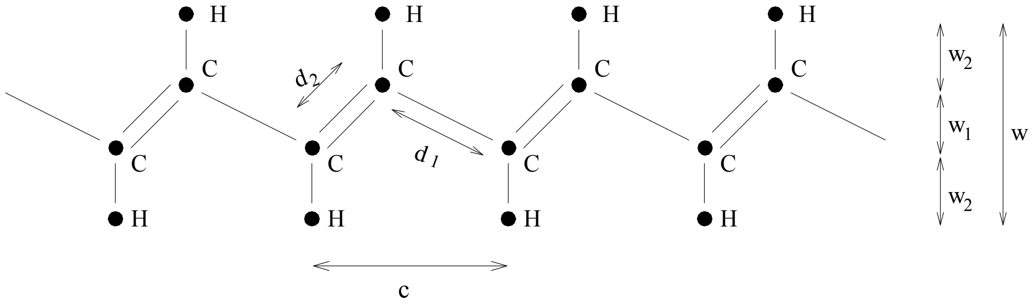

Figure 4.2: A polyacetylene polymer consists of an periodic arrangement of C_2H_2 units. The $C-C$ bond length alternates between single and double bonds.

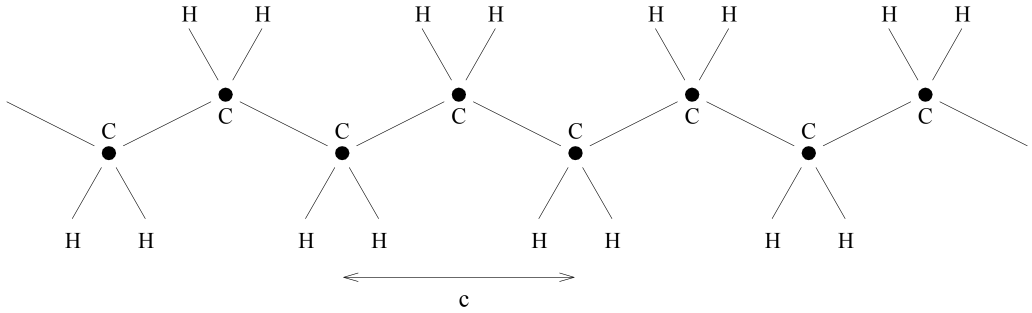

Figure 4.3: A polyethylene polymer consists of C_2H_4 units which are arranged in a linear molecule. All $C-C$ bonds have equal length.

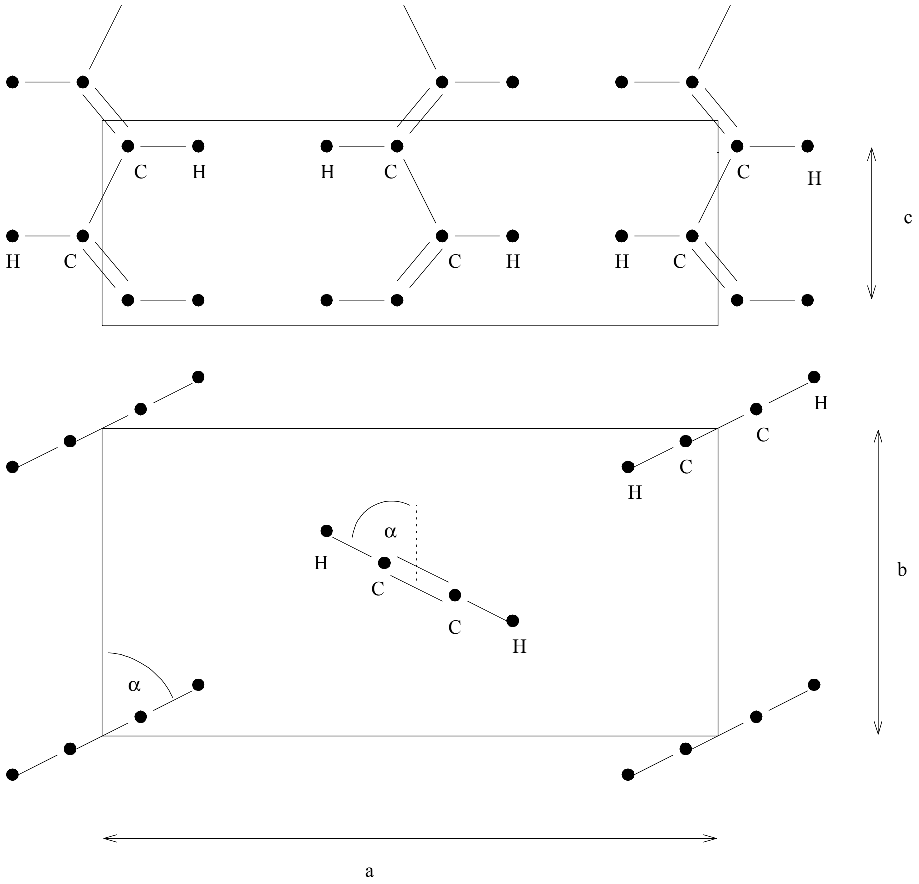

Figure 4.4: Crystal structure of polyacetylene: an orthorhombic lattice with in plane constants a, b and c along the chain axis, and the setting angle α.

4.1.2 Crystalline Polymers

In nature single polymer chains can form polymer crystals with a certain crystal structure. For example we plot the crystal structure of polyacetylene in (Fig. 4.4).

Other polymers crystallize in similar structures. If we replace each polymer chain by a wire we will loose some degrees of freedom of the real structure. The in-plane lattice constants will be the same $a, b \to a = b$, and the setting angle α becomes irrelevant.

4.2 Models for a crystallized linear polymer

4.2.1 Description of models

1. One atom per unit cell (see Fig. 4.5)

   We understand our model as a 3D crystal where one dimension is very different from the other two. Therefore we consider our model more like a 2D quadratic lattice with one wire per unit cell. For many purposes this model is already sufficient, but as we can see from the

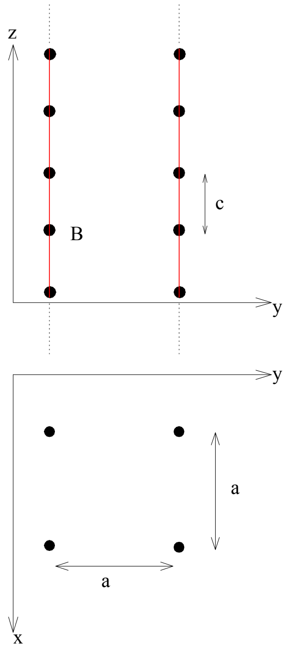

Figure 4.5: A model crystal of wires arranged in a 2D quadratic lattice with lattice constant a and wire periodicity length c with 1 atom per unit cell.

real crystal structure of polyacetylene (Fig 4.4) a model with 2 atoms per unit cell would be an improvement.

2. Two atoms per unit cell (see Fig. 4.6)

   Here we take a 2D quadratic lattice with another wire at the center of the other 4. Because one set of wires is shifted by $\frac{c}{2}$ along the chain axis, we have to describe it by using 2 atoms per unit cell.

   If the simplest model with 1 atom per unit cell is not sufficient, we will apply this model with 2 atoms per unit cell.

3. More sophisticated models

   An even more sophisticated model is sketched in (see Fig. 4.7), where each wire is not linear anymore but has more than 1 atom per 1D unit. In this model we can describe coupled rotations of the wires around their axis, which leads to the concept of librons. However this model becomes more complicated and has much more parameters which must be related to the experiment. Therefore we will not further examine it in this thesis.

4.2.2 Features

Our minimal models (1 and 2) for a crystal of linear polymers have the following features

1. The components are long, periodic, unbranched, rigid, linear polymers with periodicity c.

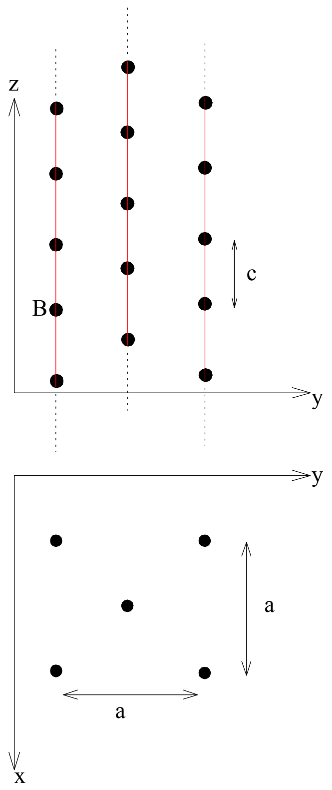

Figure 4.6: A model crystal of wires arranged in a 2D quadratic lattice with lattice constant a and wire periodicity length c with 2 atoms per unit cell.

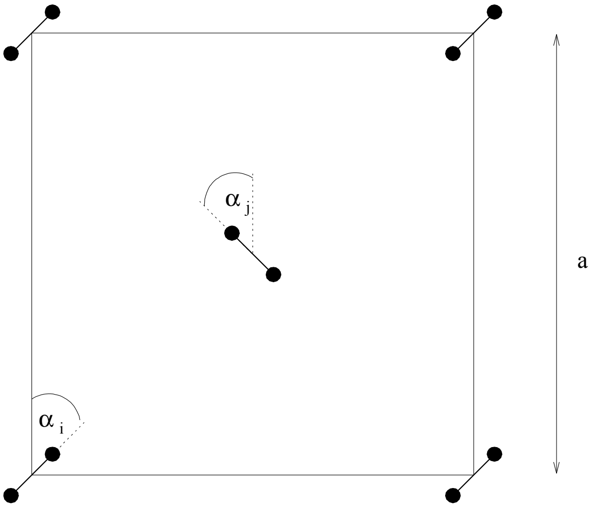

Figure 4.7: A chain is no longer linear but has itself more than 1 atom per 1D unit, which are displaced perpendicular to the axis. As another degree of freedom we can describe rotations of wires in this model.

2. In the unperturbed ideal single crystal the individual polymers are perfectly aligned, say in the z direction.

3. All chains are identical, just displaced by a set of two-dimensional displacement vectors in the $x - y$ plane forming a square lattice

$$\tau_n = \tau_{n_1,n_2} = n_1(a,0,0) + n_2(0,a,0) \ , \tag{4.1}$$

with the possible addition of a vector in the z direction

$$\tau_3 = (0,0,c/2) \ . \tag{4.2}$$

4. We assume the interactions between chains to consist of pairwise Van der Waals type attractions due to correlated charge fluctuations in pairs of polymer chains, plus short ranged repulsions due to electron overlap. We model these interactions phenomenologically by a total interaction energy

$$V = \frac{1}{2}\sum_{l\neq l'}\sum_{m,m'} v(lm, l'm') \ , \tag{4.3}$$

where $l = (l_1, l_2)$ labels the polymer chain and m the position of the monomer in a chain. We represent the interaction $v(lm, l'm')$ between two monomers in two **different** chains by a Lennard-Jones (6,12) potential,

$$v(r) = -4\epsilon\left(\left(\frac{\sigma}{r}\right)^6 - \left(\frac{\sigma}{r}\right)^{12}\right) \ , \tag{4.4}$$

whose well-depth is ϵ and whose minimum is located at $\left(2^{\frac{1}{6}}\right)\sigma$.

Extension of models

Submonomer basic units An extension of the model for a crystal of linear polymers can be constructed in the following way. One takes as a basic unit in one polymer not a monomer but a C_1H_n unit located between the respective C and H atom. Then one monomer consists of an integer number of such units, which can not be obtained from one unit by a simple translation but by a translation with a rotation.

1. For polyyne one such a unit is just one C atom and $n = 0$; two units build up one monomer C_2.

2. For polyacetylene one such unit is one $C - H$ group and $n = 1$; two units build up one monomer C_2H_2.

3. For polyethylene one such unit is one $H - C - H$ group and $n = 2$; two units build up one monomer C_2H_4.

For each basic unit one has a Lennard-Jones center, whose precise location needs to be discussed.

Individual atoms as basic units A further refinement of the model is to consider each individual atom as a Lennard Jones center. This has the advantage that the geometric structure is mimiced in a more detailed way, but also the disadvantage that one needs different Lennard Jones parameters for every different atom in the sample.

Discussion

Our term *rigid* includes strong bonds with effectively high excitation energies, both vibrational and electronic, such that internal excitations can be neglected and the relative positions of the atoms in a given chain can be considered as fixed.

4.2.3 Estimation of Lennard Jones parameters

The basic model (with 1 or 2 atoms/unit cell) has only one free bead-bead parameter σ which can be adapted to the experimental crystal structure of the solid polymer. To guarantee that one really works at the quadratic lattice constant a of the model, in the minimum of the energy in the assumed crystal structure one should determine σ by the condition

$$\frac{d}{da}V(a;c,\sigma,\epsilon)|_{a_0} = 0 \rightarrow \sigma = \sigma_0(a_0) \ . \tag{4.5}$$

The other Lennard Jones parameter ϵ only appears as a linear prefactor and therefore does not change the results in an essential way. It can be determined if an experimental value of the C_6 dispersion coefficient of the basic unit (bead) is known:

$$4\epsilon\sigma^6 = C_6 \ , \ \epsilon = \frac{C_6}{4\sigma^6}. \tag{4.6}$$

4.2.4 Universality

Because of the scaling property of the Lennard Jones potential given by

$$v(r;\epsilon,\sigma) = v(sr;\epsilon,s\sigma) = \epsilon f(r/\sigma) \ , \tag{4.7}$$

there is just one dimensionless parameter which specifies the basic model. This is the ratio $x = \frac{\sigma}{c}$ of the Lennard Jones length and the primitive periodicity constant of the chain and represents somehow the difference between the covalent bond length to the VDW bond length.

4.2.5 Different energy scales in the model

There are 3 essentially different energy scales involved in our model of a crystalline linear polymer:

1. the intrachain covalent bonds and quantities depending on them
2. the change of interchain distance
3. the relative sliding of two different chains without change of interchain distance

In the remainder we will not consider quantities depending on intrachain properties.

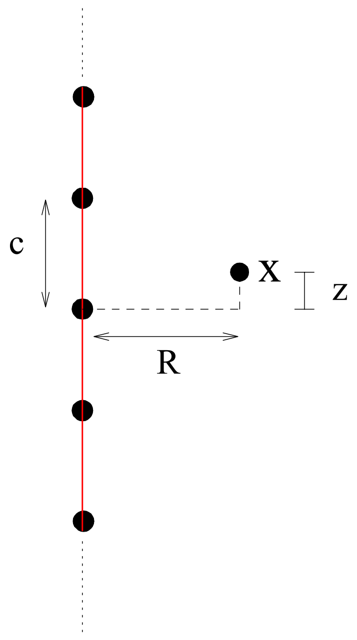

Figure 4.8: A wire and a bead of another parallel wire at a normal distance R and a z-translation z.

4.3 Results for the minimal model

In this section various physical properties of this model have been calculated.

4.3.1 Potential of one wire

Geometry: Infinitely long periodic mono-atomic chain (in z direction) with a primitive periodicity c.

The $1D$ lattice is defined by

$$\begin{aligned} \mathcal{T} &= \{na\mathbf{e}_3 : n \in \mathbb{Z}\} \ , && (4.8) \\ \mathcal{T}^* &= \left\{nb\mathbf{e}_3 = n\frac{2\pi}{a}\mathbf{e}_3 : n \in \mathbb{Z}\right\} \ , && (4.9) \end{aligned}$$

where $\mathbf{e}_3$ is the unit vector in the z-direction and $b = \frac{2\pi}{c}$ is the reciprocal lattice constant.
Let v be a single atom potential of an atom at the origin of the coordinate system:

$$v(x, y, z) = v(z; R) \ , \tag{4.10}$$

then for $R^2 = x^2 + y^2 > 0$ the 1-dimensional Fourier transform with respect to z is given by

$$\tilde{v}(k; x, y) = \tilde{v}(k; R) = \frac{1}{2\pi} \int_{\mathbb{R}} \left(v(z; R)e^{-ikz}\right) dz \ . \tag{4.11}$$

The Fourier transform of the sum of linear periodically arranged potentials is given by

$$\tilde{V}(k;x,y) = \tilde{V}(k;R) = \frac{1}{2\pi}\int_{\mathbb{R}}\sum_{n\in\mathbb{Z}} v(z-nc;R)e^{-ikz}dx = \tag{4.12}$$

$$= \frac{1}{2\pi}\sum_{n\in\mathbb{Z}}\left(\int_{\mathbb{R}} v(z;R)e^{-ikz}dz\right)e^{-ikna} = \left[|b|\sum_{n\in\mathbb{Z}}\delta\left(k-G_n\right)\right]\tilde{v}(k,R) = \tag{4.13}$$

$$= \left[|b|\sum_{n\in\mathbb{Z}}\delta\left(k-G_n\right)\tilde{v}(G_n,R)\right] . \tag{4.14}$$

The inverse Fourier transform leads to

$$V(z,R) = \int_{\mathbb{R}}\widetilde{V}(k;R)e^{ikz}dk = b\sum_{n\in\mathbb{Z}}\tilde{v}(nb,R)e^{inbz} = \tag{4.15}$$

$$= b\tilde{v}(0,R) + 2b\sum_{n\in\mathbb{N}}\tilde{v}(nb,R)\cos\left(nbz\right) . \tag{4.16}$$

We now evaluate the above formula for just the attractive and the repulsive part of our atom-atom potential. If v is a single purely attractive VdW potential then

$$v(z;x,y) = v(z;R) = -C(x^2+y^2+z^2)^{-3} = -Cr^{-6} = -C(z^2+R^2)^{-3} , \tag{4.17}$$

where C is the VdW interaction constant between two atoms with the dimensions $[energy * length^6]$. Then for $R^2 = x^2+y^2 > 0$ the 1-dimensional Fourier transform with respect to z exists and is given by

$$\tilde{v}(k,R) = \frac{1}{2\pi}\int_{\mathbb{R}} -C(z^2+R^2)^{-3}e^{-ikz}dz = \frac{1}{2}\frac{\partial^2}{\partial\left(R^2\right)^2}\left(\frac{1}{2\pi}\int_{\mathbb{R}} -C\frac{1}{z^2+R^2}e^{-ikz}dz\right) = \tag{4.18}$$

$$= \frac{-C}{4\pi}\frac{\partial^2}{\partial\left(R^2\right)^2}\left(\pi\frac{e^{-|k|R}}{R}\right) = \frac{-C}{16R^5}\left(3+3|k|R+k^2R^2\right)e^{-|k|R} . \tag{4.19}$$

This leads to

$$V(z;R) = b\sum_{n\in\mathbb{Z}}\tilde{v}(nb,R)e^{inbz} = b\tilde{v}(0,R) + 2b\sum_{n\in\mathbb{N}}\tilde{v}(nb,R)\cos\left(nbz\right) , \tag{4.20}$$

where the first harmonic terms are the most important ones:.

$$V(x,R) = b\tilde{v}(0,R) + 2b\tilde{v}(b,R)\cos(bz) + 2b\tilde{v}(2b,R)\cos(2bz) + \ldots \tag{4.21}$$

The Hamaker sum (of the attractive interaction alone, without replacement of the summation by an integration) of pairwise London interactions is therefore given by

$$V(x,y,z) = V(z,R) =$$

$$= -\frac{C}{c^6}\left[\frac{3\pi}{8}\left(\frac{c}{R}\right)^5 + \frac{\pi}{4}\sum_{n=1}^{\infty}\left[\left(3\left(\frac{c}{R}\right)^5 + 6\pi n\left(\frac{c}{R}\right)^4 + 4\pi^2n^2\left(\frac{c}{R}\right)^3\right)e^{-n2\pi\frac{R}{c}}\cos\left(n2\pi\frac{z}{c}\right)\right]\right] =$$

$$= -C\left[\frac{3}{16}bR^{-5} + \frac{1}{8}bR^{-5}\sum_{n=1}^{\infty}\left[\left(3+3G_nR+G_n^2R^2\right)e^{-G_nR}\cos\left(G_nx\right)\right]\right] . \tag{4.22}$$

The same procedure can be applied for possible present forms of the repulsive part of the interatomic potential,

$$v_{rep}(r) = +C_{12}r^{-12}, v(r) = v_0 e^{-\kappa(r-r_0)} = \lambda e^{-\kappa r}, v(r) = +C_9 r^{-9}. \tag{4.23}$$

Then for $R^2 = x^2 + y^2 > 0$ the 1-dimensional Fourier transform with respect to z exists. Only for $+C_{12}r^{-12}$ we can evaluate the integral analytically

$$\tilde{v}_{rep}(k; x, y) = \tilde{v}_{rep}(k; R) = \frac{1}{2\pi}\int_{\mathbb{R}} \left(C_{12}(z^2 + R^2)^{-6} e^{-ikz}\right) dz = \tag{4.24}$$

$$= \frac{C_{12}}{7680}\frac{e^{-|k|R}}{R^{11}}\left(945 + 945|k|R + 420\left(|k|R\right)^2 + 105\left(|k|R\right)^3 + 15\left(|k|R\right)^4 + \left(|k|R\right)^5\right) \tag{4.25}$$

This leads to a total potential energy (per bead unit) of two wires, parallel to each other, of

$$\begin{array}{rcl}
\tilde{v}(k; R) & = & \dfrac{-C_6 e^{-|k|R}}{16R^5}\left(3 + 3|k|R + k^2R^2\right) + \\
 & & +\dfrac{C_{12}}{7680}\dfrac{e^{-|k|R}}{R^{11}}\left(945 + 945|k|R + 420\left(|k|R\right)^2 + 105\left(|k|R\right)^3 + 15\left(|k|R\right)^4 + \left(|k|R\right)^5\right) \\
V(R, z) & = & \displaystyle\sum_{n\in\mathbb{Z}} v\left(\sqrt{R^2 + (z - nc)^2}\right) = \sum_{n\in\mathbb{Z}} (v_{att} + v_{rep})\left(\sqrt{R^2 + (z - nc)^2}\right) \\
 & = & \displaystyle\sum_{n\in\mathbb{Z}} V_n(R)\left(e^{in\frac{2\pi}{c}z}\right) = V_0(R) + 2\sum_{n=1}^{\infty} V_n(R)\cos\left(n\frac{2\pi}{c}z\right) = \\
 & = & \displaystyle\frac{2\pi}{c}\widetilde{v}(R; k = 0) + \frac{4\pi}{c}\sum_{n=1}^{\infty}\widetilde{v}\left(R; k = n\frac{2\pi}{c}\right)\cos\left(n\frac{2\pi}{c}z\right) .
\end{array}$$

with

$$V_0(R) \text{ being a polynomial in } R^{-1}, \text{ and } V_n(R), n \geq 1 \xrightarrow{R\to\infty} e^{-\frac{2\pi}{c}R} .$$

For many purposes it is enough to examine

$$V_0(R) = \frac{2\pi}{c}\widetilde{v}(R; k = 0) = \frac{\pi\epsilon\sigma^6}{64c}\left(63\sigma^6 R^{-11} - 96R^{-5}\right) ,$$

which is independent of z. For example the equilibrium distance is mainly determined by $V_0(R)$:

$$\frac{d}{dR}V_0(R) = 0 \Rightarrow R_0 = \left(\frac{693}{480}\right)^{\frac{1}{6}}\sigma < (2)^{\frac{1}{6}}\sigma .$$

and is therefore slightly smaller than the bead-bead equilibrium distance. The cohesive energy (per bead unit) between two wires at the equilibrium is given by

$$V_0(R_0) = -\epsilon\frac{48\pi}{11}\left(\frac{5}{77}\right)^{\frac{5}{6}} 6^{\frac{1}{6}}\frac{\sigma}{c} \approx -\epsilon\left(1.89\frac{\sigma}{c}\right) ,$$

which is confirmed by a rough approximation that all beads at the other wire with $z \in [-\sigma, +\sigma]$ contribute to the sum with $-\epsilon$. If the equilibrium position of the two wires is at $z = 0$ or $z = \frac{c}{2}$

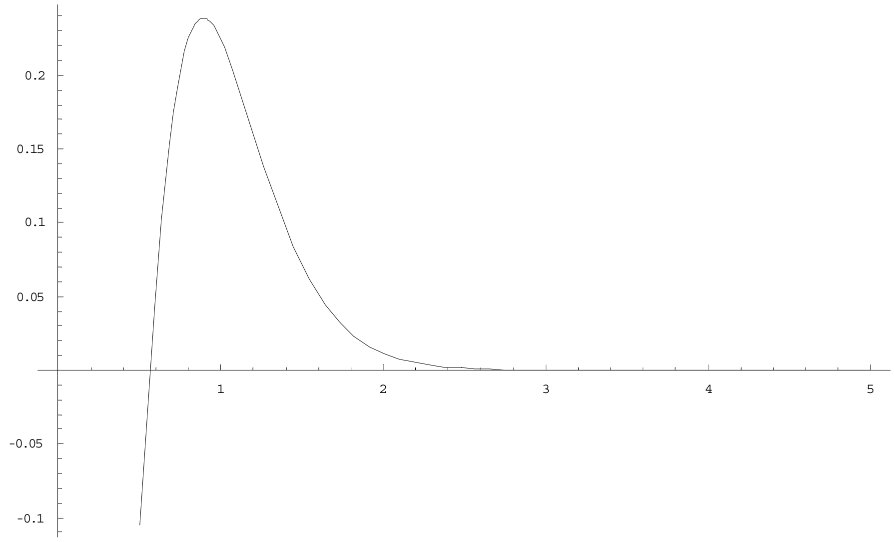

Figure 4.9: The function $\frac{4\pi}{c}\widetilde{v}(R_0; k = \frac{2\pi}{c})$ plotted against $\frac{\sigma}{c}$, therefore for $\frac{\sigma}{c} \approx 2$ the equilibrium is when the two wires are translated by $\frac{c}{2}$ in the z direction.

(and R_0 normal distance) depends on the ratio of $\frac{\sigma}{c}$. Because $e^{-n\frac{2\pi}{c}R}$ becomes small rather quickly with n growing we limit ourselves to the next term with $n = 1$,

$$\frac{4\pi}{c}\widetilde{v}\left(R; k = \frac{2\pi}{c}\right)\cos\left(\frac{2\pi}{c}z\right) \ ,$$

such that

$$\begin{aligned} \frac{4\pi}{c}\widetilde{v}\left(R_0; k = \frac{2\pi}{c}\right) &> 0 \Rightarrow R_0, z_{\min} = \frac{c}{2} \ , \\ \frac{4\pi}{c}\widetilde{v}\left(R_0; k = \frac{2\pi}{c}\right) &< 0 \Rightarrow R_0, z_{\min} = 0 \ . \end{aligned}$$

A plot (Fig. 4.9) of $\frac{4\pi}{c}\widetilde{v}(R_0; k = \frac{2\pi}{c})$ versus $\frac{\sigma}{c}$ shows that for $\frac{\sigma}{c} \approx 2$ the two wires are translated by $\frac{c}{2}$.

4.3.2 Cohesive energy

One can calculate the cohesive energy (sublimation energy) of the array of wires similar to the well known case of FCC rare gas crystals, where the cohesive energy is given by:

$$V(a; \epsilon, \sigma) = \frac{1}{2}\sum_{j\neq 0} v(j) = \frac{1}{2}\sum_{j\neq 0} -4\epsilon\left(\left(\frac{\sigma}{r_j}\right)^6 - \left(\frac{\sigma}{r_j}\right)^{12}\right) = \epsilon F(a/\sigma) \ ,$$

where F is a universal function for one lattice type (e.g. FCC) that depends only on the ratio of the lattice constant and the atom-atom Lennard Jones value σ.

For our array of wires we get

$$V\left(a;c,\epsilon,\sigma\right)=\frac{1}{2}\sum_{j\neq 0}v_{ww}\left(j\right)=\epsilon F\left(a/\sigma;c/\sigma\right)\ ,$$

where F is a universal function for one structure (e.g., 2D quadratic with 1 atom/cell) that depends only on the ratio of the lattice constant and the unit-unit (bead-bead) interaction length value σ, (and c/σ as further parameter of F).

4.3.3 Elastic constants

Let σ_{ij} be the usual stress (Cartesian stress tensor) applied to a (inner) plane with orientation i in the direction j (a surface with normal vector $\mathbf{e}_i$, where stress vector points in the direction $\mathbf{e}_j$), and ϵ_{kl} the resulting strain $\epsilon_{kl}=\frac{\triangle a_k}{a_l}$, the ratio of displacement $\triangle a_k$ to the original size a_l. Linear elasticity theory relies on the fact that

$$\sigma_{ij}=c_{ijkl}\epsilon_{kl}\ ,\ \ \epsilon_{ij}=s_{ijkl}\sigma_{kl}\ , \tag{4.26}$$

where the s_{ijkl} are so called compliance constants and the c_{ijkl} stiffness constants. Because not all components are independent one can reduce the tensor equation (4.26) to a lower dimensionality. Our crystals of linear polymers show highly anisotropic properties, because of different bond types along and perpendicular to the chain axis. Since we don't want to describe the covalent bond along the wire axis, we consider one chain as infinitely rigid. Then there are 2 qualitatively different types of stress possible, namely normal stress and shear stress as sketched in Fig. 4.10 and Fig. 4.11. For simplicity we limit ourselves to the case of only 1 wire per 2D unit cell.

Normal stress

In order to find the change in energy we need the energy per unit cell as a function of the lattice parameters $a_1=a_0+x, a_2=a_0$,

$$\Phi_{UC}\left(a_0+x,a_0;c,\sigma,\epsilon\right)\ . \tag{4.27}$$

If x is small we can approximate Φ_{UC} by

$$\Phi_{UC}\left(x\right)=\Phi_{UC}\left(0\right)+\frac{1}{2}\frac{\partial^2\Phi_{UC}}{\partial x^2}\bigg|_0 x^2\ .$$

The work done by the stress is

$$\left(ac\right)\sigma x=\Phi_{UC}\left(x\right)-\Phi_{UC}\left(0\right)=\frac{1}{2}\frac{\partial^2\Phi_{UC}}{\partial x^2}\bigg|_0 x^2\ ,$$

from which follows that

$$\sigma=\frac{1}{2ac}\frac{\partial^2\Phi_{UC}}{\partial x^2}\bigg|_0 x=\frac{1}{2c}\frac{\partial^2\Phi_{UC}}{\partial x^2}\bigg|_0\frac{x}{a}=\frac{1}{2c}\frac{\partial^2\Phi_{UC}}{\partial x^2}\bigg|_0\epsilon\ ,$$

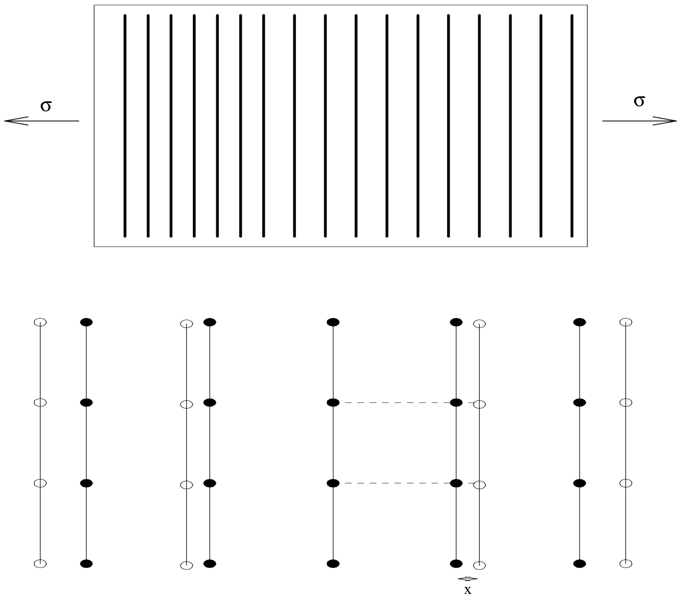

Figure 4.10: Above: a macroscopic crystalline piece of matter under normal stress $\sigma_{11} = \sigma_{xx}$. Below: while the lattice constants in y, z direction remain almost unchanged, the lattice constant in x direction changes.

and the Young modulus is given by

$$\frac{\sigma}{\frac{x}{a}} = \frac{1}{2c} \left. \frac{\partial^2 \Phi_{UC}}{\partial x^2} \right|_0 = \frac{1}{2a^2 c} \left(a^2 \left. \frac{\partial^2 \Phi_{UC}}{\partial x^2} \right|_0 \right) .$$

For a numerical evaluation of $\Phi_{UC}(x)$ we need to take into account the fact that the symmetry of the lattice is reduced by the distortion sketched in Fig. 4.10.

Shear stress

In order to find the change in energy when shear stress is applied, we need the energy per unit cell of a system where every wire is displaced by z with respect to its neighbor in x direction, while the $2D$ x, y lattice positions are unchanged and determined by the lattice constant $a_1 = a_2 = a_0$

$$\Phi_{UC}(z, a_0; c, \sigma, \epsilon) \ . \tag{4.28}$$

If z is small we can approximate Φ_{UC} by

$$\Phi_{UC}(z) = \Phi_{UC}(0) + \frac{1}{2} \left. \frac{\partial^2 \Phi_{UC}}{\partial x^2} \right|_0 z^2 \ .$$

The work done by the stress is

$$(ac)\,\sigma z = \Phi_{UC}(z) - \Phi_{UC}(0) = \frac{1}{2} \left. \frac{\partial^2 \Phi_{UC}}{\partial x^2} \right|_0 z^2 \ ,$$

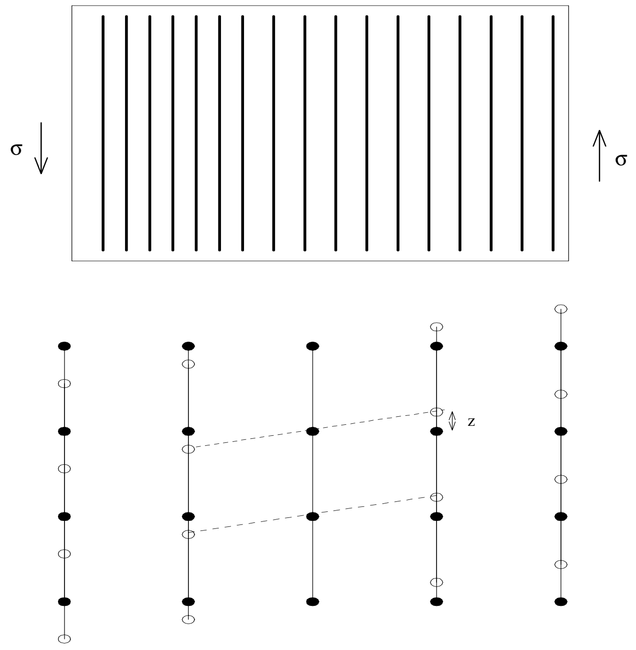

Figure 4.11: Above: a macroscopic crystalline piece of matter under shear stress $\sigma_{13} = \sigma_{xz}$ Below: while the lattice constants in the x, y direction remain almost unchanged, the chains are displaced along the axis by z.

from which it follows that

$$\sigma = \frac{1}{2ac} \left. \frac{\partial^2 \Phi_{UC}}{\partial x^2} \right|_0 z = \frac{1}{2c} \left. \frac{\partial^2 \Phi_{UC}}{\partial x^2} \right|_0 \frac{z}{a} = \frac{1}{2c} \left. \frac{\partial^2 \Phi_{UC}}{\partial x^2} \right|_0 \epsilon \ ,$$

and the Shear modulus is given by

$$\frac{\sigma}{\frac{z}{a}} = \frac{1}{2c} \left. \frac{\partial^2 \Phi_{UC}}{\partial x^2} \right|_0 = \frac{1}{2c^3} \left(c^2 \left. \frac{\partial^2 \Phi_{UC}}{\partial x^2} \right|_0 \right) \ .$$

For a numerical evaluation of $\Phi_{UC}(z)$ we need to take into account the fact that the symmetry of the lattice is reduced by the distortion sketched in Fig. 4.11 (here the array of wires is not periodic anymore for general z).

4.3.4 Vibrational spectrum:

One atom per unit cell

To start with an easy example we first consider just one atom per unit cell, so that the coordinates of all wires are given by.

$$\mathbf{x} = (\ldots, \mathbf{x}_j, \ldots) = (\ldots, x_{jm}, \ldots) \ \text{with} \ j = (j_1, j_2) \in \mathbb{Z}^2, m \in \{1, 2, 3\}$$

and the displacements from the equilibrium positions by

$$\mathbf{u} = \mathbf{x} - \mathbf{x}_0 = (\ldots, u_{jm}, \ldots) \ \text{with} \ j = (j_1, j_2) \in \mathbb{Z}^2, m \in \{1, 2, 3\} \ ,$$

where $j = (j_1, j_2)$ labels the cell and m the 3 Cartesian coordinates. The potential energy for small derivations from the equilibrium is then given by (in harmonic approximation)

$$V(\mathbf{x}) = V(\mathbf{x}_0) + \frac{1}{2}\sum_{jm}\sum_{j'm'} \left.\frac{\partial^2 V}{\partial u_{jm}\partial u_{j'm'}}\right|_{\mathbf{x}_0} u_{jm}u_{j'm'} \ .$$

The classical equation of motion,

$$M_\alpha \ddot{\mathbf{u}}(t) = -\frac{d}{d\mathbf{u}} V(\mathbf{u}) \ ,$$

therefore reads as

$$M_\alpha \ddot{u}_{jm}(t) = -\sum_{j'm'} \left.\frac{\partial^2 V}{\partial u_{jm}\partial u_{j'm'}}\right|_{\mathbf{0}} u_{j'm'} \ .$$

For our potential the second derivatives depend only on the relative position between j and j' ,

$$D_{m,m'}(j-j') = \left.\frac{\partial^2 V}{\partial u_{jm}\partial u_{j'm'}}\right|_{\mathbf{0}} = \left.\frac{\partial^2 V}{\partial u_{j-j'm}\partial u_{0m'}}\right|_{\mathbf{0}} \ ,$$

where $D_{m,m'}(j)$ is a 3×3 matrix for every lattice translation $\mathbf{t}_j$ and

$$M_\alpha \ddot{u}_{jm}(t) = -\sum_{j'm'} D_{m,m'}(j-j')\, u_{j'm'} \ .$$

With the Ansatz $u_{jm} = e^{i\left(k\cdot u_j^0 - \omega t\right)} a_m$ we arrive at

$$\begin{aligned} \omega^2(k)\, a_m &= \sum_{m'} K_{m,m'}(k)\, a_{m'} \ , \\ K_{m,m'}(k) &= \frac{1}{M}\left(\sum_j D_{m,m'}(j)\, e^{-i\mathbf{k}\cdot\mathbf{R}_j}\right) \ . \end{aligned} \tag{4.29}$$

Evaluation of $\frac{\partial^2}{\partial u_{jm}\partial u_{j'm'}} V$ Our potential of the array of wires is just the sum of pairwise wire-wire (per unit in z direction) potentials

$$V(\ldots, \mathbf{x}_j, \ldots) = \frac{1}{2}\sum\sum_{j'\neq j''} v_{ww}(\mathbf{x}_{j'} - \mathbf{x}_{j''}) \ .$$

Therefore,

$$\begin{aligned} \frac{\partial V}{\partial u_{jm}} &= \sum_{j'', j''\neq j} \frac{\partial}{\partial x_m} v_{ww}(\mathbf{x}_j - \mathbf{x}_{j''}) \ , \\ D_{m,m'}(j-j') &= \frac{\partial^2 V}{\partial u_{jm}\partial u_{j'm'}} = \left\{ \begin{array}{ll} j = j' & \sum_{j'', j''\neq j} \frac{\partial^2}{\partial x_m \partial x_{m'}} v_{ww}(\mathbf{x}_j - \mathbf{x}_{j''}) \\ j \neq j' & -\frac{\partial^2}{\partial x_m \partial x_{m'}} v_{ww}(\mathbf{x}_j - \mathbf{x}_{j'}) \end{array} \right. \ . \end{aligned}$$

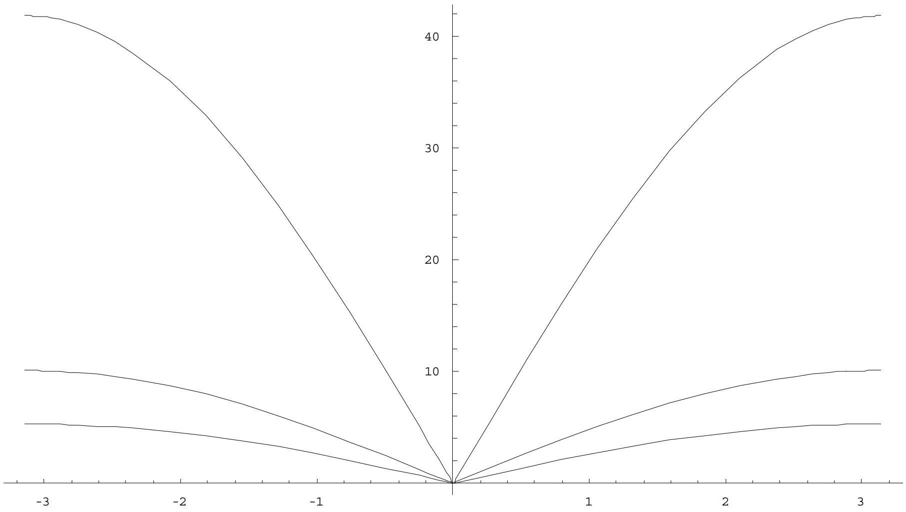

Figure 4.12: Dispersion relation for a quadratic array of wires in the symmetry direction $\mathbf{k}_0 = (1,0)$, the different $\omega_j(k)$ belong to physically different modes of the system.

Evaluating the Fourier transform we get

$$\sum_j D_{m,m'}(j)\, e^{-i\mathbf{k}\cdot\mathbf{R}_j} = \sum_{j\neq 0} \frac{\partial^2}{\partial x_m \partial x_{m'}} v_{ww}(\mathbf{x}_0 - \mathbf{x}_j) \left(1 - e^{-i\mathbf{k}\cdot\mathbf{R}_j}\right).$$

Therefore it is enough to evaluate the derivatives of the wire-wire potential v_{ww} at the distance of the first few $j = (j_1, j_2) = (0,0)$ neighboring wires.

Dispersion relation The 3×3 eigenvalue problem (4.29) with the 2D propagation vector $\mathbf{k} = (k_1, k_2, 0)$, restricted to the first reciprocal unit cell $\mathbf{k} = (k_1, k_2) \in \left[-\frac{\pi}{a}, \frac{\pi}{a}\right] \times \left[-\frac{\pi}{a}, \frac{\pi}{a}\right]$, and the polarization vector $\mathbf{a} = (a_x, a_y, a_z)$ reads in short matrix notation:

$$\underline{K}(\mathbf{k})\,\mathbf{a} = \omega^2(\mathbf{k})\,\mathbf{a} \tag{4.30}$$

(4.30) has a 3 eigenvectors, written as pairs of (eigenvalues,eigenvectors),

$$(\omega_1(\mathbf{k}), \mathbf{a}_1), (\omega_2(\mathbf{k}), \mathbf{a}_2), (\omega_3(\mathbf{k}), \mathbf{a}_3)\ . \tag{4.31}$$

For a given direction $\mathbf{k}$ one can plot $\omega_j(\mathbf{k}(\mathbf{s})), \mathbf{k}(\mathbf{s}) = s\mathbf{k}_0$ as a function of s. If we take the symmetry direction $\mathbf{k}_0 = (1,0)$, the results are plotted in (4.12). If we number the frequencies according to $\omega_1(\mathbf{k}) \leq \omega_2(\mathbf{k}) \leq \omega_3(\mathbf{k})$, then the polarization vector determines the type of elastic wave in the crystal:

$$\begin{aligned} \mathbf{a}_1 &= (0,1,0) \text{ normal distance between wires not changed} && (4.32)\\ \mathbf{a}_2 &= (0,0,1) \text{ normal distance between wires not changed} \\ \mathbf{a}_3 &= (1,0,0) \text{ normal distance between wires changed} \end{aligned}$$

The different energies involved in these distortions (see (4.2.5)) explain the different frequencies of the modes.

More than one atom per unit cell

There are a few changes for more than one atom per unit cell that have to be taken into account. The new index $\alpha \in \{1, \ldots, N_{atom}\}$ labels the nonequivalent atoms in one unit cell,

$$\mathbf{x} = (\ldots, \mathbf{x}_{j\alpha}, \ldots) = (\ldots, x_{j\alpha m}, \ldots) \text{ with } j = (j_1, j_2) \in \mathbb{Z}^2, \alpha \in \{1, \ldots, N_{atom}\}, m \in \{1, 2, 3\} \ ,$$

and the displacements from the equilibrium positions are determined by

$$\mathbf{u} = \mathbf{x} - \mathbf{x}_0 = (\ldots, u_{j\alpha m}, \ldots) \text{ with } j = (j_1, j_2) \in \mathbb{Z}^2, \alpha \in \{1, \ldots, N_{atom}\}, m \in \{1, 2, 3\}$$

where $j = (j_1, j_2)$ labels the cell, α the bead in the cell and m the 3 Cartesian coordinates. Then the potential energy for small derivations from the equilibrium is given by

$$V(\mathbf{x}) = V(\mathbf{x}_0) + \frac{1}{2} \sum_{j\alpha m} \sum_{j'\alpha' m'} \frac{\partial^2}{\partial u_{j\alpha m} \partial u_{j'\alpha' m'}} V|_{\mathbf{x}_0} u_{j\alpha m} u_{j'\alpha' m'} \ .$$

The classical equation of motion

$$M_\alpha \ddot{\mathbf{u}}(t) = -\frac{d}{d\mathbf{u}} V(\mathbf{u})$$

therefore reads with this notation

$$M_\alpha \ddot{u}_{j\alpha m}(t) = -\sum_{j'\alpha' m'} \frac{\partial^2}{\partial u_{j\alpha m} \partial u_{j'\alpha' m'}} V|_{\mathbf{0}} u_{j'\alpha' m'} \ .$$

For our potential the second derivatives depend only on the relative position between j and j'

$$D_{\alpha m, \alpha' m'}(j - j') = \frac{\partial^2}{\partial u_{j\alpha m} \partial u_{j'\alpha' m'}} V|_{\mathbf{0}} = \frac{\partial^2}{\partial u_{j-j'\alpha m} \partial u_{0\alpha' m'}} V|_{\mathbf{0}} \ ,$$

and therefore

$$M_\alpha \ddot{u}_{j\alpha m}(t) = -\sum_{j'\alpha' m'} D_{\alpha m, \alpha' m'}(j - j') u_{j'\alpha' m'} \ .$$

With the Ansatz

$$u_{j\alpha m} = e^{i\left(k \cdot u^0_{j\alpha} - \omega t\right)} a_{\alpha m} = e^{i\left(k \cdot u^0_{j\alpha} - \omega t\right)} \frac{1}{\sqrt{M_\alpha}} \overline{a}_{\alpha m} \ ,$$

in order to keep the symmetry in α, α' we have to scale the amplitude by the square root of the mass M_α, we get:

$$\begin{aligned} \omega^2(k) \overline{a}_{\alpha m} &= \sum_{\alpha' m'} K_{\alpha m, \alpha' m'}(k) \overline{a}_{\alpha' m'} \ , \qquad (4.33) \\ K_{\alpha m, \alpha' m'}(k) &= \frac{1}{\sqrt{M_\alpha M_{\alpha'}}} \left(\left(\sum_j D_{\alpha m, \alpha' m'}(j) e^{-ik \cdot R_j} \right) e^{-ik \cdot \left(x^0_\alpha - x^0_{\alpha'}\right)} \right) \ . \end{aligned}$$

Evaluation of $\frac{\partial^2}{\partial u_{j\alpha m}\partial u_{j'\alpha' m'}}V$

Our potential of an array of wires is just the sum of pairwise wire-wire (per unit in z direction) potentials,

$$V\left(\ldots,\mathbf{x}_{j\alpha},\ldots\right)=\frac{1}{2}\sum\sum_{j'\alpha'\neq j''\alpha''}v_{ww}\left(\mathbf{x}_{j'\alpha'}-\mathbf{x}_{j''\alpha''}\right)\ .$$

Therefore

$$\begin{aligned}\frac{\partial V}{\partial u_{j\alpha m}} &= \sum_{(j'',\alpha'')\neq(j,\alpha)}\frac{\partial}{\partial x_m}v_{ww}\left(\mathbf{x}_{j\alpha}-\mathbf{x}_{j''\alpha''}\right)\ ,\\ \frac{\partial^2 V}{\partial u_{j\alpha m}\partial u_{j'\alpha' m'}} &= \begin{cases}(j,\alpha)=(j',\alpha') & \sum_{(j'',\alpha'')\neq(j,\alpha)}\frac{\partial^2}{\partial x_m\partial x_{m'}}v_{ww}\left(\mathbf{x}_{j\alpha}-\mathbf{x}_{j''\alpha''}\right)\\ (j,\alpha)\neq(j',\alpha') & -\frac{\partial^2}{\partial x_m\partial x_{m'}}v_{ww}\left(\mathbf{x}_{j\alpha}-\mathbf{x}_{j'\alpha'}\right)\end{cases}\ .\end{aligned}$$

Evaluating the Fourier transform we get

$$\sum_j D_{\alpha m,\alpha' m'}\left(j\right)e^{-i\mathbf{k}\cdot\mathbf{R}_j}=$$

$$=\begin{cases}\alpha=\alpha': & \sum_{j\neq 0}\frac{\partial^2}{\partial x_m\partial x_{m'}}v_{ww}\left(\mathbf{x}_{j\alpha}-\mathbf{x}_{0\alpha}\right)\left(1-e^{-i\mathbf{k}\cdot\mathbf{R}_j}\right)+\sum_{\alpha''\neq\alpha}\sum_j\frac{\partial^2}{\partial x_m\partial x_{m'}}v_{ww}\left(\mathbf{x}_{j\alpha''}-\mathbf{x}_{0\alpha}\right)\\ \alpha\neq\alpha': & -\sum_j\frac{\partial^2}{\partial x_m\partial x_{m'}}v_{ww}\left(\mathbf{x}_{j\alpha'}-\mathbf{x}_{0\alpha}\right)e^{-i\mathbf{k}\cdot\mathbf{R}_j}\end{cases}\ .$$

Thus it is enough to evaluate the derivatives of the wire-wire potential v_{ww}. The solution of the eigenvalue problem in (4.33) leads to the eigenvalues $\omega^2\left(k\right)$ and the corresponding polarization vectors $a_{\alpha m}$.

Dispersion relation for two atoms per unit cell The 6×6 eigenvalue problem for a quadratic lattice with 2 atoms per unit cell (with propagation vector $\mathbf{k}=\left(k_1,k_2,0\right)$, restricted to the first reciprocal unit cell, $\mathbf{k}=\left(k_1,k_2\right)\in\left[-\frac{\pi}{a},\frac{\pi}{a}\right]\times\left[-\frac{\pi}{a},\frac{\pi}{a}\right]$, the index for the two non-equivalent atom types $\alpha\in\{1,2\}$ and the polarization vector $\mathbf{a}=\left(\mathbf{a}_1,\mathbf{a}_2\right)=\left(a_{1x},a_{1y},a_{1z},a_{2x},a_{2y},a_{2z}\right)$), is written as

$$\begin{aligned}\omega^2\left(\mathbf{k}\right)a_{\alpha m} &= \sum_{\alpha' m'}K_{\alpha m,\alpha' m'}\left(\mathbf{k}\right)a_{\alpha' m'}\ ,\\ \underline{K}\left(\mathbf{k}\right)\mathbf{a} &= \omega^2\left(\mathbf{k}\right)\mathbf{a}\ .\end{aligned}$$

The 6 solutions, written as pairs of (eigenvalues,eigenvectors), are

$$\left(\omega_1\left(\mathbf{k}\right),\mathbf{a}_1\right),\ldots,\left(\omega_6\left(\mathbf{k}\right),\mathbf{a}_6\right)\tag{4.34}$$

For a certain direction $\mathbf{k}_0$ one can plot $\omega_j\left(\mathbf{k}(\mathbf{s})\right),\mathbf{k}(\mathbf{s})=s\mathbf{k}_0$ as a function of s. For the symmetry direction $\mathbf{k}_0=\left(1,0\right)$ the dispersion relation is plotted in Fig.4.13. If we number the frequencies according to $\omega_1\left(\mathbf{k}\right)\leq\ldots\leq\omega_6\left(\mathbf{k}\right)$ then we have 3 acoustic and 3 optical modes with different physical meaning as explained before in (4.32).

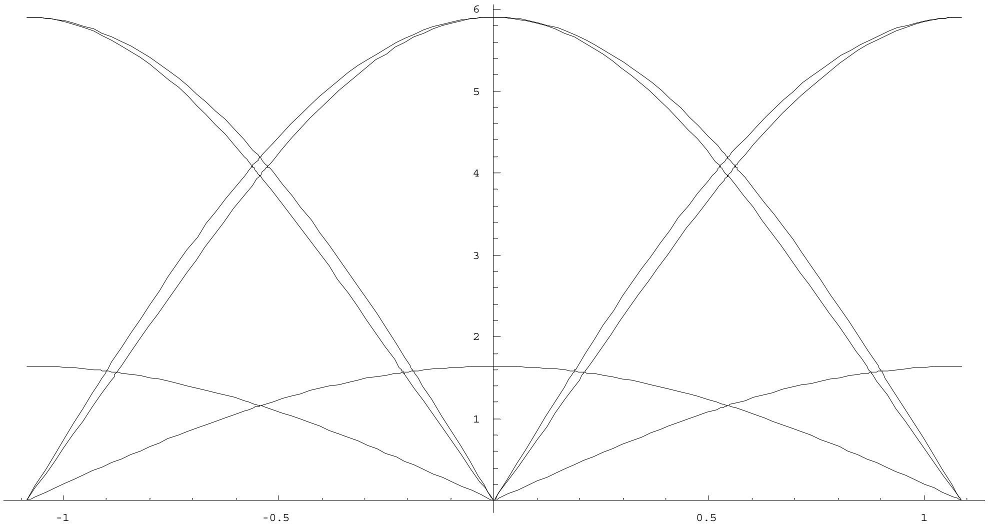

Figure 4.13: Dispersion relation for a quadratic lattice with 2 atoms per unit cell of wires in the symmetry direction $\mathbf{k}_0 = (1,0)$ and the different $\omega_j(k)$ belong to physically different modes of the system.

Thermodynamics

The different energy regions of the elastic waves should be visible in a thermodynamical study of the specific heat. But the situation is complicated by further degrees of freedom for the physical system (e.g. rotations of chains around their axis) and the low stability of the organic crystal.

4.3.5 Large amplitude slipping and plastic flow

An interesting but theoretically difficult property to access is the reaction to normal stress applied parallel to the chain axis. The dominant mechanism for the final break of the material is not the breaking of the covalent intrachain bonds (which are very stable) but is related to the fact that all chains are long (many beads) on atomic scales, but short compared to the macroscopic dimension of the specimen. Wires will slip against each other when normal stress is applied, see Fig. 4.14, the specimen tears without breaking of covalent bonds.

In order to estimate the stress necessary to tear the polymer crystal in this way we have the situation displayed in (Fig. 4.15) in mind. One wire is attached (for example over other wires) to a force which pulls it upwards, while its neighboring wires do not extent as far to the upper boundary and are not influenced by this external force. If we calculate the energy as a function of z for this situation, V_{UC}, then the size of the energy barrier mainly determines the force necessary to be applied:

$$\begin{aligned} V_{UC}\left(z_{\max}\right) - V_{UC}\left(z_0\right) &= \Delta V \\ F\frac{c}{2} &\approx \Delta V, \sigma \approx \frac{2}{a^2 c}\Delta V \end{aligned}$$

In order to obtain numerical values one only needs an estimation of the Lennard Jones parameter

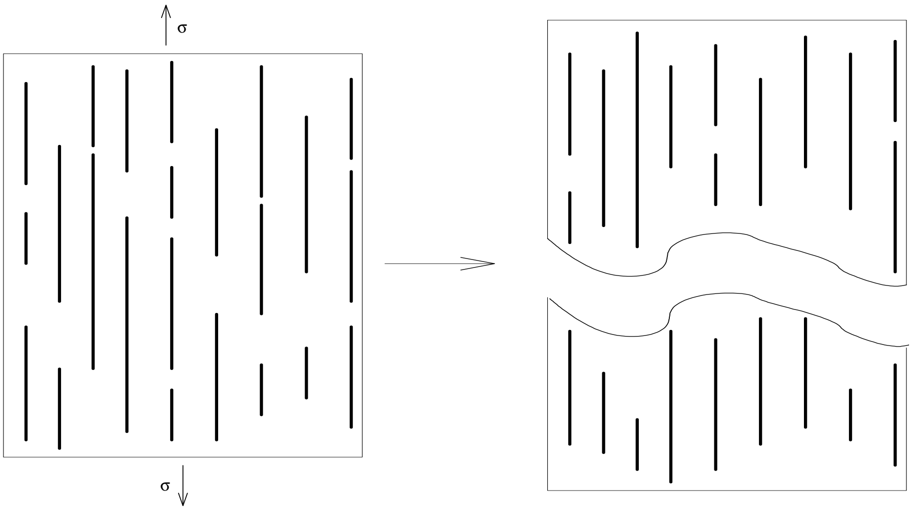

Figure 4.14: When normal stress parallel to the wire axis is applied, wires slip against each other and the specimen tears without a break of covalent bonds.

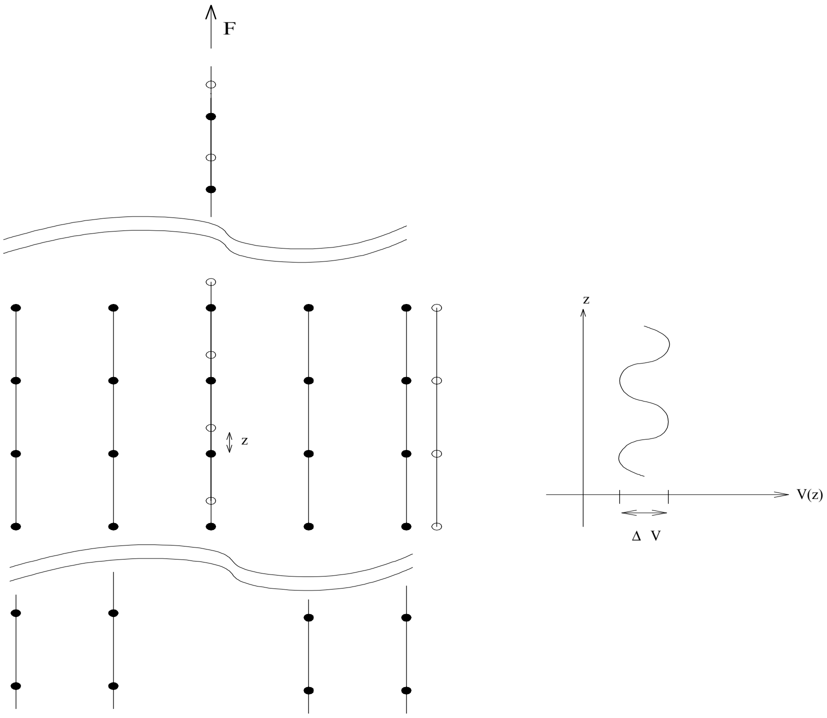

Figure 4.15: One wire is attached to the upper force which pulls it up, while its neighboring wires remain unchanged.

and data of the crystal structure.

4.4 Concluding remarks and limits of the model

The model treats the dispersion interaction energy between two chains as the sum of pairwise monomer-monomer interaction energies, which of course is only a rough estimate of the physical situation, since the dispersion interaction between two long molecules is not just the sum of the dispersion interactions between its constituent monomers. The covalent bond between the monomers inside a chain changes the electronic structure and therefore the dispersion interaction completely. In this part detailed numerical numbers are not given, because one needs the respective bead-bead Lennard Jones parameters. But values for Polyacetylene show the right order of magnitude of the results.

Part II

The Full-potential Korringa-Kohn-Rostoker (KKR) method

Chapter 5

Shape functions in the KKR method

5.1 Lower dimensional examples

5.1.1 A 1D example

Although a 1D example can only contain rudiments of the situation in 3D we try to find as many formal analogies as possible.

The most general cell in 1D is an interval $[-a, +b]$ and the characteristic function of the cell is (see Fig. 5.1)

$$\sigma : \left\{ \begin{array}{lll} \mathbb{R} & \rightarrow & \mathbb{R} \\ x & \mapsto & \sigma\left(x\right) = \Theta_{[-a,b]}(x) = \left\{ \begin{array}{ll} 1 & x \in [-a, +b] \\ 0 & x \notin [-a, +b] \end{array} \right. \end{array} \right. .$$

We define a radial coordinate and a (discrete) angle

$$x = |x| \operatorname{sgn}\left(x\right) = r\ s \text{ with } r \in \mathbb{R}_0^+, s \in \{-1, +1\}$$

The unit sphere in 1D is

$$S_0 = \{-1, +1\}$$

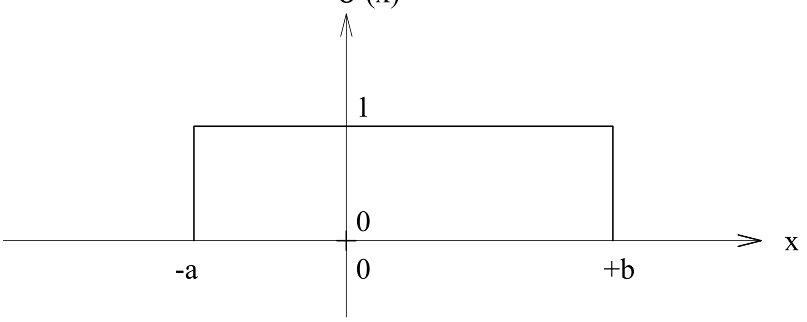

Figure 5.1: The cell in 1D is an intervall $[-a, +b]$, with positive real constants a, b.

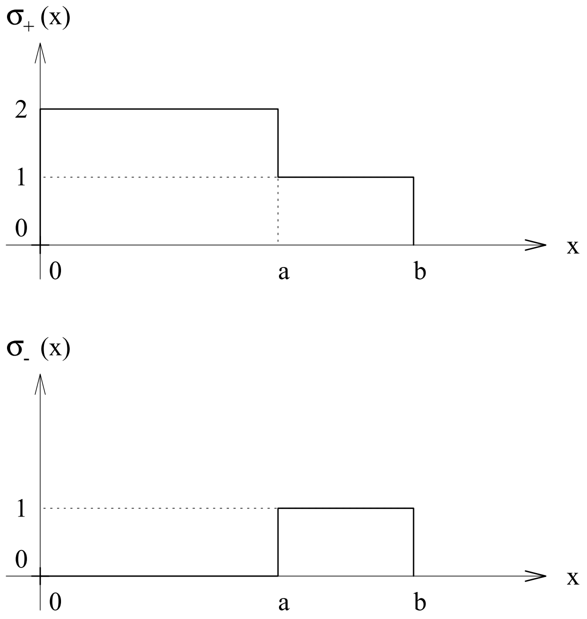

Figure 5.2: Shape functions $\sigma_{+}\left(r\right), \sigma_{-}\left(r\right)$, times $\sqrt{2}$ for 0<a<b.

with the orthonormal system $\{Y_{+}, Y_{-}\}$ on the *sphere in 1D* (the analogy of the spherical harmonics)

$$Y_{+}:\left\{\begin{array}{ccc} S_0 & \rightarrow & \mathbb{C} \\ s & \mapsto & \frac{1}{\sqrt{2}} \end{array}\right., Y_{-}:\left\{\begin{array}{ccc} S_0 & \rightarrow & \mathbb{C} \\ s & \mapsto & \frac{1}{\sqrt{2}} sgn(s) \end{array}\right. .$$

To expand the characteristic function of the cell we get

$$\sigma\left(x\right)=\sigma\left(r,s\right)=\sigma_{+}\left(r\right)Y_{+}\left(s\right)+\sigma_{-}\left(r\right)Y_{-}\left(s\right)$$

with

$$\begin{aligned} \sigma_{+}\left(r\right) &= \int_{S_0}\left(\sigma\left(x\right)Y_{+}^{*}\left(s\right)\right)ds=\sigma\left(r,s=1\right)Y_{+}\left(1\right)+\sigma\left(r,s=-1\right)Y_{+}\left(-1\right)= \\ &= \frac{1}{\sqrt{2}}\left[\Theta_{[0,b]}\left(r\right)+\Theta_{[0,a]}\left(r\right)\right]=\frac{1}{\sqrt{2}}\left\{\begin{array}{ll} 2 & r<\min\left(a,b\right) \\ 1 & \min\left(a,b\right)<r<\max(a,b) \\ 0 & r>\max\left(a,b\right) \end{array}\right. \end{aligned}$$

and

$$\begin{aligned} \sigma_{-}\left(r\right) &= \int_{S_0}\left(\sigma\left(x\right)Y_{-}^{*}\left(s\right)\right)ds=\sigma\left(r,s=1\right)Y_{-}\left(1\right)+\sigma\left(r,s=-1\right)Y_{-}\left(-1\right)= \\ &= \frac{1}{\sqrt{2}}\left[\Theta_{[0,b]}\left(r\right)-\Theta_{[0,a]}\left(r\right)\right]=\frac{1}{\sqrt{2}}\left\{\begin{array}{ll} 0 & r<\min\left(a,b\right) \\ sgn(b-a) & \min\left(a,b\right)<r<\max(a,b) \\ 0 & r>\max\left(a,b\right) \end{array}\right. \end{aligned}$$

Plots of $\sigma_{+}\left(r\right)$ and $\sigma_{-}\left(r\right)$ are shown in Fig. 5.2. There are two critical radii $r_{C1}=r_{MT}=a$ and $r_{C2}=r_{BS}=b$, all other important concepts do not have an analogy in 1D.

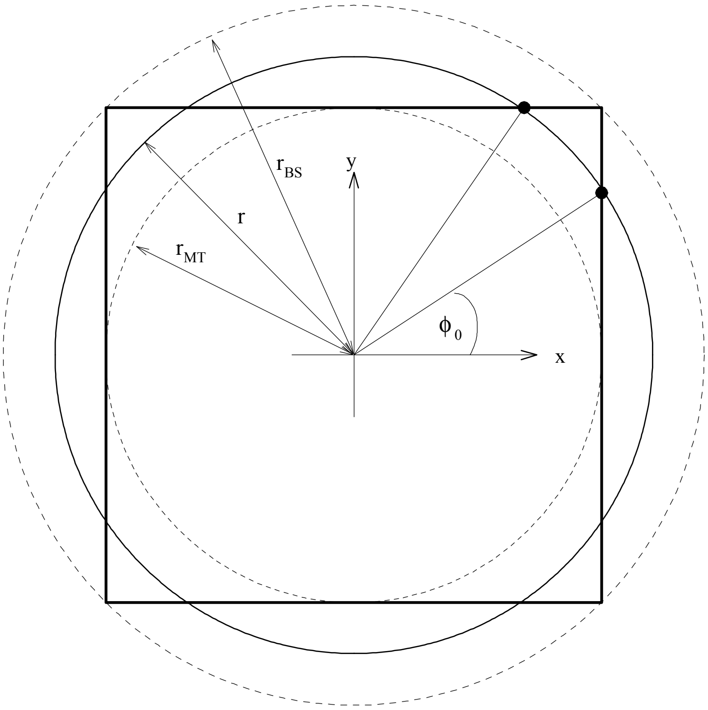

Figure 5.3: A quadratic cell with inscribed MT radius r_{MT} a general radius r and the bounding sphere radius r_{BS} .

5.1.2 A 2D example

Because a 1D model does not contain the essential features, we choose a 2D quadratic cell to present the other main ideas. We try to find as many analogies as possible to the 3D case, in which we are really interested later on (we fix the lattice parameter by $a = 1$). We define 2D polar coordinates by

$$\mathbf{x} = r \begin{pmatrix} \cos\varphi \\ \sin\varphi \end{pmatrix} \quad \text{with } r \in \mathbb{R}_0^+, \varphi \in [0, 2\pi[\ .$$

The shape function $\sigma(\mathbf{x})$ is 1 inside the quadratic unit cell, 0 outside. The orthonormal system for the angular integration is chosen as

$$y_m(\varphi) = \frac{1}{\sqrt{2\pi}} e^{im\varphi}, \ m \in \mathbb{Z} \ .$$

If we consider σ as a function of the angle φ for given radius r we get a 2π periodic function $\sigma(\varphi; r)$, which is either 0 or 1. We have to define 2 **critical radii** where the φ-region of nonzero shape function changes abruptly.

$$r_{C1} = r_{MT} = \frac{1}{2} \ ,$$
$$r_{C2} = r_{BS} = \frac{1}{\sqrt{2}} \ .$$

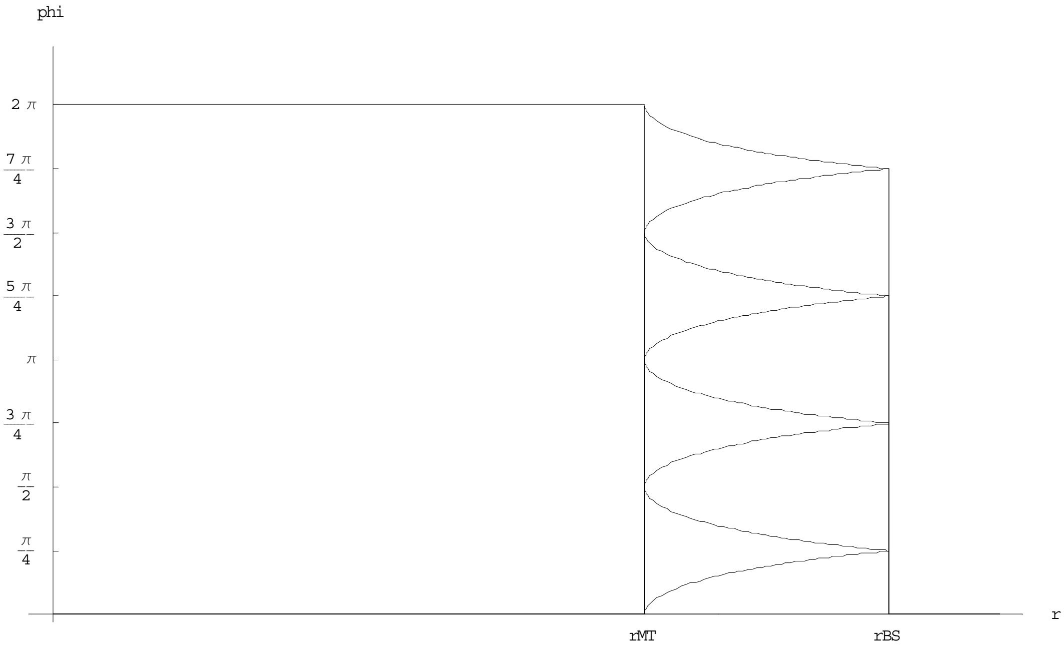

Figure 5.4: The region in the $(r,\varphi)-$plane where the shape function fulfills $\sigma(r,\varphi)=1$ and the two critical radii r_{MT} and r_{BS}.

For $0\le r\le r_{MT}$ the φ-region is the full interval $[0,2\pi]$, while for $r\ge r_{BS}$ the φ-region is the empty set $\emptyset$, between $r_{MT}\le r\le r_{BS}$ the φ-region is a union of disjunct intervals

$$\left[\varphi_0,\frac{\pi}{2}-\varphi_0\right]\cup\left[\frac{\pi}{2}+\varphi_0,\frac{2\pi}{2}-\varphi_0\right]\cup\left[\frac{2\pi}{2}+\varphi_0,\frac{3\pi}{2}-\varphi_0\right]\cup\left[\frac{3\pi}{2}+\varphi_0,\frac{4\pi}{2}-\varphi_0\right]$$

and $\sigma\left(r;\varphi\right)$ is a discontinuous multiple step function, see (Fig. 5.5). The expansion in the $\{y_m(\varphi)\}$ system is nothing else but the complex Fourier series of this periodic function,

$$\sigma\left(\mathbf{x}\right)=\sigma\left(r,\varphi\right)\sim\sum_{m}\sigma_m\left(r\right)y_m(\varphi)=\sum_{m=-\infty}^{\infty}\sigma_m\left(r\right)y_m(\varphi)$$

with the shape functions as expansion coefficients determined by

$$\sigma_m\left(r\right)=\int\limits_0^{2\pi}d\varphi\;\sigma\left(r,\varphi\right)y_m^*(\varphi)\ . \tag{5.1}$$

This integration can be done **analytically**. Looking at (Fig. 5.3) we see that for $r_{MT}<r<r_{BS}$ there are 8 **critical angles**

$$\varphi=0\pm\varphi_0,\frac{\pi}{2}\pm\varphi_0,\pi\pm\varphi_0,\frac{3\pi}{2}\pm\varphi_0\quad\text{with }\varphi_0\left(r\right)=\arccos\left(\frac{1}{2r}\right)\ ,$$

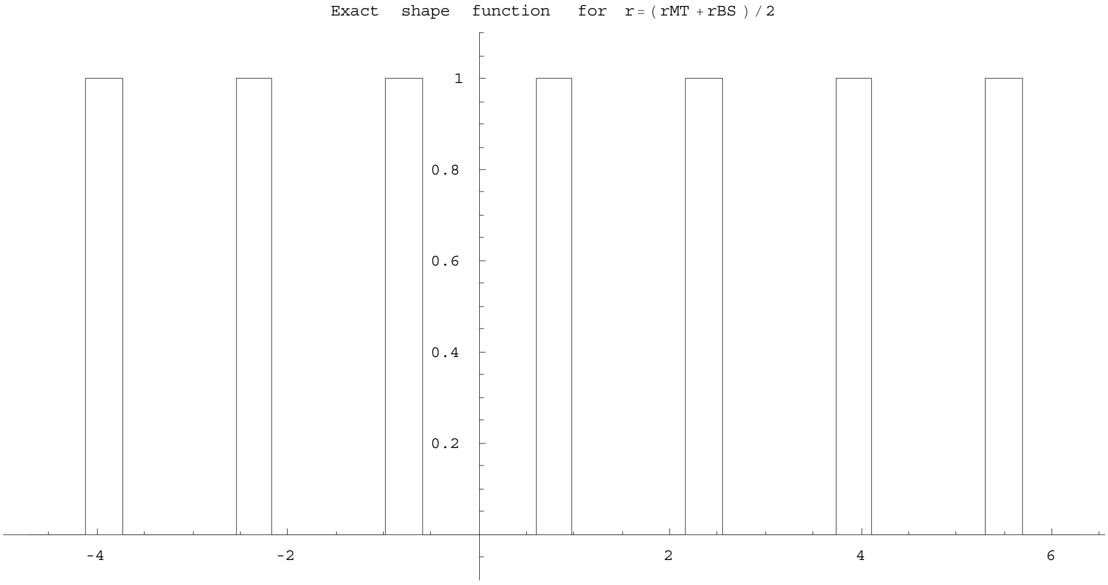

Figure 5.5: The exact shape function $\sigma(r;\varphi)$ for $r = (r_{MT} + r_{BS})/2$ as a periodic multiple step function with respect to φ. For all $r_{MT} < r < r_{BS}$ the form is principally the same.

and therefore (5.1) can be simplified to

$$\begin{aligned}\sigma_m(r) &= \sum_{j=0}^{3} \int_0^{\frac{\pi}{2}} d\varphi \left(\sigma(r,\varphi) \frac{1}{\sqrt{2\pi}} e^{-im\left(\varphi + j\frac{\pi}{2}\right)} \right) = \\ &= \sum_{j=0}^{3} \left(e^{-im\frac{\pi}{2}}\right)^j \int_0^{\frac{\pi}{2}} d\varphi \left(\sigma(r,\varphi) \frac{1}{\sqrt{2\pi}} e^{-im\varphi} \right) .\end{aligned}$$

Hence we see that only for $m \in 4\mathbb{Z}$ the result can be different from zero,

$$\sigma_m(r) = 4 \int_0^{\frac{\pi}{2}} d\varphi \left(\sigma(r,\varphi) \frac{1}{\sqrt{2\pi}} e^{-im\varphi} \right) = \frac{4}{\sqrt{2\pi}} \int_{\varphi_0}^{\frac{\pi}{2}-\varphi_0} d\varphi\, e^{-im\varphi} , \tag{5.2}$$

while for

$$m \notin 4\mathbb{Z} \quad \sigma_m(r) \equiv 0.$$

If we evaluate (5.2) we get the final result for $m = 0$

$$\sigma_0(r) = \begin{cases} \sqrt{2\pi} & r < r_{MT} \\ \sqrt{2\pi}\left(1 - \frac{4}{\pi}\varphi_0(r)\right) & r_{MT} < r < r_{BS} \\ 0 & r > r_{BS} \end{cases} \tag{5.3}$$

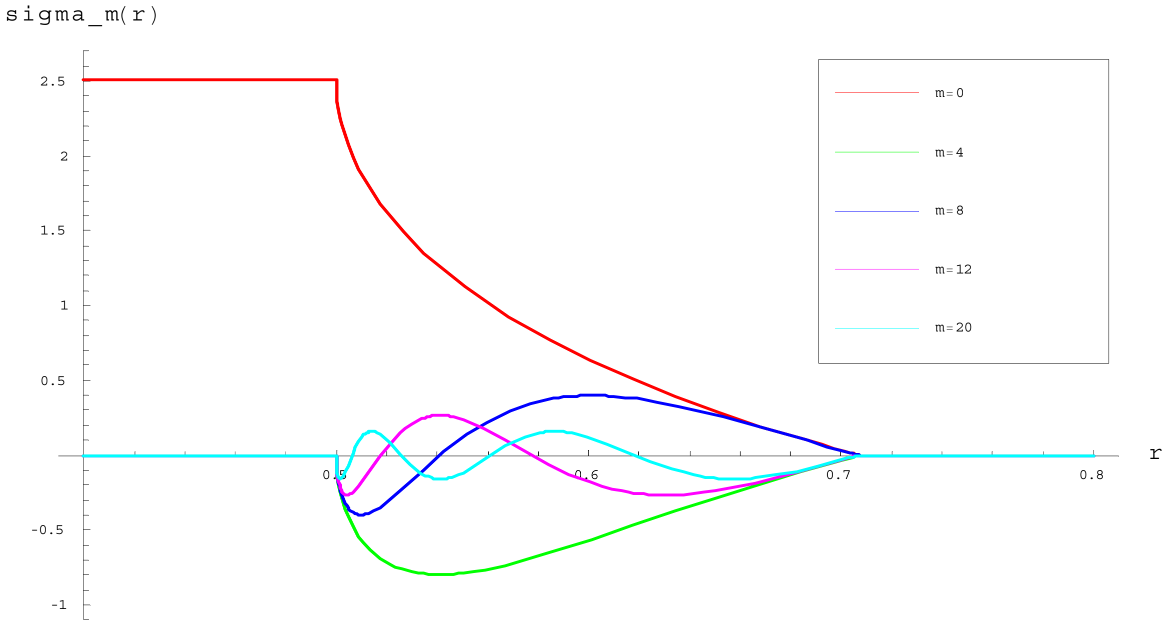

Figure 5.6: Shape functions $\sigma_m(r)$ for a quadratic cell. The shape functions are continuous but not smooth at the critical radii r_{MT}, r_{BS}.

and for $m \in 4\mathbb{Z}\setminus\{0\}$

$$\sigma_m(r) = \begin{cases} 0 & r < r_{MT} \\ \sqrt{2\pi}\left(\frac{-4}{m\pi}\sin\left(m\varphi_0(r)\right)\right) & r_{MT} < r < r_{BS} \\ 0 & r > r_{BS} \end{cases} . \tag{5.4}$$

Fig. 5.6 shows the shape functions for a quadratic cell. It is obvious that with higher m the $\sigma_m(r)$ have more radial nodes.

An important numerical question is the quality of the approximation of the exact shape function (Fig. 5.5) with only a finite number of $\sigma_m(r)$. We define $\sigma^M(r,\varphi)$ as the expansion up to $|m| \leq M$.

$$\sigma^M(r,\varphi) = \sum_{m=-M}^{M} \sigma_m(r)\, y_m(\varphi)$$

In Fig. 5.7 we plot $\sigma^M(r,\varphi)$ for a given r, with $r_{MT} < r = 0.6 < r_{BS}$ for various M. We see the slow convergence and the well known Gibbs phenomenon at the points of discontinuity. These problems are inherent to the method because the shape function $\sigma(\mathbf{x}) = \sigma(r;\varphi)$ is not a continuous function of φ. Even if we calculate the $\sigma_m(r)$ with good precision we are limited by the number of m's $|m| \leq M$, which is a serious limitation to the numerical precision also in the 3D case.

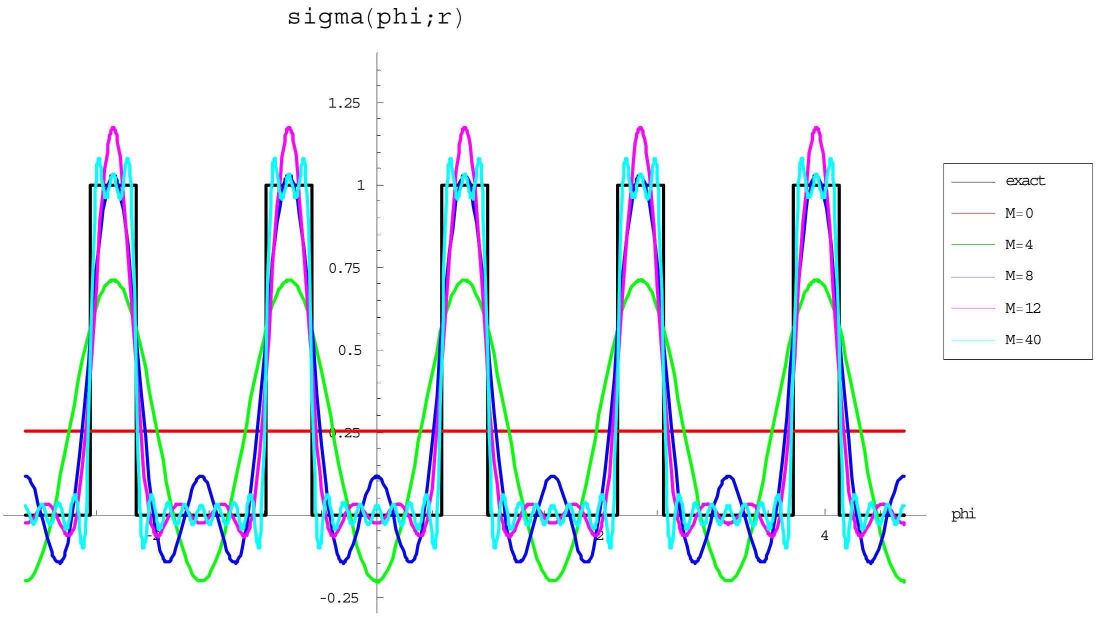

Figure 5.7: The exact shape functions $\sigma\left(\varphi;r\right)$ and the approximations $\sigma^{M}\left(\varphi;r\right)$ for given $r=0.6$.

5.2 3D Shape functions

5.2.1 The construction of shape functions in 3D

The construction of the shape functions is central to the full-potential method and therefore it is summarized here. Our approach is based on the description published in ([45]).

Let $\mathcal{V}$ be the region of the convex polyhedron containing one atom at the origin of the coordinates. Then the shape function of the region is defined as

$$\sigma\left(\mathbf{x}\right)=\begin{cases}1 & \mathbf{x}\in\mathcal{V}\\ 0 & \mathbf{x}\notin\mathcal{V}\end{cases}$$

Let $Y_L(\widehat{\mathbf{x}})=Y_{lm}(\widehat{\mathbf{x}})=C_L P_m^l(\cos\theta)e^{im\varphi}$ be the usual complex spherical harmonics. For a fixed chosen coordinate system one considers $\sigma\left(\mathbf{x}\right)$ as a function of spherical variables $\sigma\left(r;\theta,\varphi\right)$ then for every fixed r the spherical function $\sigma\left(r;\Omega\right)$ can be expanded (therefore $\sim$ instead of $=$) into spherical harmonics,

$$\sigma\left(r;\Omega\right)\sim\sum_{L}\sigma_L\left(r\right)Y_L(\Omega)=\sum_{l=0}^{\infty}\sum_{m=-l}^{l}\sigma_{lm}\left(r\right)Y_{lm}(\Omega)\ ,$$

with the shape functions as expansion coefficients determined by

$$\sigma_L\left(r\right)=\int\limits_{\Omega}d\Omega\ \left(\sigma\left(r,\Omega\right)Y_L^{*}(\Omega)\right)\ . \tag{5.5}$$

For the construction of the Voronoy polyhedron (nearest neighbor cell) we have a set of potential boundary planes, all given by their normal vector $\mathbf{R}_i$ with magnitude R_i equal to its normal distance from the origin. The polyhedron can be precisely characterized as

$$\mathbf{x} \in \mathcal{V} \Leftrightarrow \forall i \left(\mathbf{x} \cdot \mathbf{R}_i \leq R_i^2\right) \ . \tag{5.6}$$

Interception of one boundary plane of the polyhedron and a sphere

Consider one potential boundary plane $\mathbf{R}_i$ and a sphere with given radius r, the normal vector $\mathbf{R}_i$ can be split into $\mathbf{R}_i = \mathbf{R}_{i,\|} + Z_i \mathbf{e}_z$. If $\mathbf{R}_{i,\|} = \mathbf{0}$ and $\mathbf{R}_i$ therefore points in z direction we have a special case, to be considered separately. We can always rotate our coordinate system by an angle $\phi_0 = \arccos\left(\frac{X_i}{\sqrt{X_i^2+Y_i^2}}\right)$ around the z axis, so that $\mathbf{R}_{i,\|} = X_i \mathbf{e}_x$ (see right plot of Fig. 5.8). A typical situation after rotation is shown in the left plot of Fig.5.8. Now we can easily see that all points

$$\mathbf{x} = \begin{pmatrix} x & y & z \end{pmatrix} = \begin{pmatrix} r\sin\theta\cos\varphi & r\sin\theta\sin\varphi & r\cos\theta \end{pmatrix}$$

on the intersection circle (the ellipse in the left lower plot of Fig. 5.8) of the sphere and the plane have a θ value fulfilling the condition

$$\left|\frac{R_i^2 - Z_i r\cos\theta}{\sqrt{X_i^2+Y_i^2} r\sin\theta}\right| \leq 1. \tag{5.7}$$

If θ does not fulfill (5.7) there are no intersection points. For a given θ fulfilling (5.7) the plane intercepts the sphere when φ is given by

$$\begin{aligned} \text{new coord. system} \quad &: \quad \varphi_i^{(\pm)} = \pm\alpha, \alpha = \arccos\left(\frac{R_i^2 - Z_i r\cos\theta}{\sqrt{X_i^2+Y_i^2} r\sin\theta}\right) \\ \text{old coord. system} \quad &: \quad \varphi_i^{(\pm)} = \arccos\left(\frac{X_i}{\sqrt{X_i^2+Y_i^2}}\right) \pm \arccos\left(\frac{R_i^2 - Z_i r\cos\theta}{\sqrt{X_i^2+Y_i^2} r\sin\theta}\right) \ . \end{aligned}$$

If the pair (r,θ) does not fulfill (5.7) then the plane $\mathbf{R}_i$ is not involved in the construction of the polyhedron at these (r,θ) values and needs not to be considered.

Semi analytical evaluation of $\sigma_L(r)$

If one repeats the same procedure of subsection 5.2.1 for every possible boundary plane $\mathbf{R}_i$, one gets for every pair (r,θ) a set of $\left\{\varphi_i^{(\pm)}, i = 1,\ldots,N\right\}$, which can be ordered such that $0 \leq \varphi_1 \leq \ldots \leq \varphi_{2N} \leq 2\pi \leq \varphi_{2N+1} = \varphi_1 + 2\pi$. This can be used to solve the φ integral analytically

$$\sigma_L(r) = \int\limits_{\Omega} d\Omega\, \sigma(r,\Omega)\, Y_L^*(\Omega) = C_L \int\limits_0^{\pi} d\theta \left(\sin\theta P_m^l(\cos\theta)\left(\int\limits_0^{2\pi} d\varphi\sigma(r,\theta;\varphi)\, e^{-im\varphi}\right)\right) \ .$$

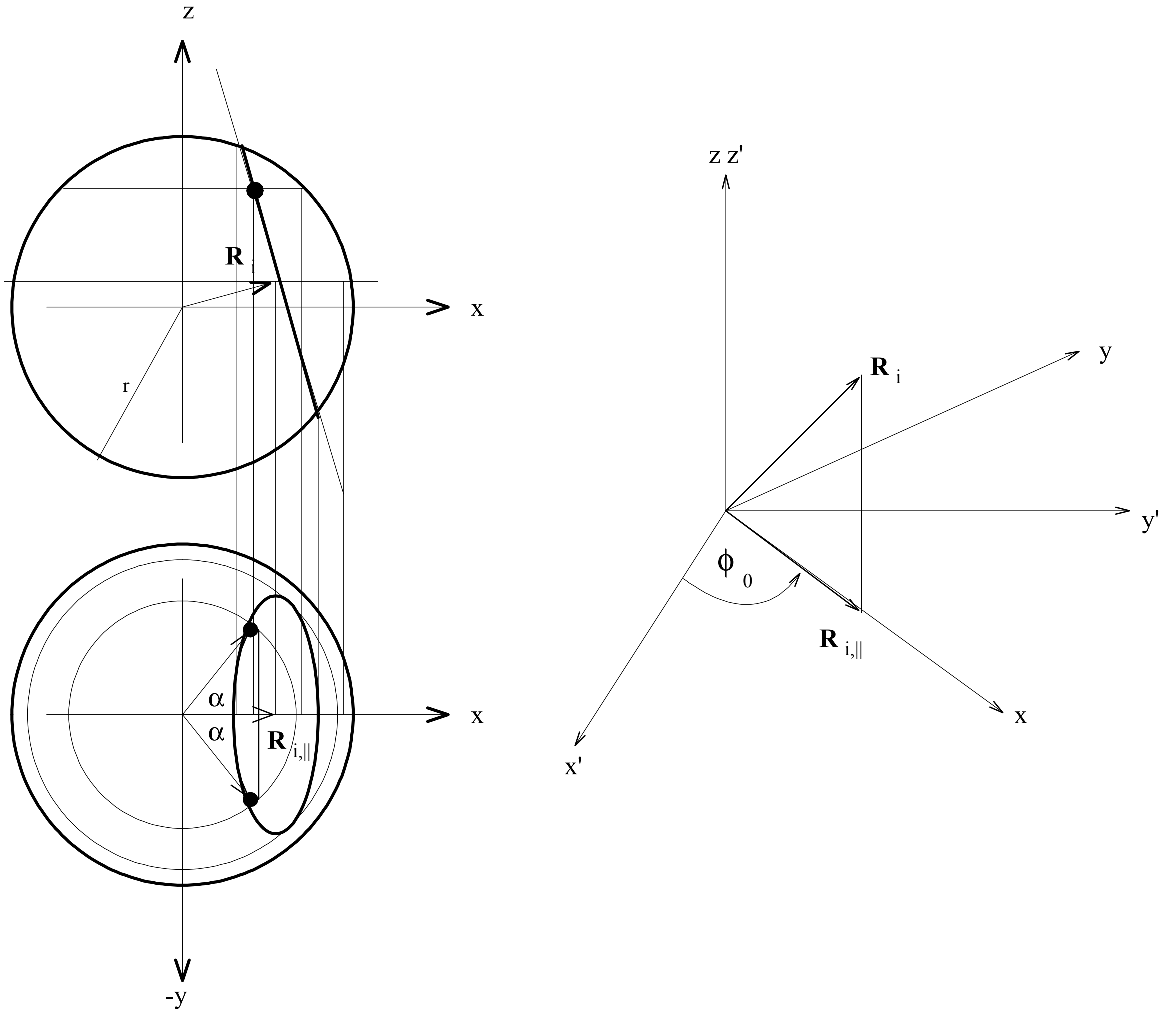

Figure 5.8: Right plot: The coordinate system is rotated around the z axis such that $\mathbf{R}_{i,\|}$ points in x direction.
Left plot: view from the top (below) and the side (above) of the plane intersecting the sphere.

With the help of the above ordered list one can solve the φ integral

$$\begin{aligned} f_m(r,\cos\theta) &= \left(\int_0^{2\pi} d\varphi\sigma(r,\theta;\varphi)\,e^{-im\varphi}\right) = \\ &= \begin{cases} \sum\limits_{j=1}^{2N}\left(\varphi_{j+1}-\varphi_j\right)\sigma\left(r,\theta,\varphi_j^M\right) & m=0 \\ \frac{i}{m}\sum\limits_{j=1}^{2N}\left(e^{-im\varphi_{j+1}}-e^{-im\varphi_j}\right)\sigma\left(r,\theta,\varphi_j^M\right) & m\neq 0 \end{cases} \end{aligned}$$

where $\sigma\left(r,\theta,\varphi_j^M\right)$ is 1 if, for $\varphi_j^M=\left(\varphi_{j+1}-\varphi_j\right)/2$, the point represented by

$$\mathbf{x}^M = \left(\begin{array}{ccc} r\sin\theta\cos\varphi_j^M & r\sin\theta\sin\varphi_j^M & r\cos\theta \end{array}\right)$$

is inside the polyhedron and 0 otherwise, which can be easily verified with (5.6). The remaining θ integral has to be evaluated numerically

$$\sigma_L(r) = C_L\int_0^{\pi} d\theta\left(\sin\theta P_m^l(\cos\theta)f_m(r;\cos\theta)\right) = C_L\int_1^{1} du\left[P_m^l(u)f_m(r;u)\right] \ .$$

The $f_m(r;\cos\theta)$ are not smooth functions of $\cos\theta$, they are only smooth between K irregular points

$$\{\theta_k=\theta_k(r)\,,k=1,\ldots,K\}\ ,$$

so that one splits the θ integration into several intervals

$$\sigma_L(r) = C_L\sum_{k=1}^{K-1}\left(\int_{\theta_k}^{\theta_{k+1}} d\theta\left(\sin\theta P_m^l(\cos\theta)f_m(r;\cos\theta)\right)\right) \ . \tag{5.8}$$

5.2.2 Shape functions of the FCC cell

As an example we discuss the construction of the shape functions for a simple FCC cell, with cubic lattice constant a. In the FCC lattice we have 12 nearest neighbors, each one giving rise to one boundary plane of the Wigner Seitz cell at a normal distance $\frac{\sqrt{2}a}{4}$. These planes intercept with each other in a total of 24 edges, each one is equivalent and at a normal distance $\frac{a}{\sqrt{6}}$. The edges intercept in total at 14 corners, where 8 are 'near corners' at the distance $\frac{\sqrt{3}a}{4}$ and 6 are 'far corners' at the distance $\frac{2a}{4}$. Therefore we have the following critical radii:

$$0<\left(r_{C1}=r_{MT}=\frac{\sqrt{2}a}{4}\right)<\left(r_{C2}=\frac{a}{\sqrt{6}}\right)<\left(r_{C3}=\frac{\sqrt{3}a}{4}\right)<\left(r_{C4}=r_{BS}=\frac{2a}{4}\right) \tag{5.9}$$

Only at the critical radii the number K of irregular θ values, $\{\theta_k, k=1,\ldots,K\}$ can change, while for given r the number N of φ interception points, $\left\{\varphi_i^{(\pm)}, i=1,\ldots,N\right\}$, can only change at an irregular θ_k. While all the above features are independent of the orientation of the coordinate system, many results depend on it. As an example for a property dependent on the coordinate system we compare the neighborhood of $\theta = 0$ between coordinate systems with $\mathbf{e}_z \parallel [100]$, $\mathbf{e}_z \parallel [110]$ and $\mathbf{e}_z \parallel [111]$. The respective z axis intersects the polyhedron at the following points:

$$\begin{array}{lll} [100] & H \text{ at } r_{BS} = \frac{1}{2}a & \text{'far corner'} \\ [110] & N \text{ at } r_{MT} = \frac{\sqrt{2}}{4}a & \text{'plane center'} \\ [111] & P \text{ at } r_{C3} = \frac{\sqrt{3}}{4}a & \text{'near corner'} \end{array}$$

To examine the situation around $\theta = 0$ we take a radius next to the corresponding critical radius.

The [100] case

For the [100] we choose a radius r_2 a bit smaller then r_{BS} (the situation for $r \geq r_{BS}$ is trivial). At this radius all points with a constant θ define a circle and we make a planar plot of the situation in the plane of the circle (the plane given by $z = r_2 \cos\theta$), for θ varying from 0 to small positive values (right column of figure (5.9)). For $\theta = 0$ the circle is reduced to a point and the plane cuts a square out of the polyhedron (4 edges meet at the corner H), with θ increasing the circle gets bigger until it touches the (also increasing) square from the inside at an irregular $\theta-$value θ_2 then the circle intercepts with the square until the square touches the circle at an irregular $\theta-$value θ_3, afterwards the circle is outside the polyhedron. For $r_2 \rightarrow r_{BS}^{(-)}$ the irregular θ points $0 = \theta_1 \leq \theta_2 \leq \theta_3$ all approach 0.

The [110] case

The situation is different in the case of the z axis pointing in the [110] direction. We choose a radius r_1 a bit bigger then r_{MT} (the situation for $r \leq r_{MT}$ is trivial), for this radius all points with a constant θ value define a circle and we make a planar plot of the situation in the plane of the circle (plane given by $z = r_1 \cos\theta$), for θ varying from 0 to small positive values (left column of figure (5.9)). For $\theta = 0$ the circle is reduced to a point and this plane does not intersect with the polyhedron (N is the MT-point of the boundary plane), with θ increasing the circle gets bigger but is still completely outside the polyhedron until at an irregular $\theta-$value θ_2 the circle is in the plane of the bounding plane, afterwards this bounding plane of the polyhedron is no longer involved in the construction. For $r_1 \rightarrow r_{MT}^{(+)}$ the irregular θ points $0 = \theta_1 \leq \theta_2$ all approach 0.

The [111] case

For the [111] the situation is more complicated since the z axis intercepts the polyhedron at a 'near corner' P, where 3 edges meet, see figure (5.10). Therefore we have to examine the situation for different radii r, namely $r_1 < r_2 = r_{C3} < r_3$ smaller, equal to or bigger then the critical radius.

First we choose a radius r_1 a bit smaller then r_{C3} (left column of figure (5.11)). For $\theta = 0$ the circle is reduced to a point and the plane cuts a triangle out of the polyhedrons (3 edges meet at the 'near corner' P), with θ increasing the circle gets bigger until it touches the (also increasing) triangle from inside at an irregular $\theta-$value θ_2 then the circle intercepts with the triangle. For $r_1 \rightarrow r_{C3}^{(-)}$ the irregular θ points $0 = \theta_1 \leq \theta_2$ all approach 0. If we choose a radius r_2 equal to the

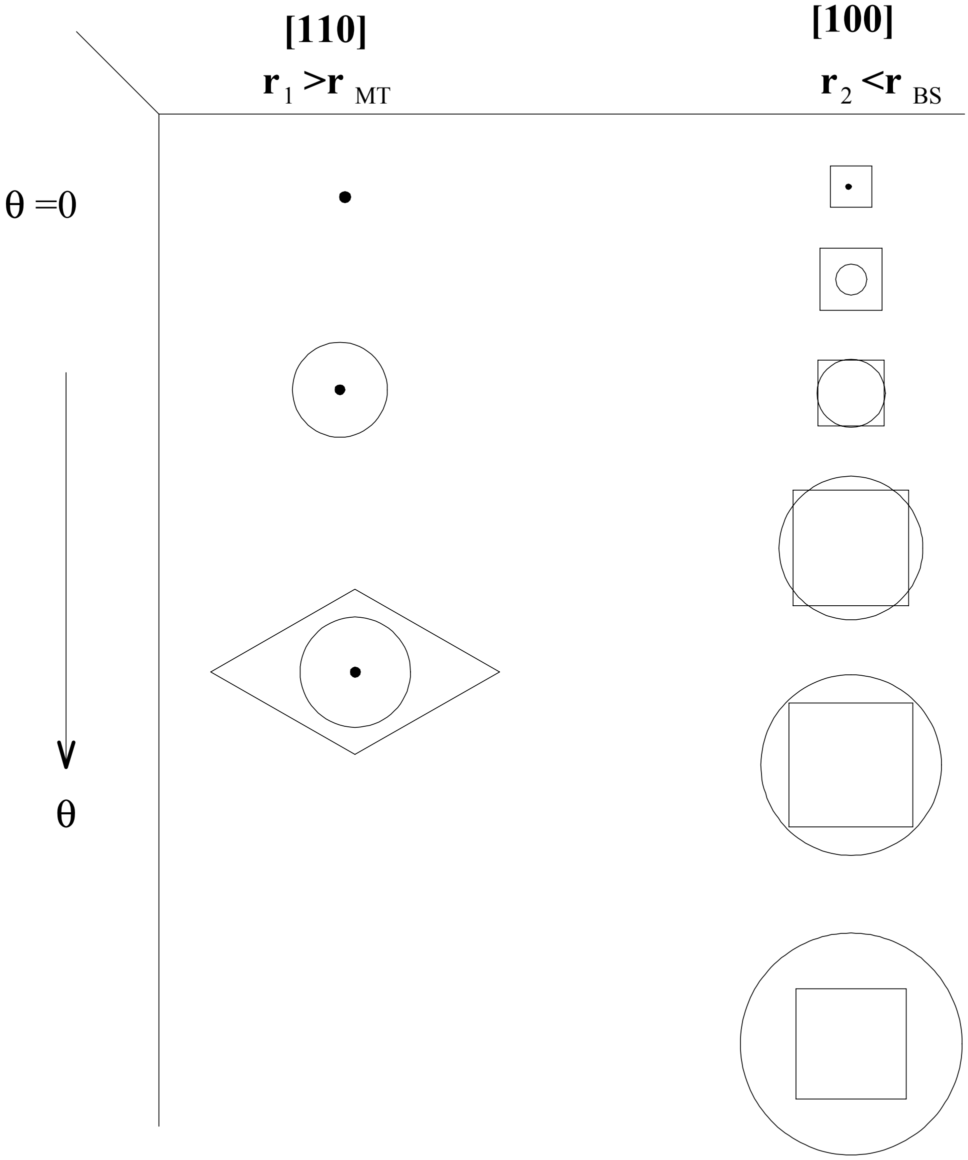

Figure 5.9: Right column: For $\theta = 0$ the circle is reduced to a point and the plane cuts a square out of the polyhedron, with θ increasing the circle gets bigger until it touches the (also increasing) square from inside at an irregular $\theta-$value θ_2 then the circle intercepts with the square until the square touches the circle at an irregular $\theta-$value θ_3, afterwards the circle is outside the polyhedron. Left column: For $\theta = 0$ the circle is reduced to a point and this plane does not intersect with the polyhedron, with θ increasing the circle gets bigger but is still completely outside the polyhedron until at an irregular $\theta-$value θ_2 the circle is in the plane of the bounding plane, afterwards this bounding plane of the polyhedron is no longer involved in the construction.

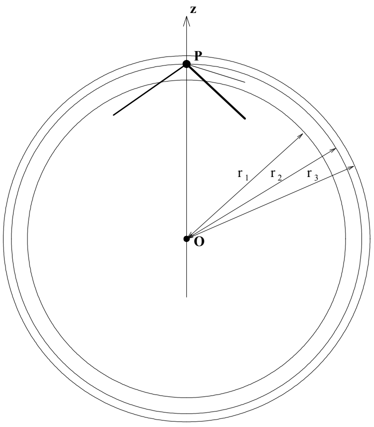

Figure 5.10: The 'near corner P' where 3 edges come together and spheres with radii smaller, equal to or bigger than the critical radius $r_1 < r_2 = r_{C3} < r_3$

r_{C3} (middle column of figure (5.11)) for $\theta = 0$ the circle and the triangle is reduced to a point, with θ increasing the circle and the triangle get bigger and intercept with each other, there is no other irregular $\theta-$value except $\theta_1 = 0$. Finally we choose a radius r_3 a bit bigger then r_{C3} (right column of figure (5.11)). For $\theta = 0$ the circle is reduced to a point which is outside the polyhedron, with θ increasing the triangle inside the circle gets bigger until it touches the (also increasing) circle from inside at an irregular $\theta-$value θ_2, then the circle intercepts with the triangle. For $r_3 \to r_{C3}^{(+)}$ the irregular θ points $0 = \theta_1 \leq \theta_2$ all approach 0.

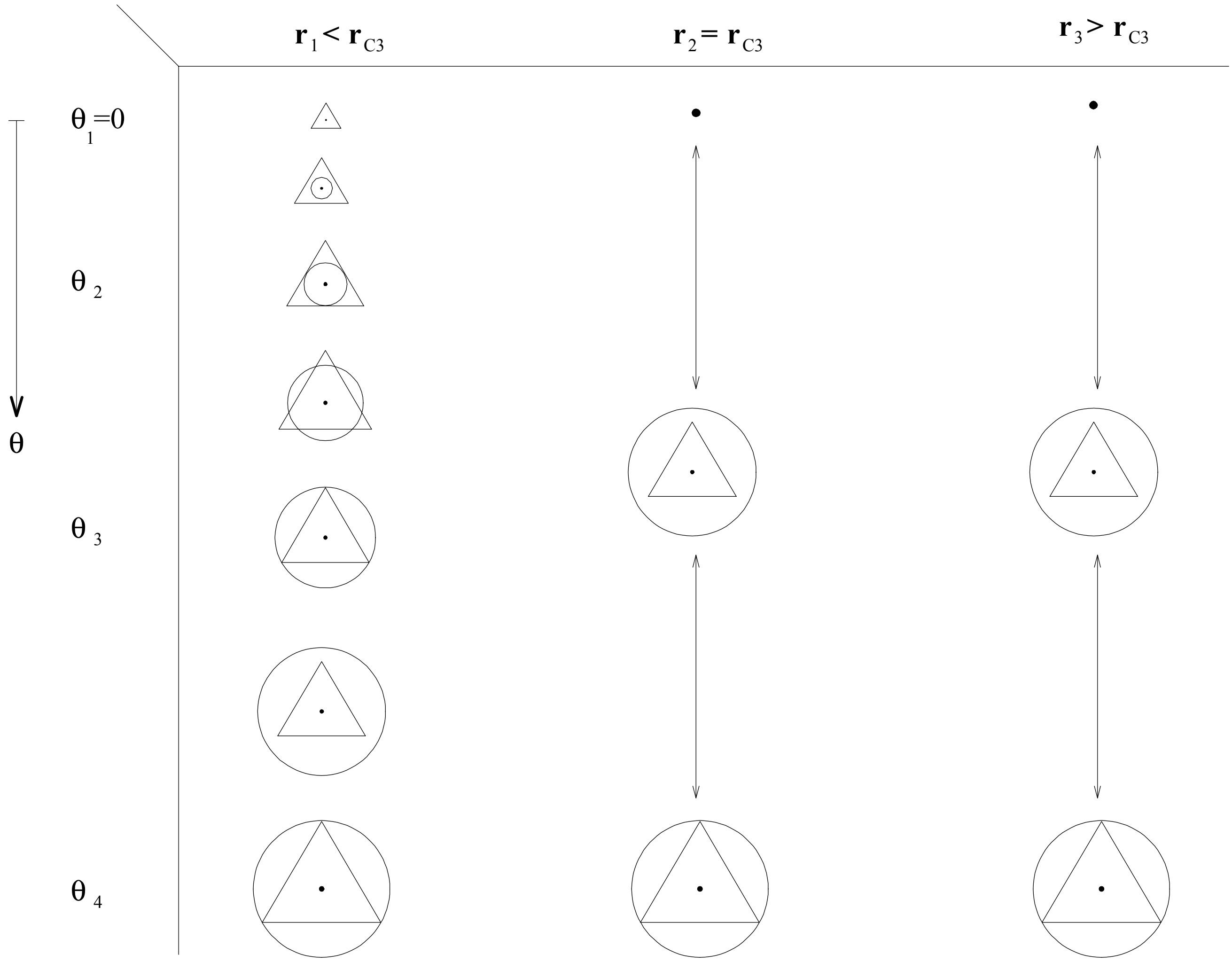

Figure 5.11: Left column: $r_1 < r_{C3}$ For $\theta = 0$ the circle is reduced to a point and the plane cuts a triangle out of the polyhedron, the sequence of θ increasing.
Middle column: $r_2 = r_{C3}$ For $\theta = 0$ the circle and the triangle is reduced to a point, sequence for θ increasing.
Right column: $r_3 > r_{C3}$ For $\theta = 0$ the circle is reduced to a point which is outside the polyhedron, sequence for θ increasing

Chapter 6

Electrostatic potential of a charge density with 2D or 3D translational symmetry - Madelung constants

6.1 Introduction

This chapter summarizes the theory behind the numerical programming of the electrostatic potential in the SKKR software code. The idea was first developed by Laszlo Szunyogh by adapting the Kambe papers of the Structure constants of LEED theory, major changes, corrections and completions were part of these thesis. The implementation of the corresponding numerical procedures for the 'simple lattice full-potential SKKR code', mainly developed by Jan Zabloudil, was done following this document by the author. The theory as well as all program routines also work for the 'complex structure SKKR code'.

6.2 Basic definitions

Using atomic Rydberg units ($m_e = \frac{1}{2}, \hbar = 1, e^2 = 2$) the (now dimensionless) Poisson equation reads as

$$\Delta V(\mathbf{r}) = -8\pi\rho(\mathbf{r}) \ . \tag{6.1}$$

The corresponding Green function $G(\mathbf{r},\mathbf{r}')$ is defined by

$$\Delta G(\mathbf{r},\mathbf{r}') = -4\pi\delta(\mathbf{r},\mathbf{r}') \ , \tag{6.2}$$

with the solution

$$G(\mathbf{r},\mathbf{r}') = G_0(\mathbf{r},\mathbf{r}') + F(\mathbf{r},\mathbf{r}') \ , \tag{6.3}$$

where

$$G_0(\mathbf{r},\mathbf{r}') = \frac{1}{|\mathbf{r}-\mathbf{r}'|} \quad \text{and} \quad \Delta F(\mathbf{r},\mathbf{r}') = 0 \ . \tag{6.4}$$

For a point in the neighborhood of a nucleus $\mathbf{R}$ its coordinates $\mathbf{r}$ are measured from this nucleus position. The *intercell contribution to the electrostatic potential* around an atomic position $\mathbf{R}$ is given by

$$V_{\mathbf{R}}(\mathbf{r}) = 2 \sum_{\substack{\mathbf{R}' \\ (\mathbf{R}' \neq \mathbf{R})}} \left(\int_{\Omega_{\mathbf{R}'}} d^3r' (G_0(\mathbf{r}+\mathbf{R}, \mathbf{r}'+\mathbf{R}')\rho_{\mathbf{R}'}(\mathbf{r}')) \right) \qquad (\mathbf{r} \in \Omega_{\mathbf{R}}) \tag{6.5}$$

The *intracell contribution to the electrostatic potential* at the atomic position $\mathbf{R}$ is given by

$$V_{\mathbf{R}}(\mathbf{r}) = 2 \int_{\Omega_{\mathbf{R}}} d^3r' \, (G_0(\mathbf{r}, \mathbf{r}')\rho_{\mathbf{R}}(\mathbf{r}')) \qquad (\mathbf{r} \in \Omega_{\mathbf{R}}) \tag{6.6}$$

We write the angular momentum index as $L = (l,m) = l(l+1)+m+1 \in \mathbb{N}$.

6.3 Intracell contribution

First we treat the contribution coming from the central cell $\mathcal{V}$, with

$$\mathbf{x} \in \mathcal{V} \Rightarrow |\mathbf{x}| = r \leq r_{BS} \ .$$

Let $\bar{\rho}(\mathbf{x})$ be the (shape truncated) charge density of the central cell with an expansion in spherical harmonics (Y_L^* in agreement with the common literature of KKR),

$$\bar{\rho}(\mathbf{x}) = \rho(\mathbf{x})\sigma_{\mathcal{V}}(\mathbf{x}) = \sum_L \bar{\rho}_L(r) Y_L^*(\widehat{\mathbf{x}}) \ .$$

The potential of this charge distribution fulfills the equation

$$V(\mathbf{x}) = 2 \int_{\mathcal{V}} \frac{1}{|\mathbf{x}-\mathbf{x}'|} \bar{\rho}(\mathbf{x}') d^3x'$$

With the expansion (A.44) for $\frac{1}{|\mathbf{x}-\mathbf{x}'|}$ this can be written as

$$V_{Intra}(\mathbf{x}) = \sum_L \frac{8\pi}{2l+1} \left[r^l \left(\int_r^{r_{BS}} \frac{\bar{\rho}_L(r')}{(r')^{l-1}} dr' \right) + \frac{1}{r^{l+1}} \left(\int_0^r (r')^{l+2} \bar{\rho}_L(r') dr' \right) \right] Y_L^*(\widehat{\mathbf{x}}) \ . \tag{6.7}$$

Remark 1 ***Symmetries in*** $L = (l,m)$***:***
For all real quantities $X(\mathbf{x})$ *(like* $\bar{\rho}(\mathbf{x})$*) one only needs to evaluate the* X_{lm} *for* $m \geq 0$ *and use the relation*

$$X_{l-m} = (-1)^m \left(X_{lm} \right)^* \ . \tag{6.8}$$

For a system with inversion symmetry with respect to the center $\mathbf{R}$ *(e.g. all simple structures with* 1 *atom per unit cell) we have the selection rule*

$$X_{lm} = 0 \ \ \forall l \ odd \ . \tag{6.9}$$

If the z axis of the coordinate system is a n-fold rotational symmetry axis (of the whole system), we have the selection rule

$$m = \ldots, -n, 0, n, \ldots \ , \tag{6.10}$$

which e.g. leads only to the following nonvanishing contributions for the cubic systems (with 1 *atom per unit cell) dependent on the choice of the coordinate system*

z-axis	*2D lattice inplane*	n
[100]	*quadratic lattice*	4
[110]	*rectangular lattice*	2
[111]	*hexagonal lattice*	3

From (6.7) it is clear that V_{Intra} has the same symmetry as $\bar{\rho}(\mathbf{x})$ and only the corresponding (l, m) have to be calculated. The $\bar{\rho}_L$ are the coefficients of the shape truncated charge density, they are expressed with the shape functions $\sigma_{L''}(r)$ and the untruncated ones as

$$\bar{\rho}_L(r) = \sum_{L'L''} C^{L'}_{L''L} \rho_{L'}(r) \sigma_{L''}(r) \ .$$

If one needs the expansion of $V_{Intra}(\mathbf{x})$ in Y_L then (6.7) reads as

$$V_{Intra}(\mathbf{x}) = \sum_L \frac{8\pi}{2l+1} \left[r^l \left(\int_r^{r_{BS}} \frac{1}{(r')^{l-1}} \left(\sum_{L'L''} C^{L'}_{L''L} \rho_{L'}(r') \sigma_{L''}(r') \right) dr' \right) + \right. \tag{6.11}$$
$$\left. + \frac{1}{r^{l+1}} \left(\int_0^r (r')^{l+2} \left(\sum_{L'L''} C^{L'}_{L''L} \rho_{L'}(r') \sigma_{L''}(r') \right) dr' \right) \right]^* Y_L(\widehat{\mathbf{x}})$$

The radial grid for the numerical evaluation of the integral is determined by the shape functions. The numerics are performed best by first evaluating the sum and then perform the integration, complex conjugation only done at the very end.

$$V_{Intra,L}(r) = \frac{8\pi}{2l+1} \left[r^l \int_r^{r_{BS}} \frac{1}{(r')^{l-1}} \left(\sum_{L'L''} C^{L'}_{L''L} \rho_{L'}(r') \sigma_{L''}(r') \right) dr' + \right. \tag{6.12}$$
$$\left. + \frac{1}{r^{l+1}} \int_0^r (r')^{l+2} \left(\sum_{L'L''} C^{L'}_{L''L} \rho_{L'}(r') \sigma_{L''}(r') \right) dr' \right]^* \ . \tag{6.13}$$

Because $V_{Intra}(\mathbf{x})$ is a real function, we immediately obtain the relation

$$V_{Intra,l-m}(r) = (-1)^m \left(V_{Intra,lm}(r) \right)^* . \tag{6.14}$$

Remark 2 *Alternatively one could calculate the intracell contribution with the untruncated charge density, in the hope of compensating the nearest neighbor error discussed later on in (6.20).*

Before we discuss the intercell contribution some general considerations are necessary.

6.4 Multipole expansion in real space

6.4.1 Charge density

In our problem the space is divided in non-overlapping, space-filling cells such that the total charge density is the sum of localized densities centered around atomic positions $\mathbf{R}_\alpha$

$$\rho(\mathbf{x}) = \sum_\alpha \bar{\rho}_{R_\alpha}(\mathbf{x}), \quad \bar{\rho}_{R_\alpha}(\mathbf{x}) = \rho(\mathbf{R}_{\boldsymbol{\alpha}} + \mathbf{x})\sigma_\alpha(\mathbf{R}_{\boldsymbol{\alpha}} + \mathbf{x}) \ . \tag{6.15}$$

One such local charge density $\bar{\rho}_{R_\alpha}(\mathbf{x})$ is only unequal zero in a neighborhood of $\mathbf{x} = \mathbf{0}$. This charge density can be expanded in spherical harmonics,

$$\bar{\rho}_{R_\alpha}(\mathbf{x}) = \sum_L \bar{\rho}_{R_\alpha,L}(r) Y_L^*(\widehat{\mathbf{x}}) \ . \tag{6.16}$$

Furthermore, the spherical multipole moments of the localized charge density are defined by

$$Q_R^L = \frac{\sqrt{4\pi}}{2l+1} \int_{V_R} r^l \bar{\rho}_{R_\alpha}(\mathbf{x}) Y_L(\widehat{\mathbf{x}}) d^3x \tag{6.17}$$

and can be expressed in terms of the untruncated coefficients as

$$Q_R^L = \frac{\sqrt{4\pi}}{2l+1} \int_0^{r_{BS}} r^{l+2} \bar{\rho}_{R_\alpha,L}(r) dr = \frac{\sqrt{4\pi}}{2l+1} \sum_{L'L''} C^{L'}_{L''L} \left(\int_0^\infty r^{l+2} \rho_{R_\alpha,L'}(r) \sigma_{R_\alpha,L''}(r) dr \right) \tag{6.18}$$

The multipole moments are defined such that $Q_{\mathbf{R}}^{00} = Q_{\mathbf{R}}$ and it is obvious that they fulfill the same selection rules as $\bar{\rho}_{\mathbf{R}}(\mathbf{x})$, the charge distribution in the cell centered around the position $\mathbf{R}$. Because the charge density $\bar{\rho}(\mathbf{x})$ is real, we have the symmetry condition

$$Q_R^{l-m} = (-1)^m (Q_R^{lm})^* \tag{6.19}$$

The set of atomic positions $\mathbf{R}_{\boldsymbol{\alpha}}$ with the corresponding spherical multipole moments $Q_{\mathbf{R}_\alpha}^L$ (for all L) of its local charge density $\bar{\rho}_{\mathbf{R}_\alpha}$ are the input data for the Poisson problem. The intercell potential depends only on the multipole moments of the other cells but not on their detailed charge density distribution.

6.4.2 Lattice translational symmetry

In the following we will have two cases

1. 3D periodic (complex) crystal structure:

$$\begin{array}{rcl} \mathbf{R}_\alpha & = & \mathbf{R}_{\mathbf{n}\boldsymbol{\mu}} = \mathbf{T}_{\mathbf{n}} + \mathbf{a}_{\boldsymbol{\mu}} \\ \mathbf{T}_{\mathbf{n}}, \mathbf{n} & \in & \mathbb{Z}^3 \text{ a 3D lattice translation,} \\ \mathbf{a}_{\boldsymbol{\mu}}, \mu & \in & \{1, .., n_{atom}\} \text{ atomic position,} \end{array}$$

   n_{atom} is this finite, rather small number of non equivalent atomic positions, (e.g. for FCC Cu, $n_{atom} = 1$, for hcp Co $n_{atom} = 2$)

2. 2D periodic (complex) crystal structure:

$$\begin{aligned} \mathbf{R}_\alpha &= \mathbf{R}_{\mathbf{np}} = \mathbf{T}_\mathbf{n} + \mathbf{c}_\mathbf{p} \\ \mathbf{T}_\mathbf{n}, \mathbf{n} &\in \mathbb{Z}^2 \text{ a 2D lattice translation }, \\ \mathbf{c}_\mathbf{p}, p &\in \{..., 0, 1, .., n_{\mathbf{intfc}}, n_{\mathbf{intfc}} + 1, ...\}, \end{aligned}$$

$\mathbf{c}_p$ is one non equivalent atomic position per layer, they are numbered in such a way that for $p \leq q, c_{p\perp} \leq c_{q\perp}$ and by definition the layer with $p = 0$ is the last layer of the semi-infinite left region and $p = n_{intfc}$ is the last layer in the selfconsistent treated film. On the left and right side might be either vacuum or a semi-infinite material (there is no other restriction). Also for some layers $p \neq q, c_{p\perp} = c_{q\perp}$ is possible, a 2D plane with more than 1 non equivalent atom .

6.4.3 Relation between Green function and Madelung constants

Using the expansions (A.44) and (A.45), the Green function connecting just 2 different positions $G_0(\mathbf{r} + \mathbf{R}, \mathbf{r}' + \mathbf{R}')$ can be evaluated for

$$r < |\mathbf{r}' - \mathbf{R} + \mathbf{R}'| \text{ and } r' < |\mathbf{R} - \mathbf{R}'| \tag{6.20}$$

as

$$G_0(\mathbf{r} + \mathbf{R}, \mathbf{r}' + \mathbf{R}') = \frac{1}{|\mathbf{r} + \mathbf{R} - \mathbf{r}' - \mathbf{R}'|} = \sum_L \frac{4\pi}{2\ell + 1} r^\ell Y_L^*(\hat{\mathbf{r}}) \frac{Y_L(\widehat{\mathbf{r}' - \mathbf{R} + \mathbf{R}'})}{|\mathbf{r}' - \mathbf{R} + \mathbf{R}'|^{\ell+1}} = \tag{6.21}$$

$$= \sum_L \sum_{L'} r^\ell Y_L^*(\hat{\mathbf{r}}) \left\{ (-1)^\ell \frac{(4\pi)^2 [2(\ell + \ell') - 1]!!}{(2\ell + 1)!!(2\ell' + 1)!!} C^{\ell' m'}_{\ell m, (\ell + \ell')(m' - m)} \frac{Y^*_{(\ell+\ell')(m'-m)}(\widehat{\mathbf{R} - \mathbf{R}'})}{|\mathbf{R} - \mathbf{R}'|^{\ell + \ell' + 1}} \right\} (r')^{\ell'} Y_{\ell' m'}(\hat{\mathbf{r}}') \,. \tag{6.22}$$

With the definition (6.17) of the spherical multipole moments of the charge density it makes sense to recast the expansion (6.22) as follows

$$G_0(\mathbf{r} + \mathbf{R}, \mathbf{r}' + \mathbf{R}') = \sum_L \sum_{L'} \frac{\sqrt{4\pi}}{2\ell + 1} r^\ell Y_L^*(\hat{\mathbf{r}}) \, A^{LL'}_{\mathbf{RR}'} \frac{\sqrt{4\pi}}{2\ell' + 1} (r')^{\ell'} Y_{L'}(\hat{\mathbf{r}}') \,, \tag{6.23}$$

and define the *real-space Madelung constants* (for only 2 atomic positions as)

$$A^{LL'}_{\mathbf{RR}'} = (-1)^\ell \frac{4\pi [2(\ell + \ell') - 1]!!}{(2\ell - 1)!!(2\ell' - 1)!!} C^{\ell' m'}_{\ell m, (\ell + \ell')(m' - m)} \frac{Y^*_{(\ell+\ell')(m'-m)}(\widehat{\mathbf{R} - \mathbf{R}'})}{|\mathbf{R} - \mathbf{R}'|^{\ell + \ell' + 1}} \,. \tag{6.24}$$

This treatment is only valid if $r < |\mathbf{r}' - \mathbf{R} + \mathbf{R}'|$ and $r' < |\mathbf{R} - \mathbf{R}'|$ which means that the bounding spheres of the 2 cells must not overlap. By neglecting the near-field correction for these neighboring cells, the intercell potential (6.5) can than be expressed as direct space sum of terms as above

$$V_{\mathbf{R}}(\mathbf{r}) = 2 \sum_{\mathbf{R}'(\neq \mathbf{R})} \sum_{L} \sum_{L'} \frac{\sqrt{4\pi}}{2\ell+1} r^{\ell} Y_L^*(\widehat{\mathbf{r}})\, A_{\mathbf{RR}'}^{LL'}\, Q_{\mathbf{R}'}^{L'} = 2 \sum_{L} \frac{\sqrt{4\pi}}{2\ell+1} \left(\sum_{L'} \sum_{\mathbf{R}'(\neq \mathbf{R})} A_{\mathbf{RR}'}^{LL'}\, Q_{\mathbf{R}'}^{L'} \right) r^{\ell} Y_L^*(\widehat{\mathbf{r}}) =$$

$$= \sum_{L} \frac{4\sqrt{\pi}}{2\ell+1} \left(\sum_{\mathbf{R}'(\neq \mathbf{R})} \sum_{L'} A_{\mathbf{RR}'}^{LL'}\, Q_{\mathbf{R}'}^{L'} \right)^{*} r^{\ell} Y_L(\widehat{\mathbf{r}}) = \sum_{L} V_{\mathbf{R},L}(r) Y_L(\widehat{\mathbf{r}}) \tag{6.25}$$

$$V_{\mathbf{R},L}(r) = \frac{4\sqrt{\pi}}{2\ell+1} \left(\sum_{\mathbf{R}'(\neq \mathbf{R})} \sum_{L'} A_{\mathbf{RR}'}^{LL'}\, Q_{\mathbf{R}'}^{L'} \right)^{*} r^{\ell} \tag{6.26}$$

If one considers only (piecewise around each atomic position) spherically symmetric potentials, namely, by taking only the $\ell = 0$ term above, this expression reduces to a constant value at the origin of the cell, although all higher multipole moments of the charge densities have to be taken into account.

$$V_{\mathbf{R}}^{ASA} = V_{\mathbf{R}}(\mathbf{0}) = 2 \sum_{\mathbf{R}'(\neq \mathbf{R})} \sum_{L'} A_{\mathbf{RR}'}^{00,L'}\, Q_{\mathbf{R}'}^{L'} \, . \tag{6.27}$$

6.4.4 Alternative relation between the Green function and the Madelung constants → Reduced Madelung constants

Making use of the fact that $G_0(\mathbf{r}+\mathbf{R}, \mathbf{r}'+\mathbf{R}')$ directly depends only on the difference vector $\mathbf{r}-\mathbf{r}'$,

$$G_0(\mathbf{r}+\mathbf{R}, \mathbf{r}'+\mathbf{R}') = G_0(\mathbf{r}-\mathbf{r}'+\mathbf{R}-\mathbf{R}') \, , \tag{6.28}$$

at least for small $\mathbf{r}$ and $\mathbf{r}'$, namely $|\mathbf{r}-\mathbf{r}'| < |\mathbf{R}-\mathbf{R}'|$ it can be expanded as

$$G_0(\mathbf{r}+\mathbf{R}, \mathbf{r}'+\mathbf{R}') = \sum_{L} |\mathbf{r}-\mathbf{r}'|^{\ell}\, Y_L(\widehat{\mathbf{r}-\mathbf{r}'}) \frac{4\pi}{2\ell+1} \frac{Y_L^*(\widehat{\mathbf{R}'-\mathbf{R}})}{|\mathbf{R}-\mathbf{R}'|^{\ell+1}} = \tag{6.29}$$

$$= \sum_{L} |\mathbf{r}-\mathbf{r}'|^{\ell}\, Y_L(\widehat{\mathbf{r}-\mathbf{r}'}) G_{\mathbf{RR}'}^{L} \, . \tag{6.30}$$

The $G_{\mathbf{RR}'}^{L}$ are usually termed as the *reduced Madelung constants.* Inserting expansion (A.49) for $|\mathbf{r}-\mathbf{r}'|^{\ell}\, Y_L(\widehat{\mathbf{r}-\mathbf{r}'})$ into eq. (6.29) yields

$$G_0(\mathbf{r}+\mathbf{R}, \mathbf{r}'+\mathbf{R}') = \sum_{L,L'} r^{\ell} Y_L^*(\widehat{\mathbf{r}}) \frac{4\pi(-1)^{\ell'}[2(\ell+\ell')+1]!!}{(2\ell+1)!!(2\ell'+1)!!} \mathcal{C}_{\ell m,(\ell+\ell')(m'-m)}^{\ell' m'} G_{\mathbf{RR}'}^{(\ell+\ell')(m'-m)} \, (r')^{\ell'} Y_{L'}(\widehat{\mathbf{r}}') \, . \tag{6.31}$$

Comparing eq. (6.23) with eq. (6.31) implies the following relationship between the Madelung constants and the reduced ones

$$A_{\mathbf{RR}'}^{LL'} = (-1)^{\ell'} \frac{[2(\ell+\ell')+1]!!}{(2\ell-1)!!(2\ell'-1)!!} \mathcal{C}_{\ell m,(\ell+\ell')(m'-m)}^{\ell' m'} G_{\mathbf{RR}'}^{(\ell+\ell')(m'-m)} = \tag{6.32}$$

$$= 2\sqrt{\pi}(-1)^{\ell'} \frac{\Gamma(\ell+\ell'+\frac{3}{2})}{\Gamma(\ell+\frac{1}{2})\Gamma(\ell'+\frac{1}{2})} \mathcal{C}_{\ell m,(\ell+\ell')(m'-m)}^{\ell' m'} G_{\mathbf{RR}'}^{(\ell+\ell')(m'-m)} \, , \tag{6.33}$$

which also evidently follows from eq. (6.24) by observing that

$$G^L_{\mathbf{R}\mathbf{R}'} = \frac{4\pi}{2\ell+1} \frac{Y^*_L(\widehat{\mathbf{R}'-\mathbf{R}})}{|\mathbf{R}-\mathbf{R}'|^{\ell+1}} = \frac{4\pi\,(-1)^\ell}{2\ell+1} \frac{Y^*_L(\widehat{\mathbf{R}-\mathbf{R}'})}{|\mathbf{R}-\mathbf{R}'|^{\ell+1}} \; . \tag{6.34}$$

Every reduced Madelung constant $G^L_{\mathbf{R}\mathbf{R}'}$ leads with (6.33) to one or more Madelung constants $A^{LL'}_{\mathbf{R}\mathbf{R}'}$, which themselves are determined by only one reduced one.

One straight forward possibility to calculate the Madelung constants for a periodic system is the direct space summation of the Madelung constants as given in (6.34), by exploiting the fact that the multipole moments do not depend on $\mathbf{n} \in \mathbb{Z}^d$, $(\mathbf{R}_{p,n} = \mathbf{a}_p + \mathbf{T}_n)$

$$V_{\mathbf{R}_p,L}(r) = \frac{4\sqrt{\pi}}{2\ell+1} \left(\sum_q \sum_{\substack{n\in\mathbb{Z}^d \\ (p=q,n\neq 0)}} \sum_{L'} A^{LL'}_{R_p R_{q,n}} \, Q^{L'}_{\mathbf{R}_q} \right)^* r^\ell = \tag{6.35}$$

$$= \frac{4\sqrt{\pi}}{2\ell+1} \left(\sum_{q,L'} \left(\sum_{\substack{n\in\mathbb{Z}^d \\ (p=q,n\neq 0)}} A^{LL'}_{R_p R_{q,n}} \right) Q^{L'}_{\mathbf{R}_q} \right)^* r^\ell \tag{6.36}$$

$$V_{p,L}(r) = \frac{4\sqrt{\pi}}{2\ell+1} \left(\sum_{q,L'} A^{LL'}_{pq} Q^{L'}_q \right)^* r^\ell \; , \; A^{LL'}_{pq} \text{ calculated from } G^L_{pq} \tag{6.37}$$

$$G^L_{pq} = \frac{4\pi\,(-1)^\ell}{2\ell+1} \sum_{\substack{\mathbf{n}\in\mathbb{Z}^d \\ (p=q,n\neq 0)}} \frac{Y^*_L(\widehat{\mathbf{R}_p - \mathbf{R}_{q,n}})}{|\mathbf{R}_p - \mathbf{R}_{q,n}|^{\ell+1}} \tag{6.38}$$

Eq. (6.38) is a series which is (if at all) **only slowly converging**, absolute convergence is guaranteed if $\ell \geq d$, but also then the convergence is only polynomial, it becomes better with large ℓ. It can be used as a straightforward test of other methods. In the following, for systems with 3D and 2D translational symmetry we proceed by taking the lattice Fourier transform of $G_0(\mathbf{r}+\mathbf{R}, \mathbf{r}'+\mathbf{R}')$ and we make use of the definition in (6.29) rather than to perform the direct lattice sum of eq. (6.38). Because of numerical efficiency we express all formulas with the reduced Madelung constants $G^L_{\mathbf{R}\mathbf{R}'}$ instead of $A^{LL'}_{pq}$.

6.5 Complex 3D lattice - bulk case

We have a structure with translational lattice vectors $\mathbf{T}_n \in \mathcal{L}^3$ and non equivalent atomic positions $\mathbf{a}_\mu \notin \mathcal{L}^3$ such that a general atomic position is given by

$$\mathbf{R}_{n\mu} = \mathbf{T}_n + \mathbf{a}_\mu \; (\mathbf{T}_n \in \mathcal{L}^3, \mathbf{a}_\mu \notin \mathcal{L}^3), \quad \rho_{\mathbf{R}_{n\mu}}(\mathbf{r}) = \rho_\mu(\mathbf{r}) \; . \tag{6.39}$$

6.5.1 Evaluation of the Green function

Evidently, in this case the total electrostatic potential depends only on the index μ,

$$V(\mathbf{R}_{\mathbf{n}\boldsymbol{\mu}} + \mathbf{r}) = V(\mathbf{a}_{\boldsymbol{\mu}} + \mathbf{r}) = V_\mu(\mathbf{r}) = 2\sum_{n\nu} \int_{V_\nu} d^3r' G_0(\mathbf{a}_{\boldsymbol{\mu}} + \mathbf{r}, \mathbf{a}_{\boldsymbol{\nu}} + \mathbf{T}_{\mathbf{n}} + \mathbf{r}')\rho_\nu(\mathbf{r}') \quad , \mathbf{r} \in V_\mu \tag{6.40}$$

In order to separate the part independent of the charge density we perform the $\mathbf{n} \in \mathbb{Z}^3$ summation first,

$$V_\mu(\mathbf{r}) = \sum_\nu 2 \int_{\Omega_\nu} d^3r' G_{\mu\nu}(\mathbf{r}, \mathbf{r}')\rho_\nu(\mathbf{r}') \qquad (\mathbf{r} \in \Omega_\mu), \tag{6.41}$$

where $G_{\mu\nu}(\mathbf{r}, \mathbf{r}')$ is given by the following lattice sum

$$G_{\mu\nu}(\mathbf{r}, \mathbf{r}') = \sum_{\substack{n \\ (\mu=\nu, n\neq 0)}} G_0(\mathbf{r} + \mathbf{a}_\mu, \mathbf{r}' + \mathbf{T}_n + \mathbf{a}_\nu) \ . \tag{6.42}$$

Remark 3 *The $G_{\mu\nu}(\mathbf{r}, \mathbf{r}')$ depend only on the lattice and not on the charge density, therefore they can not contain information about the necessity of an overall charge neutral system and must have certain mathematical difficulties with respect to convergence.*

Now we use 2 different methods to evaluate $G_{\mu\nu}(\mathbf{r}, \mathbf{r}')$.

Method A

Let us split (6.42) into

$$G_{\mu\nu}(\mathbf{r}, \mathbf{r}') = D_{\mu\nu}(\mathbf{r}, \mathbf{r}') - \delta_{\mu\nu} G_0(\mathbf{r}, \mathbf{r}') \ , \tag{6.43}$$

namely into a sum over all cells minus the part for the intracell contribution, where

$$D_{\mu\nu}(\mathbf{r}, \mathbf{r}') = \sum_n G_0(\mathbf{r} + \mathbf{a}_\mu, \mathbf{r}' + \mathbf{T}_n + \mathbf{a}_\nu) = D(\mathbf{r} + \mathbf{a}_\mu - \mathbf{r}' - \mathbf{a}_\nu) \ , \tag{6.44}$$

and

$$D(\mathbf{r}) \equiv \sum_n G_0(\mathbf{r} - \mathbf{T}_n) = \sum_n \frac{1}{|\mathbf{r} - \mathbf{T}_n|} \ . \tag{6.45}$$

The above infinite sum (6.45) is trivially divergent to $+\infty$ because of the long-range contributions, additionally it does not exist if $\mathbf{r}$ is equal to a lattice vector ($\mathbf{r} \in \mathcal{L}^3$). But only the sum of the contributions of all atoms make the Madelung potential finite in case of a neutral crystal. In order to facilitate the calculation of the contributions of the individual sublattices, the divergencies will be dropped systematically from all terms, such that the sum, i.e., the proper Madelung potential is conserved. Furthermore there is a singularity of $D(\mathbf{r})$ at all lattice translations $\mathbf{T}_n$, but finally we have to evaluate D only at $(\mathbf{r} + \mathbf{a}_\mu) - (\mathbf{r}' + \mathbf{a}_\nu)$ and therefore $(\mathbf{r} + \mathbf{a}_\mu) - (\mathbf{r}' + \mathbf{a}_\nu) = \mathbf{T}_n$, but because $(\mathbf{r} + \mathbf{a}_\mu) \in \mathcal{V}_\mu, (\mathbf{r}' + \mathbf{a}_\nu) \in \mathcal{V}_\nu$ this can only happen for $\mathbf{T}_n = 0$. Replacing the identity (A.62) into eq. (6.45), $D(\mathbf{r})$ can be split into two parts

$$D(\mathbf{r}) = D_1(\mathbf{r}) + D_2(\mathbf{r}) \ , \tag{6.46}$$

where

$$D_1(\mathbf{r}) = \frac{2}{\sqrt{\pi}} \sum_n \int_0^{1/2\sigma} dx \exp(-\left|\mathbf{r}-\mathbf{T}_n\right|^2 x^2) \ , \tag{6.47}$$

$$D_2(\mathbf{r}) = \frac{2}{\sqrt{\pi}} \sum_n \int_{1/2\sigma}^{\infty} dx \exp(-\left|\mathbf{r}-\mathbf{T}_n\right|^2 x^2) \ , \tag{6.48}$$

and σ is the so called Ewald parameter.
With exception of $\mathbf{r}=0$ (the case will be considered at the end of this section), eq. (6.48) can be evaluated easily:

$$D_2(\mathbf{r}) = \sum_n \frac{1}{\left|\mathbf{r}-\mathbf{T}_n\right|} \left\{ \frac{2}{\sqrt{\pi}} \int_{\left|\mathbf{r}-\mathbf{T}_n\right|/2\sigma}^{\infty} dx \exp(-x^2) \right\} = \sum_n \frac{1}{\left|\mathbf{r}-\mathbf{T}_n\right|} \mathrm{erfc}(\left|\mathbf{r}-\mathbf{T}_n\right|/2\sigma) \ , \tag{6.49}$$

which, as $\lim_{z\to\infty} \mathrm{erfc}(z) = e^{-z^2}/(\sqrt{\pi}z)$, is rapidly convergent. Utilizing the identity (A.63), eq. (6.47) can be rewritten as

$$D_1(\mathbf{r}) = \frac{2\pi}{V} \sum_j \exp(i\mathbf{G}_j \cdot \mathbf{r}) \int_0^{1/2\sigma} \frac{dx}{x^3} \exp(-\mathbf{G}_j^2/4x^2) \ , \tag{6.50}$$

where $\mathbf{G}_j$ denote vectors of the reciprocal lattice. The divergence mentioned above appears in the term for $\mathbf{G}_j = \mathbf{0}$. Therefore, from this term we keep only that part that depends on σ and drop an infinite constant,

$$\frac{2\pi}{V} \int_0^{1/2\sigma} \frac{dx}{x^3} = -\frac{\pi}{V} \left[\frac{1}{x^2} \right]_0^{1/2\sigma} = -\frac{4\pi\sigma^2}{V} \ (\ + \infty \ ) \ ,$$

and instead of (6.50) we write

$$D_1(\mathbf{r}) = \frac{2\pi}{V} \sum_{\substack{j \\ (\mathbf{G}_j \neq \mathbf{0})}} \exp(i\mathbf{G}_j \cdot \mathbf{r}) \int_0^{1/2\sigma} \frac{dx}{x^3} \exp(-\mathbf{G}_j^2/4x^2) - \frac{4\pi\sigma^2}{V} \ . \tag{6.51}$$

The integral in eq. (6.51) can be easily performed

$$\int_0^{1/2\sigma} \frac{1}{x^3} \exp(-\mathbf{G}_j^2/4x^2) dx = \frac{2}{\mathbf{G}_j^2} \int_{-\infty}^{-\mathbf{G}_j^2\sigma^2} dy \exp(y) = \frac{2\exp(-\mathbf{G}_j^2\sigma^2)}{\mathbf{G}_j^2} \ , \tag{6.52}$$

therefore,

$$D_1(\mathbf{r}) = \frac{4\pi}{V} \sum_{\substack{j \\ (\mathbf{G}_j \neq \mathbf{0})}} \exp(i\mathbf{G}_j\mathbf{r}) \frac{\exp(-\mathbf{G}_j^2\sigma^2)}{\mathbf{G}_j^2} - \frac{4\pi\sigma^2}{V} \ . \tag{6.53}$$

Setting $\mathbf{r} = \mathbf{r} + \mathbf{a}_{\mu\nu}$ ($\mathbf{a}_{\mu\nu} = \mathbf{a}_\mu - \mathbf{a}_\nu$) in eqs. (6.49) and (6.51) yields

$$D_{1,\mu\nu}(\mathbf{r}) = \frac{4\pi}{V} \sum_{\substack{j \\ (\mathbf{G}_j \neq \mathbf{0})}} \exp(i\mathbf{G}_j\mathbf{r}) \exp(i\mathbf{G}_j\mathbf{a}_{\mu\nu}) \frac{\exp(-\mathbf{G}_j^2\sigma^2)}{\mathbf{G}_j^2} - \frac{4\pi\sigma^2}{V} \ , \tag{6.54}$$

$$D_{2,\mu\nu}(\mathbf{r}) = \sum_{\substack{n \\ (\mathbf{T}_n - \mathbf{a}_{\mu\nu} \neq \mathbf{0})}} \frac{1}{\left|\mathbf{r}+\mathbf{a}_{\mu\nu}-\mathbf{T}_n\right|} \mathrm{erfc}(\left|\mathbf{r}+\mathbf{a}_{\mu\nu}-\mathbf{T}_n\right|/2\sigma) \ , \tag{6.55}$$

while the missing term in (6.55) and the last term in eq. (6.42) lead to a contribution,

$$D_{3,\mu\nu}(\mathbf{r}) = \delta_{\mu\nu}\frac{\operatorname{erfc}(|\mathbf{r}|/2\sigma)-1}{|\mathbf{r}|} = -\delta_{\mu\nu}\frac{\operatorname{erf}(|\mathbf{r}|/2\sigma)}{|\mathbf{r}|}\ , \tag{6.56}$$

such that

$$G_{\mu\nu}(\mathbf{r},\mathbf{r}') = D_{1,\mu\nu}(\mathbf{r}-\mathbf{r}') + D_{2,\mu\nu}(\mathbf{r}-\mathbf{r}') + D_{3,\mu\nu}(\mathbf{r}-\mathbf{r}')\ . \tag{6.57}$$

Note that $D_{3,\mu\nu}(\mathbf{r})$ is finite for $r \to 0$

$$\lim_{r\to 0} D_{3,\mu\nu}(\mathbf{r}) = -\delta_{\mu\nu}\frac{1}{\sqrt{\pi}\sigma}\ . \tag{6.58}$$

Method B

From eq. (6.5) it is clear that the potential produced by the point charges

$$\rho(\mathbf{r}) = \sum_{\mu}\sum_{n} Q_\mu \delta(\mathbf{r}-\mathbf{a}_\mu-\mathbf{T}_n)\ , \tag{6.59}$$

is given by

$$V_\mu(\mathbf{r}) = 2\sum_{\nu}\sum_{n} Q_\nu G_0(\mathbf{r}+\mathbf{a}_\mu, \mathbf{a}_\nu+\mathbf{T}_n) = 2\sum_{\nu} Q_\nu G_{\mu\nu}(\mathbf{r}) + \frac{2Q_\mu}{|\mathbf{r}|}\ . \tag{6.60}$$

Thus, the problem of calculating $G_{\mu\nu}(\mathbf{r})$ can be led back to one of calculating $V_\mu(\mathbf{r})$ by solving the corresponding Poisson equation. As what follows, we require charge neutrality for the system, i.e.,

$$\sum_{\mu} Q_\mu = 0\ . \tag{6.61}$$

Adding to and subtracting from the charge density a charge distribution of the form

$$\rho_I(\mathbf{r}) = \sum_{\mu}\sum_{n} Q_\mu \frac{1}{8\sigma^3\pi^{3/2}} \exp\left(-(\mathbf{r}-\mathbf{a}_\mu-\mathbf{T}_n)^2/4\sigma^2\right)\ , \tag{6.62}$$

$$\left(\int d^3r\rho_I(\mathbf{r}) = \sum_{\mu}\sum_{n} Q_\mu = 0\right)$$

the Poisson equation can be solved separately for

$$\rho_S(\mathbf{r}) = \sum_{\mu}\sum_{n} Q_\mu \left(\delta(\mathbf{r}-\mathbf{a}_\mu-\mathbf{T}_n) - \frac{1}{8\sigma^3\pi^{3/2}} \exp\left(-(\mathbf{r}-\mathbf{a}_\mu-\mathbf{T}_n)^2/4\sigma^2\right)\right) \tag{6.63}$$

and $\rho_I(\mathbf{r})$, since

$$\rho(\mathbf{r}) = \rho_S(\mathbf{r}) + \rho_I(\mathbf{r})\ . \tag{6.64}$$

It is easy to show that

$$V_S(\mathbf{r}) = \sum_\mu \sum_n 2Q_\mu \frac{\mathrm{erfc}(|\mathbf{r}-\mathbf{a}_\mu-\mathbf{T}_n|/2\sigma)}{|\mathbf{r}-\mathbf{a}_\mu-\mathbf{T}_n|} + C \ . \tag{6.65}$$

Namely,

$$\begin{aligned}\Delta\left(\frac{\mathrm{erfc}(r/2\sigma)}{r}\right) = \Delta\left(\frac{1-\mathrm{erf}(r/2\sigma)}{r}\right) &= -4\pi\delta\left(\mathbf{r}\right) - \frac{1}{r}\frac{d^2}{dr^2}\left(r\frac{\mathrm{erf}(r/2\sigma)}{r}\right) = \\ &= -4\pi\delta\left(\mathbf{r}\right) - \frac{1}{2\sigma^3\pi^{1/2}}\exp\left(-r^2/4\sigma^2\right) \ ,\end{aligned}$$

therefore,

$$\Delta V_S(\mathbf{r}) = -8\pi\rho_S(\mathbf{r}) \ . \tag{6.66}$$

By expressing the potential $V_I(\mathbf{r})$ and the charge density $\rho_I(\mathbf{r})$ in lattice Fourier series

$$V_I(\mathbf{r}) = \sum_j V_I(\mathbf{G}_j)\exp\left(i\mathbf{G}_j\mathbf{r}\right) \tag{6.67}$$

$$\rho_I(\mathbf{r}) = \sum_j \rho_I(\mathbf{G}_j)\exp\left(i\mathbf{G}_j\mathbf{r}\right) \ , \tag{6.68}$$

eq. (6.1) implies that

$$V_I(\mathbf{G}_j) = -\frac{8\pi}{\mathbf{G}_j^2}\rho_I(\mathbf{G}_j) \ . \tag{6.69}$$

The lattice Fourier transform of $\rho_I(\mathbf{r})$ can be calculated as

$$\rho_I(\mathbf{G}_j) = \frac{1}{NV}\int d^3r\, \rho_I(\mathbf{r})\exp\left(-i\mathbf{G}_j\mathbf{r}\right) = \tag{6.70}$$

$$= \frac{1}{NV}\sum_\mu\sum_n Q_\mu \frac{1}{8\sigma^3\pi^{3/2}}\int d^3r \exp\left(-(\mathbf{r}-\mathbf{a}_\mu-\mathbf{T}_n)^2/4\sigma^2\right)\exp\left(-i\mathbf{G}_j\mathbf{r}\right) = \tag{6.71}$$

$$= \frac{1}{V}\sum_\mu Q_\mu \exp\left(-i\mathbf{G}_j\mathbf{a}_\mu\right)\underbrace{\frac{1}{8\sigma^3\pi^{3/2}}\int d^3r \exp\left(-\mathbf{r}^2/4\sigma^2\right)\exp\left(-i\mathbf{G}_j\mathbf{r}\right)}_{=\frac{1}{\pi^{3/2}}\int d^3u \exp\left(-u^2\right)\exp\left(-i2\sigma\mathbf{G}_j\mathbf{u}\right)} \ . \tag{6.72}$$

For $\mathbf{G}_j = \mathbf{0}$ the above integral equals to 1, therefore, $\rho_I\left(\mathbf{G}_j = \mathbf{0}\right) = 0$, while for $\mathbf{G}_j \neq \mathbf{0}$

$$\begin{aligned}&\frac{1}{\pi^{3/2}}\int d^3u \exp\left(-\mathbf{u}^2/4\sigma^2\right)\exp\left(-i2\sigma\mathbf{G}_j\mathbf{u}\right) = \\ &= \frac{2}{\pi^{1/2}}\int_0^\infty du\, u^2\exp\left(-u^2\right)\int_{-1}^{1} dx \exp\left(-i2\sigma G_j ux\right) = \\ &= \frac{2}{\pi^{1/2}\sigma G_j}\int_0^\infty du\, u \exp\left(-u^2\right)\sin(2\sigma G_j u) = \exp(-G_j^2\sigma^2) \ ,\end{aligned}$$

thus,

$$\rho_I(\mathbf{G}_j) = \frac{1}{V}\sum_{\mu} Q_\mu \exp\left(-i\mathbf{G}_j\mathbf{a}_\mu\right)\exp(-G_j^2\sigma^2) \; . \tag{6.73}$$

Consequently,

$$V_I(\mathbf{G}_j) = -\frac{8\pi}{V}\sum_{\mu} Q_\mu \frac{\exp\left(-i\mathbf{G}_j\mathbf{a}_\mu\right)\exp(-G_j^2\sigma^2)}{\mathbf{G}_j^2} \; , \tag{6.74}$$

and

$$V_I(\mathbf{r}) = -\frac{4\pi}{V}\sum_{\mu} 2Q_\mu \sum_{\substack{j\\(\mathbf{G}_j\neq\mathbf{0})}} \frac{\exp\left(i\mathbf{G}_j\cdot(\mathbf{r}-\mathbf{a}_\mu)\right)\exp(-G_j^2\sigma^2)}{\mathbf{G}_j^2} \; . \tag{6.75}$$

Therefore, we obtain

$$V(\mathbf{r}) = \sum_{\nu} 2Q_\nu \left\{ -\frac{4\pi}{V}\sum_{\substack{j\\(\mathbf{G}_j\neq\mathbf{0})}} \frac{\exp\left(i\mathbf{G}_j(\mathbf{r}-\mathbf{a}_\nu)\right)\exp(-G_j^2\sigma^2)}{\mathbf{G}_j^2} + \sum_{n}\frac{\operatorname{erfc}(\left|\mathbf{r}-\mathbf{a}_\nu-\mathbf{T}_n\right|/2\sigma)}{\left|\mathbf{r}-\mathbf{a}_\nu-\mathbf{T}_n\right|} + C \right\} \; , \tag{6.76}$$

where, in order to ensure independence of the ν-like terms from the parameter σ, $C = -\frac{4\pi\sigma^2}{V}$ has to be chosen. Replacing $\mathbf{r}$ by $\mathbf{r}+\mathbf{a}_\mu$ and comparing with eq. (6.60), the expression of $G_{\mu\nu}(\mathbf{r})$ is identical to the ones in the previous sections.

6.5.2 Derivation of the Madelung constants

According to (6.29), for small r, the $D_{i,\mu\nu}(\mathbf{r})$ ($i = 1,2,3$) have to be expanded as

$$D_{i,\mu\nu}(\mathbf{r}) = \sum_{L} D_{i,\mu\nu}^{L} r^\ell Y_L(\widehat{\mathbf{r}}) \; . \tag{6.77}$$

(The expansion in r and r' follows from the one of $|\mathbf{r}-\mathbf{r}'|$) Conveniently, this is done by performing the following operation

$$D_{i,\mu\nu}^{L} = \lim_{r\to 0}\left(\frac{1}{r^\ell}\int d\widehat{\mathbf{r}} D_{i,\mu\nu}(\mathbf{r}) Y_L^*(\widehat{\mathbf{r}})\right) \; . \tag{6.78}$$

(The limit $r \to 0$ is necessary because the relation is only strictly valid for small r).

Derivation of the reciprocal sum component $D_{1,\mu\nu}^{L}$

Inserting the identity (A.50) into eq. (6.54) yields

$$\int d\widehat{\mathbf{r}} D_{1,\mu\nu}(\mathbf{r}) Y_L^*(\widehat{\mathbf{r}}) = \tag{6.79}$$

$$= \frac{(4\pi)^2 i^\ell}{V}\sum_{\substack{j\\(\mathbf{G}_j\neq\mathbf{0})}} j_\ell(G_j r) Y_L^*(\widehat{\mathbf{G}}_j)\exp(i\mathbf{G}_j\mathbf{a}_{\mu\nu})\frac{\exp(-\mathbf{G}_j^2\sigma^2)}{\mathbf{G}_j^2} - \delta_{L,00}\frac{(4\pi)^{3/2}\sigma^2}{V} \; . \tag{6.80}$$

Recalling that

$$\lim_{z\to 0} j_\ell(z) = \frac{z^\ell}{(2\ell+1)!!} = \frac{\sqrt{\pi}}{2^{\ell+1}\Gamma(\ell+\frac{3}{2})} z^\ell \ , \tag{6.81}$$

one gets

$$D^L_{1,\mu\nu} = \frac{(4\pi)^2\sqrt{\pi}\, i^\ell}{V 2^{\ell+1}\Gamma(\ell+\frac{3}{2})} \sum_{\substack{j \\ (\mathbf{G}_j\neq\mathbf{0})}} Y^*_L(\widehat{\mathbf{G}}_j)\exp(i\mathbf{G}_j\mathbf{a}_{\mu\nu}) G_j^{\ell-2}\exp(-\mathbf{G}_j^2\sigma^2) - \delta_{L,00}\frac{(4\pi)^{3/2}\sigma^2}{V} \ . \tag{6.82}$$

At the evaluation one should exploit the (l,m) symmetries.

Derivation of the direct sum component $D^L_{2,\mu\nu}$

In order to evaluate $D^L_{2,\mu\nu}$ we return to the integral representation of the erfc function (see eq. (6.49)),

$$D_{2,\mu\nu}(\mathbf{r}) = \frac{2}{\sqrt{\pi}} \sum_{\substack{n \\ (\mathbf{T}_n-\mathbf{a}_{\mu\nu}\neq\mathbf{0})}} \int_{1/2\sigma}^{\infty} dx \exp(-\left|\mathbf{r}+\mathbf{a}_{\mu\nu}-\mathbf{T}_n\right|^2 x^2) \ , \tag{6.83}$$

and expand the integrand as follows (with complex continuation of (A.50))

$$\begin{aligned} \exp(-\left|\mathbf{r}+\mathbf{a}_{\mu\nu}-\mathbf{T}_n\right|^2 x^2) &= \exp(-r^2x^2)\exp(-\left|\mathbf{a}_{\mu\nu}-\mathbf{T}_n\right|^2 x^2)\exp(-2\mathbf{r}(\mathbf{a}_{\mu\nu}-\mathbf{T}_n)x^2) \\ &= \exp(-r^2x^2)\exp(-\left|\mathbf{a}_{\mu\nu}-\mathbf{T}_n\right|^2 x^2)\times \\ &\quad 4\pi\sum_L i^\ell j_\ell(i2r\left|\mathbf{a}_{\mu\nu}-\mathbf{T}_n\right| x^2) Y^*_L(\widehat{\mathbf{a}_{\mu\nu}-\mathbf{T}_n}) Y_L(\widehat{\mathbf{r}}) \ . \end{aligned}$$

We then get (the dx integral is still convergent even that $j_l(ix)$ is exponentially increasing with x)

$$\begin{aligned} \int d\widehat{r} D_{2,\mu\nu}(\mathbf{r}) Y^*_L(\widehat{\mathbf{r}}) &= 8\sqrt{\pi} i^\ell \sum_{|\mathbf{a}_\mu-\mathbf{a}_\nu-\mathbf{T}_n|\neq 0} Y^*_L(\widehat{\mathbf{a}_{\mu\nu}-\mathbf{T}_n})\times \\ \times \int_{1/2\sigma}^{\infty} & dx\, j_\ell(i2r\left|\mathbf{a}_{\mu\nu}-\mathbf{T}_n\right| x^2)\exp(-r^2x^2)\exp(-\left|\mathbf{a}_{\mu\nu}-\mathbf{T}_n\right|^2 x^2) \ , \end{aligned} \tag{6.84}$$

and, consequently, by taking $\lim_{r\to 0}\frac{1}{r^\ell}$ we get

$$\begin{aligned} D^L_{2,\mu\nu} &= \frac{4\pi(-1)^\ell}{\Gamma(\ell+\frac{3}{2})} \sum_{|\mathbf{a}_\mu-\mathbf{a}_\nu-\mathbf{T}_n|\neq 0} Y^*_L(\widehat{\mathbf{a}_{\mu\nu}-\mathbf{T}_n})\left|\mathbf{a}_{\mu\nu}-\mathbf{T}_n\right|^\ell \int_{1/2\sigma}^{\infty} dx\, x^{2\ell}\exp(-\left|\mathbf{a}_{\mu\nu}-\mathbf{T}_n\right|^2 x^2) = \\ &= \frac{4\pi(-1)^\ell}{\Gamma(\ell+\frac{3}{2})} \sum_{\substack{n \\ (\mathbf{T}_n-\mathbf{a}_{\mu\nu}\neq\mathbf{0})}} \frac{Y^*_L(\widehat{\mathbf{a}_{\mu\nu}-\mathbf{T}_n})}{\left|\mathbf{a}_{\mu\nu}-\mathbf{T}_n\right|^{\ell+1}} \int_{|\mathbf{a}_{\mu\nu}-\mathbf{T}_n|/2\sigma}^{\infty} dx\, x^{2\ell}\exp(-x^2) \ , \end{aligned} \tag{6.85}$$

or, introducing the incomplete gamma function according to eq. (A.65)

$$D^L_{2,\mu\nu} = \frac{2\pi(-1)^\ell}{\Gamma(\ell+\frac{3}{2})} \sum_{\substack{n \\ (\mathbf{T}_n-\mathbf{a}_{\mu\nu}\neq\mathbf{0})}} Y^*_L(\widehat{\mathbf{a}_{\mu\nu}-\mathbf{T}_n}) \frac{\Gamma(\ell+\frac{1}{2}, \left|\mathbf{a}_{\mu\nu}-\mathbf{T}_n\right|^2/4\sigma^2)}{\left|\mathbf{a}_{\mu\nu}-\mathbf{T}_n\right|^{\ell+1}} \ . \tag{6.86}$$

From eq. (6.56) one easily derives

$$\underline{D^L_{3,\mu\nu} = -\delta_{\mu\nu}\delta_{L,00}\frac{2}{\sigma}\,.} \tag{6.87}$$

The 3D Madelung constants $A^{LL'}_{\mu\nu}$ are obtained from eq. (6.33) when replacing $G^L_{\mathbf{RR'}}$ by

$$\underline{G^L_{\mu\nu} = D^L_{1,\mu\nu} + D^L_{2,\mu\nu} + D^L_{3,\mu\nu}}\,. \tag{6.88}$$

With the reduced 3D Madelung constants $G^L_{\mu\nu}$ the potential can be written as

$$\underline{V_\mu(\mathbf{x}) = \sum_L \frac{4\pi}{\Gamma(\ell+\frac{3}{2})}\left(\sum_{L'} \frac{(-1)^{\ell'}\Gamma(\ell+\ell'+\frac{3}{2})}{\Gamma(\ell'+\frac{1}{2})}\mathcal{C}^{\ell'm'}_{\ell m,(\ell+\ell')(m'-m)}\left(\sum_\nu G^{\ell+\ell',m'-m}_{\mu\nu}Q^{L'}_\nu\right)\right)^* r^\ell Y_L(\hat{\mathbf{x}})} \tag{6.89}$$

The expansion coefficients in spherical harmonics are therefore given by

$$\underline{V_{\mu,lm}(r) = \frac{4\pi}{\Gamma(\ell+\frac{3}{2})}\left(\sum_{L'} \frac{(-1)^{\ell'}\Gamma(\ell+\ell'+\frac{3}{2})}{\Gamma(\ell'+\frac{1}{2})}\mathcal{C}^{\ell'm'}_{\ell m,(\ell+\ell')(m'-m)}\left(\sum_\nu G^{\ell+\ell',m'-m}_{\mu\nu}Q^{L'}_\nu\right)\right)^* r^\ell} \tag{6.90}$$

Since the intercell potential $V_\mu(\mathbf{x})$ is real, one only needs to evaluate (6.90) for $m \geq 0$ and use the relation

$$V_{\mu,l-m}(r) = (-1)^m\left(V_{\mu,l-m}(r)\right)^* \tag{6.91}$$

Because the multipole moments Q^{lm}_ν and the reduced Madelung constants $G^{lm}_{\mu\nu}$ fulfill the selection rules, also the intercell potential fulfills all the (lm) selection rules explained before in (1).

It should be noted that the Madelung constants $G^L_{\mu,\nu}$ depend (also in the bulk case) on the choice of the coordinate system and have to be transformed for comparison between two different coordinate systems. If one calculates the same bulk structure with two different choices of the coordinate system one gets Madelung constants $G^L_{\mu\nu}, \tilde{G}^L_{\mu\nu}$ which have to fulfill the condition

$$\sum_{m=-l}^{l}\left|G^{lm}_{\mu\nu}\right|^2 = \sum_{m=-l}^{l}\left|\tilde{G}^{lm}_{\mu\nu}\right|^2 \tag{6.92}$$

$$G^{00}_{\mu\nu} = \tilde{G}^{00}_{\mu\nu} \tag{6.93}$$

In case one is only interested in a ASA potential, we get

$$\underline{V_{ASA,\mu} = V_\mu(\mathbf{0}) = \sum_{L'}(-1)^{\ell'}\frac{2\ell'+1}{\sqrt{\pi}}\left(\sum_\nu G^{\ell',m'}_{\mu\nu}Q^{L'}_\nu\right)} \tag{6.94}$$

Note that again also here we need all reduced Madelung constants and all multipole moments. Increasing the number of considered multipole moments in an ASA calculation therefore already improves the results.

6.6 Complex 2D lattice - structures with surfaces

We have a structure with translational lattice vectors $\mathbf{T}_n \in \mathcal{L}^2$ and non equivalent atomic positions $\mathbf{c}_p$ such that a general atomic position is given by

$$\mathbf{R}_{np} = \mathbf{T}_n + \mathbf{c}_p,\ (\mathbf{T}_n \in \mathcal{L}^2,\ \mathbf{c}_p \notin \mathcal{L}^2), \rho_{\mathbf{R}_{np}}(\mathbf{r}) = \rho_p(\mathbf{r})$$

Note that the lattice vectors $\mathbf{T}_n$ have no components perpendicular to the planes

$$\mathbf{T}_n = \mathbf{T}_{n\|} + \mathbf{T}_{n\perp} = \mathbf{T}_{n\|}\ ,$$

whereas $\mathbf{c}_p$ are, in general, 3D vectors also with components in plane

$$\mathbf{c}_p = \mathbf{c}_{p\|} + \mathbf{c}_{p\perp}\ .$$

Note that we do not demand that the atomic positions give rise to a *3D parent lattice.* The case of a 2D *complex structure* with more than 1 non equivalent atom in one plane is, however, obviously included if one allows $c_{p\perp} - c_{q\perp} = 0$ for $(p \neq q)$.

6.6.1 Evaluation of the Green function

The potential depends only on the layer index p,

$$V_p(\mathbf{r}) = V(\mathbf{c}_p+\mathbf{r}) = 2\sum_q \int_{\Omega_q} d^3r' G_{pq}(\mathbf{r},\mathbf{r}')\rho_q(\mathbf{r}') \qquad (\mathbf{r} \in \Omega_p), \tag{6.95}$$

where $G_{pq}(\mathbf{r},\mathbf{r}')$ is given by the following lattice sum ($\sum_n$ means now $\sum_{n\in Z^2}$)

$$G_{pq}(\mathbf{r},\mathbf{r}') = \sum_{\substack{n \\ (\mathbf{T}_n+\mathbf{c}_q-\mathbf{c}_p\neq\mathbf{0})}} G_0(\mathbf{r}+\mathbf{c}_p, \mathbf{r}'+\mathbf{T}_n+\mathbf{c}_q) = D_{pq}(\mathbf{r},\mathbf{r}') - \delta_{pq}G_0(\mathbf{r},\mathbf{r}')\ . \tag{6.96}$$

$D_{pq}(\mathbf{r},\mathbf{r}')$ is then defined as

$$D_{pq}(\mathbf{r},\mathbf{r}') = \sum_n G_0(\mathbf{r}+\mathbf{c}_p, \mathbf{r}'+\mathbf{T}_n+\mathbf{c}_q) = D(\mathbf{r}+\mathbf{c}_p-\mathbf{r}'-\mathbf{c}_q)\ , \tag{6.97}$$

where, by using the notation $\mathbf{r} = (\mathbf{r}_\|, z)$, one can write

$$D(\mathbf{r}) = \frac{2}{\sqrt{\pi}}\sum_n \int_0^\infty dx \exp(-\left|\mathbf{r}-\mathbf{T}_n\right|^2 x^2)\ = \tag{6.98}$$

$$= \frac{2}{\sqrt{\pi}} \int_0^\infty dx \exp(-z^2x^2) \underbrace{\sum_n \exp(-\left|\mathbf{r}_\|-\mathbf{T}_n\right|^2 x^2)}_{=\frac{\pi}{Ax^2}\sum_j \exp\left(-\mathbf{G}_j^2/4x^2+i\mathbf{G}_j\mathbf{r}_\|\right)} \tag{6.99}$$

$$= \frac{2\sqrt{\pi}}{A}\sum_j \left(\exp\left(i\mathbf{G}_j\mathbf{r}_\|\right)\int_0^\infty dx\frac{1}{x^2}\exp\left(-z^2x^2-\mathbf{G}_j^2/4x^2\right)\right)\ , \tag{6.100}$$

with the $\mathbf{G}_j$ being 2D reciprocal lattice vectors and A the area of the 2D unit cell (we used again the identity (A.63)). For the case of $\mathbf{G}_j \neq \mathbf{0}$ the integral in (6.100) can be performed (see eq.(A.75)), while for $\mathbf{G}_j = \mathbf{0}$ it is divergent. It will be shown, however, that this term corresponds to a one-dimensional (normal to planes) Poisson equation and all other terms vanish for $z \to \pm\infty$. Thus, the $G_j = 0$ term has to be treated separately and used for imposing appropriate boundary conditions for the potential in $z \to \pm\infty$. Therefore, as what follows, we exclude the $G_j = 0$ term from eq. (6.100),

$$D(\mathbf{r}) = \frac{2\sqrt{\pi}}{A} \sum_{\substack{j \\ (\mathbf{G}_j \neq \mathbf{0})}} \exp\left(i\mathbf{G}_j\mathbf{r}_\parallel\right) \int_0^\infty dx \frac{1}{x^2} \exp(-z^2x^2 - \mathbf{G}_j^2/4x^2) = \tag{6.101}$$

$$= \frac{2\pi}{A} \sum_{\substack{j \\ (\mathbf{G}_j \neq \mathbf{0})}} \frac{1}{G_j} \exp\left(i\mathbf{G}_j\mathbf{r}_\parallel\right) \exp(-G_j\,|z|)\ . \tag{6.102}$$

It is obvious that (6.102) converges very slowly for small z, especially for $z = 0$, therefore, similar to the 3D case, we split the integral in (6.101) into,

$$D(\mathbf{r}) = D_1(\mathbf{r}) + D_2(\mathbf{r})\ , \tag{6.103}$$

where

$$D_1(\mathbf{r}) = \frac{2\sqrt{\pi}}{A} \sum_{\substack{j \\ (\mathbf{G}_j \neq \mathbf{0})}} \exp\left(i\mathbf{G}_j\mathbf{r}_\parallel\right) \int_0^{1/2\sigma} dx \frac{1}{x^2} \exp(-z^2x^2 - \mathbf{G}_j^2/4x^2)\ , \tag{6.104}$$

$$D_2(\mathbf{r}) = \frac{2\sqrt{\pi}}{A} \sum_{\substack{j \\ (\mathbf{G}_j \neq \mathbf{0})}} \exp\left(i\mathbf{G}_j\mathbf{r}_\parallel\right) \int_{1/2\sigma}^\infty dx \frac{1}{x^2} \exp(-z^2x^2 - \mathbf{G}_j^2/4x^2)\ . \tag{6.105}$$

It is easy to see that the infinite sum involved in $D_1(\mathbf{r})$ is well-converging,

$$|D_1(\mathbf{r})| \leq \frac{2\sqrt{\pi}}{A} \sum_{\substack{j \\ (\mathbf{G}_j \neq \mathbf{0})}} \int_0^{1/2\sigma} dx \frac{1}{x^2} \exp(-\mathbf{G}_j^2/4x^2) = \frac{2\pi}{A} \sum_{\substack{j \\ (\mathbf{G}_j \neq \mathbf{0})}} \frac{1}{G_j} \mathrm{erfc}(G_j\sigma) < \infty\ , \tag{6.106}$$

in particular,

$$D_1(\mathbf{r}_\parallel, z = 0) = \frac{2\pi}{A} \sum_{\substack{j \\ (\mathbf{G}_j \neq \mathbf{0})}} \frac{1}{G_j} \exp\left(i\mathbf{G}_j\mathbf{r}_\parallel\right) \mathrm{erfc}(G_j\sigma)\ . \tag{6.107}$$

By changing the variable of integration in the integral ($y = \frac{1}{x^2}$) on the right hand side of (6.104) one can also write,

$$D_1(\mathbf{r}) = \frac{\sqrt{2\pi}}{A} \sum_{\substack{j \\ (\mathbf{G}_j \neq \mathbf{0})}} \exp\left(i\mathbf{G}_j\mathbf{r}_\parallel\right) \int_{2\sigma^2}^\infty y^{-\frac{1}{2}} \exp\left(-\frac{1}{2}(z^2/y + \mathbf{G}_j^2 y)\right) dy\ . \tag{6.108}$$

In order to return to the real-lattice summation in (6.105) the $G_j = 0$ term has to be added and subtracted,

$$D_2(\mathbf{r}) = \frac{2\sqrt{\pi}}{A}\int_{1/2\sigma}^{\infty} dx\,\exp(-z^2x^2)\underbrace{\frac{1}{x^2}\sum_j \exp\left(i\mathbf{G}_j\mathbf{r}_{\|} - \mathbf{G}_j^2/4x^2\right)+}_{=\frac{A}{\pi}\sum_n \exp(-\left|\mathbf{r}_{\|}-\mathbf{T}_n\right|^2x^2)} \tag{6.109}$$

$$-\frac{2\sqrt{\pi}}{A}\int_{1/2\sigma}^{\infty} dx\frac{1}{x^2}\exp(-z^2x^2),$$

therefore,

$$D_2(\mathbf{r}) = \sum_n \frac{1}{|\mathbf{r}-\mathbf{T}_n|}\operatorname{erfc}(|\mathbf{r}-\mathbf{T}_n|/2\sigma) - \frac{2\sqrt{\pi}}{A}\int_{1/2\sigma}^{\infty} dx\frac{1}{x^2}\exp(-z^2x^2)\ . \tag{6.110}$$

Due to eq. (A.81) the second term on the right hand side proves to be

$$-\frac{2\sqrt{\pi}}{A}\int_{1/2\sigma}^{\infty} dx\frac{1}{x^2}\exp(-z^2x^2) = -\frac{4\sqrt{\pi}\sigma}{A}\exp\left(-\frac{z^2}{4\sigma^2}\right) - \frac{2\pi|z|}{A}\operatorname{erf}\left(\frac{|z|}{2\sigma}\right) + \frac{2\pi|z|}{A}\ . \tag{6.111}$$

Without the $\mathbf{G}_j = 0$ contribution, the Green function for a 2D translational invariant system can then be written as

$$G_{pq}(\mathbf{r},\mathbf{r}') = D_{1,pq}(\mathbf{r}-\mathbf{r}') + D_{2a,pq}(\mathbf{r}-\mathbf{r}') + D_{2b,pq}(\mathbf{r}-\mathbf{r}') + D_{3,pq}(\mathbf{r}-\mathbf{r}')\ , \tag{6.112}$$

where

$$D_{1,pq}(\mathbf{r}) = \frac{\sqrt{2\pi}}{A}\sum_{\substack{j\\(\mathbf{G}_j\neq\mathbf{0})}} \exp\left(i\mathbf{G}_j\mathbf{r}_{\|}\right)\exp\left(i\mathbf{G}_j\mathbf{c}_{pq\|}\right)\int_{2\sigma^2}^{\infty} y^{-\frac{1}{2}}\exp\left(-\frac{1}{2}\left[(z+c_{pq\perp})^2/y + \mathbf{G}_j^2y\right]\right)dy\ , \tag{6.113}$$

$$D_{2a,pq}(\mathbf{r}) = \sum_{\substack{n\\(\mathbf{T}_n-\mathbf{c}_{pq}\neq\mathbf{0})}} \frac{1}{|\mathbf{r}+\mathbf{c}_{pq}-\mathbf{T}_n|}\operatorname{erfc}(|\mathbf{r}+\mathbf{c}_{pq}-\mathbf{T}_n|/2\sigma) \tag{6.114}$$

$$D_{2b,pq}(\mathbf{r}) = -\left(1-\delta_{c_{pq\perp},0}\right)\frac{2\sqrt{\pi}}{A}\int_{1/2\sigma}^{\infty} dx\frac{1}{x^2}\exp(-\left(z+c_{pq\perp}\right)^2x^2) \tag{6.115}$$

$$-\delta_{c_{pq\perp},0}\left(\frac{4\sqrt{\pi}\sigma}{A}\exp\left(-\frac{z^2}{4\sigma^2}\right) + \frac{2\pi|z|}{A}\operatorname{erf}\left(\frac{|z|}{2\sigma}\right)\right) \tag{6.116}$$

$$D_{3,pq}(\mathbf{r}) = \delta_{pq}\frac{1}{|\mathbf{r}|}\left(\operatorname{erfc}\left(\frac{|\mathbf{r}|}{2\sigma}\right)-1\right) = -\delta_{pq}\frac{\operatorname{erf}(|\mathbf{r}|/2\sigma)}{|\mathbf{r}|}\ , \tag{6.117}$$

and we introduced the notation $\mathbf{c}_{pq} = \mathbf{c}_p - \mathbf{c}_q$. Note that the term $\delta_{c_{pq\perp},0}\frac{2\pi|z|}{A}$ in (6.116) has been passed to the $\mathbf{G}_j = 0$ contribution of the Green function to be discussed in the next section, leading there to a new term D_0.

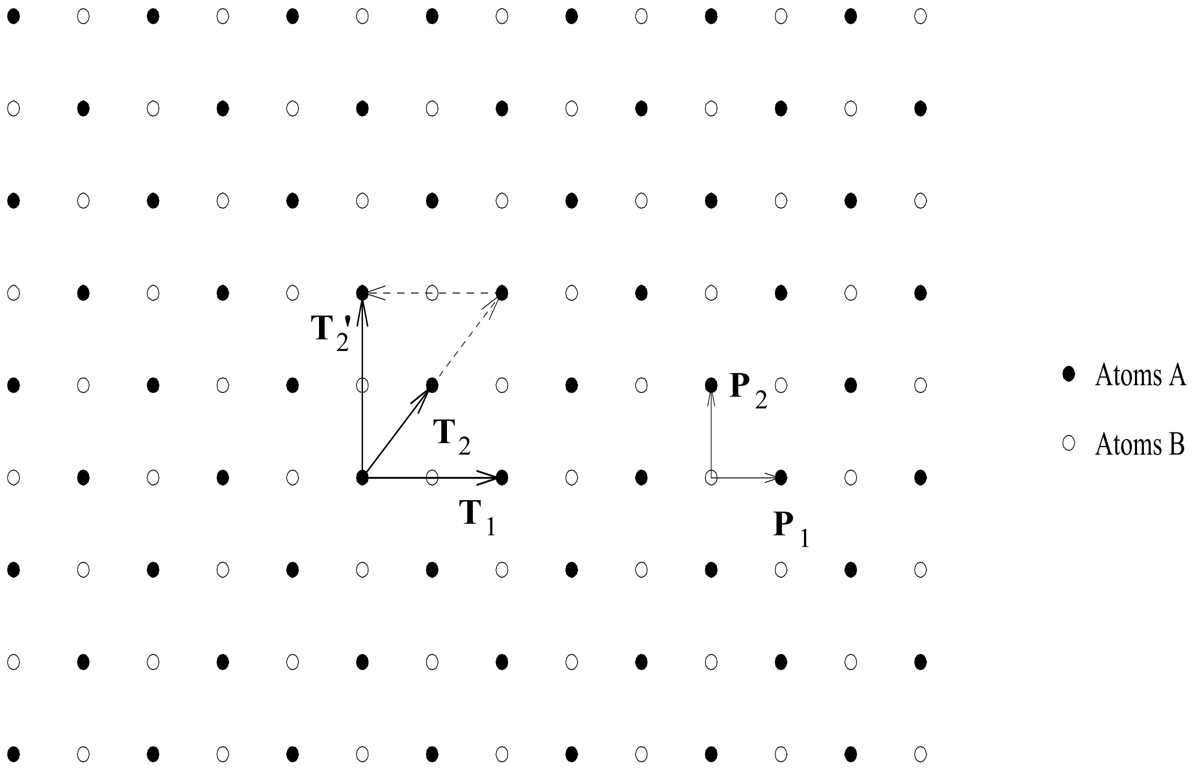

Figure 6.1: We have a structure with 2 non equivalent atoms per unit cell.
The lattice $\mathcal{L} = \{n_1\mathbf{T}_1 + n_2\mathbf{T}_2 : n_1, n_2 \in \mathbb{Z}\}$ contains exactly all translational symmetries of the system. All atomic positions are given by $\mathbf{a}_\mu + \mathbf{T}_n, \mu \in \{1,2\}\,,\, n \in \mathbb{Z}^2$
The parent lattice $\mathcal{P} = \{n_1\mathbf{P}_1 + n_2\mathbf{P}_2 : n_1, n_2 \in \mathbb{Z}\}$ is only fictitious, it does not only contain translational symmetries of the system. It could be described as 'the lattice formed by all atomic positions'. All atomic positions are given by $\mathbf{P}_n, n \in \mathbb{Z}^2$.
The lattice $\mathcal{L}' = \{n_1\mathbf{T}_1 + n_2\mathbf{T}'_2 : n_1, n_2 \in \mathbb{Z}\}$ is a sublattice (subgroup) of $\mathcal{L}$, which contains only (but not all) translational symmetries of the system. All atomic positions are given by $\mathbf{a}_{\mu,i} + \mathbf{T}'_n, \mu \in \{1,2\}\,, i \in \{0,1\}\; n \in \mathbb{Z}^2$, $\mathbf{a}_{\mu,i} = \mathbf{a}_\mu + i\;\mathbf{T}_2$.

The $\mathbf{G}_j = \mathbf{0}$ contribution

Special Case of a 3D translational symmetry In principle we could have had a 3D translational symmetry but have only exploited the 2D symmetry so far.

This paragraph explains how we can regain the 3D symmetry in this special case. Note that **this formalism is only possible**, if we have a **system** which indeed does **have 3D lattice translational symmetry**, not only a 3D parent lattice in a system which only has 2D translational symmetry (see Fig. 6.1).

In a 3D symmetry system where the crystal structure is given by

$$\mathbf{a}_\mu + \mathbf{T}_n : n \in \mathbb{Z}^3, \mu \in \{1, \ldots, n_{atom}\} \ ,$$

with $\mathbf{T}_n \in \mathcal{L}^3$ and $\mathbf{a}_\mu$ the non equivalent atomic positions in the unit cell, we can choose a Bravais-matrix $(\mathbf{T}_1, \mathbf{T}_2, \mathbf{T}_3)$,

$$\mathcal{L}^3 = \{n_1\mathbf{T}_1 + n_2\mathbf{T}_2 + n_3\mathbf{T}_3 : n_1, n_2, n_3 \in \mathbb{Z}\} \ ,$$

such that $T_{1,\perp} = T_{2,\perp} = 0$ and $\mathbf{T}_3 = \mathbf{T}_{3,\parallel} + T_{3,\perp}\widehat{\mathbf{z}}$, $T_{3,\perp} = d$, where d is the minimum lattice translational length in the z (normal) direction. The 2D lattice is formed by definition by $(\mathbf{T}_1, \mathbf{T}_2)$

$$\mathcal{L}^2 = \{n_1\mathbf{T}_1 + n_2\mathbf{T}_2 : n_1, n_2 \in \mathbb{Z}\}$$

Suppose there exists a $N \in \mathbb{N}$ and a 2D lattice vector $\mathbf{T}_\parallel$ such that $N\,\mathbf{T}_{3,\parallel} = \mathbf{T}_\parallel$ then

$$\mathbf{T}_3' = N\,\mathbf{T}_3 - \mathbf{T}_\parallel = N\,d\,\widehat{\mathbf{z}}.$$

Then by repeating N-times the unit cell and defining the new Bravais-matrix $(\mathbf{T}_1', \mathbf{T}_2', \mathbf{T}_3')$ with $\mathbf{T}_1' = \mathbf{T}_1$, $\mathbf{T}_2' = \mathbf{T}_2$ and $\mathbf{T}_3' = N\,d\,\widehat{\mathbf{z}}$ we have a new lattice (a subgroup of $\mathcal{L}^3$)

$$\mathcal{L}'^3 = \{n_1\mathbf{T}_1' + n_2\mathbf{T}_2' + n_3\mathbf{T}_3' : n_1, n_2, n_3 \in \mathbb{Z}\}\,.$$

But we need a bigger basis of the crystal structure, namely $n_{atom} \cdot N$ atoms, to describe the same crystal structure, the basis vectors are given by

$$\mathbf{a}_{i\mu} = \mathbf{a}_\mu + i\mathbf{T}_3 \ \ (i = 0, 1, 2, \ldots, N-1) \ .$$

The corresponding reciprocal lattice vectors of $\mathcal{L}'^3$ can be written as

$$\mathbf{G}' = \mathbf{G}_j + (2\pi k/Nd)\,\widehat{\mathbf{z}} \qquad \left(j \in \mathbb{Z}^2, k \in \mathbb{Z}\right)$$

with $\mathbf{G}_j$ the 2D reciprocal lattice vectors. We then recall the expression of the 3D Greens function $(\sigma = 0)$

$$G'_{ij,\mu\nu}(\mathbf{r}, \mathbf{r}') = \frac{4\pi}{NV} \sum_{\mathbf{G}' \neq \mathbf{0}} \frac{\exp\left(i\mathbf{G}'\left[\mathbf{r} - \mathbf{r}' + \mathbf{a}_{\mu\nu} + (i-j)\,\mathbf{T}_3\right]\right)}{\mathbf{G}'^2} \quad , \tag{6.118}$$

which is related to the Greens function of the original lattice by

$$G_{\mu\nu}(\mathbf{r}, \mathbf{r}') = \sum_{t=1}^{N} G'_{0t,\mu\nu}(\mathbf{r}, \mathbf{r}') = \frac{4\pi}{NV} \sum_{t=1}^{N} \sum_{\mathbf{G}' \neq \mathbf{0}} \frac{\exp\left(i\mathbf{G}'\left[\mathbf{r} - \mathbf{r}' + \mathbf{a}_{\mu\nu} - t\mathbf{T}_3\right]\right)}{\mathbf{G}'^2} \quad . \tag{6.119}$$

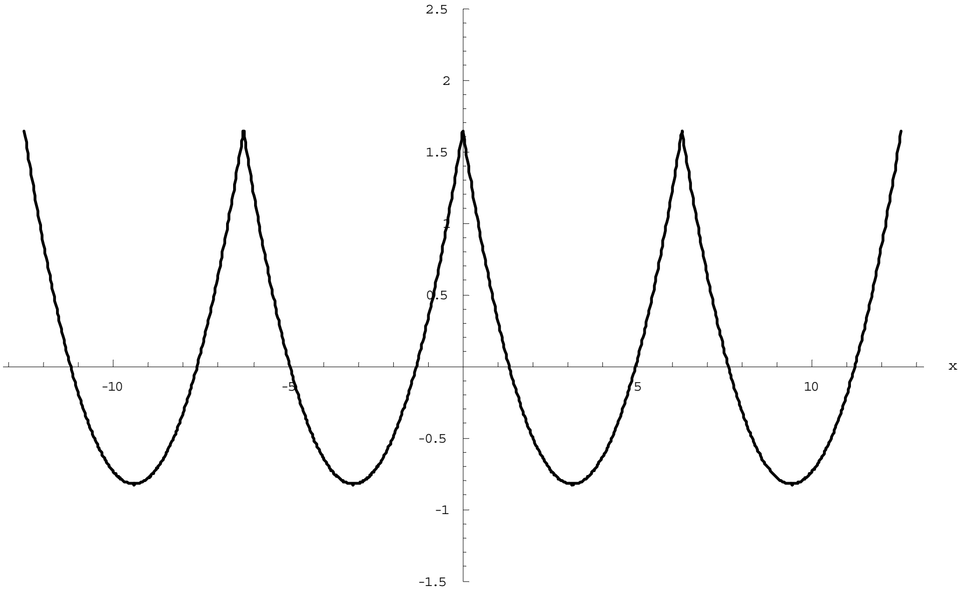

Figure 6.2: The periodic continuation of the function $f(x) = \frac{3x^2 - 6\pi x + 2\pi^2}{12}, x \in [0, 2\pi]$.

Taking the $\mathbf{G}_j = \mathbf{0}$ contribution yields

$$
\begin{aligned}
D_{0,\mu\nu}(\mathbf{r}) &= \frac{4\pi}{NV} \sum_{t=1}^{N} \sum_{k \in \mathbb{Z} \backslash \{0\}} \frac{\exp\left(i\left(2\pi k/Nd\right)\left[z + a_{\mu\nu\perp} - td\right]\right)}{\left(2\pi k/Nd\right)^2} = \\
&= \frac{Nd}{A\pi} \sum_{t=1}^{N} \sum_{k \in \mathbb{Z} \backslash \{0\}} \frac{\exp\left(i\left(2\pi k/Nd\right)\left[z + a_{\mu\nu\perp} - td\right]\right)}{k^2} = \\
&= \frac{2Nd}{A\pi} \sum_{t=1}^{N} \sum_{k=1}^{\infty} \frac{\cos\left(k \frac{2\pi\left(td - \left|z + a_{\mu\nu\perp}\right|\right)}{Nd}\right)}{k^2} \quad .
\end{aligned}
\tag{6.120}
$$

With ([16], formula 1.443.3.) for $0 \leq x \leq 2\pi$ (otherwise one needs the 2π periodic continuation of the polynomial, see Fig.6.2)

$$
\sum_{k=1}^{\infty} \frac{\cos(kx)}{k^2} = \frac{3x^2 - 6\pi x + 2\pi^2}{12} \, , \tag{6.121}
$$

$$\begin{aligned}
D_{0,\mu\nu}(\mathbf{r}) &= \frac{Nd}{6A\pi}\sum_{t=1}^{N}\left(\frac{12\pi^2}{N^2d^2}\left(td-|z+a_{\mu\nu\perp}|\right)^2-\frac{12\pi^2}{Nd}\left(td-|z+a_{\mu\nu\perp}|\right)+2\pi^2\right)= \\
&= \frac{Nd}{6A\pi}\sum_{t=1}^{N}\left(\frac{12\pi^2}{N^2d^2}\left(z+a_{\mu\nu\perp}\right)^2+\frac{12\pi^2}{N^2}t^2-\frac{24\pi^2}{N^2d}\left|z+a_{\mu\nu\perp}\right|t-\frac{12\pi^2}{N}t+\frac{12\pi^2}{Nd}\left|z+a_{\mu\nu\perp}\right|+2\pi^2\right)= \\
&= \frac{\pi}{A}\left(\frac{2}{d}\left(z+a_{\mu\nu\perp}\right)^2-2\left|z+a_{\mu\nu\perp}\right|\right)+\frac{2d\pi}{NA}\underbrace{\sum_{t=1}^{N}\left(t^2-Nt+\frac{N^2}{6}\right)}_{\frac{2N^3+3N^2+N}{6}-\frac{N^2(N+1)}{2}+\frac{N^3}{6}}= \\
&= \frac{\pi}{A}\left(\frac{2}{d}\left(z+a_{\mu\nu\perp}\right)^2-2\left|z+a_{\mu\nu\perp}\right|+\frac{d}{3}\right)\quad . \qquad (6.122)
\end{aligned}$$

Taking into account also the term missing from eq. (6.116)

$$D_{0,\mu\nu}(\mathbf{r}) = \frac{\pi}{A}\left(\frac{2}{d}\left(z+a_{\mu\nu\perp}\right)^2-2\left|z+a_{\mu\nu\perp}\right|\left(1-\delta_{a_{\mu\nu\perp},0}\right)+\frac{d}{3}\right)\quad . \qquad (6.123)$$

The general case: No translational symmetry in z direction In general our system will not have a further translational symmetry except the 2D lattice, because of e.g. an interface or surface. If we could still define a parent lattice or not is of no importance here.

Inserting the 2D lattice Fourier representation of the potential

$$V(\mathbf{r}) = \sum_j V_{\mathbf{G}_j}(z)\exp(i\mathbf{G}_j\mathbf{r}_\parallel)\ , \qquad (6.124)$$

and the charge density

$$\rho(\mathbf{r}) = \sum_j \rho_{\mathbf{G}_j}(z)\exp(i\mathbf{G}_j\mathbf{r}_\parallel)\ , \qquad (6.125)$$

into eq. (6.1) one gets

$$\left(\frac{d^2}{dz^2}-G_j^2\right)V_{\mathbf{G}_j}(z) = -8\pi\rho_{\mathbf{G}_j}(z)\ , \qquad (6.126)$$

which for $\mathbf{G}_j = \mathbf{0}$ simply reads as

$$\frac{d^2}{dz^2}V_0(z) = -8\pi\rho_0(z)\ , \qquad (6.127)$$

with

$$\rho_0(z) = \rho_{(00)}(z) = \frac{1}{A}\int_{\Omega_{2D}} d^2r_\parallel\,\rho(\mathbf{r}_\parallel, z)\ , \qquad (6.128)$$

where Ω_{2D} denotes the 2D Wigner-Seitz cell having the 2D volume (area) A. The Green function of eq. (6.127) defined as

$$\frac{d^2}{dz^2}\widehat{G}_0(z,z') = -4\pi\delta(z-z')\ , \qquad (6.129)$$

is given by

$$\widehat{G}_0(z,z') = -2\pi\,|z-z'|\ . \tag{6.130}$$

$V_0(z)$ can then be written as

$$V_{(00)}(z) = V_0(z) = 2\int_{-\infty}^{\infty} dz'\widehat{G}_0(z,z')\rho_0(z') + \mathcal{A}\,z + \mathcal{B} \tag{6.131}$$

$$= 2\int_{-\infty}^{\infty} dz' \int_{\Omega_{2D}} d^2r'_{\|}\frac{1}{A}\widehat{G}_0(z,z')\rho(\mathbf{r}') + \mathcal{A}\,z + \mathcal{B} \tag{6.132}$$

$$= 2\sum_q \int_{\Omega_q} d^3r'\frac{1}{A}\widehat{G}_0(z,z')\rho_q(\mathbf{r}') + \mathcal{A}\,z + \mathcal{B}\ , \tag{6.133}$$

where we made use of the 2D translational invariance of $\rho(\mathbf{r})$ and an additional term, $\mathcal{A}\,z+\mathcal{B}$, has been added to the potential which will be used to satisfy appropriate boundary conditions. The expression above is for the global coordinate system, but we have at every atomic position a center of the coordinate system, therefore in analogy to eq. (6.95), for $\mathbf{r}\in\Omega_p$ one can write (with z measured from every $\mathbf{c}_p$)

$$V_{0,p}(z) = V_0(\mathbf{c}_p + z) = 2\sum_q \int_{\Omega_q} d^3r' G_{0,pq}(z,z')\rho_q(\mathbf{r}') + \mathcal{A}\,(z + c_{p\perp}) + \mathcal{B}\ , \tag{6.134}$$

where

$$G_{0,pq}(z,z') = -\frac{2\pi}{A}\,|z - z' + c_{pq\perp}|\ . \tag{6.135}$$

Thus, by adding the term left out from eq. (6.115) one can define

$$D_{0,pq}(z) = -\left(1-\delta_{c_{pq\perp},0}\right)\frac{2\pi}{A}\,|z + c_{pq\perp}|\ , \tag{6.136}$$

from which the only Madelung constants non-vanishing for $|c_{pq\perp}|\to\infty$ can be derived. (See the section for imposing boundary conditions.)

6.6.2 Derivation of the Madelung constants

Again, the expansion coefficients of the function $D_{i,\mu\nu}(\mathbf{r})$ $(i = 0, 1, 2a, 2b, 3)$ are called Madelung constants and are calculated as

$$D^L_{i,pq} = \lim_{r\to 0}\,(\frac{1}{r^\ell}\int d\widehat{r} D_{i,pq}(\mathbf{r})Y^*_L(\widehat{\mathbf{r}})\ ). \tag{6.137}$$

Derivation of the reciprocal sum component $D^L_{1,pq}$

By inserting the following Taylor expansion,

$$\exp\left(-\frac{1}{2}(z+c_{pq\perp})^2/y\right) = \exp\left(-\frac{1}{2}c^2_{pq\perp}/y\right)\exp\left(-\frac{1}{2}(z^2+2zc_{pq\perp})/y\right) =$$

$$= \exp\left(-\frac{1}{2}c^2_{pq\perp}/y\right)\sum_{n=0}^{\infty}\frac{1}{n!}\left(-\frac{1}{2}(z^2+2zc_{pq\perp})\right)^n y^{-n}\ ,$$

into eq. (6.113) yields

$$
\begin{aligned}
D_{1,pq}(\mathbf{r}) \; &= \; \frac{\sqrt{2\pi}}{A} \sum_{\substack{j \\ (\mathbf{G}_j \neq \mathbf{0})}} \exp\left(i\mathbf{G}_j \mathbf{r}_\parallel\right) \exp\left(i\mathbf{G}_j \mathbf{c}_{pq\parallel}\right) \sum_{n=0}^{\infty} \frac{1}{n!} \left(-\frac{1}{2}\right)^n (z^2 + 2zc_{pq\perp})^n \times \\
& \int_{2\sigma^2}^{\infty} y^{-\frac{1}{2}-n} \exp\left(-\frac{1}{2}(c_{pq\perp}^2/y + \mathbf{G}_j^2 y)\right) \, dy \; . \qquad (6.138)
\end{aligned}
$$

Using the notation $\mathbf{r}_\parallel = (r\sin(\Theta)\cos(\phi), r\sin(\Theta)\sin(\phi))$, $z = r\cos(\Theta)$, $\mathbf{G}_j = (G_j\cos(\phi_j), G_j\sin(\phi_j))$, thus, $\mathbf{G}_j\mathbf{r}_\parallel = G_j r\sin(\Theta)\cos(\phi_j - \phi)$, and also the Condon-Shortly phase convention (eq. (A.43)) in

$$
\begin{aligned}
D_{1,pq}^L = \lim_{r\to 0} \frac{1}{r^\ell} \int d\widehat{r} D_{1,pq}(\mathbf{r}) Y_L^*(\widehat{\mathbf{r}}) \; &= \; \frac{i^{m+|m|}}{A} \sqrt{\frac{2\ell+1}{2} \frac{(\ell-|m|)!}{(\ell+|m|)!}} \sum_{\substack{j \\ (\mathbf{G}_j \neq \mathbf{0})}} \exp\left(i\mathbf{G}_j \mathbf{c}_{pq\parallel}\right) \times \\
& \times \sum_{n=0}^{\infty} \frac{1}{n!} \left(-\frac{1}{2}\right)^n \left\{ \int_{2\sigma^2}^{\infty} y^{-\frac{1}{2}-n} \exp\left(-\frac{1}{2}(c_{pq\perp}^2/y + \mathbf{G}_j^2 y)\right) \, dy \right\} \qquad (6.139) \\
& \times \lim_{r\to 0} \frac{1}{r^\ell} \int_0^\pi \sin(\Theta) d\Theta \int_0^{2\pi} d\phi \exp\left(i\mathbf{G}_j \mathbf{r}_\parallel\right) P_\ell^{|m|}(\cos(\Theta)) \exp(-im\phi)(z^2 + 2zc_{pq\perp})^n \; ,
\end{aligned}
$$

the following integral with respect to ϕ occurs (see proof in the Appendix (A.4)),

$$
\int_0^{2\pi} \exp(-im\phi + iG_j r\sin(\Theta)\cos(\phi_j - \phi)) d\phi = 2\pi \, i^{|m|} \exp(-im\phi_j) \, J_{|m|}(G_j r\sin(\Theta)) \; . \qquad (6.140)
$$

Eq. (6.139) can then be written as

$$
\begin{aligned}
D_{1,pq}^L = \frac{2\pi i^{-m}}{A} & \sqrt{\frac{2\ell+1}{2} \frac{(\ell-|m|)!}{(\ell+|m|)!}} \sum_{\substack{j \\ (\mathbf{G}_j \neq \mathbf{0})}} \exp(-im\phi_j) \exp\left(i\mathbf{G}_j \mathbf{c}_{pq\parallel}\right) \times \qquad (6.141) \\
& \times \sum_{n=0}^{\infty} \frac{1}{n!} \left(-\frac{1}{2}\right)^n \left\{ \int_{2\sigma^2}^{\infty} y^{-\frac{1}{2}-n} \exp\left(-\frac{1}{2}(c_{pq\perp}^2/y + \mathbf{G}_j^2 y)\right) \, dy \right\} \lim_{r\to 0} \frac{1}{r^\ell} I_n \; ,
\end{aligned}
$$

where we denoted the integral with respect to Θ by

$$
I_n = \int_0^\pi d\Theta \sin(\Theta) P_\ell^{|m|}(\cos(\Theta)) J_{|m|}(G_j r\sin(\Theta)) (r^2\cos^2(\Theta) + 2rc_{pq\perp}\cos(\Theta))^n \; . \qquad (6.142)
$$

Expanding the Bessel function into a power series, eq. (A.84), and using the binomial theorem, eq. (A.85), results in

$$\frac{1}{r^\ell} I_n = \sum_{k=0}^{\infty} \sum_{s=0}^{n} \frac{(-1)^k}{k!\,(|m|+k)!} \left(\frac{G_j}{2}\right)^{|m|+2k} \binom{n}{s} (2c_{pq\perp})^{n-s}\; r^{|m|+2k+n+s-\ell} \times \tag{6.143}$$

$$\times \int_0^\pi d\Theta \sin\Theta P_\ell^{|m|}(\cos(\Theta)) \sin^{|m|+2k}(\Theta) \cos^{n+s}(\Theta) =$$

$$= \sum_{k=0}^{\infty} \sum_{s=0}^{n} \binom{n}{s} \frac{(-1)^k 2^{n-s-2k-|m|}}{k!\,(|m|+k)!} G_j^{|m|+2k} c_{pq\perp}^{n-s}\; r^{|m|+2k+n+s-\ell} \int_{-1}^{1} dx \left(1-x^2\right)^{\frac{|m|+2k}{2}} x^{n+s} P_\ell^{|m|}(x)\;. \tag{6.144}$$

From the above expression the lowest order of r only should be considered (which has to be zero, otherwise we are in trouble in the limit $r \to 0$). But for that reason we have to keep not only the $k=0$ term, because for higher $\ell - |m|$ also the higher k terms can contribute. In the Appendix it is shown that the lowest value of $n+s$ is $\ell - |m| - 2k$ such that the integral does not vanish, thus the lowest order term of r in eq.(6.144) is indeed zero. How many k have to be considered depends on $l - |m|$. The contribution to the limits from the k terms are given by

$$\lim_{r\to 0} \frac{1}{r^\ell} I_n = \sum_{k=0}^{\infty} \binom{n}{\ell - |m| - n - 2k} \frac{\sqrt{\pi} 2^{2n-2\ell}}{k!(|m|+k)!} \frac{\Gamma(\ell + |m| + 1)}{\Gamma(\ell + \frac{3}{2})} G_j^{|m|+2k}\, c_{pq\perp}^{2n-\ell+|m|+2k} \tag{6.145}$$

(only if $(\frac{\ell - |m|}{2} - k \le n \le \ell - |m| - 2k)$ is fulfilled they really occur in the n sum). (See also Appendix, note that also different definitions for P_ℓ^m are in use). By inserting (6.145) into eq. (6.141) and taking into account all occurring terms gives

$$\underline{D^L_{1,pq}} = \frac{\pi^{\frac{3}{2}} i^{-m}}{2^{2\ell-1} A} \frac{\sqrt{(2\ell+1)\,\Gamma\left(\ell+|m|+1\right)\Gamma\left(\ell-|m|+1\right)}}{\Gamma\left(\ell+\frac{3}{2}\right)} \sum_{\substack{j \\ (\mathbf{G}_j \neq \mathbf{0})}} \exp(-im\phi_j) \exp\left(i\mathbf{G}_j \mathbf{c}_{pq\|}\right) \times$$

$$\times \sum_{k=0}^{\frac{\ell-|m|}{2}} \sum_{n=\frac{\ell-|m|}{2}-k}^{\ell-|m|-2k} \left(\frac{(-1)^n\, c_{pq\perp}^{2n-\ell+|m|+2k} G_j^{|m|+2k}}{\Gamma\left(2n-\ell+|m|+2k+1\right)\Gamma\left(\ell-|m|-n-2k+1\right)\Gamma(k+1)\Gamma\left(|m|+k+1\right)} \times \right.$$

$$\left. \times \left\{ \int_{2\sigma^2}^{\infty} y^{-\frac{1}{2}-n} \exp\left(-\frac{1}{2}(c_{pq\perp}^2/y + \mathbf{G}_j^2 y)\right)\, dy \right\} \right) =$$

$$= \frac{\pi^{\frac{3}{2}} i^{-m}}{2^{2\ell-1} A} \frac{\sqrt{(2\ell+1)!\,(\ell+|m|)!\,(\ell-|m|)!}}{\Gamma\left(\ell+\frac{3}{2}\right)} \sum_{\substack{j \\ (\mathbf{G}_j \neq \mathbf{0})}} \exp(-im\phi_j) \exp\left(i\mathbf{G}_j \mathbf{c}_{pq\|}\right) \times$$

$$\times \sum_{k=0}^{\frac{\ell-|m|}{2}} \sum_{n=\frac{\ell-|m|}{2}-k}^{\ell-|m|-2k} \frac{(-1)^n\, c_{pq\perp}^{2n-\ell+|m|+2k} G_j^{2n+|m|+2k-1}}{(2n-\ell+|m|+2k)!\,(\ell-|m|-n-2k)!k!\,(|m|+k)!} I_n\left(G_j\sigma, \frac{|c_{pq\perp}|\,G_j}{2}\right)\;. \tag{6.146}$$

In the Appendix it is shown how to calculate the integral

$$I_n\left(G_j\sigma, \frac{|c_{pq\perp}|\,G_j}{2}\right) = \int_{G_j^2\sigma^2}^{\infty} x^{-\frac{1}{2}-n} \exp\left(-\frac{c_{pq\perp}^2 G_j^2}{4x} - x\right) dx \ ,$$

in a numerically efficient way in terms of recurrence relations and the error function.

For $\underline{c_{pq\perp} = 0}$ only the term corresponding to $n = \frac{\ell-|m|}{2} - k$ yields a nonzero contribution, which is **only** the case **for even** $\ell - |m|$. In that case the above formula reduces to

$$\underline{D_{1,pq}^L} = \frac{\pi^{\frac{3}{2}} i^{\ell-m-|m|}}{2^{2\ell-1}A} \frac{\sqrt{(2\ell+1)\,\Gamma\left(\ell+|m|+1\right)\Gamma\left(\ell-|m|+1\right)}}{\Gamma\left(\ell+\frac{3}{2}\right)} \times$$
$$\times \sum_{\substack{j \\ (\mathbf{G}_j \neq \mathbf{0})}} \exp(-im\phi_j) \exp\left(i\mathbf{G}_j \mathbf{c}_{pq\|}\right) G_j^{\ell-1} \sum_{k=0}^{\frac{\ell-|m|}{2}} \frac{(-1)^k \Gamma(\frac{1}{2} - \frac{\ell-|m|}{2} + k, G_j^2\sigma^2)}{(|m|+k)!k!(\frac{\ell-|m|}{2} - k)!} \ . \tag{6.147}$$

Derivation of the direct sum component $D_{2a,pq}^L$

Eq. (6.114) is analogous to (6.55), therefore the result of (6.86) applies. One has to take care that $\mathbf{T}_n$ is a 2D lattice vector, whereas $\mathbf{c}_{pq}$ is in general a 3D vector.

$$D_{2a,pq}^L = \frac{2\pi(-1)^\ell}{\Gamma(\ell+\frac{3}{2})} \sum_{\substack{n\in Z^2 \\ (\mathbf{T}_n - \mathbf{c}_{pq} \neq \mathbf{0})}} Y_L^*(\widehat{\mathbf{c}_{pq} - \mathbf{T}_n}) \frac{\Gamma(\ell+\frac{1}{2}, \left|\mathbf{c}_{pq} - \mathbf{T}_n\right|^2/4\sigma^2)}{\left|\mathbf{c}_{pq} - \mathbf{T}_n\right|^{\ell+1}} \ . \tag{6.148}$$

Derivation of the components $D_{0,pq}^L$, $D_{2b,pq}^L$

In order to evaluate $D_{0,pq}^L$ and $D_{2b,pq}^L$ let us first consider the coefficients of a general function which depends only on $z = r\cos\Theta$ in a power series

$$f(z) = \sum_{n=0}^{\infty} f_n z^n$$

$$f^L = \sum_{n=0}^{\infty} f_n \lim_{r\to 0}\left[r^{n-\ell} \int d\widehat{r} \cos^n(\Theta) Y_L^*(\widehat{\mathbf{r}})\right] \ . \tag{6.149}$$

Integration with respect to ϕ immediately implies the selection rule $m = 0$:

$$f^L = \delta_{m0}\sqrt{\pi}\sqrt{2\ell+1} \sum_{n=0}^{\infty} f_n \lim_{r\to 0} r^{n-\ell} \left(\int_{-1}^{1} dx\, x^n P_\ell(x)\right) \ . \tag{6.150}$$

According to ([16], formula 7.222.1) the integral contained by the above formula vanishes for $n < \ell$. Therefore, the lowest power of r, that corresponds to $n = \ell$, proves again to be zero. By using eq. (A.91) one gets

$$f^L = \delta_{m0}\sqrt{\pi}\sqrt{2\ell+1} f_\ell \int_{-1}^{1} dx\, x^\ell P_\ell(x) \ = \delta_{m0} \frac{\pi\sqrt{2\ell+1}}{2^\ell} \frac{\Gamma(\ell+1)}{\Gamma(\ell+\frac{3}{2})} f_\ell \ . \tag{6.151}$$

$D^L_{0,\mu\nu}$ for the 3D translational symmetry case of a bulk system If we indeed have a system with 3D lattice symmetry we get (since for small z, $|z{+}a_{\mu\nu\perp}| = |a_{\mu\nu\perp}| + \operatorname{sign}(a_{\mu\nu\perp})\, z$),

$$D_{0,\mu\nu}(z) = \frac{\pi}{A}\left(\frac{2}{d}z^2 + \frac{4a_{\mu\nu\perp}}{d}z + \frac{2}{d}a^2_{\mu\nu\perp} - 2\,|a_{\mu\nu\perp}| - 2\operatorname{sign}(a_{\mu\nu\perp})\,(1-\delta_{a_{\mu\nu\perp},0})\,z + \frac{d}{3}\right) \tag{6.152}$$

and (note that there is also a quadrupole contribution)

$$\underline{D^L_{0,\mu\nu} = 2\frac{\pi^{\frac{3}{2}}}{A}\delta_{m0}\left(\delta_{\ell 0}\left(\frac{2}{d}a^2_{\mu\nu\perp} - 2\,|a_{\mu\nu\perp}| + \frac{d}{3}\right) +\right.} \tag{6.153}$$

$$\underline{\left. +\delta_{\ell 1}\frac{2\sqrt{3}}{3}\left(\frac{2a_{\mu\nu\perp}}{d} - \operatorname{sign}(a_{\mu\nu\perp})\,(1-\delta_{a_{\mu\nu\perp},0})\right) + \delta_{\ell 2}\left(\frac{4\sqrt{5}}{15d}\right)\right).} \tag{6.154}$$

These terms can be used to compare the sum of the 2D Madelung constants with the 3D Madelung constants. If there is a 3D translational invariant system with N atoms per 3D unit cell, then the layers can be numbered so that every N^{th} layer is equivalent, by choosing layer $p = 1$ to consist of $\mu = 1$ atoms in the 3D system we get a mapping $f(p) = p \bmod N$

$$\begin{array}{l} f : p \in \mathbb{Z} \to \mu \in \{1,\dots N\} \\ \downarrow \begin{array}{c} p \\ \mu \end{array} \left\| \begin{array}{cccccc} \dots & 1 & \dots & N & N+1 & \dots \\ \dots & 1 & \dots & N & 1 & \dots \end{array} \right. \end{array}$$

Now if we sum up the 2D Madelung constants, $2D{-}G^L_{pq}$, for fixed p with $f(p) = \mu$ over all layers q with $f(q) = \nu$ we must get the following identity

$$3D{-}G^L_{\mu\nu} = \left[\sum_{\substack{q=-\infty \\ f(q)=\nu}}^{\infty} \left(D^L_{1,pq} + D^L_{2a,pq} + D^L_{2b,pq} + D^L_{3,pq}\right)\right] + D^L_{0,\mu\nu}\ . \tag{6.155}$$

Because the correction terms $D^L_{0,\mu\nu}$ are identical zero for $\ell \geq 3$, then (6.155) reduces to

$$\forall \ell \geq 3, (f(p) = \mu)\ \ 3D{-}G^L_{\mu\nu} = \left[\sum_{\substack{q=-\infty \\ f(q)=\nu}}^{\infty} 2D{-}G^L_{pq}\right]. \tag{6.156}$$

$D^L_{0,pq}$ for the general only 2D translational invariant case Since for small z,

$$|z + c_{pq\perp}| = |c_{pq\perp}| + \operatorname{sign}(c_{pq\perp})z \quad (c_{pq\perp} \neq 0),$$

one can immediately derive

$$\underline{D^L_{0,pq} = -\left(1 - \delta_{c_{pq\perp},0}\right)\delta_{m0}\frac{4\pi}{A}\left(\delta_{\ell 0}\sqrt{\pi}\,|c_{pq\perp}| + \delta_{\ell 1}\frac{\sqrt{3\pi}}{3}\operatorname{sign}(c_{pq\perp})\right)}\ . \tag{6.157}$$

Evaluation of $D^L_{2,pq}$ To evaluate $D^L_{2b,pq}$ **for** $\underline{c_{pq\perp}\neq 0}$ we have to perform the expansion

$$\begin{aligned}
\exp(-\left(z+c_{pq\perp}\right)^2 x^2) &= \exp(-c^2_{pq\perp}x^2)\exp(-\left(z^2+2c_{pq\perp}z\right)x^2) \\
&= \exp(-c^2_{pq\perp}x^2)\sum_{n=0}^{\infty}\frac{\left(-1\right)^n\left(z^2+2c_{pq\perp}z\right)^n x^{2n}}{n!} \\
&= \exp(-c^2_{pq\perp}x^2)\sum_{n=0}^{\infty}\frac{\left(-1\right)^n x^{2n}}{n!}\sum_{\ell=n}^{2n}\binom{n}{\ell-n}2^{2n-\ell}c^{2n-\ell}_{pq\perp}z^{\ell} \\
&= \sum_{\ell=0}^{\infty}\left(\exp(-c^2_{pq\perp}x^2)\sum_{\frac{\ell}{2}\le n\le\ell}\frac{\left(-1\right)^n 2^{2n-\ell}c^{2n-\ell}_{pq\perp}x^{2n}}{\Gamma\left(\ell-n+1\right)\Gamma\left(2n-\ell+1\right)}\right)z^{\ell}
\end{aligned}$$

from which we obtain (**only for** $c_{pq\perp}\neq 0$)

$$\begin{aligned}
\underline{D^L_{2b,pq}} &= -\,\delta_{m0}\,\mathrm{sign}\left(c_{pq\perp}\right)\frac{2\pi}{A}\frac{\sqrt{\pi\left(2\ell+1\right)}}{4^{\ell}c^{\ell-1}_{pq\perp}}\frac{\Gamma(\ell+1)}{\Gamma(\ell+\frac{3}{2})}\times \\
&\times\sum_{\frac{\ell}{2}\le n\le\ell}\frac{\left(-1\right)^n 4^n}{\Gamma\left(\ell-n+1\right)\Gamma\left(2n-\ell+1\right)}\int_{\left|c_{pq\perp}\right|/2\sigma}^{\infty}dx\,x^{2n-2}\exp(-x^2) = \\
&= -\,\delta_{m0}\,\mathrm{sign}\left(c_{pq\perp}\right)\frac{\pi}{A}\frac{\sqrt{\pi\left(2\ell+1\right)}}{4^{\ell}c^{\ell-1}_{pq\perp}}\frac{\Gamma(\ell+1)}{\Gamma(\ell+\frac{3}{2})}\times \\
&\underline{\times\sum_{\frac{\ell}{2}\le n\le\ell}\frac{\left(-1\right)^n 4^n}{\Gamma\left(\ell-n+1\right)\Gamma\left(2n-\ell+1\right)}\Gamma\left(n-\frac{1}{2},c^2_{pq\perp}/4\sigma^2\right)}\,. \qquad (6.158)
\end{aligned}$$

Manipulating the Taylor expansion

$$\begin{aligned}
&-\frac{4\sqrt{\pi}\sigma}{A}\exp(-\frac{z^2}{4\sigma^2})-\frac{2\pi\left|z\right|}{A}\mathrm{erf}(\frac{\left|z\right|}{2\sigma}) = \\
&= -\frac{4\sqrt{\pi}\sigma}{A}\sum_{n=0}^{\infty}\frac{\left(-1\right)^n z^{2n}}{n!4^n\sigma^{2n}}-\frac{4\sqrt{\pi}\sigma}{A}\sum_{n=0}^{\infty}\frac{\left(-1\right)^n z^{2n+2}}{n!(2n+1)2^{2n+1}\sigma^{2n+2}} = \\
&= -\frac{4\sqrt{\pi}\sigma}{A}-\frac{4\sqrt{\pi}\sigma}{A}\sum_{n=1}^{\infty}\frac{\left(-1\right)^n z^{2n}}{n!4^n\sigma^{2n}}\left(1-\frac{2n!}{(n-1)!(2n-1)}\right) = \\
&= \frac{4\sqrt{\pi}\sigma}{A}\sum_{n=0}^{\infty}\frac{\left(-1\right)^n}{n!\left(2n-1\right)\left(2\sigma\right)^{2n}}z^{2n}\,,
\end{aligned}$$

yields **for** $c_{pq\perp}=0$ that **for odd** ℓ $D^L_{2b,pq}=0$, while **for even** $\ell\,(=2n)$

$$\begin{aligned}
\underline{D^L_{2b,pq}} &= \delta_{m0}\frac{4\sqrt{\pi}\sigma}{A}\frac{\pi\sqrt{4n+1}}{2^{2n}}\frac{\Gamma(2n+1)}{\Gamma(2n+\frac{3}{2})}\frac{\left(-1\right)^n}{n!\left(2n-1\right)\left(2\sigma\right)^{2n}} \\
&= \underline{\delta_{m0}\frac{2\pi}{A}\frac{\left(-1\right)^n\sqrt{4n+1}}{4^n\sigma^{2n-1}}\frac{\Gamma(n-\frac{1}{2})}{\Gamma(2n+\frac{3}{2})}}\,. \qquad (6.159)
\end{aligned}$$

Finally, similar to eq. (6.87)

$$\underline{D^L_{3,pq} = -\delta_{pq}\delta_{L,00}\frac{2}{\sigma}} \, . \tag{6.160}$$

The 2D Madelung constants $A^{LL'}_{pq}$ can then be again obtained from eq. (6.33) if we replace $G^L_{\mathbf{RR'}}$ by

$$\underline{G^L_{pq} = \sum_{i=0,1,2a,2b,3} D^L_{i,pq}} \, . \tag{6.161}$$

With the reduced 2D Madelung constants G^L_{pq} and the $\mathbf{G} = \mathbf{0}$ terms the potential can be written as

$$\underline{\begin{array}{c} V_p(\mathbf{x}) = \sum_L \frac{4\pi}{\Gamma(\ell+\frac{3}{2})} \left(\sum_{L'} \frac{(-1)^{\ell'}\Gamma(\ell+\ell'+\frac{3}{2})}{\Gamma(\ell'+\frac{1}{2})} \mathcal{C}^{\ell' m'}_{\ell m,(\ell+\ell')(m'-m)} \left(\sum_q G^{\ell+\ell',m'-m}_{pq} Q^{L'}_q \right) \right)^* r^\ell Y_L(\hat{x}) + \\ + \mathcal{A}\sqrt{\frac{4\pi}{3}} r Y_{10}(\hat{x}) + (\mathcal{A}c_{p\perp} + \mathcal{B})\sqrt{4\pi} Y_{00}(\hat{x}) \end{array}} \tag{6.162}$$

The expansion coefficients in spherical harmonics are therefore given by

$$\underline{V_{p,lm}(r)} = \begin{array}{c} \underline{\frac{4\pi}{\Gamma(\ell+\frac{3}{2})} \left(\sum_{L'} \frac{(-1)^{\ell'}\Gamma(\ell+\ell'+\frac{3}{2})}{\Gamma(\ell'+\frac{1}{2})} \mathcal{C}^{\ell' m'}_{\ell m,(\ell+\ell')(m'-m)} \left(\sum_q G^{\ell+\ell',m'-m}_{pq} Q^{L'}_q \right) \right)^* r^\ell +} \\ \underline{+ \mathcal{A}\sqrt{\frac{4\pi}{3}} r \delta_{L,3} + (\mathcal{A}c_{p\perp} + \mathcal{B})\sqrt{4\pi}\delta_{L,1}} \end{array} \tag{6.163}$$

Since the intercell potential $V_p(\mathbf{x})$ is real 1 applies.

In case one is only interested in the ASA potential, we get

$$\underline{V_{ASA,p} = V_p(\mathbf{0}) = \sum_{L'} \frac{(-1)^{\ell'}(2\ell'+1)}{\sqrt{\pi}} \left(\sum_q G^{\ell',m'}_{pq} Q^{L'}_q \right) + (\mathcal{A}c_{p\perp} + \mathcal{B})} \tag{6.164}$$

Note that also for the ASA case all reduced Madelung constants and multipole moments enter.

The case of $L = (\ell, 0)$

$$\begin{aligned} D^{\ell 0}_{1,pq} = {} & \frac{\pi^{\frac{3}{2}}}{2^{\ell-1}A} \frac{\ell!\sqrt{2\ell+1}}{\Gamma\left(\ell+\frac{3}{2}\right)} \sum_{\substack{j \\ (\mathbf{G}_j \neq \mathbf{0})}} \exp\left(i\mathbf{G}_j \mathbf{c}_{pq\|}\right) \times \\ & \times \sum_{\frac{\ell}{2} \leq n \leq \ell} \frac{(-1)^n \, c^{2n-\ell}_{pq\perp} G^{2n-1}_j}{\Gamma(2n-\ell+1)\,\Gamma(\ell-n+1)} I_n\left(G_j\sigma, \frac{|c_{pq\perp}|\,G_j}{2}\right) \, , \end{aligned} \tag{6.165}$$

$$I_n(G_j\sigma, \frac{|c_{pq\perp}|\,G_j}{2}) = \int_{G^2_j\sigma^2}^{\infty} x^{-\frac{1}{2}-n} \exp\left(-\frac{c^2_{pq\perp}G^2_j}{4x} - x\right) dx \, , \tag{6.166}$$

6.6.3 Determining the constants $\mathcal{A}$ and $\mathcal{B}$

In the following we do not need the dependence of the potential inside the cell and therefore write

$$V_p = V_p(\mathbf{x} = \mathbf{0}).$$

For given Madelung constants $A_{pq}^{LL'}$ the Madelung potentials of a layered system V_p can be determined via eq. (6.27) to which, however, according to eq. (6.134), the term $\mathcal{A}c_{p\perp} + \mathcal{B}$ has to be added. As what follows we split V_p into two parts

$$V_p = \widehat{V}_p + V_{\perp,p} \ , \tag{6.167}$$

where $V_{\perp,p}$ is the part remaining for $p \longrightarrow \infty$

$$V_{\perp,p} = 2 \sum_L \sum_q A_{0,pq}^{00,L} Q_q^L + \mathcal{A}c_{p\perp} + \mathcal{B} \ , \tag{6.168}$$

and

$$\widehat{V}_p = 2 \sum_{i=1,2a,2b,3} \sum_L \sum_q A_{i,pq}^{00,L} Q_q^L \ , \tag{6.169}$$

with

$$A_{i,pq}^{00,L} = (-1)^\ell \frac{\ell + \frac{1}{2}}{\sqrt{\pi}} D_{i,pq}^L \qquad (i = 0, 1, 2a, 2b, 3) \ , \tag{6.170}$$

the later is based on eq. (6.33).

$V_{\perp,\mu}$ for the 3D translational invariant case In particular, from eq. (6.153) one obtains

$$A_{0,\mu\nu}^{00,L} = \frac{2\pi}{A} \delta_{m0} \left(\delta_{\ell 0} \left(\frac{1}{d} a_{\mu\nu\perp}^2 - |a_{\mu\nu\perp}| + \frac{d}{6} \right) - \delta_{\ell 1} \sqrt{3} \left(\frac{2a_{\mu\nu\perp}}{d} - \operatorname{sign}(a_{\mu\nu\perp}) \right) \right) \tag{6.171}$$

and

$$V_{\perp,\mu} = \frac{4\pi}{A} \sum_\nu Q_\nu^{00} \left(\frac{1}{d} a_{\mu\nu\perp}^2 - |a_{\mu\nu\perp}| \right) - \frac{4\pi}{A} \sum_\nu \sqrt{3} Q_\nu^{10} \left(\frac{2a_{\mu\nu\perp}}{d} - \operatorname{sign}(a_{\mu\nu\perp}) \right) \ , \tag{6.172}$$

where we made use of the charge neutrality in a bulk unit cell and used the convention sign(0) = 0.

$V_{\perp,\mu}$ for a general 2D translational invariant case In particular, by using eq. (6.157) yields

$$A_{0,pq}^{00,L} = -\left(1 - \delta_{c_{pq\perp},0}\right) \delta_{m0} \frac{2\pi}{A} \left(\delta_{\ell 0} |c_{pq\perp}| - \delta_{\ell 1} \sqrt{3} \operatorname{sign}(c_{pq\perp}) \right) \ , \tag{6.173}$$

and, consequently,

$$V_{\perp,p} = -\frac{4\pi}{A} \sum_q \left(|c_{pq\perp}| Q_q^{00} - \operatorname{sign}(c_{pq\perp}) \sqrt{3} Q_q^{10} \right) + \mathcal{A}c_{p\perp} + \mathcal{B} \ , \tag{6.174}$$

where in terms of the convention sign(0) $= 0$ the restriction for $D^L_{0,pq}$, namely, $|c_{pq\perp}| \neq 0$ is automatically fulfilled.

Suppose that in a typical layered system for layers $p \leq 0$ the local physical quantities (charges, moments, potentials etc.) are identical to those of a complex 3D bulk system (left semi-infinite region, L), while for $p \geq N+1$, to those of either a complex 3D bulk, or, to mimic vacuum, the charge density is zero (right semi-infinite region, R). The layers $1 \leq p \leq N$ form the interface (central) region I. Conveniently, we choose the layer indices such that

$$c_{p\perp} \geq c_{q\perp} \quad \text{if} \quad p > q \; ,$$
$$c_{0\perp} < c_{1\perp} \quad \text{and} \quad c_{N\perp} < c_{N+1,\perp} \; .$$

As we require continuity for the Madelung potential between regions L and I as well as between I and R, the constants $\mathcal{A}$ and $\mathcal{B}$ can be uniquely determined.

"Bulk" from the left

The properties of the material in the left region are not changed during the film calculation but give rise to boundary conditions for the film layers. Suppose the material in the L region on its one corresponds to a bulk 3D complex lattice with n nonequivalent atoms, then it can be decisive which layer of the left bulk material is the one closest to the film layers, therefore we need the following derivation.

The numbering of the layers of the 2D invariant system is as follows

Layer (p)	atom type (μ)
0	1
-1	2
⋮	⋮
-n+1	n
-n	1
-n-1	2
⋮	⋮

The above table clearly defines a mapping μ_p for $p \leq 0$. This means for the moments of the charge density the following condition has to apply

$$Q^{\ell m}_p = Q^{\ell m}_{L,\mu_p} \qquad (p \leq 0) \; , \tag{6.175}$$

where the subscript L refers to the left bulk region and V_{Left} is the value of the Intercellpotential (in the bulk calculation) of the uppermost bulk layer (which is layer $p = 0$). Continuity between regions L and I implies for the Madelung potentials

$$V_{Left} = V_{p=0}(\mathbf{r} = \mathbf{0}) = \widehat{V}_0 - \frac{4\pi}{A} \sum_q \left(|c_{0q\perp}| \, Q^{00}_q - \text{sign}(c_{0q\perp}) \sqrt{3} Q^{10}_q \right) + \mathcal{A} c_{0\perp} + \mathcal{B} \; , \tag{6.176}$$

from which the constant $\mathcal{B}$ can be expressed,

$$\underline{\mathcal{B} = V_{Left} - 2 \sum_L \sum_q \frac{(-1)^\ell \, (2\ell + 1)}{\sqrt{\pi}} G^L_{0q} Q^L_q} \tag{6.177}$$

and inserted into eq. (6.174) $(p \geq 0)$ yields

$$V_{\perp,p} = -\frac{4\pi}{A}\sum_q \Big(Q_q^{00}\left(|c_{pq\perp}| - |c_{0q\perp}|\right) - \sqrt{3}Q_q^{10}\left(\text{sign}(c_{pq\perp}) - \text{sign}(c_{0q\perp})\right)\Big) + \mathcal{A}c_{p0\perp} + V_{L,1} - \widehat{V}_0 \; . \tag{6.178}$$

For $p \geq 1$

$$|c_{pq\perp}| - |c_{0q\perp}| = \begin{cases} c_{p0\perp} & \text{if } \; q \leq 0 \\ c_{pq\perp} - c_{q0\perp} = c_{p0\perp} - 2c_{q0\perp} & \text{if } 1 \leq q \leq p \\ -c_{p0\perp} & \text{if } p < q \end{cases} \tag{6.179}$$

$$\text{sign}(c_{pq\perp}) - \text{sign}(c_{0q\perp}) = \begin{cases} 0 & \text{if } \; c_{q\perp} < c_{0\perp} \\ 1 & \text{if } \; c_{q\perp} = c_{0\perp} \\ 2 & \text{if } \; q \geq 1 \text{ and } c_{q\perp} < c_{p\perp} \\ 1 & \text{if } \; q \geq 1 \text{ and } c_{q\perp} = c_{p\perp} \\ 0 & \text{if } \; q \geq 1 \text{ and } c_{q\perp} > c_{p\perp} \end{cases} \; , \tag{6.180}$$

and because of the charge neutrality in L, one thus gets

$$\begin{aligned} V_{\perp,p} = -\frac{4\pi}{A}\sum_{q\geq 1} Q_q^{00}\left(|c_{pq\perp}| - c_{q0\perp}\right) + \frac{4\pi}{A}\sum_{\substack{q\leq 0 \\ (c_{q0\perp}=0)}} \sqrt{3}Q_q^{10} + \frac{8\pi}{A}\sum_{\substack{q\geq 1 \\ (c_{q\perp}<c_{p\perp})}} \sqrt{3}Q_q^{10} + \\ + \frac{4\pi}{A}\sum_{\substack{q\geq 1 \\ (c_{q\perp}=c_{p\perp})}} \sqrt{3}Q_q^{10} + \mathcal{A}c_{p0\perp} + V_{L,1} - \widehat{V}_0 \; . \end{aligned} \tag{6.181}$$

Vacuum from the right If there is vacuum in the right region of the film calculation it means that for

$$\forall p \geq N+1 \quad \rho_p(\mathbf{r}) = 0 \; , V_p(\mathbf{r}) = const. \; (\mathbf{r} \in \Omega) \; ,$$

i.e. $V_p = V_p(\mathbf{0}) = const.$ $(\, p \geq N+1)$, and therefore the following boundary condition is imposed

$$\forall p \geq N+1 \;\; \frac{d}{dc_{p\perp}}V_{\perp,p} = 0 \; . \tag{6.182}$$

Remembering that $c_{N+1,\perp} > c_{p\perp}$ $(p \leq N)$, eq. (6.181) implies for $p > N$

$$V_{\perp,p} \;\; = \;\; \left(-\frac{4\pi}{A}\sum_{q=1}^{N} Q_q^{00} + \mathcal{A}\right) c_{p0\perp} + \frac{8\pi}{A}\sum_{q=1}^{N} Q_q^{00}c_{q0\perp} + \tag{6.183}$$

$$+\frac{4\pi}{A}\sum_{\substack{q\leq 0 \\ (c_{q0\perp}=0)}} \sqrt{3}Q_q^{10} + \frac{8\pi}{A}\sum_{q=1}^{N} \sqrt{3}Q_q^{10} + V_{L,1} - \widehat{V}_0 \; , \tag{6.184}$$

therefore, the Vacuum boundary condition (6.182) implies

$$\underline{\mathcal{A} = \frac{4\pi}{A}\sum_{q=1}^{N} Q_q^{00}} \; , \tag{6.185}$$

and

$$V_{vac} \equiv V_{\perp,p>N} = \frac{8\pi}{A} \sum_{q=1}^{N} \left(Q_q^{00} c_{q0\perp} + \sqrt{3} Q_q^{10} \right) + \frac{4\pi}{A} \sum_{\substack{q\leq 0 \\ (c_{q0\perp}=0)}} \sqrt{3} Q_q^{10} + V_{L,1} - \widehat{V}_0 \tag{6.186}$$

$$V_{vac} \equiv \frac{4\pi}{A} \sum_{q} \left(Q_q^{00} c_{q0\perp} + \sqrt{3} Q_q^{10} \right) + \mathcal{B}. \tag{6.187}$$

Furthermore, for $1 \leq p \leq N$ one gets

$$\begin{aligned} V_{\perp,p} = {} & V_{L,1} - \widehat{V}_0 + \frac{8\pi}{A} \sum_{q=1}^{N} Q_q^{00} \min(c_{p0\perp}, c_{q0\perp}) \\ & + \frac{4\pi}{A} \sum_{\substack{q\leq 0 \\ (c_{q0\perp}=0)}} \sqrt{3} Q_q^{10} + \frac{8\pi}{A} \sum_{\substack{q\geq 1 \\ (c_{q\perp}<c_{p\perp})}} \sqrt{3} Q_q^{10} + \frac{4\pi}{A} \sum_{\substack{q\geq 1 \\ (c_{q\perp}=c_{p\perp})}} \sqrt{3} Q_q^{10} . \end{aligned} \tag{6.188}$$

"Bulk" from the right Suppose the material in the R region on its own corresponds again to a bulk 3D complex lattice with m non equivalent atoms, forming layers of the 2D invariant system numbered as follows,

Layer (p)	atom type (μ)
N+1	1
N+2	2
$\vdots$	$\vdots$
N+m	m
N+m+1	1
N+m+2	2
$\vdots$	$\vdots$

,

which defines a unique mapping μ_p for $p \geq N+1$. The multipole moments in these layers are given by the multipole moments of the bulk calculation of this material

$$Q_p^{\ell m} = Q_{R,\mu_p}^{\ell m} \qquad (p \geq N+1) , \tag{6.189}$$

continuity between regions I and R implies

$$\begin{aligned} V_{R,1} = {} & V_{N+1} = \widehat{V}_{N+1} - \frac{4\pi}{A} \sum_{q=1}^{N} Q_q^{00} \left(c_{N+1,0\perp} - 2 c_{q0\perp} \right) \\ & + \frac{4\pi}{A} \sum_{\substack{q\leq 0 \\ (c_{q0\perp}=0)}} \sqrt{3} Q_q^{10} + \frac{8\pi}{A} \sum_{q=1}^{N} \sqrt{3} Q_q^{10} + \frac{4\pi}{A} \sum_{\substack{q\geq N+1 \\ (c_{q\perp}=c_{N+1,\perp})}} \sqrt{3} Q_q^{10} + \mathcal{A} c_{N+1,0\perp} + V_{L,1} - \widehat{V}_0 , \end{aligned} \tag{6.190}$$

where we made use of eq. (6.181) and the charge neutrality of the R bulk region. Thus, in that case

$$\mathcal{A} = \frac{1}{c_{N+1,0\perp}} \left(V_{R,1} - V_{L,1} + \widehat{V}_0 - \widehat{V}_{N+1} + \frac{4\pi}{A} \sum_{q=1}^{N} Q_q^{00} \left(c_{N+1,0\perp} - 2c_{q0\perp} \right) + \right.$$

$$\left. - \frac{4\pi}{A} \sum_{\substack{q\leq 0 \\ (c_{q0\perp}=0)}} \sqrt{3} Q_q^{10} - \frac{8\pi}{A} \sum_{q=1}^{N} \sqrt{3} Q_q^{10} - \frac{4\pi}{A} \sum_{\substack{q\geq N+1 \\ (c_{q\perp}=c_{N+1,\perp})}} \sqrt{3} Q_q^{10} \right) , \tag{6.191}$$

which should be inserted into eq. (6.181),

$$\underline{\mathcal{A} = \frac{1}{c_{N+1,0\perp}} \left(V_{Right} - V_{Left} + \sum_{L} \sum_{q} \frac{(-1)^{\ell}(2\ell+1)}{\sqrt{\pi}} \left(G_{0q}^{L} - G_{N+1q}^{L} \right) Q_q^{L} \right).} \tag{6.192}$$

Slab In electronic structure calculations, a *slab* is defined by a **finite number** of atomic layers surrounded by vacuum on both sides, i.e.,

$$Q_p^L = 0 \qquad \text{for} \quad p \leq 0 \quad \text{and} \quad p > N \; , \tag{6.193}$$

thus, from Eq. (6.174) we have

$$V_{\perp,p} = -\frac{4\pi}{A} \sum_{q=1}^{N} \left(\left| c_{pq\perp} \right| Q_q^{00} - \operatorname{sign}(c_{pq\perp}) \sqrt{3} Q_q^{10} \right) + \mathcal{A} c_{p\perp} + \mathcal{B} \; . \tag{6.194}$$

One boundary condition is again set by restriction that the potential becomes a constant in the vacuum

$$\forall p \geq N+1 \;\; \frac{d}{dc_{p\perp}} V_{\perp,p} = 0 \; .$$

$$\begin{aligned} V_{\perp,p} &= -\frac{4\pi}{A} \sum_{q=1}^{N} \left(c_{pq\perp} Q_q^{00} - \sqrt{3} Q_q^{10} \right) + \mathcal{A} c_{p\perp} + \mathcal{B} = \\ &= \left(-\frac{4\pi}{A} \sum_{q=1}^{N} Q_q^{00} + \mathcal{A} \right) c_{p\perp} + \frac{4\pi}{A} \sum_{q=1}^{N} Q_q^{00} c_{q\perp} + \frac{4\pi}{A} \sum_{q=1}^{N} \sqrt{3} Q_q^{10} + \mathcal{B} \; , \end{aligned} \tag{6.195}$$

therefore,

$$\mathcal{A} = \frac{4\pi}{A} \sum_{q=1}^{N} Q_q^{00} \; , \tag{6.196}$$

and, consequently, for $1 \leq p \leq N$

$$V_p = -\frac{4\pi}{A} \sum_{q=1}^{N} \left(\left(\left| c_{pq\perp} \right| - c_{p\perp} \right) Q_q^{00} - \operatorname{sign}(c_{pq\perp}) \sqrt{3} Q_q^{10} \right) + \mathcal{B} + \widehat{V}_p \; . \tag{6.197}$$

In the center of the slab, the bulk properties should pertain, hence we impose the corresponding bulk value for the Madelung potential. Let p^* denote the layer in the center of the slab which we associate with the sublattice α^* of the bulk. Then one can write

$$V_{b,\alpha^*} = -\frac{4\pi}{A}\sum_{q=1}^{N}\Big(\left(|c_{p^*q\perp}| - c_{p^*\perp}\right)Q_q^{00} - \mathrm{sign}(c_{p^*q\perp})\sqrt{3}Q_q^{10}\Big) + \mathcal{B} + \widehat{V}_{p^*}\,, \tag{6.198}$$

from which yields

$$\mathcal{B} = V_{b,\alpha^*} + \frac{4\pi}{A}\sum_{q=1}^{N}\Big(\left(|c_{p^*q\perp}| - c_{p^*\perp}\right)Q_q^{00} - \mathrm{sign}(c_{p^*q\perp})\sqrt{3}Q_q^{10}\Big) - \widehat{V}_{p^*}\ , \tag{6.199}$$

and

$$\begin{aligned} V_p = -\frac{4\pi}{A}\sum_{q=1}^{N}\Big(\Big(|c_{pq\perp}| - |c|_{p^*q\perp} + c_{p^*p\perp}\Big)Q_q^{00} - \left(\mathrm{sign}(c_{pq\perp}) - \mathrm{sign}(c_{p^*q\perp})\right)\sqrt{3}Q_q^{10}\Big) + \\ + \widehat{V}_p + V_{b,\alpha^*} - \widehat{V}_{p^*}\ . \end{aligned} \tag{6.200}$$

$$\mathcal{B} = V_{central} - 2\sum_{L}\sum_{q} A_{p^*q}^{00,L} Q_q^L - \mathcal{A}c_{p^*\perp} \tag{6.201}$$

$$V_{Vac} = \mathcal{B} + 2\sum_{L}\sum_{q} A_{N+1q}^{00,L} Q_q^L \tag{6.202}$$

Chapter 7

Single Site Scattering Green Function

The following chapter summarizes some important properties of the single site problem, where we have a potential $V(\mathbf{x})$ with just one attractive center at the origin. For the considerations here it is not important whether the potential is spherically symmetric or not, therefore we restrict ourselves in the beginning to the easier case of a spherically symmetric potential.

7.1 One dimensional examples

In order to demonstrate the principle ideas we start with an example in one dimension.

7.1.1 Free particle in one dimension

Spectrum and complete set of eigenfunctions

If the potential is identically zero

$$V(x) \equiv 0$$

the Schrödinger equation is given by

$$-\frac{d^2}{dx^2}\psi(x) = E\psi(x) \tag{7.1}$$

There is only a continuous spectrum

$$\sigma = \sigma_p \cup \sigma_c = \{\} \cup [0, +\infty[\subset \mathbb{R} \tag{7.2}$$

A complete, orthonormal set of generalized eigenfunctions is given by

$$\left\{\phi_k(x) = \frac{1}{\sqrt{2\pi}} e^{ikx}, k \in \mathbb{R}\right\}, E_k = k^2 \tag{7.3}$$

Orthonormal:

$$\int_{\mathbb{R}} \phi_k(x)\phi^*_{k'}(x)dx = \frac{1}{2\pi}\int_{\mathbb{R}} e^{i(k-k')x}dx = \delta(k-k') \tag{7.4}$$

Complete:

$$\int_{\mathbb{R}} |\phi_k >< \phi_k| dk = \hat{1} \ , \ \frac{1}{2\pi} \int_{\mathbb{R}} e^{ik(x-x')} dk = \delta(x-x') \tag{7.5}$$

Another complete, orthonormal set of generalized eigenfunctions is given by (note the $k = 0$ problem)

$$\begin{aligned} \{\phi_{+,k}(x) &= \pi^{-\frac{1}{2}} \cos(kx), k \in]0, \infty[\}, E_k = k^2 & (7.6) \\ \{\phi_{-,k}(x) &= \pi^{-\frac{1}{2}} \sin(kx), k \in]0, \infty[\}, E_k = k^2 & (7.7) \end{aligned}$$

By denoting the symmetry with the two-valued variable $L \in \{+,-\}$:

Orthonormal:

$$\int_{\mathbb{R}} \phi_{L,k}(x) \phi^*_{L',k'}(x) dx = \delta_{LL'} \delta(k-k') \tag{7.8}$$

Complete:

$$\sum_{L \in \{+,-\}} \int_0^{\infty} \phi_{L,k}(x) \phi_{L,k}(x') dk = \delta(x-x') \tag{7.9}$$

Regular and Irregular solutions

Similar to the radial equation in the 3 dimensional case there exists a radial differential equation also in the 1-dimensional case. We take

$$x = |x| \operatorname{sgn}(x) = r \ s \text{ with } r \in \mathbb{R}_0^+, s \in \{-1, +1\}$$

and define an orthonormal system $\{Y_+, Y_-\}$ on the *sphere in 1D* (the analogy of the spherical harmonics)

$$\text{sphere in 1D: } S_0 = \{-1, +1\}$$

$$Y_+ : \left\{ \begin{array}{ccc} S_0 & \to & \mathbb{C} \\ s & \mapsto & \frac{1}{\sqrt{2}} \end{array} \right. , Y_- : \left\{ \begin{array}{ccc} S_0 & \to & \mathbb{C} \\ s & \mapsto & \frac{1}{\sqrt{2}} \operatorname{sgn}(s) \end{array} \right.$$

Our Ansatz to solve the differential equation

$$\left[-\frac{d^2}{dx^2} - z \right] \psi(x) = 0 \ , \tag{7.10}$$

for general $z \in \mathbb{C}$, $z = p^2, \operatorname{Im} p > 0$ (see A.1) is

$$\psi(x) = f(|x|) Y_L(\operatorname{sgn}(x)) = f(r) Y_L(s)$$

The radial differential equation is just the same for every $L \in \{+,-\}$

$$\left[-\frac{d^2}{dr^2} - z \right] f(r) = 0 \ . \tag{7.11}$$

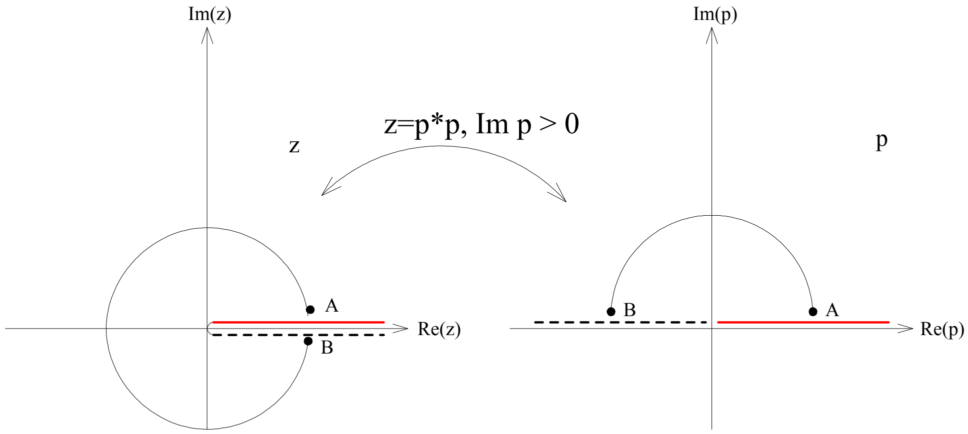

Figure 7.1: Spectrum of a free particle and the complex square root function.

Considered as linear homogenous second order differential equation there exists a 2 dimensional solution space, which can be spanned by one regular and one irregular solution.
The regular solution is characterized by the fact that it fulfills the differential equation

$$\left[-\frac{d^2}{dx^2} - z\right] \psi(x) = 0 \tag{7.12}$$

for all $x \in \mathbb{R}$. An irregular solution does not fulfill the differential equation (7.12) at the origin $x = 0$, where it is only fulfilled up to a δ like singularity. Different to the 3D case the 'irregular solutions' are not necessarily irregular at the origin, but only their derivatives might be. This is simply related to the fact that

$$\begin{array}{ll} \text{1D:} & \frac{d^2}{dx^2}\left[\frac{1}{2}|x|\right] = \delta(x) \\ \text{3D:} & \triangle\left[\frac{-1}{4\pi}\frac{1}{|\mathbf{x}|}\right] = \delta^{(3)}(\mathbf{x}) \end{array} .$$

where $\delta^{(3)}(\mathbf{x}) = \delta(x_1)\delta(x_2)\delta(x_3)$ is the usual delta function in the $3D$ case.

Even functions, $L = (+)$ For $L = (+)$ we have a pair of solutions:

$$\begin{array}{rl} \text{regular solution:} & Z_{+,p}(x) = \frac{1}{\sqrt{\pi}}\cos(pr) = \left(\frac{1}{\sqrt{2}}\right)\left(\sqrt{\frac{2}{\pi}}\cos(px)\right) \\ \text{irregular solution:} & I_{+,p}(x) = \frac{1}{\sqrt{\pi}}\sin(p|x|) = \left(\frac{1}{\sqrt{2}}\right)\left(\sqrt{\frac{2}{\pi}}\sin(pr)\right) \\ \text{outgoing waves:} & H_{+,p}(x) = Z_{+,p}(x) + iI_{+,p}(x) = \frac{1}{\sqrt{\pi}}\left(\cos(pr) + i\sin(pr)\right) = \frac{1}{\sqrt{\pi}}e^{ipr} \end{array}$$

Here the regular solution fulfills the differential equation for all $x \in \mathbb{R}$, while the irregular has a δ singularity at the origin.

$$\left[-\frac{d^2}{dx^2} - z\right] I_{+,p}(x) = \frac{2p}{\sqrt{\pi}}\delta(x)$$

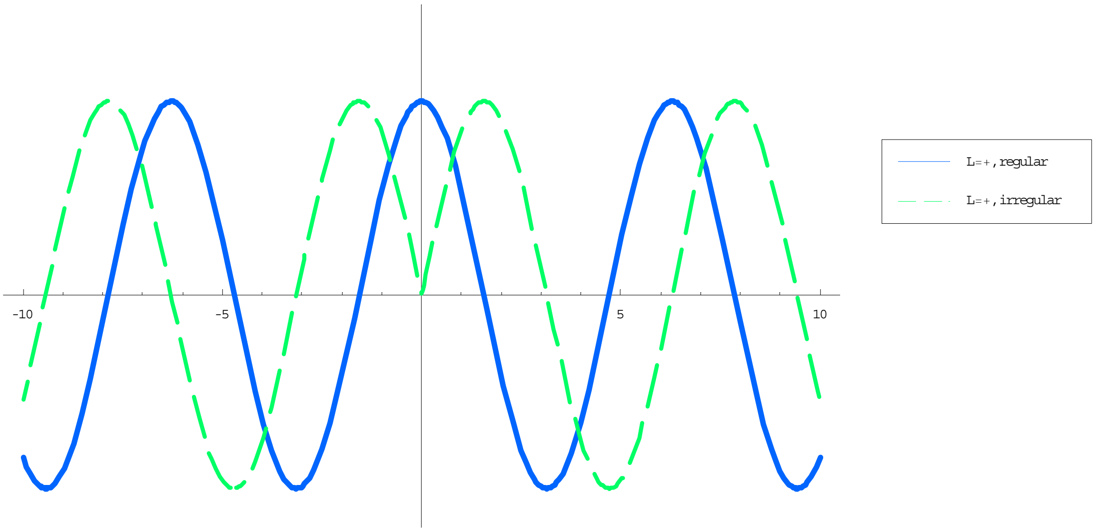

Figure 7.2: Regular and irregular even solution for a free particle.

The Green function of the 1 dimensional free particle is given by

$$\begin{aligned} G(x,x';z) &= g(|x-x'|;z) = g_p(|x-x'|) = \frac{\sin\left(p|x-x'|\right)}{2p} - i\frac{\cos\left(p|x-x'|\right)}{2p} = && (7.13)\\ &= \frac{e^{ip|x-x'|}}{2ip} = \frac{\sqrt{\pi}}{2p} I_{+,p}(x-x') - i\frac{\sqrt{\pi}}{2p} Z_{+,p}(x-x') && (7.14)\end{aligned}$$

and fulfills

$$\left[-\frac{d^2}{dx^2} - z\right] g_p(|x-x'|) = \delta(x-x') \qquad (7.15)$$

While for every constant c the function $g_p(|x-x'|) + cZ_{+,p}\left(x-x'\right)$ fulfills the same differential equation, the Green function is **uniquely** defined because of the boundary conditions for $|x-x'| \to \infty$.

Odd functions, $L = (-)$ For $L = (-)$ we have a pair of solutions:

$$\begin{array}{rl} \text{regular solution:} & Z_{-,p}(x) = \frac{1}{\sqrt{\pi}} \sin\left(px\right) = \left(\frac{1}{\sqrt{2}} \operatorname{sgn}\left(x\right)\right)\left(\sqrt{\frac{2}{\pi}} \sin\left(pr\right)\right) \\ \text{irregular solution:} & I_{-,p}\left(x\right) = \frac{1}{\sqrt{\pi}} sgn\left(x\right) \cos p|x| = \left(\frac{1}{\sqrt{2}} \operatorname{sgn}\left(x\right)\right)\left(\sqrt{\frac{2}{\pi}} \cos\left(pr\right)\right) = \\ \text{outgoing waves:} & H_{-,p}\left(x\right) = Z_{-,p}\left(x\right) - iI_{-,p}\left(x\right) = \frac{-i}{\sqrt{\pi}} \operatorname{sgn}\left(x\right)\left(\cos\left(pr\right) + i\sin\left(pr\right)\right) = \left(-\frac{i}{\sqrt{\pi}} \operatorname{sgn}\left(x\right)\right) e^{ipr} \end{array}$$

Here the regular solution fulfills the differential equation everywhere, while the irregular has a δ' singularity at the origin.

$$\left[-\frac{d^2}{dx^2} - z\right] I_{-,p}(x) = \frac{2}{\sqrt{\pi}} \delta'\left(x\right) \qquad (7.16)$$

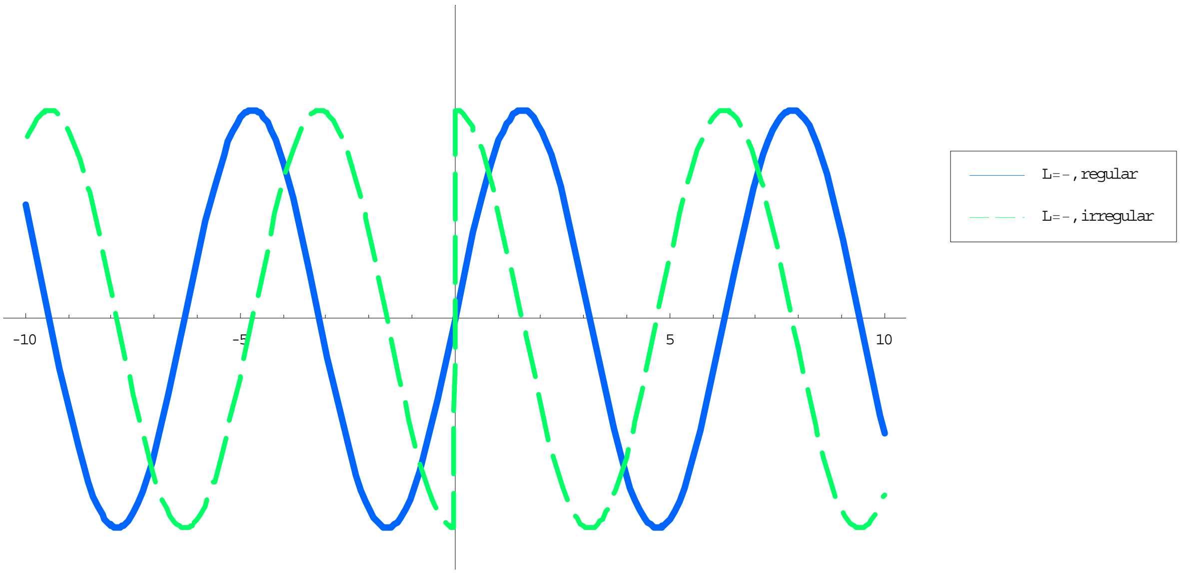

Figure 7.3: Odd solutions for a free particle.

The derivative of the delta function is given by

$$\int_{\mathbb{R}} \left(\delta^{'}(x)f(x)\right) dx = -\int_{\mathbb{R}} \left(\delta(x)f^{'}(x)\right) dx = -f^{'}(0) \tag{7.17}$$

Symmetry of the solutions in p

While $L \in \{+,-\}$ determines the symmetry of the regular and irregular solution for $x \to -x$, we also want to choose solutions with symmetry in p

Even solutions, $L = (+)$ A regular solution is only given up to a multiplicative constant of absolute value 1 if still normed properly. Therefore all normed regular, even (in x) solutions are given by

$$e^{i\beta(p)}\pi^{-1/2}\cos{(px)} \tag{7.18}$$

with $\beta(p)$ being a real function of p. One possibility is to choose $\beta = 0$ which leads to our function, which is also even in p :

$$Z_{+,-p}(x) = \pi^{-1/2}\cos(-px) = Z_{+,p}(x) \tag{7.19}$$

For an irregular solution there are more degrees of freedom, because one can always add a regular solution. The one given above is the only real, normed, even (in x) solution which is odd in p.

$$I_{+,-p}(x) = \pi^{-1/2}\sin(-p|x|) = -I_{+,p}(x) \tag{7.20}$$

Odd solutions, $L = (-)$ Once again a regular solution is only given up to a multiplicative constant of absolute value 1 if normed properly. Therefore all normed regular, odd (in x) solutions are given by

$$e^{i\beta(p)}\pi^{-1/2}\sin(px) \tag{7.21}$$

with $\beta(p)$ being a real function of p. Now one possibility is to choose $\beta = 0$ which leads to our function, which is also odd in p.

$$Z_{-,-p}(x) = \pi^{-1/2}\sin(-px) = -Z_{+,p}(x) \tag{7.22}$$

For the irregular solution there are again more degrees of freedom, because one can always add a regular solution. The one given above is the only real, normed, odd (in x) solution which is even in p

$$I_{-,-p}(x) = \pi^{-1/2}\sigma(x)\cos(-p|x|) = I_{-,p}(x)\ . \tag{7.23}$$

Green function

With a complete, orthonormal (generalized) eigenbasis given, the Green function can always be expressed in the spectral resolution

$$G(x,x';z) = \sum\int d\mu\,(\lambda)\,\frac{1}{z-E(\lambda)}\phi_\lambda(x)\phi^*_\lambda(x')\ . \tag{7.24}$$

where λ labels any complete set of eigenfunctions (and $.\sum\int d\mu\,(\lambda)$ is the summation and integration over the spectrum)
One possibility (and the easiest here) is to take the plane waves (7.3)

$$\begin{aligned}
G(x,x';z) &= \int_{\mathbb{R}} dk \left[\frac{1}{z-k^2}\left(\frac{1}{2\pi}e^{ik(x-x')}\right)\right] dk = && (7.25)\\
&= \frac{1}{2\pi}\oint_{C+}\left(\frac{e^{ik|x-x'|}}{z-k^2}\right) dk = \frac{1}{2\pi}\oint_{C+}\left(\frac{-e^{ik|x-x'|}}{(k-p)\,(k+p)}\right) dk = && (7.26)\\
&= 2\pi i\left(\frac{1}{2\pi}\frac{-e^{ip|x-x'|}}{2p}\right) = \frac{e^{ip|x-x'|}}{2ip} = && (7.27)\\
g(|x-x'|\,;z &= p^2) = \frac{\sin(p|x-x'|)}{2p} - i\frac{\cos(p|x-x'|)}{2p} && (7.28)
\end{aligned}$$

Because we will need a similar derivation later on, we also derive the Green function with the other eigenbasis of even and odd functions defined in (7.6)

$$\begin{aligned}
G(x,x';z) &= \sum_{L\in\{+,-\}} \int_0^\infty dk \left[\frac{1}{z-k^2}\left(Z_{L,k}(x)Z^*_{L,k}(x')\right)\right] = \\
&= \sum_{L\in\{+,-\}} \frac{1}{2}\int_{\mathbb{R}} dk \left(\frac{1}{z-k^2} Z_{L,k}(x)Z_{L,k}(x')\right) = \\
&= \sum_{L\in\{+,-\}} \frac{1}{2}\int_{\mathbb{R}} dk \left(\frac{1}{z-k^2} Z_{L,k}(r_<)\left(Z_{L,k}(r_>)+c_{L,k}I_{L,k}(r_>)\right)\right) = \\
&= \sum_{L\in\{+,-\}} \frac{1}{2}\oint_{C^+} dk \left(\frac{1}{z-k^2} Z_{L,k}(r_<)\left(Z_{L,k}(r_>)+c_{L,k}I_{L,k}(r_>)\right)\right) = \\
&= \ldots = \frac{e^{ip|x-x'|}}{2ip} = \\
&= \frac{\pi}{2ip} \sum_{L\in\{+,-\}} Z_{L,p}(r_<)H_{L,p}(r_>) = G(x,x';z=p^2) \qquad (7.29\text{a})
\end{aligned}$$

Where the constants $c_{L,k}$ are chosen such that one can close the arc in the complex plane by a half circle with $\mathrm{Im}(k) > 0$. The value of the integral is not changed because Z and I have always different symmetry in p and therefore $\int_{\mathbb{R}}$ vanishes.
Here the constants $c_{L,k}$ are given by

$$L = (+) \quad : \quad \frac{1}{\sqrt{\pi}} e^{ikr_>} = \frac{1}{\sqrt{\pi}}(\cos(kr_>) + i\sin(kr_>)), \quad c_{+,k} = +i \qquad (7.30)$$

$$L = (-) \quad : \quad \frac{1}{\sqrt{\pi}}\sigma(x_>)(-ie^{ikr_>}) = \frac{1}{\sqrt{\pi}}\sigma(x)(\sin(kr) - i\cos(kr)), \quad c_{-,k} = -i \qquad (7.31)$$

which are the irregular solutions named outgoing waves, which make the complex upper half circle harmless.

7.1.2 Particle in 1D potential with bound states

Spectrum and complete set of eigenfunctions

If the potential is given by

$$V(x) = -2B\delta(x)$$

the Schrödinger equation can be written as

$$\left[-\frac{d^2}{dx^2} + V(x)\right]\psi(x) = E\psi(x) \qquad (7.32)$$

By integrating the differential equation $\int_{-\epsilon}^{+\epsilon}$ for $\epsilon \to 0$, one gets the necessary condition

$$\psi'|_{0^-}^{0^+} = -2B\psi(0) \qquad (7.33)$$

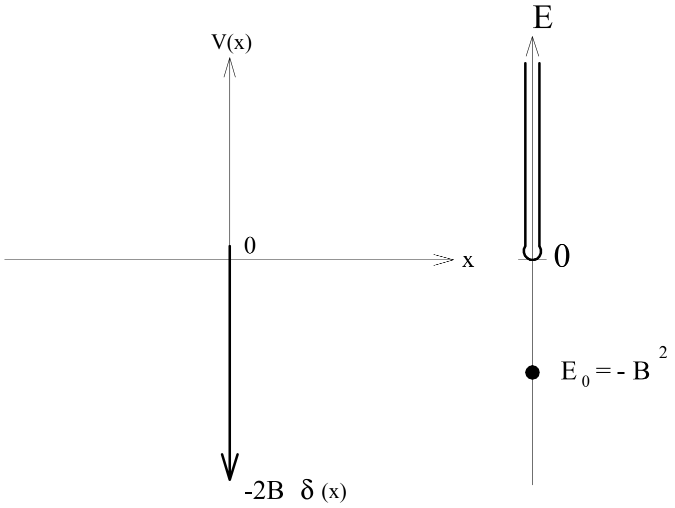

Figure 7.4: A potential with one attractive δ function at the origin gives rise to a spectrum $\sigma = \sigma_p \cup \sigma_c = \{-B^2\} \cup [0, +\infty]$.

for the discontinuity of the first derivative at $x = 0$.
There is a point spectrum as well as a continuous spectrum, see (Fig.7.4)

$$\sigma = \sigma_p \cup \sigma_c = \{-B^2\} \cup [0, +\infty] \tag{7.34}$$

The one and only bound state is given by

$$\phi_{0,+}(x) = \sqrt{B} e^{-B|x|}, E_0 = -B^2 \tag{7.35}$$

where one can see that it is an even function of x.
For the continuous spectrum various different sets of complete, orthonormal generalized eigenfunctions can be given. We try to follow the line chosen for a free particle.

Regular and Irregular solutions

Similar to 3D there exists for every $L \in \{+, -\}$ a 2 dimensional solution space, which can be spanned by one regular and one irregular solution.
The regular solution is characterized by the fact that it fulfills the differential equation

$$\left[-\frac{d^2}{dx^2} - 2B\delta(x) \right] \psi(x) = E\psi(x) \tag{7.36}$$

everywhere in $\mathbb{R}$. All irregular solutions do not fulfill the differential equation at the origin $x = 0$, where they have an additional δ like singularity. Because the potential itself has already a δ singularity at the origin the situation is more complicated.
The radial differential equation is the same for every L (even and odd functions) but we see that the odd functions are not affected by the δ singularity at the origin, because they vanish for $x = 0$.

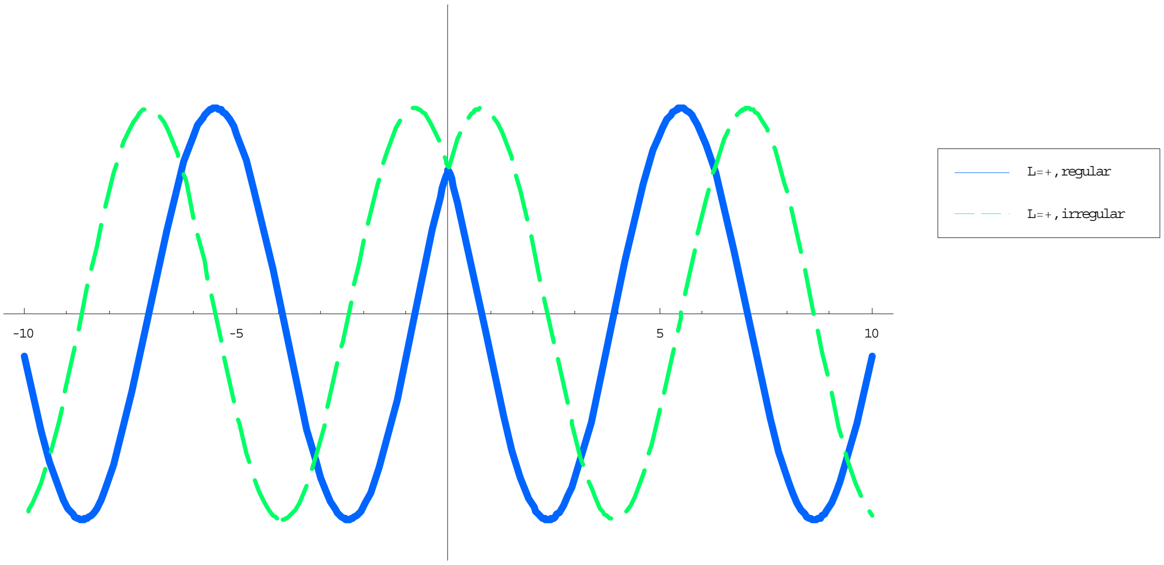

Figure 7.5: Regular and irregular even solution for a particle under the influence of the δ potential at the origin..

Even functions, $L = (+)$ The even functions can be affected by the potential (see Fig. 7.5 compared to Fig. 7.2)

$$\begin{array}{rl}
\text{regular solution} & Z_{+,k}(x) = \frac{1}{\sqrt{\pi}}\cos(k|x| + \alpha_k) = \frac{1}{\sqrt{\pi}}\cos(kr + \alpha_k) \\
\text{irregular solution} & I_{+,k}(x) = \frac{1}{\sqrt{\pi}}\sin\left(k\,|x| + \alpha_k\right) = \frac{1}{\sqrt{\pi}}\sin\left(kr + \alpha_k\right) \\
\text{outgoing waves:} & I_{+,k}(x) = \frac{1}{\sqrt{\pi}}e^{i(k|x|+\alpha_k)} = \frac{1}{\sqrt{\pi}}e^{i(kr+\alpha_k)}
\end{array}$$

The 'phase shifts' α_k fulfill the relation

$$\tan\alpha_k = \frac{B}{k} \tag{7.37}$$

which implies that they are an odd function of k with a step-singularity at $k = 0.$, see (Fig.7.6) Since for $B = 0$ the phase shifts should be identically zero, $\alpha_k \equiv 0$ for all k, we choose the branch of the arctan with $\arctan(0) = 0$. Furthermore, one gets the relations

$$\cos^2\alpha_k = \frac{k^2}{B^2 + k^2} \tag{7.38}$$

$$\sin^2\alpha_k = \frac{B^2}{B^2 + k^2} \tag{7.39}$$

$$\sin\alpha_k\cos\alpha_k = \frac{Bk}{B^2 + k^2}\ . \tag{7.40}$$

Odd functions, $L = (-)$ The odd solutions are not affected by the δ potential

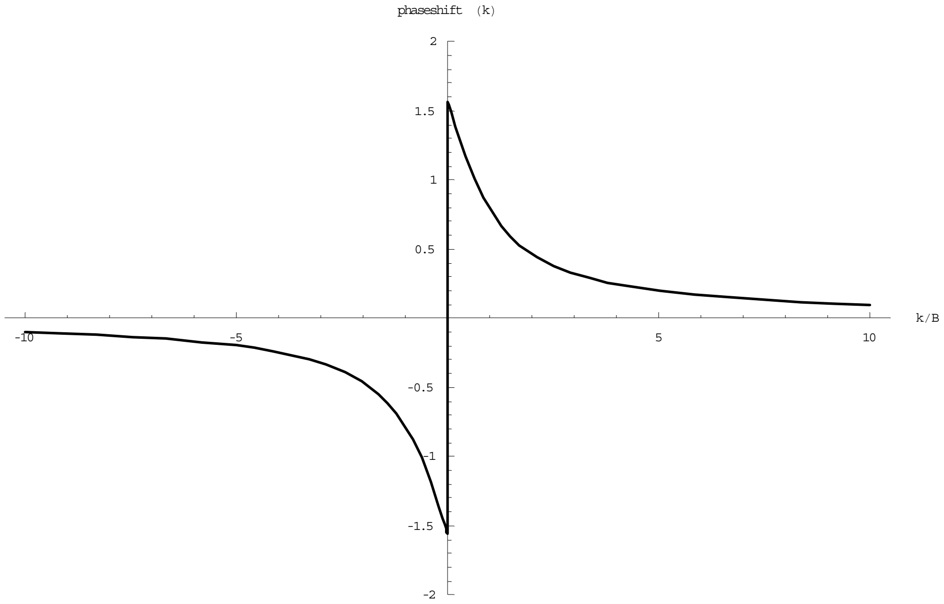

Figure 7.6: .

regular solution	$Z_{-,k}(x)=\frac{1}{\sqrt{\pi}}\sin kx=\frac{1}{\sqrt{\pi}}\sigma(x)\sin kr$
irregular solution	$I_{-,k}(x)=\frac{1}{\sqrt{\pi}}\sigma(x)\cos kr=\frac{1}{\sqrt{\pi}}\sigma(x)\cos k\vert x\vert$
	$H_{-,p}(x)=\left(-\frac{i}{\sqrt{\pi}}\operatorname{sgn}(x)\right)e^{ipr}$

Symmetry of the solutions in k

While $L\in\{+,-\}$ determines the symmetry of the regular and irregular solution as a function of x, we also chose solutions with symmetry in k.

Even solutions The regular solution fulfills

$$Z_{+,-k}(x)=\pi^{-1/2}\cos(-kr+\alpha_{-k}))=Z_{+,+k}(x) \tag{7.41}$$

and is even in k, while for the irregular solutions we took an odd function in k

$$I_{+,-k}(x)=\pi^{-1/2}\sin(-k|x|)=-I_{+,+k}(x) \tag{7.42}$$

Odd solutions The regular solution is odd in k

$$Z_{-,-k}(x)=\pi^{-1/2}\sin(-kx)=-Z_{-,+k}(x) \tag{7.43}$$

The irregular solution is even in k

$$I_{-,-k}(x)=\pi^{-1/2}\sigma(x)\cos(-k|x|)=I_{-,+k}(x) \tag{7.44}$$

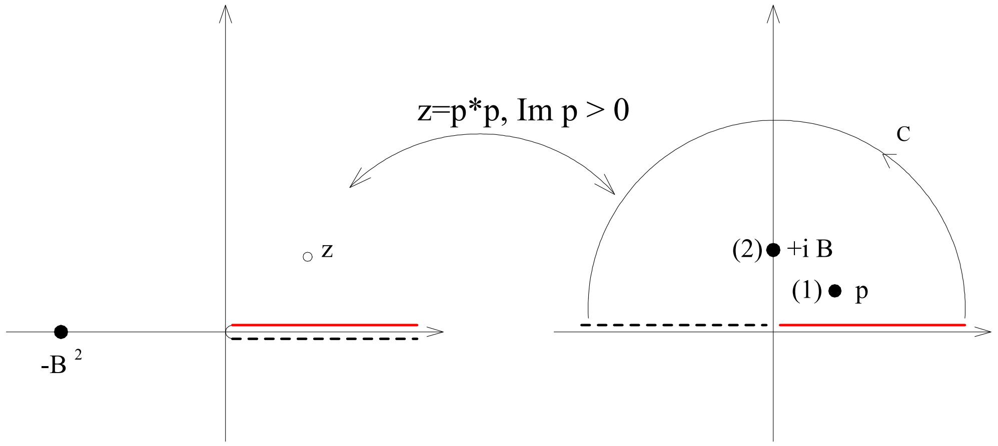

Figure 7.7: left plot: The complex energy z plane with the continuous spectrum at the positive real axis and the eigenvalue at $z = -B^2$
right plot: The complex p plane, after the bijective mapping $z \mapsto p$ on the upper complex halfplane. The halfcircle C contains the point $+iB$ and the point p.

Green function

Now we come to the most important part which illustrates what happens to the bound states in the Green function. Given a complete, orthonormal (generalized) eigenbasis the Green function can always be expressed in the spectral resolution

$$G(x,x';z) = \sum \int d\lambda \frac{1}{z - E(\lambda)} \phi_\lambda(x)\phi_\lambda(x') \ , \tag{7.45}$$

where λ labels any complete set of eigenfunctions.With a point spectrum and continuous spectrum we have to write

$$\begin{aligned} G(x,x';z) &= G_p(x,x';z) + G_c(x,x';z) = \\ &= \sum_{E_n \in \sigma_p} \frac{1}{z - E_n} \left(\phi_{0,n}(x)\phi^*_{0,n}(x')\right) + \sum_{L \in \{+,-\}} \int_0^\infty dk \left(\frac{1}{z - k^2} Z_{L,k}(x) Z^*_{L,k}(x') \right) = \\ &= \frac{B}{z + B^2} e^{-B(r+r')} + \frac{1}{\pi} \int_0^\infty dk \left[\frac{1}{z - k^2} \left(\cos(kr + \alpha_k)\cos(kr' + \alpha_k) + \sin(kx)\sin(kx')\right) \right] \end{aligned} \tag{7.46}$$

If we add another function in order to be able to close the integral path in the complex plane without changing the result of the integral we arrive at

$$\begin{aligned} G(x,x';z) &= \frac{B}{z + B^2} e^{-B(r+r')} + \frac{1}{2\pi} \int_{-\infty}^\infty dk \left(\frac{1}{z - k^2} (\cos(kr_< + \alpha_k) \times \right. \\ &\times (\cos(kr_> + \alpha_k) + i\sin(kr_> + \alpha_k)) + \sigma(x)\sigma(x')\sin kr_< (\sin kr_> - i\cos kr_>))) = \\ &= \frac{B}{z + B^2} e^{-B(r+r')} + \frac{1}{2\pi} \oint_C dk \frac{1}{z - k^2} (\cos(kr_< + \alpha_k) e^{i\alpha_k} - i\sigma(x)\sigma(x')\sin kr_<) e^{ikr_>} \end{aligned} \tag{7.47}$$

Here the real integral could be transferred to a complex contour integral by adding specific functions to the regular solutions which make

- the integrand vanish for the upper complex half circle
- the integrand a meromorphic function of $k \in \mathbb{C}$

Now the integrand has 2 different kind of poles in the upper half plane,

- one pole of first order at $k = p$; $p^2 = z$, $Im(p) > 0$ where the $(z - k^2)^{-1}$ has a pole
- poles at all those k values where the functions of the phase shifts have a pole, which are exactly the roots of the energy of the bound states

In this specific example we only have one bound state at $E = -B^2, k = iB$, which leads to a term which exactly cancels the first term from the bound states. What remains is to evaluate the functions at $k = p = \sqrt{z}$, which leads to

$$\begin{aligned} G(x, x'; z) &= \frac{-i}{2p}\left[\cos(pr_< + \alpha_p)e^{i\alpha_p} - i\sigma(x)\sigma(x')\sin(pr_<)\, e^{ipr_>}\right] = \\ &= \frac{-i}{2p}\left[e^{ip|x-x'|} + \frac{iB}{p-iB}e^{ip(r_<+r_>)}\right] = \frac{e^{ip|x-x'|}}{2ip} + \frac{B}{2p(p-iB)}e^{ip(r_<+r_>)} \end{aligned}$$

So we found an expression for the Green function.

7.2 Free particle in 3 dimensions

7.2.1 Spectrum and complete set of eigenfunctions

If the potential is identically zero

$$V(x) \equiv 0$$

the Schrödinger equation is written

$$-\triangle\psi(x) = z\psi(x) \tag{7.48}$$

There is only a continuous spectrum

$$\sigma = \sigma_p \cup \sigma_c = \{\} \cup [0, +\infty] \tag{7.49}$$

A complete, orthonormal set of generalized eigenfunctions is given by

$$\left\{\phi_{\mathbf{k}}(\mathbf{x}) = \frac{1}{\sqrt{(2\pi)^3}}e^{i\mathbf{k}\cdot\mathbf{x}}, \mathbf{k} \in \mathbb{R}^3\right\}, E_{\mathbf{k}} = \mathbf{k}\cdot\mathbf{k} \tag{7.50}$$

Orthonormal:

$$\int_{\mathbb{R}^3} (\phi_k(\mathbf{x})\phi^*_{k'}(\mathbf{x}))\, d^3\mathbf{x} = \frac{1}{(2\pi)^3}\int_{\mathbb{R}^3} e^{i(\mathbf{k}-\mathbf{k}')\cdot\mathbf{x}} d^3\mathbf{x} = \delta^{(3)}(\mathbf{k}-\mathbf{k}') = \delta(\mathbf{k}-\mathbf{k}') \tag{7.51}$$

Complete:

$$\int_{\mathbb{R}^3} |\phi_k >< \phi_k| d^3k = \hat{1} \ , \ \frac{1}{(2\pi)^3} \int_{\mathbb{R}^3} e^{i\mathbf{k}\cdot(\mathbf{x}-\mathbf{x}')} d^3k = \delta(\mathbf{x}-\mathbf{x}') \tag{7.52}$$

To find another complete, orthonormal set of generalized eigenfunctions we apply the usual separation

$$\psi(\mathbf{x}) = f(r) Y(\widehat{\mathbf{x}}) \tag{7.53}$$

and the solutions of the angular equations in the form of spherical harmonics

$$Y_L(\widehat{\mathbf{x}}) = Y_{lm}(\widehat{\mathbf{x}}), \quad l \in \{0, 1, \ldots\}, m \in \{-l, \ldots, +l\}$$

lead to the radial equation

$$\left[-\frac{1}{r^2} \frac{d}{dr} (r^2 \frac{d}{dr}) + \frac{l(l+1)}{r^2} - z \right] f(r) = 0 \tag{7.54}$$

or with $g(r) = rf(r)$ to

$$\left[-\frac{d^2}{dr^2} + \frac{l(l+1)}{r^2} - z \right] g(r) = 0 \tag{7.55}$$

A regular, normed solution is given by ($z = E = k^2 \in \mathbb{R}^+$)

$$Z_{l,k}(r) = \sqrt{\frac{2}{\pi}} k j_l(kr) \tag{7.56}$$

Therefore a complete set of generalized eigenfunctions is given by

$$\left\{ \sqrt{\frac{2}{\pi}} k j_l(kr) Y_L(\widehat{\mathbf{x}}), L = (lm), k \in \mathbb{R}^+ \right\} \tag{7.57}$$

which is orthonormal

$$\int_{\mathbb{R}^3} \left(\sqrt{\frac{2}{\pi}} k j_l(kr) Y_L(\widehat{\mathbf{x}}) \sqrt{\frac{2}{\pi}} k' j_{l'}(k'r) Y^*_{L'}(\widehat{\mathbf{x}}) \right) d^3x = \delta\left(k - k'\right) \delta_{LL'} \tag{7.58}$$

and complete

$$\sum_L \int_{\mathbb{R}^+} dk \left(\sqrt{\frac{2}{\pi}} k j_l(kr) Y_L(\widehat{\mathbf{x}}) \sqrt{\frac{2}{\pi}} k j_l(kr') Y^*_{L'}(\widehat{\mathbf{x}}') \right) = \delta^{(3)}\left(\mathbf{x} - \mathbf{x}'\right) = \delta\left(\mathbf{x} - \mathbf{x}'\right) \tag{7.59}$$

7.2.2 Regular and Irregular solutions

For every L there exists a 2 dimensional solution space, which is spanned by one regular and one irregular solution.
A regular solution is characterized by the fact that it fulfills the differential equation

$$\left[-\frac{d^2}{dr^2} + \frac{l(l+1)}{r^2} - z \right] (rf(r)) = 0 \tag{7.60}$$

everywhere in $[0,\infty]$. All irregular solutions do not fulfill the differential equation at the origin $\mathbf{x} = \mathbf{0}$ ($\mathbf{r} = \mathbf{0}$), where they have a δ like singularity.
Different to the 1D case the radial differential equation depends on L and only the 'irregular solutions' are really irregular at the origin.

$$\begin{aligned} L = (l,m) \quad \text{regular solution:} \quad & Z_{l,k}(r) = \sqrt{\tfrac{2}{\pi}}kj_l(kr) \\ \text{irregular solution:} \quad & I_{l,k}(r) = \sqrt{\tfrac{2}{\pi}}kn_l(kr) \end{aligned}$$

Here the regular solution fulfills the differential equation everywhere, while e.g. the irregular for $l = 0$

$$[-\triangle - z]\, I_{l=0,p}(r) = [-\triangle - z]\frac{1}{\sqrt{2}\pi}\frac{\cos(kr)}{r} = 2\sqrt{2}\delta(\mathbf{x}) \tag{7.61}$$

7.2.3 Symmetry of the solutions in p

While L determines the symmetry of the regular and irregular solution as a function of the angle of $\mathbf{x}$, we chose solutions with symmetry with respect to $k \to -k$

Regular solutions

The symmetry of a regular solution is given by the symmetry of the spherical Bessel function:

$$Z_{l,-k}(r) = \sqrt{\frac{2}{\pi}}\,(-kj_l(-kr)) = (-1)^{l+1} Z_{l,k}(r) \tag{7.62}$$

Irregular solutions

For the irregular solutions there are more degrees of freedom, because one can always add a regular solution. The one given above is the only real, normed solution which has symmetry in k.

$$I_{l,-k}(r) = \sqrt{\frac{2}{\pi}}\,(-kn_l(-kr)) = (-1)^l I_{l,k}(r) \tag{7.63}$$

Therefore the product of this regular and irregular solutions is always odd in $k \in \mathbb{R}$.

7.2.4 Green function

With a complete, orthonormal (generalized) eigenbasis the Green function can always be expressed in the spectral resolution.

$$G(x,x';z) = \sum_\lambda \int d\lambda \frac{1}{z - E(\lambda)}\phi_\lambda(x)\phi^*_\lambda(x')\ , \tag{7.64}$$

where λ labels any complete set of eigenfunctions.
One possibility and the easiest here is to take plane waves (with $p^2 = z$)

$$\begin{aligned} G(x,x';z) &= \int_{\mathbb{R}^3} d\mathbf{k}\frac{1}{z-k^2}\frac{1}{(2\pi)^3}e^{i\mathbf{k}\cdot(\mathbf{x}-\mathbf{x}')}d^3k = && (7.65)\\ &= \frac{1}{(2\pi)^3}\int_{S_2} d\widehat{\mathbf{k}}\int_0^\infty dk\frac{k^2}{z-k^2}e^{i|\mathbf{k}||\mathbf{x}-\mathbf{x}'|\cos\theta} = && (7.66)\\ &= \ldots = && (7.67)\\ &= -\frac{e^{ip|\mathbf{x}-\mathbf{x}'|}}{4\pi|\mathbf{x}-\mathbf{x}'|} && (7.68) \end{aligned}$$

Another expression is given by taking the basis defined in paragraph (7.2.2)

$$\begin{aligned} G(x,x';z) &= \sum_L \int_0^\infty dk\frac{1}{z-k^2}Z_{L,k}(x)Z^*_{L,k}(x') = && (7.69)\\ &= \sum_L \frac{1}{2}\int_{\mathbb{R}} dk\frac{1}{z-k^2}Z_{L,k}(x)Z_{L,k}(x') = && (7.70)\\ &= \sum_L \frac{1}{2}\int_{\mathbb{R}} dk\left(\frac{1}{z-k^2}Z_{l,k}(r_<)(Z_{l,k}(r_>)+c_{l,k}I_{l,k}(r_>))Y_L(\widehat{\mathbf{x}})Y^*_L(\widehat{\mathbf{x}}')\right) = && (7.71)\\ &= ip\sum_L j_l(pr_<)h_l(pr_>)Y_L(\widehat{\mathbf{x}})Y^*_L(\widehat{\mathbf{x}}')\ , && (7.72) \end{aligned}$$

where the constants $c_{l,k}$ are chosen such that one can close the arc in the complex plane by a half circle with $\mathrm{Im}(k) > 0$. The value of the integral is not changed because Z and I have always different symmetry in k.
Here it would be the following function,

$$L : (j_l(kr) + in_l(kr)) \qquad (7.73)$$

which is the outgoing Hankel function that goes to 0 for $k \to \infty$, $Im(k) > 0$.

7.3 Constant shift of the potential, dependence on shift parameter

In this section we deal with the consequences of the choice of the zero of energy for the KKR method.

7.3.1 Fullcell geometry - theoretical independence of results

In a fullcell geometry description the lattice periodic potential V is a sum of localized potentials $V_{\mu,n}$

$$V(\mathbf{x}) = \sum_{n\in\mathbb{Z}^d}\sum_\mu V_{\mu,n}(\mathbf{x}) = \sum_{n\in\mathbb{Z}^d}\sum_\mu \sigma_{\mu,n}(\mathbf{x})V(\mathbf{x})$$

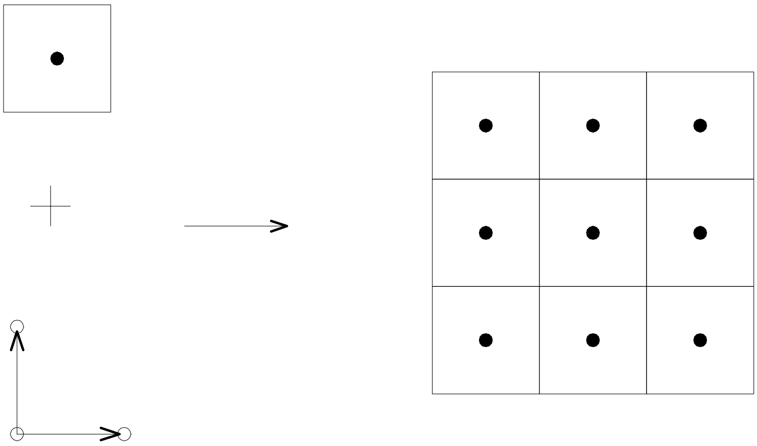

Figure 7.8: In a full-cell geometry the union of all cells covers the space without overlap or uncovered regions.

Where each $V_{\mu,n}$ is a localized potential and identical zero outside the corresponding cell $\mathcal{V}_{\mu,n}$, which is given by the Wigner-Seitz construction. The theory of KKR demands that these cells must not overlap, then the multiple scattering problem can be separated in a single center problem and the geometrical structure constants (see Fig. 7.8).

This is fulfilled by our nearest neighbor cell construction. In principle one is free to add a constant to the **periodic potential**, which should leave the results unchanged. $V(\mathbf{x}) \to V(\mathbf{x}) + W$, because

$$\forall \mathbf{x} \in \mathbb{R}^d \left(\sum_{n \in \mathbb{Z}^d} \sum_{\mu} \sigma_{\mu,n}(\mathbf{x}) = 1 \right),$$

this constant can be transferred into each single center potential

$$\left[V_{\mu,n}(\mathbf{x}) + W \right] \sigma_{\mu,n}(\mathbf{x})$$

which might be advantageous so that one can shift the potential to a certain energy region

$$V(\mathbf{x}) + W = \left(\sum_{n \in \mathbb{Z}^d} \sum_{\mu} V_{\mu,n}(\mathbf{x}) \right) + W = \sum_{n \in \mathbb{Z}^d} \sum_{\mu} \left[V_{\mu,n}(\mathbf{x}) + W \right] \sigma_{\mu,n}(\mathbf{x})$$

7.3.2 Fullcelll geometry - practical dependence on shift parameter

While a fullcell geometry description theoretically leads to results independent of the shift parameter W in practice one is limited to a certain $l_{\max}$ in the expansion of the shape functions

$$\sigma^{[l_{\max}]}(\mathbf{x}) = \sum_{L=(l,m)}^{l_{\max}} \sigma_L(r) Y_L(\widehat{x})$$

Therefore the identity

$$1 = \sum_{n \in \mathbb{Z}^d} \sum_{\mu} \sigma_{\mu,n}(\mathbf{x})$$

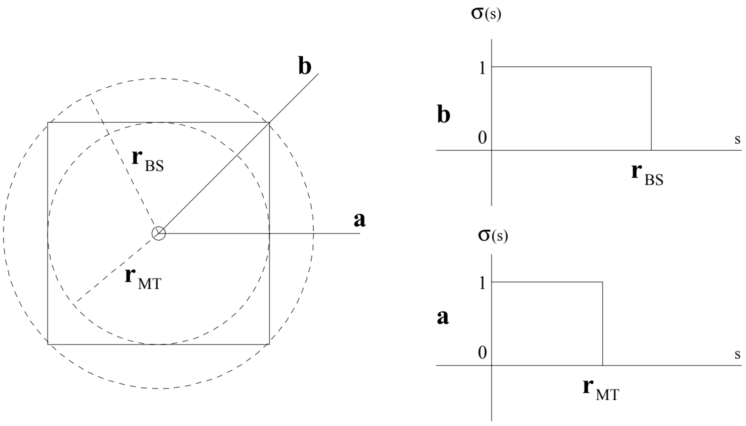

Figure 7.9: Ideal form of $\sigma\left(\mathbf{x}(r)\right)$ in a quadratic unit cell for a given direction $\mathbf{x}_0$ as a function of the radial distance $\mathbf{x}(r) = r\ \mathbf{x}_0$. The discontinuous jump is not reproduced by $\sigma^{[l_{\max}]}(\mathbf{x}(r))$.

is not exactly fulfilled anymore, which can be seen by plotting the shape function along specific directions out of the cell centre. Let r be the parameter along the path $\mathbf{x}(r)$ then $\sigma(\mathbf{x}(r))$ should be a step function changing from 1 to the value 0 at the cell boundary (see Fig 7.9), in practice this is not fulfilled and $\sigma^{[l_{\max}]}(\mathbf{x}(r))$ will deviate from the theoretical curve, due to the mathematical Gibbs Phenomenon (see Fig 7.10 in MT direction and Fig 7.11 in BS direction) this effect would also be present for $\mathrm{l}_{\max} \to \infty$ and is a serious limitation to the method.

The Gibbs Phenomenon has smallest disturbing influence, if the potential is shifted by a constant

$$V'\left(\mathbf{x}\right) = V\left(\mathbf{x}\right) + W = \left(\sum_{L} V'_L(r) Y_L(\widehat{x})\right)$$

so that the $L = (0,0) = 1$ (with $L = l(l+1) + m + 1$) component fulfills

$$V'_{L=(00)}(r_{MT}) = V_{L=(00)}(r_{MT}) + W = 0\ .$$

7.3.3 ASA geometry - theoretical dependence of results on shift parameter

In the case of a spherical cell geometry (MT, ASA,..) every single center potential is limited to a ball (sphere) $B_{\mu,n}$ centered around the atomic position $\mathbf{R}_{\mu,n}$. These balls overlap $B_{\mu,n} \cap B_{\nu,m} \neq \emptyset$ and/or leave some space which is not covered by any cell,

$$\exists \mathbf{x} \in \mathbb{R}^d : \forall \mu, n \left(\mathbf{x} \notin B_{\mu,n}\right)\ .$$

If we still denote the characteristic function of the set $B_{\mu,n}$ with $\sigma_{\mu,n}(\mathbf{x}) = \sigma_{B_{\mu,n}}(\mathbf{x})$, then

$$\sum_{n\in\mathbb{Z}^d}\sum_{\mu}\sigma_{\mu,n}(\mathbf{x}) = \begin{cases} 0 & \mathbf{x} \notin B_{\mu,n} \\ 1 & \mathbf{x} \in 1\ B_{\mu,n} \\ 2 & \mathbf{x} \in 2\ B_{\mu,n} \\ \cdots & \cdots \\ n & \mathbf{x} \in n \text{ Balls} \end{cases}$$

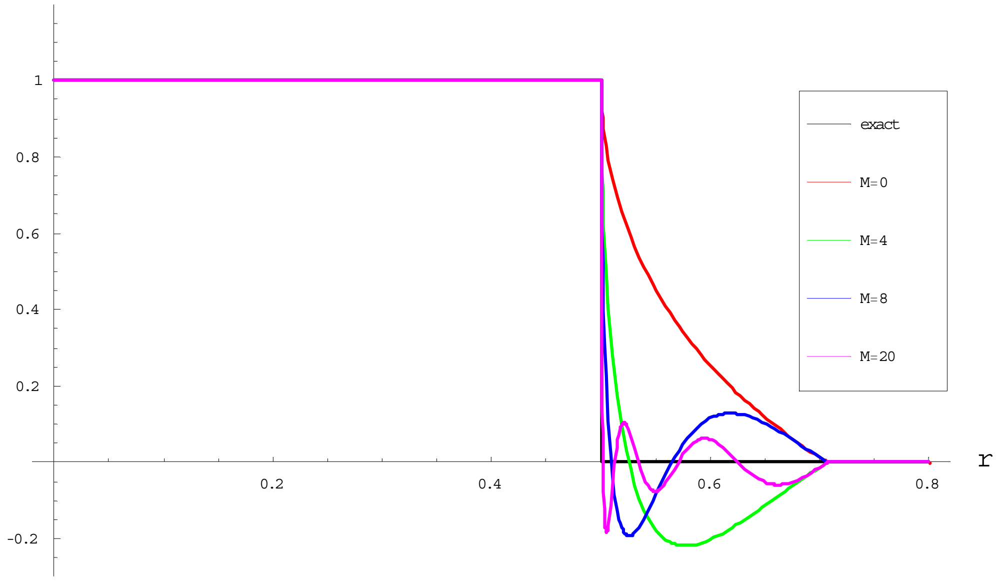

Figure 7.10: The exact shape function $\sigma(\mathbf{x}(r))$ and approximations $\sigma^{[l_{\max}]}(\mathbf{x}(r))$ for various $l_{\max}$ in a MT direction of the 2D quadratic unit cell.

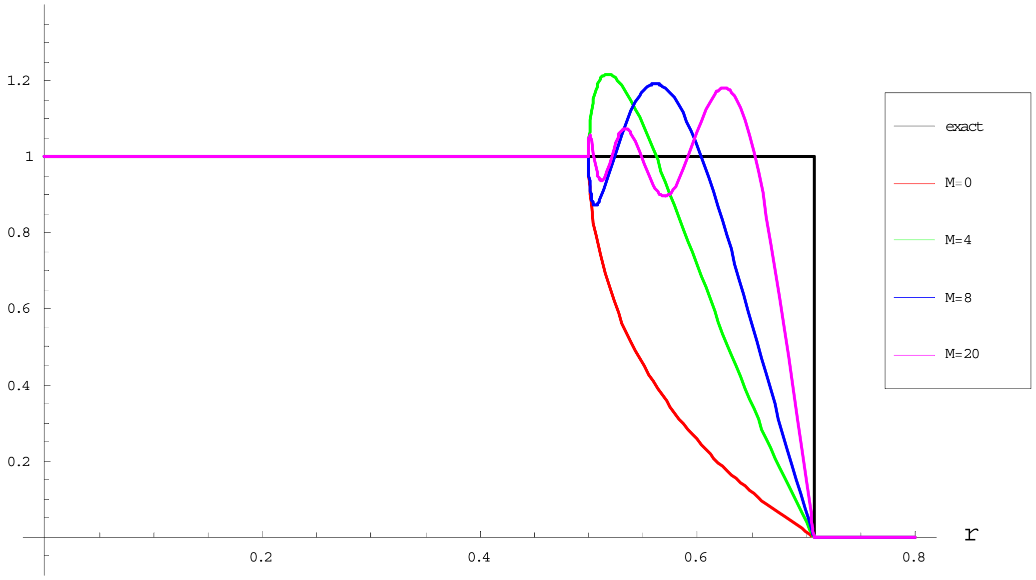

Figure 7.11: The exact shape function $\sigma(\mathbf{x}(r))$ and approximations $\sigma^{[l_{\max}]}(\mathbf{x}(r))$ for various $l_{\max}$ in a BS direction of the 2D quadratic unit cell.

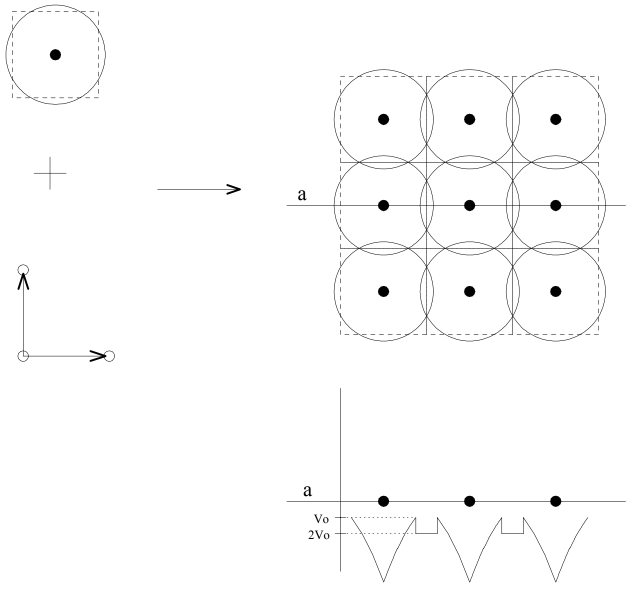

Figure 7.12: Unit cell and ASA spheres: if put together there are overlap regions and uncovered regions. The sum of the potentials is not only shifted by a constant.

is not identically 1 anymore, but has an integer value equal to the number of balls which contain $\mathbf{x}$ (see Fig. 7.12). For a MT-geometry only the values 0 and 1 arise, while for an ASA geometry 0,1 and 2 arise. Therefore in all sphere geometry cases one can not transfer the shift constant W to the single site problems

$$V(\mathbf{x}) + W = \left(\sum_{n \in \mathbb{Z}^d} \sum_{\mu} V_{\mu,n}(\mathbf{x}) \right) + W \neq \sum_{n \in \mathbb{Z}^d} \sum_{\mu} \left(V_{\mu,n}(\mathbf{x}) + W \right) \sigma_{\mu,n}(\mathbf{x})$$

and the results will have a dependence on the value of W. Especially at the boundary of the balls the relevant periodic potential is not continuous anymore (see Fig. 7.14). These jumps can be minimized by shifting the single site potential to 0 at r_{ASA} (see Fig. 7.13).

Note that also in a MT-description this problem still occurs as long as one does not further describe the interstitial region.

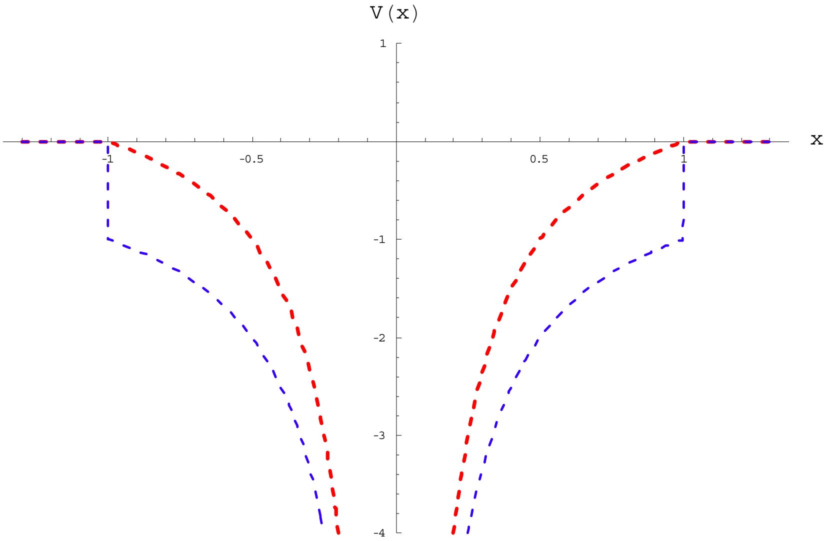

Figure 7.13: A single center potential $V(r)$, unshifted and shifted such that $V(r_{ASA}) = 0$.

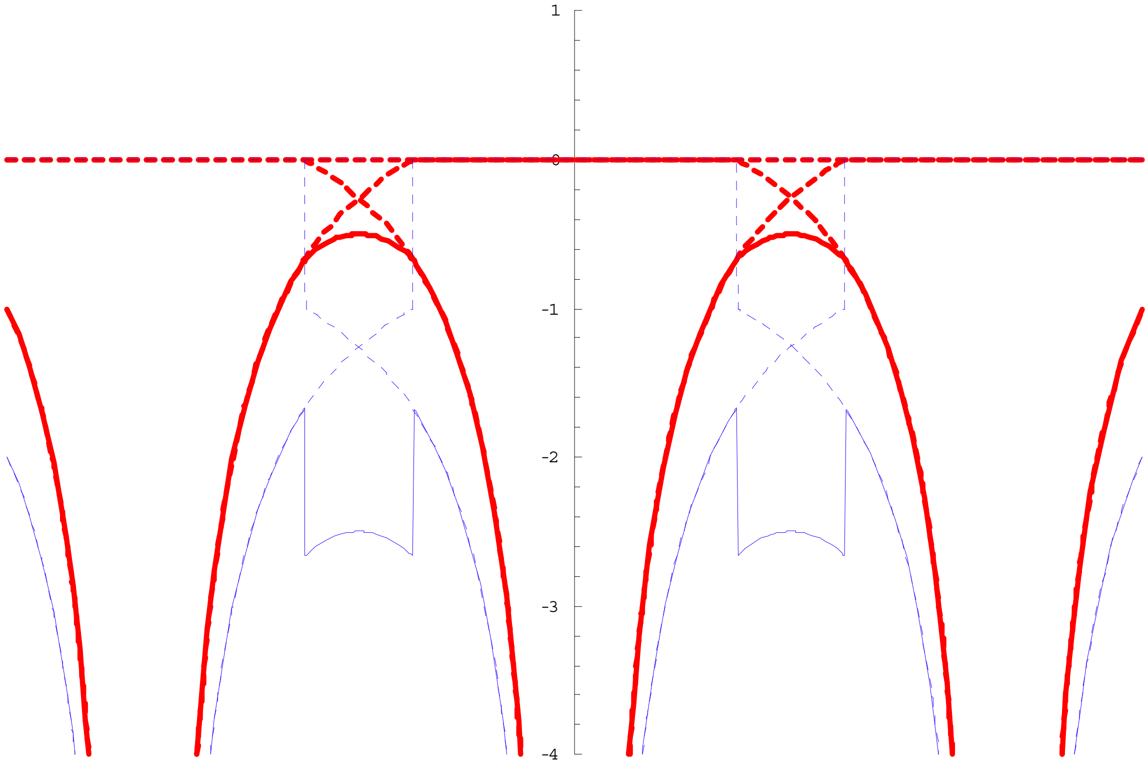

Figure 7.14: Dashed lines are single site potentials, full lines are total, periodic potentials, the lower potential is not shifted to zero at r_{ASA} and therefore the total potential has a discontinuity (lower full line).

Chapter 8

Structural Green function for m-dimensional lattices in n dimensional space

A general expression for the structural Green function for a system exhibiting lattice translational symmetry in m dimensions and natural boundary conditions in the remaining $n - m$ dimensions is developed and mathematically rigorously proofed.

For the case of $m = n = 3$ an expression has been given by [25], for $m = 2, n = 3$ by [23], and for $m = 2, n = 2$ by [14]. Future applications contain Quantum wires for $m = 1, n = 3$ and quasicrystals for $n \geq 4$. Both, a direct lattice summation and a reciprocal lattice summation technique are given and an Ewald-technique is applicable for a combined summation.

8.1 Overview:

We find an expression for the structural Green function for m-dimensional lattices in n-dimensional real space. The expansion of the structural Green function leads to the structure constants.

Both are given either in terms of a reciprocal lattice sum or a direct lattice sum. In general the expression for the structural Green function is the sum of a product of a free particle Green function times an exponential function. Using the Ewald technique the reciprocal and direct lattice sums can be combined for numerical evaluation. Applications to the special cases of ($m = 1, n = 2$), ($m = 1, n = 3$), and ($m = 2, n = 3$), are finally discussed.

8.2 Free Particle Green Function:

The free particle Hamiltonian in n dimensions is defined as (b.c. means boundary conditions)

$$\hat{A}_0^{(n)} = \begin{cases} -\Delta & \text{in}\, \mathcal{H} = L_2(\mathbb{R}^n; \mathbb{C}) \\ +\text{ natural b.c.} & \end{cases} \tag{8.1}$$

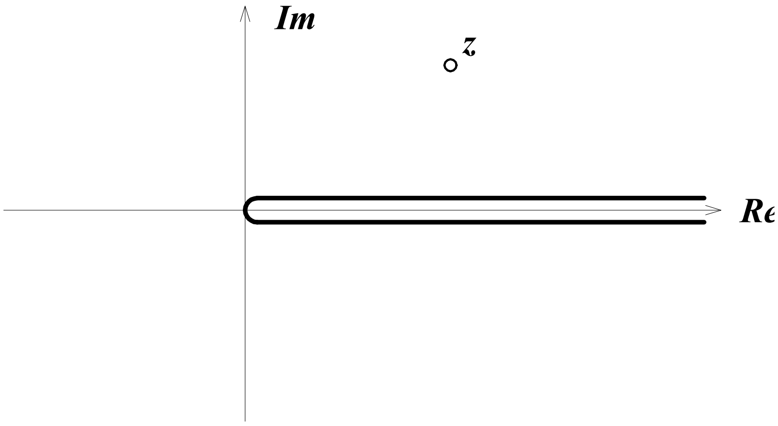

Figure 8.1: The spectrum of the free particle Hamiltonian $\sigma\left(\hat{A}_0^{(n)}\right) = [0, \infty[$ independent of the dimension n.

8.2.1 Spectrum of the operator:

The spectrum is a purely continuous one:

$$\sigma\left(\hat{A}_0^{(n)}\right) = [0, +\infty[$$

Resolvent:

The resolvent operator is defined only for $z \notin \sigma\left(\hat{A}_0^{(n)}\right)$ as

$$\hat{G}_0^{(n)}(z) = \left(z - \hat{A}_0^{(n)}\right)^{-1}$$

In the real space representation a state is described by a wavefunction $(\Phi(\mathbf{x}), \mathbf{x} \in \mathbb{R}^n)$ and the Green function by

$$\left[\hat{G}_0^{(n)}(z)\,\Phi\right](\mathbf{x}) = \int\limits_{\mathbb{R}^n} d\mathbf{x}' \,\left(G_0^{(n)}(\mathbf{x}, \mathbf{x}'; z)\,\Phi(\mathbf{x}')\right) \;.$$

If the wavefunction is a proper element of the Hilbert space, $\Phi \in \mathcal{H}$, then also $\left[\hat{G}_0^{(n)}(z)\,\Phi\right] \in \mathcal{H}$, which is guaranteed by a basic mathematical theorem. A similar one is valid for generalized eigenfunctions.

The resolvent in the real space representation is given by the integral kernel $G_0^{(n)}(\mathbf{x}, \mathbf{x}'; z)$, which only depends on the absolute value of the difference vector $r = |\mathbf{x} - \mathbf{x}'|$. Further we define a bijective mapping between $z \in \rho\left(\hat{A}_0^{(n)}\right)$ and u in the upper complex halfplane $H^{(i,+)}$ (see appendix A.1). The energy is always considered just as a parameter of the Green function.

$$z = u^2 \quad , \quad \operatorname{Im} u > 0$$

We distinguish between these two functions to emphasize their importance:

$$G_0^{(n)} \;:\; \left\{ \begin{array}{lcc} \mathbb{R}^n \times \mathbb{R}^n & \to & \mathbb{C} \\ (\mathbf{x}, \mathbf{x}'; z) & \mapsto & G_0^{(n)}(\mathbf{x}, \mathbf{x}'; z) = G_0^{(n)}(\mathbf{x}, \mathbf{x}'; u) \end{array} \right.$$

$$g_0^{(n)} \;:\; \left\{ \begin{array}{lcc} \mathbb{R}_0^+ & \to & \mathbb{C} \\ (r; z) & \mapsto & g_0^{(n)}(r; z) = g_0^{(n)}(r; u) \end{array} \right.$$

although there is the relation $G_0^{(n)}(\mathbf{x}, \mathbf{x}'; z) = g_0^{(n)}(|\mathbf{x} - \mathbf{x}'|; z)$

8.2.2 Expression for the free space Green function

The following table summarizes the free particle Green function in $n = 1, 2, 3, \ldots$ dimensions,

dimension	free particle Green function
$n = 1$	$g_0^{(1)}(r; u) = \frac{e^{\mathrm{i}ur}}{2\mathrm{i}u}$
$n = 2$	$g_0^{(2)}(r; u) = -\frac{\mathrm{i}}{4}\, H_0^{(+)}(ur)$
$n = 3$	$g_0^{(3)}(r; u) = -\frac{e^{\mathrm{i}ur}}{4\pi r}$
$n \geq 4$	$g_0^{(n)}(r; u)$

in which $H_0^{(+)}(ur)$ is the Hankel function of zero order of the first kind. All functions have the property that

$$\lim_{r\to\infty} g_0^{(n)}(r; u) \to e^{\mathrm{i}ur} \to 0, \text{ because } \operatorname{Im}(u) > 0 \;.$$

$g_0^{(n)}(r; u)$ is uniquely defined because of the boundary conditions for $r \to \infty$, otherwise one could as well take e.g., for $n = 3 : -\frac{\cos ur}{4\pi r}$, which is often done in the literature. Furthermore we want to emphasize that the Green function for all $z = E \in \mathbb{R}_0^+$ is 'a priori' not defined. It can only be defined as a limiting value.

8.3 A m dimensional lattice in n dimensional space

We use the term lattice for the set of translation vectors, not necessarily to be associated with the atomic positions.

We consider the vector space $\mathbb{R}^n$ and m linear independent vectors

$$\mathbf{a}_1, \ldots, \mathbf{a}_m \in \mathbb{R}^n,$$

then we define a m-dimensional lattice in $\mathbb{R}^n$ by all **integer** linear combinations of the lattice basis vectors

$$\mathcal{L}^{(m,n)} = \{\mathbf{t_k} = k_1\mathbf{a_1} + \cdots + k_m\mathbf{a_m} \,:\, k_j \in \mathbb{Z}\} \;.$$

These m vectors define also a m-dimensional subspace $\mathbf{U}$ of the $\mathbb{R}^n$

$$\mathbf{U} = \{s_1\mathbf{a_1} + \cdots + s_m\mathbf{a_m} \,:\, s_j \in \mathbb{R}\}$$

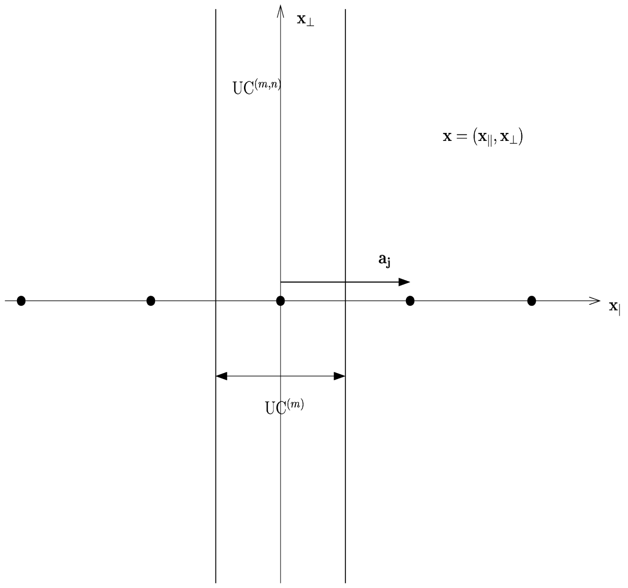

Figure 8.2: The unit cell $UC^{(m,n)}$ of a m dimensional lattice in $\mathbb{R}^n$: The m dimensional lattice defines a unit cell $UC^{(m)}$ in $\mathbb{R}^m$ and $UC^{(m,n)} = UC^{(m)} \times \mathbb{R}^{n-m}$

and we can choose a coordinate system in $\mathbb{R}^n$ such that all $\mathbf{u} \in \mathbf{U}$ are of the form

$$\mathbf{u} = (u_1, \ldots, u_m, 0, \ldots, 0) ,$$

where only the first m components are unequal from zero, while the last $n - m$ ones are identically zero. Then essentially $\mathbf{U} = \mathbb{R}^m$ and we can consider the lattice of $\mathbf{a}_1, \ldots, \mathbf{a}_m$ in $\mathbf{U} = \mathbb{R}^m$, a m-dimensional lattice in $\mathbb{R}^m$

$$\mathcal{L}^{(m)} = \mathcal{L}^{(m,m)} = \{k_1 \mathbf{a_1} + \cdots + k_m \mathbf{a_m} : k_j \in \mathbb{Z}\} .$$

For every m dimensional lattice in $\mathbb{R}^m$ a unit cell can be defined, which is denoted by $UC^{(m)}$ and is a subset of $\mathbb{R}^m$. For our purpose we always choose a simply connected region containing the lattice point $\mathbf{0}$, e.g. the Wigner-Seitz construction of a unit cell. The natural definition of the unit cell of a m-dimensional lattice in $\mathbb{R}^n$ is (see Fig. 8.2)

$$UC^{(m,n)} = UC^{(m)} \times \mathbb{R}^{(n-m)} .$$

The reciprocal lattice of $\mathcal{L}^{(m)}$ we denote by $\mathcal{L}'^{(m)} = \{\mathbf{K}_\nu : \nu \in \mathbb{Z}^m\}$ and is constructed in the usual way. The unit cell of the reciprocal lattice is called Brillioun zone and we denote it by $BZ^{(m)}$.

8.4 Laplace Operator with m-dimensional periodic boundary conditions

First we consider the Laplace operator in m dimensional space $\mathbb{R}^m$ with $\mathbf{k}$-periodic boundary conditions from a m dimensional lattice $\mathcal{L}^{(m)}$, (only functions fulfilling $\psi_\mathbf{k}(\mathbf{x} + \mathbf{t_n}) = e^{i\mathbf{k}\mathbf{t_n}} \psi_\mathbf{k}(\mathbf{x})$

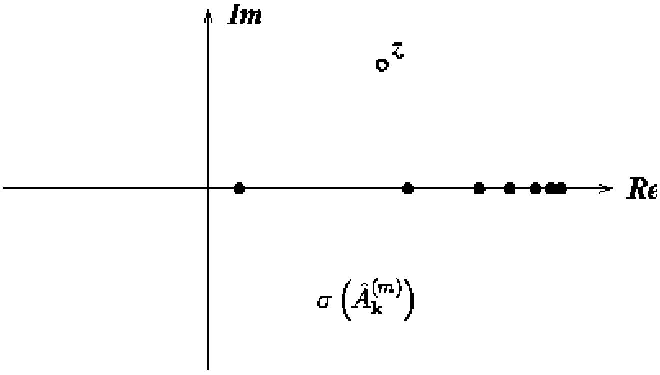

Figure 8.3: The spectrum of the m-dim. Laplacian with $\mathbf{k} \in \mathbf{BZ}^{(m)}$ periodic boundary condition. It is an only discrete but unbounded spectrum.

are allowed)

$$\text{for } \mathbf{k} \in BZ^{(m)} \ : \quad \hat{A}_{\mathbf{k}}^{(m)} = \begin{cases} -\Delta & \text{in } \mathcal{H} = L_2(\mathrm{UC}^{(m)};\mathbb{C}) \\ +\mathbf{k}\ . & \text{periodic b.c.} \end{cases} \tag{8.2}$$

If we consider the **boundary conditions as part of the operator,** $\hat{A}_{\mathbf{k}}^{(m)}$ is an essentially different operator than $\hat{A}_{0}^{(m)}$.

8.4.1 Spectrum of the operator:

The spectrum of $\hat{A}_{\mathbf{k}}^{(m)}$ is a pure point spectrum

$$\sigma\left(\hat{A}_{\mathbf{k}}^{(m)}\right) = \sigma_p\left(\hat{A}_{\mathbf{k}}^{(m)}\right) = \left\{(\mathbf{k}+\mathbf{K}_\nu)^{\mathbf{2}} : \nu \in \mathbb{Z}^m\right\} \ . \tag{8.3}$$

8.4.2 Resolvent operator:

Following (8.2.1) the resolvent operator is defined only for $z \notin \sigma\left(\hat{A}_{\mathbf{k}}^{(m)}\right)$ as

$$\hat{G}_{\mathbf{k}}^{(m)}(z) = \left(z - \hat{A}_{\mathbf{k}}^{(m)}\right)^{-1}$$

In the real space representation a state is described by a wavefunction $\left(\Phi(\mathbf{x}), \mathbf{x} \in \mathrm{UC}^{(\mathbf{m})}\right)$

$$\left[\hat{G}_{\mathbf{k}}^{(m)}(z)\,\Phi\right](\mathbf{x}) = \int\limits_{\mathrm{UC}^{(m)}} dx'\,\left(G_{\mathbf{k}}^{(m)}(\mathbf{x},\mathbf{x}';z)\,\Phi(\mathbf{x}')\right)$$

The resolvent in real space representation is given by the integral kernel $G_{\mathbf{k}}^{(m)}(\mathbf{x},\mathbf{x}';z)$, which only depends on the difference vector $\mathbf{y} = \mathbf{x} - \mathbf{x}'$. Once again we also use u instead of z for the energy parameter (see (A.1)) of the Green function.

$$z = u^2 \quad , \quad \operatorname{Im} u > 0$$

Reciprocal and direct lattice sums:

In order to find an expression for the integral kernel $G_{\mathbf{k}}^{(m)}(\mathbf{x},\mathbf{x}';z)$, we have two straightforward methods.

Reciprocal lattice sum: In general if an operator $\widehat{A}$, with spectrum

$$\sigma\left(\hat{A}\right)=\sigma_p\left(\hat{A}\right)=\{\lambda_j, j\in I\}$$

and corresponding eigenvectors $\Phi_j$is given, then the resolvent can be expressed by

$$\hat{G}(z)=\left(z-\hat{A}\right)^{-1}=\sum_{j\in I}\frac{1}{z-\lambda_j}\left|\Phi_j\right\rangle\left\langle\Phi_j\right|$$

Applying this general result to the operator $\hat{A}_{\mathbf{k}}^{(m)}$ from definition (8.2) we have the reciprocal lattice sum

$$\begin{aligned} G_{\mathbf{k}}^{(m)}(\mathbf{x},\mathbf{x}';z) &= \frac{1}{|\mathrm{UC}^{(m)}|}\sum_{\nu\in\mathbb{Z}^m}\frac{1}{z-(\mathbf{k}+\mathbf{K}_\nu)^2}\,e^{\mathrm{i}(\mathbf{k}+\mathbf{K}_\nu)\cdot(\mathbf{x}-\mathbf{x}')} = \\ &= \frac{1}{|\mathrm{UC}^{(m)}|}\sum_{\nu\in\mathbb{Z}^m}\frac{1}{z-(\mathbf{k}+\mathbf{K}_\nu)^2}\,e^{\mathrm{i}(\mathbf{k}+\mathbf{K}_\nu)\cdot\mathbf{y}} \end{aligned}$$

Direct lattice sum: The direct lattice sum expression exploits the fact that the **k** periodic Laplacian $\hat{A}_{\mathbf{k}}^{(m)}$ is related to the free Laplacian $\hat{A}_0^{(n)}$ defined in (8.1). Both of their integral kernels fulfill the same differential equation

$$[z+\Delta]\,G(\mathbf{x},\mathbf{x}';z)=\delta\left(\mathbf{x}-\mathbf{x}'\right)$$

but the boundary conditions for $G_{\mathbf{k}}^{(m)}(\mathbf{x},\mathbf{x}';z)$ are different from the ones for $G_0^{(n)}(\mathbf{x},\mathbf{x}';z)$. If we take a proper sum of translated free space solutions we can obtain a function fulfilling the **k** periodic b.c.

$$\begin{aligned} G_{\mathbf{k}}^{(m)}(\mathbf{x},\mathbf{x}';z) &= \sum_{\nu\in\mathbb{Z}^m} G_0^{(m)}(\mathbf{x}-\mathbf{R}_\nu,\mathbf{x}';z)\,e^{\mathbf{ik}\cdot\mathbf{R}_\nu} = \\ &= \sum_{\nu\in\mathbb{Z}^m} g_0^{(n)}(|\mathbf{x}-\mathbf{x}'{-}\mathbf{R}_\nu|;z)\,e^{\mathbf{ik}\cdot\mathbf{R}_\nu} = \sum_{\nu\in\mathbb{Z}^m} g_0^{(n)}(|\mathbf{y}-\mathbf{R}_\nu|;z)\,e^{\mathbf{ik}\cdot\mathbf{R}_\nu} \end{aligned}$$

If summed up to infinity we should get the same functions, numerically there are of course differences.

Mixed direct and reciprocal lattice sums: The direct and reciprocal lattice sum can be combined for quicker numerical convergence using an Ewald-technique [9]:

$$G_{\mathbf{k}}^{(m)}(\mathbf{x},\mathbf{x}';z)=G_1(z)+G_2(z)$$

$$G_1(z)=\sum_{\substack{\text{reciprocal}\\ \text{lattice}}}\ldots\quad,\quad G_2(z)=\sum_{\substack{\text{direct}\\ \text{lattice}}}\ldots$$

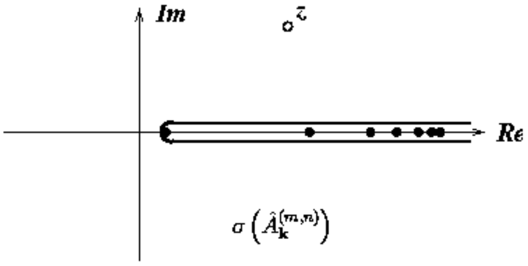

Figure 8.4: The purely continuous spectrum of $\hat{A}_{\mathbf{k}}^{(m,n)}$, the points are at the eigenvalues of $\hat{A}_{\mathbf{k}}^{(m)}$.

8.5 n-dimensional Laplace Operator with periodicity in m-dimensions

Now we deal with an operator defined in a n dimensional space with periodic boundary conditions in m dimensions and natural boundary conditions in the remaining $n-m$ dimensions.

$$\mathbf{k} \in \mathrm{BZ}^{(m)} \;:\quad \hat{A}_{\mathbf{k}}^{(m,n)} = \begin{cases} -\Delta & \text{in}\, \mathcal{H} = L_2(\mathrm{UC}^{(m,n)};\mathbb{C}) \\ \mathbf{k}-\text{periodic} & \text{b.c. in first m dimensions} \end{cases} \tag{8.4}$$

Because the Laplace operator does not mix the dimensions

$$\Delta = \frac{d^2}{dx_1^2} + \ldots \frac{d^2}{dx_m^2} + \frac{d^2}{dx_{m+1}^2} + \ldots \frac{d^2}{dx_n^2}\ ,$$

we can write

$$\hat{A}_{\mathbf{k}}^{(m,n)} = \hat{A}_{\mathbf{k}}^{(m)} \otimes \hat{\mathbf{1}}^{(n-m)} + \hat{\mathbf{1}}^{(m)} \otimes \hat{A}_0^{(n-m)}$$

as the sum of a $\mathbf{k}$ periodic Laplace operator as studied in (8.4) and a free operator as studied in (8.2).

8.5.1 Spectrum of the operator:

The spectrum of this operator $\hat{A}_{\mathbf{k}}^{(m,n)}$ is a purely continuous spectrum, starting at $\mathbf{k}$ extending to infinity, see (Fig. 8.4)

$$\sigma\left(\hat{A}_{\mathbf{k}}^{(m,n)}\right) = \left[\mathbf{k}^2, +\infty\right[$$

One can view the spectrum as the union of spectra of the form $\bigcup\limits_{\nu\in\mathbb{Z}^m} \left[(\mathbf{k}+\mathbf{K}_\nu)^2, +\infty\right[$, namely $(\mathbf{k}+\mathbf{K}_\nu)^2$ as the possible eigenvalues of $\hat{A}_{\mathbf{k}}^{(m)}$ plus an arbitrary positive number s from the continuous spectrum of $\hat{A}_0^{(n-m)}$.

8.5.2 Resolvent:

For $z \notin \sigma\left(\hat{A}_{\mathbf{k}}^{(m,n)}\right)$ the resolvent is given by

$$\hat{G}_{\mathbf{k}}^{(m,n)}(z) = \left(z - \hat{A}_{\mathbf{k}}^{(m,n)}\right)^{-1} \quad ,$$

which in real space representation is again an integral kernel

$$\left[\hat{G}_{\mathbf{k}}^{(m,n)}(z)\,\Phi\right](\mathbf{x}) = \int\limits_{\mathrm{UC}^{(m,n)}} d^3x' \, \left(G_{\mathbf{k}}^{(m,n)}(\mathbf{x},\mathbf{x}';z)\,\Phi(x')\right)$$

$G_{\mathbf{k}}^{(m,n)}$ can be again expressed in the form of direct or reciprocal lattice sums.

Reciprocal lattice sum: If we introduce for every $\nu \in \mathbb{Z}^m$, $z_\nu = z - (\mathbf{k}+\mathbf{K}_\nu)^2$ we can write the Green function as

$$G_{\mathbf{k}}^{(m,n)}(x,x';z) = \frac{1}{|\mathrm{UC}^{(m)}|} \sum_{\nu\in\mathbb{Z}^m} \left(G_0^{(n-m)}(x_\perp,x'_\perp;z_\nu)\, e^{\mathrm{i}(\mathbf{k}+\mathbf{K}_\nu)\cdot(\mathbf{x}_\parallel - \mathbf{x}'_\parallel)}\right) \quad ,$$

which is a reciprocal lattice sum using the free Green function in $n{-}m$ dimensions $G_0^{(n-m)}(\mathbf{x}_\perp,\mathbf{x}'_\perp;z_\nu)$.

Direct lattice sum: For the direct lattice sum we use again a proper summation of free particle Green function

$$G_{\mathbf{k}}^{(m,n)}(\mathbf{x},\mathbf{x}';z) = \sum_{\nu\in\mathbb{Z}^m} \left(G_0^{(n)}(\mathbf{x}-\mathbf{R}_\nu,\mathbf{x}';z)\, e^{\mathrm{i}\mathbf{k}\cdot\mathbf{R}_\nu}\right)$$

Note that here we have to use the n dimensional free space Green function $G_0^{(n)}(\mathbf{x}-\mathbf{R}_\nu,\mathbf{x}';z)$.

Combined direct and reciprocal lattice sums using Ewald-technique: Once again we can apply an Ewald technique to have a mixed reciprocal and direct space summation

$$G_{\mathbf{k}}^{(m,n)}(x,x';z) = G_1(z) + G_2(z)$$

$$G_1(z) = \sum_{\substack{\text{reciprocal}\\ \text{lattice}}} \ldots \quad , \quad G_2(z) = \sum_{\substack{\text{direct}\\ \text{lattice}}} \ldots$$

8.6 Examples and References for specific (m,n) cases:

The following table should summarize the cases already dealt within the literature.

(n, m)	physical examples	references
(1,1)	1D bulk crystal	
(2,1)	wire in 2D system	
(2,2)	2D bulk crystal	[14]
(3,1)	wire in 3D system	
(3,2)	surface of crystal	[23]
(3,3)	3D bulk crystal	[25]
n≥4	Quasicrystals	

8.6.1 The case (m,n)=(1,2)

If we have a 2 dimensional space with a 1 dimensional lattice, we write

$$\mathbf{x} = (x_1, x_2) = (x_\parallel, x_\perp)$$

and a 1 dimensional Brillioun zone with $k \in BZ_1$. We define

$$u_\nu \leftrightarrow z \;\text{ with }\; z_\nu = u_\nu^2 = z - (k + K_\nu)^2$$

and the 1 dimensional free space Green function

$$g_0^{(1)}(r, u) = \frac{e^{\mathrm{i}ur}}{2\mathrm{i}u}$$

we then get the result

$$G_k^{(1,2)}(\mathbf{x}, \mathbf{x}'; z) = \frac{1}{|UC^{(1)}|} \sum_{\nu \in \mathbb{Z}} \frac{1}{2iu_\nu} e^{iu_\nu |x_2 - x_2'|} e^{i(k+K_\nu)\left(x_2 - x_2'\right)}$$

Typical applications are surfaces/interfaces of samples with 1 dimensional periodic structures in a 2 dimensional world

8.6.2 The case (m,n)=(1,3)

If we have a 2 dimensional space with a 1 dimensional lattice, we write

$$\mathbf{x} = (x_1, x_2, x_3) = (x_\parallel, \mathbf{x}_\perp)$$

and a 1 dimensional Brillioun zone with $k \in BZ_1$. We define $u_\nu \leftrightarrow z$ with $z_\nu = u_\nu^2 = z - (k + K_\nu)^2$ and the 2 dimensional free Green function

$$g_0^{(2)}(r, u) = \frac{-\mathrm{i}}{4} H_0^{(+)}(ur) \; ,$$

then $G_k^{(1,3)}(\mathbf{x}, \mathbf{x}'; z)$ is given by

$$G_k^{(1,3)}(\mathbf{x}, \mathbf{x}'; z) = \frac{1}{|UC^{(1)}|} \sum_{\nu \in \mathbb{Z}} \frac{-i}{4} H_0^{(+)}(u_\nu \, |\mathbf{x}_\perp - \mathbf{x}_\perp'|) e^{i(k+K_\nu)\left(x_\parallel - x_\parallel'\right)}$$

Applications: samples with 1 dimensional periodic structures in 3 dimensional space, quantum wires

8.6.3 The case (m,n)=(2,3)

If we have a 3 dimensional space with a 2 dimensional lattice, we write

$$\mathbf{x} = (x_1, x_2, x_3) = (\mathbf{x}_\parallel, x_\perp)$$

and a 2 dimensional Brillioun zone with $\mathbf{k} \in BZ_2$. We define $u_\nu \leftrightarrow z$ with $z_\nu = u_\nu^2 = z - (\mathbf{k} + \mathbf{K}_\nu)^2$ and the 1 dimensional free space Green function

$$g_0^{(1)}(r, u) = \frac{e^{\mathrm{i}ur}}{2\mathrm{i}u}$$

$$G_{\mathbf{k}}^{(2,3)}(\mathbf{x}, \mathbf{x}'; z) = \frac{1}{|UC^{(2)}|} \sum_{\nu \in \mathbb{Z}^2} \frac{1}{2iu_\nu} e^{iu_\nu \left|x_3 - x_3'\right|} e^{i(\mathbf{k}+\mathbf{K}_\nu)\cdot\left(\mathbf{x}_\parallel - \mathbf{x}_\parallel{}'\right)}$$

Applications: surfaces/interfaces of samples with 2 dimensional periodic structures in 3 dimensional space

Part III

Results of KKR-ASA calculations

Chapter 9

Magnetic anisotropy of thin films of Co on Cu(111)[1]

9.1 Introduction.

Growth, morphology and magnetic structure of ultrathin films of Co on Cu(111) have been a matter of intensive experimental investigations in the near past. Prepared by molecular beam epitaxy (thermal deposition, TD) Co films (ML) grow in a face centered cubic (fcc) structure below a thickness of 2 monolayers by forming mostly 2 or 3 ML high islands [7]; above this thickness they undergo a gradual fcc→hcp transformation [41] aided by hexagonal closed packed (hcp) stacking faults. By using Pb as surfactant on Cu(111) the quality of growth of Co films has been greatly improved, however, this leads to a substantial change in the magnetic properties of the system, namely induced by a Pb overlayer [4]. A novel experimental method using pulsed layer deposition (PLD) [22] made it possible to reduce significantly the number of stacking faults during the initial growth of Co films on Cu(111) and thus to delay the fcc→hcp structural transition to about 6 ML of Co [52]: in contrast to perpendicularly magnetized thermally deposited hcp films [51] these films show an overall in-plane magnetization.

As the practically perfect layer-by-layer growth of the PLD films represents an ideal situation for theoretical investigations, the purpose of the present report is to calculate and discuss the magnetic anisotropy properties of epitaxial Co_N/Cu(111) ($1 \leq N \leq 7$) films. To our knowledge, ab initio calculations of the magnetic anisotropy energy (MAE) have been reported so far only for Co_1/Cu(111) (in fact also as capped by additional Cu overlayers) by [53]. In there a MAE of -0.31 meV per unit cell (in-plane) was found for a Co ML occupying positions of a perfect fcc Cu parent lattice, while for a selfconsistently relaxed Co monolayer ($\sim$ 7.6% inward relaxation) a MAE of -0.30 meV per unit cell was reported. In many cases the effect of layer relaxations is known to be decisive for the MAE , most prominently for Ni/Cu(100) film systems, where it gives rise to an inverse reorientation transition with increasing film thickness [42].

---

[1] The results of these calculation are published in an article [17]

9.2 Theoretical approach.

The following theoretical study of the MAE of thin films of Co on Cu(111) is performed by using the fully relativistic spin polarized screened Korringa-Kohn-Rostoker (KKR) method [47] in the context of the spin-polarized local density functional as parametrized by Vosko et al [44]. Various uniform relaxations R with respect to the interlayer distance in the substrate (fcc Cu), $-4\% \leq R \leq +3\%$, have been considered by extending this method to systems of layers sharing only the same in-plane translational symmetry but otherwise can differ in respective interlayer distances [42]. It should be noted that the same in-plane translational symmetry is a necessary requirement for making use of two-dimensional lattice Fourier transformations. For each system, i.e., for each uniform relaxation R and number of Co layers N, the electronic and magnetic structure is calculated selfconsistently for a ferromagnetic configuration corresponding to an orientation of the magnetization perpendicular to the planes of atoms. In all systems investigated, an additional buffer of three substrate Cu layers is treated selfconsistently. It was found that within the atomic sphere approximation 30 $k_{\|}$ points in the hexagonal irreducible surface Brillouin zone (ISBZ) guarantees necessary numerical accuracy for the effective potentials and effective exchange fields treated .

The magnetic anisotropy energy (MAE) E_a,

$$E_a = E(\|) - E(\perp) \ , \tag{9.1}$$

defined as the energy difference between a uniform in-plane and a uniform perpendicular orientation of the magnetization, is obtained by making use of the Magnetic Force Theorem [21], namely as a sum over the respective band energy difference ΔE_b and the magnetic dipole-dipole energy contribution ΔE_{dd},

$$E_a = \Delta E_b + \Delta E_{dd} \ . \tag{9.2}$$

It is worthwhile to mention that ΔE_b, evaluated here with 690 $k_{\|}$ points in the ISBZ in order to guarantee a relative accuracy of below 5%, can be identified as *the* contribution to the MAE induced by the spin-orbit interaction, while ΔE_{dd} is a purely classical term denoted usually as the shape anisotropy.

Denoting the magnetic moment in the cell centered around the atomic position $\mathbf{R}$ by $m_{\mathbf{R}}$ the (classical) magnetic dipole-dipole interaction energy is given (in atomic Rydberg units) by

$$E_{dd} = \frac{1}{c^2} \sum_{\mathbf{R},\mathbf{R}'}{}' \left\{ \frac{m_{\mathbf{R}} \cdot m_{\mathbf{R}'}}{|\mathbf{R}-\mathbf{R}'|^3} - 3\frac{[m_{\mathbf{R}} \cdot (\mathbf{R}-\mathbf{R}')]\,[m_{\mathbf{R}'} \cdot (\mathbf{R}-\mathbf{R}')]}{|\mathbf{R}-\mathbf{R}'|^5} \right\} . \tag{9.3}$$

This expression can be evaluated very efficiently by making use of the underlying two-dimensional translational symmetry; for further theoretical and computational details, see [40],[47]. Note that due to the definition in Eq. (1), positive/negative values of E_a imply a perpendicular/in-plane orientation of the magnetization.

9.3 Results

In Fig. 9.1 the MAE is displayed together with the corresponding band energy and magnetic dipole-dipole energy contribution for Co_N films ($1 \leq N \leq 7$) on $Cu(111)$ as a function of the

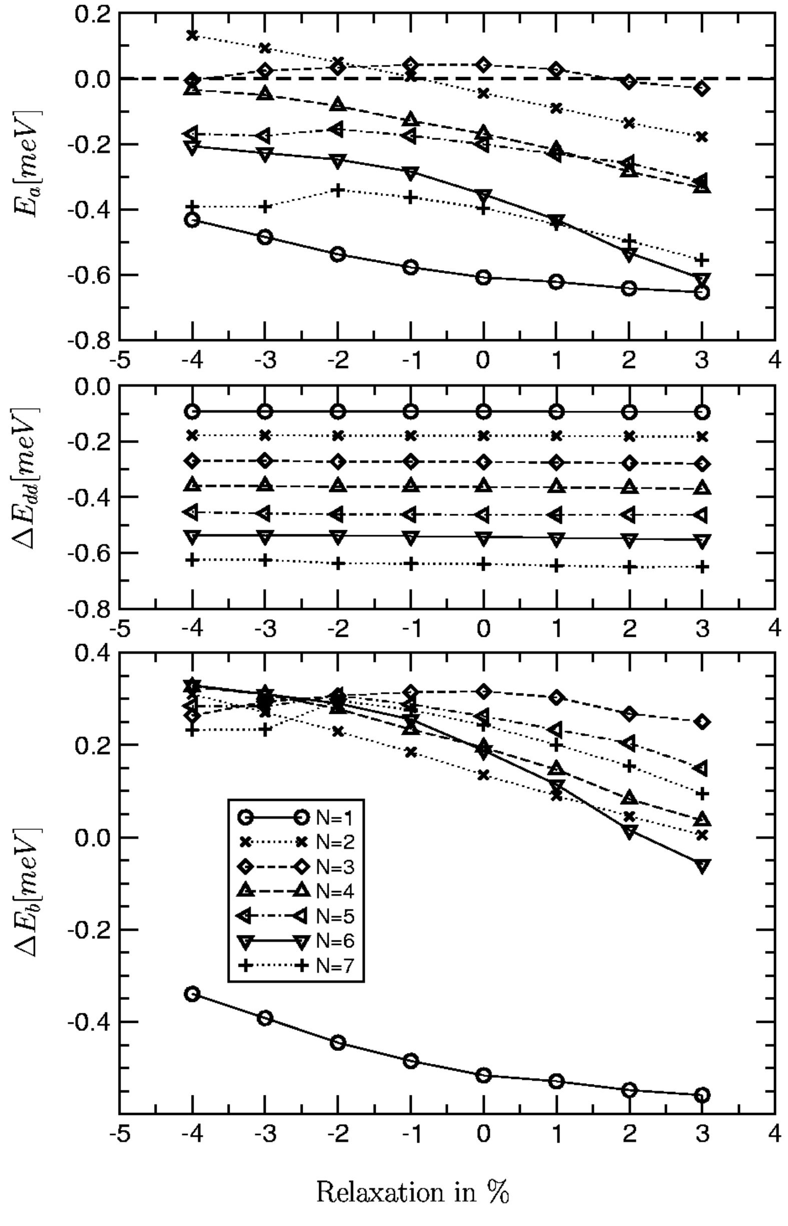

Figure 9.1: Calculated total magnetic anisotropy energies E_a, band energy anisotropies ΔE_b and magnetic dipole-dipole energy differences ΔE_{dd} for $\mathrm{Co}_N/\mathrm{Cu}(111)$ $(1 \leq N \leq 7)$ as a function of a uniform relaxation R.

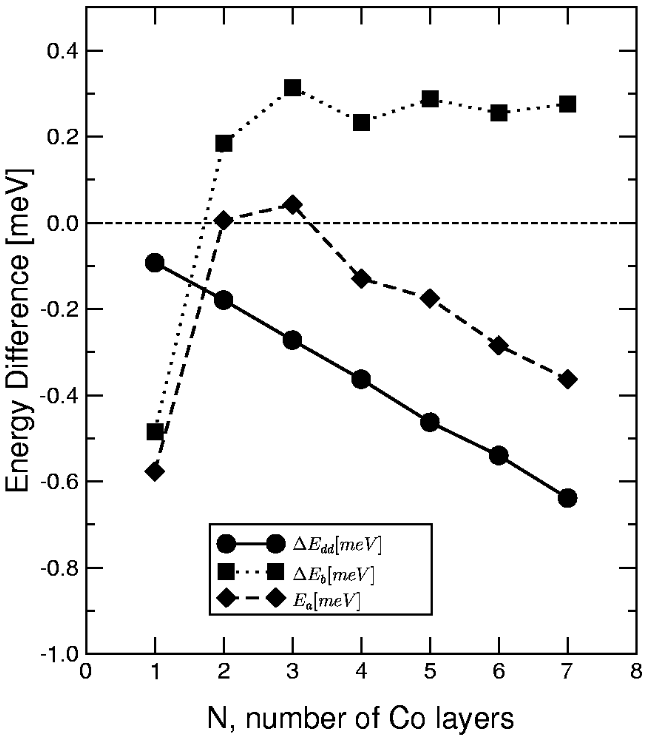

Figure 9.2: Band energy anisotropies ΔE_b (squares), dipole-dipole energy differences ΔE_{dd} (circles) and magnetic anisotropy energies E_a (diamonds) as a function of the number of Co layers for the experimentally given relaxation of $R = -1\%$.

uniform relaxation rate R of the cobalt interlayer distance. The results show that for $N = 1$ an in-plane orientation is clearly favored, while for $N = 2, 3$ the MAE is around zero; for increasing contractions a small perpendicular magnetic anisotropy occurs. For $N \geq 4$, however, an in-plane anisotropy develops with increasing film thickness. The two contributions to the MAE, namely, the band energy and the magnetic dipole dipole energy, have significantly different properties: ΔE_{dd}, favoring always an in-plane magnetization, is essentially independent of relaxations, at least in the regime investigated, and increases in good approximation linearly with the number of film layers. This simple behavior of ΔE_{dd} results from the dominating spin-only Co magnetic moments, which are fairly insensitive to both relaxations and the thickness of the film. In contrast to ΔE_{dd} the band energy difference ΔE_b does depend on both the thickness of the film and the relaxation. In agreement with the theoretical investigations of Zhong et al. [53] ΔE_b is negative for $N = 1$, however, it seems to show a more pronounced dependence on R as compared to the one that can be deduced from Ref.[53]. For not too large values of R the band energy ΔE_b favors a perpendicular magnetization for $N \geq 2$.

For the specific case of $R = -1\%$ (closest to the experiment, see Ref.[52]), the variation of the MAE and its contributions with respect to N is visualized in Fig. 9.2.

After an abrupt jump from about -0.5 meV at $N = 1$ to nearly 0.2 meV at $N = 2$, ΔE_b oscillates for $N \geq 3$ around about 0.3 meV with an amplitude that reduces by increasing the number of cobalt layers. The fact that for $N \geq 3$ the band energy difference is not significantly changing

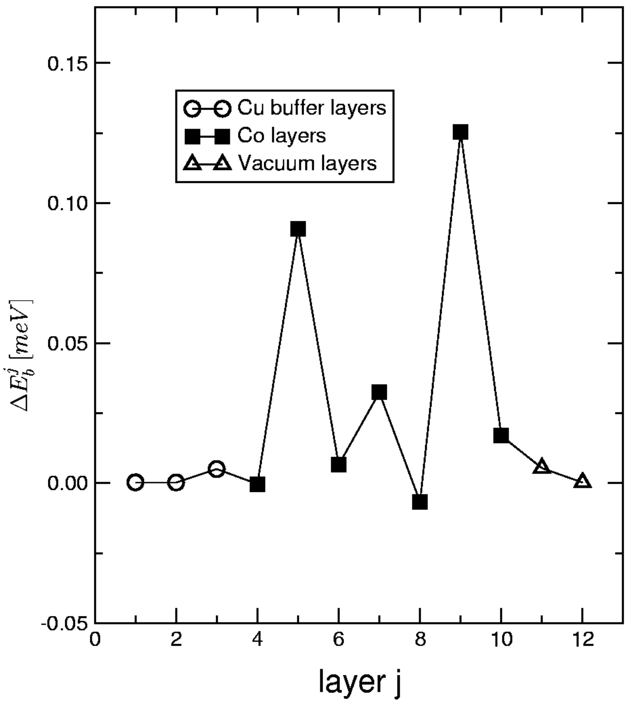

Figure 9.3: Layer-resolved band energy anisotropies ΔE_b^j for a film of 7 cobalt layers with a uniform relaxation of $R = -1\%$.

with the film thickness can be deduced from Fig. 9.3, showing the layer-resolved contributions of ΔE_b for the thickest system under consideration, $Co_7/Cu(111)$. As can be seen ΔE_b is mainly located in the cobalt layers second closest to the interface and to the surface; the corresponding contributions from the 3 most interior cobalt layers alternate in sign, but are remarkably smaller in magnitude. Therefore, the interior of the Co film does not contribute significantly to ΔE_b. It should be noted that a similar oscillating behavior of the MAE was found for Co films on Cu(100) [39]. Obviously, however, ΔE_{dd} increases in magnitude with N, and thus results in an in-plane magnetization for $N \geq 4$.

Changes in physical quantities such as charges or magnetic moments with respect to the magnetic orientation are usually very small as compared to their absolute values. In the first row of Fig. 9.4 the layer resolved total (orbital and spin) magnetic moments for the in-plane and the perpendicular orientation are shown for three (first column) and seven (second column) layers of Cobalt. In the second and third row of this figure the corresponding layer resolved orbital and spin magnetic moment differences are displayed for the same systems. One can see in Fig. 9.4 that the absolute value of the difference in the orbital magnetic moments is one order of magnitude larger than the corresponding difference in the spin magnetic moments. It should be noted, however, that considering the actual size of the anisotropy energy, see Fig. 9.2, the minute differences to be read off from Fig. 9.4, are not surprising at all.

PLD grown $Cu(111)/Co_N$ films show an in-plane easy axis of magnetization for all thicknesses investigated ($N = 2, \ldots, 15$) [51] in good agreement with our theoretical results. When comparing experimental and theoretical results, one should keep in mind, however, that for very thin films

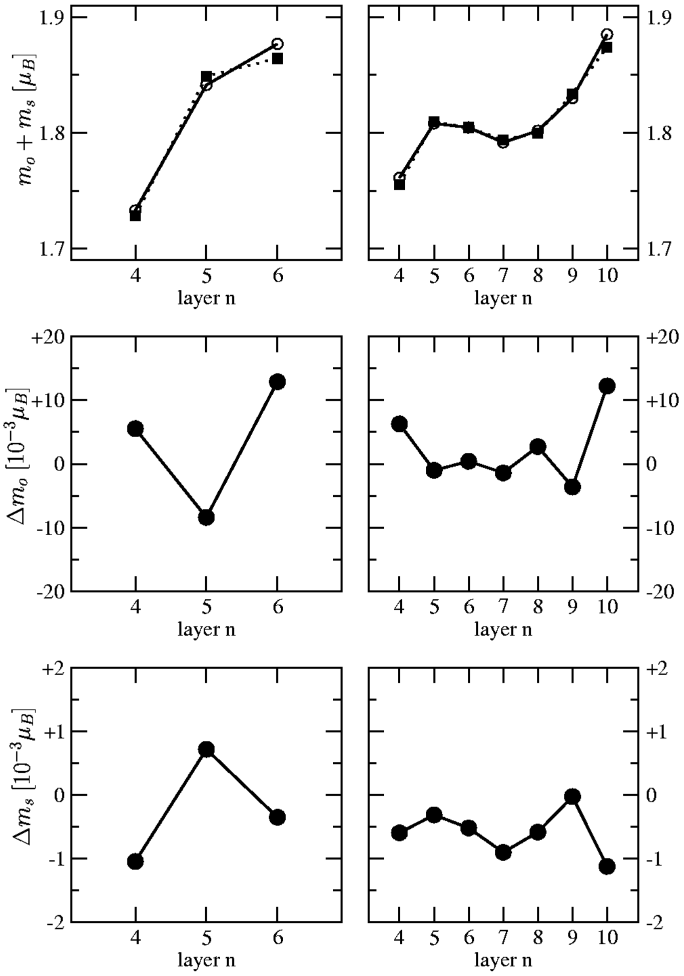

Figure 9.4: Layer resolved total magnetic moments (top; circles correspond to the perpendicular orientation of the magnetization, squares to the in-plane orientation) and differences in the orbital (middle) and spin (bottom) magnetic moments with respect to the orientation of magnetization. The left column refers to three layers thick Co film, the right column to a film with seven Cobalt layers. Only the Cobalt layers are shown.

the Curie temperature drops significantly. This means that the measurement temperature of 230 K is no longer far below T_c, see Ref. [51]. Usually, when approaching T_c from below the anisotropy falls more rapidly with increasing temperature than the magnetization. Therefore in the experiment the magnetic dipole-dipole contribution can overwhelm the tiny perpendicular band energy anisotropy, pulling the magnetization in-plane. In contrast to this behavior TD films do also show a perpendicular easy axis of magnetization for various film thicknesses, in addition to a more $3D$–like growth mode of the films. These facts and the present results prove once again the strong dependence of the magnetic properties of thin films on the experimental growth technique. Unfortunately, in ab-initio like descriptions at best the electronic temperature (via the Fermi-Dirac distribution function) for the band energy part can be taken into account. This implies that for a rigorous study of temperature effects in these systems a Heisenberg-like model with ab-initio-like parameters is needed in order to calculate corresponding free energies and to attempt to evaluate critical temperatures. Evaluation schemes for such ab-initio parameters, however, are still under discussion and at present not available.

9.4 Conclusion

We have investigated ab initio the magnetic anisotropy energy of the system $Co_N/Cu(111)$ using the fully relativistic spin-polarized screened KKR method by taking into account uniform interlayer relaxations in the Co film between $R = -4\%$ and $+3\%$. It was shown that the calculations predict an in-plane easy axis of magnetization for essentially all thicknesses and relaxations. Furthermore, the results prove that the main contributions to the magnetic anisotropy arise from the Cu/Co interface and the Co/Vac surface: relaxations therefore do not influence the anisotropy energy in a very sensitive way. This in turn justifies the simplified model of uniform relaxations used in here instead of specific relaxation profiles. The obtained results are in good agreement with the experimental findings on PLD ultrathin films of the same system. [51]

Financial support was provided by the Fonds zur Förderung der wissenschaftlichen Forschung (Project number W004), the Austrian Ministry of Science (Project number GZ 45.504) and the Hungarian National Science Foundation (OTKA T030240, T037856). The collaboration between L.S. and the Austrian partners was partially sponsored also by the Research and Technological Cooperation Project between Austria and Hungary (Contract No. A-23/01).

Chapter 10

Interlayer exchange coupling and magnetic anisotropy in prototype trilayers: *Ab initio* theory versus experiment[1]

The magnetic anisotropy energy (MAE) and the interlayer exchange coupling (IEC) of prototype $\mathrm{Cu_4Ni_8Cu_NNi_9/Cu(001)}$ trilayers are calculated using an *ab initio* approach based on the experimental lattice spacings. The results thereof are compared to ferromagnetic resonance (FMR) experiments, which allow for the quantitative determination of the MAE as well as the IEC. The tetragonal distortion of the Ni films due to the pseudomorphic growth leads to a positive MAE of the inner Ni layers favoring an out-of-plane easy axis. At the Cu/Ni interfaces a negative surface anisotropy is present which is, however, reduced compared to a Ni/vacuum interface. The MAE is clearly determined by the Ni layers only, whereas the IEC is shown to result from Ni and Cu layers at the inner Cu/Ni interfaces.

Nowadays it is well known that ultrathin ferromagnetic layers separated by a non-magnetic spacer layer may interact via the so-called interlayer exchange coupling (IEC). This interaction was found to oscillate between ferromagnetic (FM) and antiferromagnetic (AFM) alignment as function of the spacer thickness. The IEC defined as the difference between the free energy for FM and AFM coupling has been the subject of many studies. The theoretical understanding of the phenomenon nowadays mostly relies on model calculations. The most frequently used picture is probably the RKKY [38], [3] model which explains the observed oscillation periods to arise from extremal spanning vectors of the Fermi surface (the so-called calipers) of the spacer material. The magneto-optical Kerr effect (MOKE) most widely used and other static magnetometries usually yield values of the coupling only for AFM coupled layers, whereas for FM coupling in most cases no results can be obtained. A method which is capable of such a determination and sensitive enough to measure down to the monolayer(ML)-limit is the ferromagnetic resonance (FMR) [11], [29]

In this communication we present simultaneously a theoretical and an experimental study on

---

[1] The results of these calculation are published in an article [19]

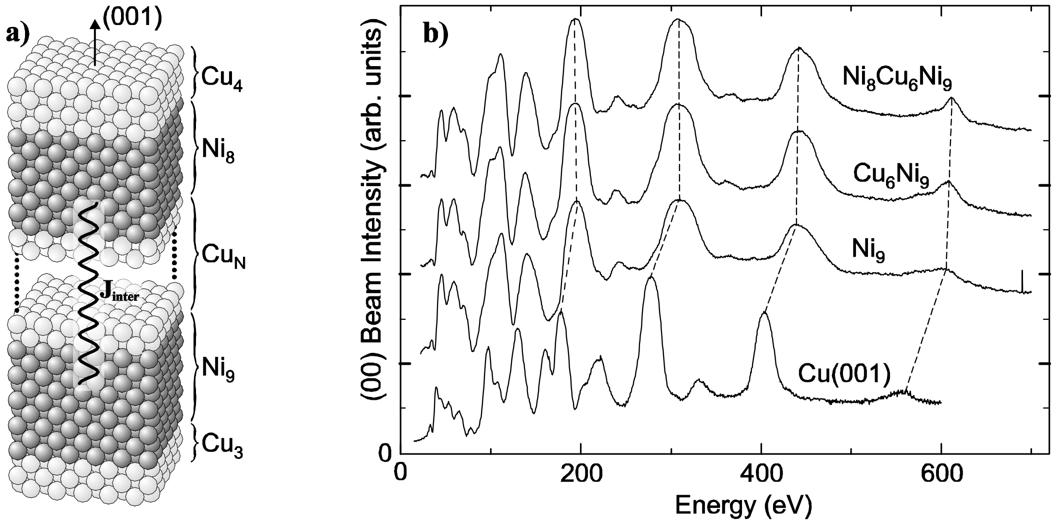

Figure 10.1: a) Hard sphere model of the $Cu_4Ni_8Cu_NNi_9$/Cu(001) trilayers. b) I/V-LEED spectra taken from the specular reflected (00) beam for (from bottom to top) Cu(001), Ni_9, Cu_6Ni_9 and $Ni_8Cu_6Ni_9$.

prototype $Cu_4Ni_8Cu_NNi_9$/Cu(001) trilayers with the focus on the behavior for small spacer thicknesses in the range $N = 2 - 10$ ML. The Ni/Cu(001) system can be viewed as a prototype system, since it implements both, structural as well as magnetic homogeneity. Details concerning the film preparation under ultrahigh vacuum conditions have been discussed elsewhere [29], [27], [31], [28] . A hard-sphere model of the trilayers is shown in Fig. 10.1(a). In order to have a limited set of parameters, only N was varied between the different trilayer systems, whereas the thicknesses of the Ni films were kept constant (8 and 9 ML, respectively). Ni films grow pseudomorphically up to at least 15 ML adopting the Cu in-plane lattice constant. In the vertical growth direction this leads to a contraction of the Ni film. A quantitative I/V-low energy electron diffraction (LEED) study [34] revealed values of 2.53(2) Å for the in-plane nearest neighbor distance and 1.70(2) Å for the interlayer separation. Relative to the Cu-bulk interlayer distance of 1.805 Å this means a contraction of about -5.5 % (if referred to the Ni-bulk value of 1.76 Å its value amounts to -3.2 %). The question whether the pseudomorphic growth continues upon capping the Ni film with the Cu spacer and, moreover, when the second Ni film is deposited on top of the spacer, has not been discussed in [34]. Since the structure is an important input for theory, this question is – in the present work – addressed via I/V-LEED experiments carried out after each evaporation step. The I/V-LEED spectra recorded for the specular reflected (00) beam during the stepwise preparation of a $Ni_8Cu_6Ni_9$/Cu(001) trilayer is shown in Fig. 10.1(b). From the position of the Bragg peaks one can extract the averaged vertical interlayer distance. If, on the other hand, the interlayer distance is known – as in the case of the Cu(001) substrate – relative shifts of the Bragg peaks can be translated directly into changes of the vertical layer separation. A shift to higher (lower) energy values indicates a contraction (expansion) of the interlayer distance. Clearly such a shift of the intensity maxima towards *higher* energies can be observed after the Ni_9 film is deposited. This shift shows the vertical contraction of the Ni film discussed already in [34]. No changes in the maxima are found after the evaporation of the Cu spacer and the topmost Ni film. Thus, one can conclude that the contraction of -5.5 % is present within the whole trilayer.

The magnetic anisotropy of the trilayers can phenomenologically be described by the part of the free energy E per unit area being anisotropic with respect to the directions of the magnetizations $\vec{M}_1$ and $\vec{M}_2$ in the two films

$$E = \sum_{i=1}^{2} \left(2\pi M_i^2 - K_{2\perp,i}\right) d_i \cos^2\theta_i - J_{inter}\frac{\vec{M}_1 \cdot \vec{M}_2}{M_1 M_2}, \tag{10.1}$$

Here the d_i are the thicknesses of the individual Ni slabs, $2\pi M_i^2$ is the shape anisotropy due to dipole-dipole interaction, and $K_{2\perp,i} = K_{2\perp,i}^{V} + (K_{2\perp,i}^{S_1} + K_{2\perp,i}^{S_2})/d_i$ denotes the intrinsic uniaxial anisotropy which can be split into a part arising from the film volume ($K_{2\perp,i}^{V}$) and a contribution from the two surfaces ($K_{2\perp,i}^{S_1}$ upper surface, $K_{2\perp,i}^{S_2}$ lower surface). In the following we set $S_1 = S_2 = S$ as our Ni films face Cu on both sides. The angles θ_i measure the magnetization directions with respect to the film normal. For $2\pi M_i^2 - K_{2\perp,i} > 0$ (< 0) the easy axis of magnetization lies in (out of) the film plane. Within the framework of Eq. (10.1) The IEC corresponds to the *macroscopic* coupling constant J_{inter} [3]. The magnetic anisotropy energy is defined as the energy difference between in- and out-of-plane orientation of the magnetization, i.e. MAE $= E\left(\theta_i = \pi/2\right) - E\left(\theta_i = 0\right)$. Ultrathin Ni films on Cu(001) present a reorientation of the easy axis of the magnetization from in to out-of-plane [2] which at room temperature occurs at about 10-11 ML [30]. Upon capping the Ni film with Cu the reorientation thickness is reduced to about 7-8 ML [30]. Consequently, both Ni films in our trilayers exhibit an out-of-plane easy axis [28]. This configuration was chosen because of enabling one to carry out additional MOKE measurements in the most sensitive polar geometry [28]. The magnetic anisotropy energies as well as the coupling between the two films were determined by means of *in situ* FMR at a microwave frequency of 9 GHz and external magnetic fields up to 15 kOe. Using in situ FMR the trilyer can be grown and measured within a step-by-step experiment: First, the bottom Ni_9 film capped with the Cu_N spacer layer is evaporated and investigated while in a second step, the topmost Cu_4Ni_8 layers are deposited. This approach allows to 'switch on' the IEC within the second step and monitor its influence on the FMR signal of the bottom Ni_9 film. Via angular dependent FMR measurements, i.e. by varying the θ_i angles of the two magnetizations $\vec{M}_i$, before and after the deposition of the topmost layers, one can separate the magnetic anisotropies being proportional to $\cos^2\theta_i$ (first term in Eq.(10.1)) from J_{inter} which scales with $\cos\left(\theta_1 - \theta_2\right)$ (second term in Eq.(10.1)). A detailed description of this procedure yielding absolute values for J_{inter} was described previously [27]. The measurements were performed in a temperature range of 50-400 K which covers almost the whole range from the low temperature regime up to the Curie-temperature.

In using the relativistic spin-polarized screened Korringa-Kohn-Rostoker method for layered systems, the theoretical aspects of which are discussed in detail in Ref. [47], the calculations were carried out for the same type of trilayers on which the FMR experiments have been done, namely those shown in Fig. 10.1(a). For the calculations shown in Fig. 10.2 different (uniform) vertical relaxations of 0 % (circles), -3.5 % (squares) and -5.5 % (diamonds) of the trilayers with respect to the Cu(001) substrate were assumed, the lattice spacing *within* the layers always being the one of Cu bulk. Three buffer layers of Cu were found to be sufficient to guarantee reliable matching to the semi-infinite Cu(001) substrate; at least two vacuum layers were used to join up to the semi-

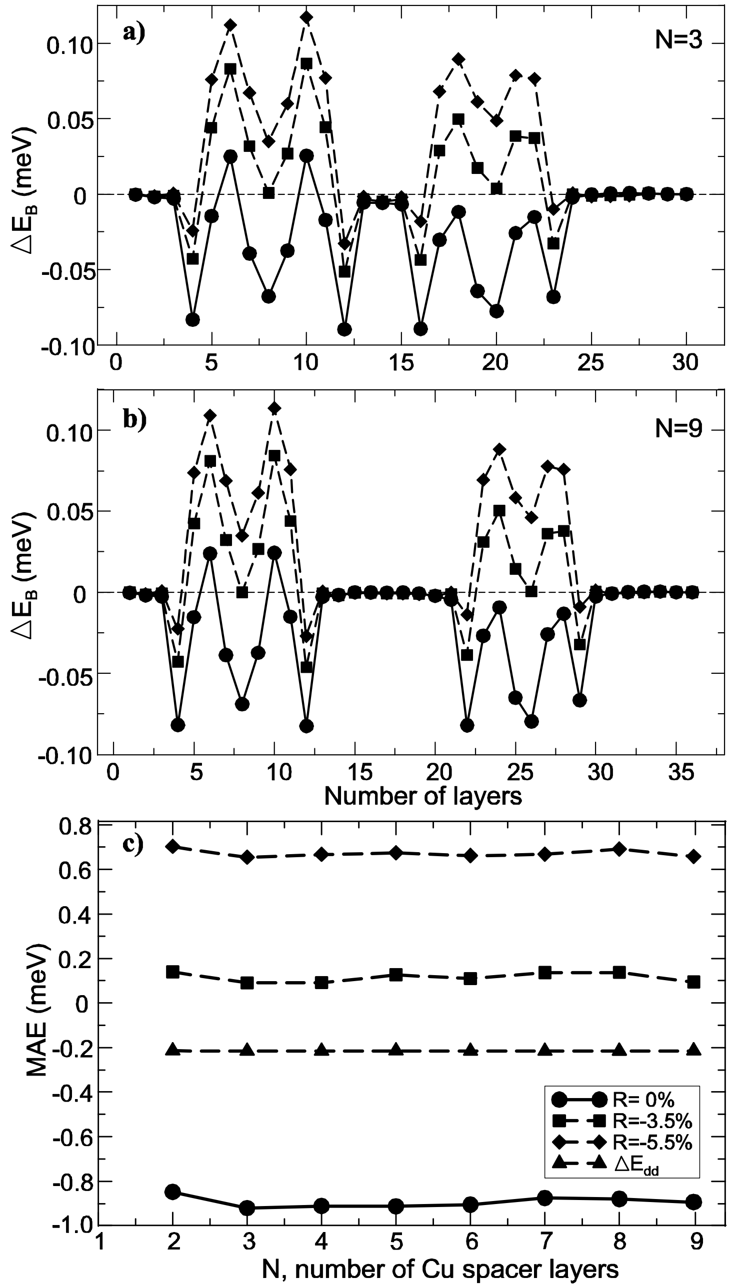

Figure 10.2: Layer-resolved band energy difference ΔE_B for a trilayer with a) $N = 3$ and b) $N = 9$. c) MAE as function of the spacer layer thickness N for the different vertical relaxations.

infinite vacuum. The MAE is calculated as the sum of differences in the magnetic dipole-dipole energy ΔE_{dd} and in the band energy ΔE_B (intrinsic contribution) between a uniform in-plane and a uniform out-of-plane orientation of the magnetization. The layer-resolved band energy differences for trilayers with $N = 3$ and $N = 9$ are presented in Fig. 10.2(a) and (b). The layer numbering starts at the three Cu buffer layers and comprises the trilayer itself, the 4 Cu capping layers and three vacuum layers (the different films within the slab are separated by dotted lines in Fig. 10.2(a) and (b)). One obtains the following results: (i) A sizeable anisotropy energy only arises from the Ni layers. (ii) The Ni layers facing Cu layers show a negative contribution, thus favoring an in-plane easy axis. (iii) Only the volume part of the Ni film presents a positive anisotropy contribution for the case that the experimentally derived distortion of -5.5 % in the film is assumed. From this it follows that in order to explain the experimentally observed positive overall MAE [28] the lattice relaxation has to be taken into account. In Fig. 10.2(c) the MAE is plotted as function of N for the three different distortions. Note that each data point in (c) corresponds to the sum of ΔE_B over all layers *including* the dipole-dipole energy ΔE_{dd} shown in this figure as triangles. As can be seen a positive MAE is only revealed for the distorted systems. Furthermore, the MAE shows no dependence on the spacer thickness N. Unlike for many other systems the shape anisotropy given by ΔE_{dd} in the investigated system is too small to lead to a negative overall MAE and thus ΔE_B dominates resulting in a MAE > 0. Dividing the theoretical value of ΔE_{dd} by the number of Ni layers yields an energy per atom, which amounts to a value of 12.7 μeV/atom for $2\pi M^2$. As compared to the experimental value for Ni bulk at $T = 0$ K, namely 12.1 μeV/atom, this indicates that the Ni moments and thus the magnetization are on the average bulk-like. This behavior was experimentally verified via an *in situ* SQUID investigation which showed that only for Ni thicknesses smaller than 5 ML a decrease of the $T = 0$ K magnetization with respect to the bulk value occurs [33].

	Experiment	Theory
$K^{V}_{2,\perp,i}$	70(20)[12]	80(20)
$K^{Ni/Cu}_{2,\perp,i}$	$-60(10)$[30]	$-20(10)$
$K^{NiVac}_{2,\perp,i}$	$-100(20)$[30]	$-100(20)$[12]

Volume and surface anisotropy constants (μeV/atom) for Ni/Cu(001) at $T = 0$ K.

In order to compare the theoretical results to the experimentally determined second order constants given by Eq. (10.1) one has to identify the energy of the interface Ni layers with the surface anisotropy $K^S_{2\perp}$ and the sum of the energy of the interior Ni layers divided by their number with the volume contribution $K^V_{2\perp}$. As can be seen from Tab. 10 very good agreement between theory and experiment concerning $K^V_{2\perp}$ applies. The experimental value for $K^{\mathrm{Ni/Cu}}_{2\perp}$, however, is by about a factor of 2 - 3 larger than found theoretically. This discrepancy most likely results from surface roughness and/or interface mixing which was not taken into account in the calculations. The driving force for the perpendicular orientation of the Ni films is therefore the positive volume contribution due to the tetragonal distortion. The surface anisotropy of the Ni/Cu interface – though still being negative – is reduced with respect to Ni/vacuum which explains the smaller reorientation thicknesses found for Cu capped Ni films [30].

Now we turn to the IEC. In Fig. 10.3(a) and (b) the calculated layer-resolved IEC for the experimental lattice relaxation of -5.5 % is plotted for two spacer thicknesses of $N = 3$ and $N = 9$, the layer numbering being the same as in Fig. 10.2. The main contribution to the IEC stems from Ni and Cu layers at or close to the Ni/Cu interface. For $N = 3$ ($N = 9$) the overall IEC energy is < 0 (> 0) indicating AFM (FM) coupling. Figure 10.3(c) shows the results of the experimental determination of the IEC for the $\mathrm{Cu_4Ni_8Cu_NNi_9/Cu(001)}$ trilayers (open squares) with N ranging from 2-10. The experimental values for the $\mathrm{Cu_4Ni_8Cu_NNi_9/Cu(001)}$ system ranging from $J_{inter} = 0$ to about 60 μeV/atom were extrapolated to $T = 0$ K in order to compare them to the theoretical calculations. This extrapolation was done using a $1 - (T/T_C)^{3/2}$ functional dependence of the IEC which was shown to correctly describe the temperature dependence of the IEC for various systems [31]. In addition to the $\mathrm{Cu_4Ni_8Cu_NNi_9/Cu(001)}$ trilayers results for $\mathrm{Ni_7Cu_NCo_2/Cu(001)}$ trilayers (open circles) are added. Note, that the experimentally determined values for the IEC are by about a factor of three larger for the $\mathrm{Ni_7Cu_NCo_2/Cu(001)}$ systems (right y-axis compared to the left one). For a detailed discussion of the $\mathrm{Ni_7Cu_NCo_2/Cu(001)}$ systems, see [31]. An oscillatory behavior is clearly seen for both systems, indicating that – except the strength – the overall behavior is not influenced upon substituting one Ni film with Co. The oscillations are also found in the *ab initio* calculation shown as crosses. However, in order to obtain the best agreement with the experiment the theoretical curve has to be upshifted by 0.7 ML, which in turn indicates that the **effective** experimental thickness seems to be by 0.7 ML smaller than the nominal evaporation rate. This can easily be understood considering a small amount of interdiffusion occuring during the film growth, a fact that is well known to happen for Ni as well as Co/Cu(001) [13]. In principle interdiffusion effects can theoretically be taken into account in terms of the inhomogenous Coherent Potential Approximation, see e.g. [20]. The profile, however, can only serve as a parametric, qualitative description as long as no reliable experimental data to compare with are available.Although the principal behavior of the IEC found experimentally is reproduced by the theory, the absolute strength of the coupling calculated [47] for the $\mathrm{Cu_4Ni_8Cu_NNi_9/Cu(001)}$ trilayers has to be scaled by a factor of 1/10 to match the experimental values. It should be noted, however, that experimentally one makes use of Eq. (10.1), i.e., of a 'macroscopical' Heisenberg ansatz. The fact that the calculated values are larger than those obtained from this procedure indicates that the 'experimental' J_{inter} displayed in Fig. 3 not necessarily is identical with the *microscopical* IEC. Only a thermodynamically averaged Heisenberg model would eventually lead to an expression as the one introduced in Eq. (10.1):

$$\begin{aligned} \langle E \rangle &= \left\langle \sum_{i,j} J_{ij} \frac{\vec{m}_i \cdot \vec{m}_j}{m_i m_j} \right\rangle \sim \left\langle J \sum_{i,j} \frac{\vec{m}_i \cdot \vec{m}_j}{m_i m_j} \right\rangle \\ &\sim \langle J \rangle \left\langle \sum_{i,j} \frac{\vec{m}_i \cdot \vec{m}_j}{m_i m_j} \right\rangle \rightarrow J_{inter} \frac{\vec{M}_1 \cdot \vec{M}_2}{M_1 M_2} \end{aligned} \tag{10.2}$$

In Eq. (10.2) the $\vec{m}_i$ refer to magnetic moments at sites i, and J_{ij} is the coupling energy between two such moments. Clearly enough also interface roughness not included in the theoretical description adds to the discrepancy in amplitudes between theory and experiment. This becomes evident by considering the fact shown in Fig. 10.3 that the IEC mainly arises from the interfaces of the films. The phases of the oscillations, however, can be expected to be in good agreement since in both cases the switching between two macroscopic magnetic configurations is mapped.

In summary we have shown for the case of prototype $\mathrm{Cu_4Ni_8Cu_NNi_9/Cu(001)}$ trilayers that a

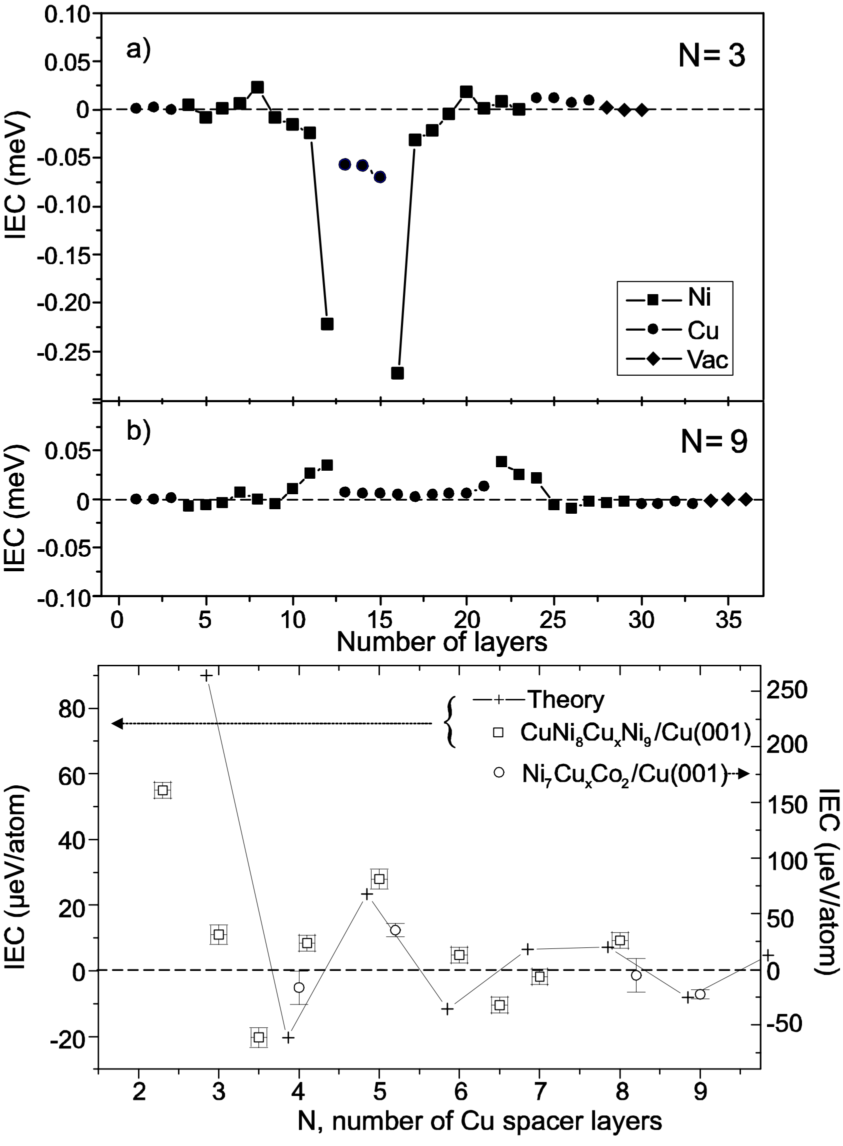

Figure 10.3: Layer-resolved IEC for a trilayer with a) $N = 3$ and $N = 9$. In c) the experimental results for both trilayer systems, indicated by the open squares and circles, are plotted as function of the numbers of spacer layers N.The theoretical IEC values (crosses) have been upshifted on the x-axis by 0.7 ML (see text).

combination of experiment and *ab initio* theory yields a better understanding of fundamental magnetic properties like the MAE and the IEC. Due to the included tetragonal distortion the results show a quantitative agreement for the volume contribution of the Ni films and thus lead to the experimentally observed easy axis perpendicular to the film plane. The surface anisotropy is negative and strongly reduced if the Ni films are capped by a Cu overlayer. Unlike the MAE which is determined by the Ni layers only and independent of the coupling between the Ni films, the IEC is strongly influenced by the Ni *and* Cu interface layers. The calculations reproduce the oscillatory behavior and the very strong dependence of the number of atomic spacer layers. As discussed above, namely because of inherent conceptual differences, the theoretical IEC will not be identical to the experimental J_{inter} (projected on a Heisenberg Hamiltonian, influence of interface roughness and/or interface mixing); nevertheless the numerical agreement can be expected to be very good.

This work was supported by the Fonds zur Förderung der wissenschaftlichen Forschung (Project Number W004), the Austrian Ministry of Science (Project number GZ 45.490) and by the DFG Sfb290, TP A2. K. Lenz is acknowledged for helpful discussions.

Chapter 11

On the reorientation transition in Cu(100)/Ni$_N$/H[1]

11.1 Abstract

Using also results of a previous study in terms of the scalar-relativistic full potential linearized augmented plane wave method (FLAPW) the fully relativistic screened Korringa-Kohn-Rostoker approach (SKKR) is applied in order to describe the shift in the critical thickness for the so-called inverse reorientation transition from in-plane to perpendicular in Ni films on Cu(100) upon loading with hydrogen. It is argued that on the average by loading with H the interlayer distances in the Ni films would have to be reduced by about 3%, or, expressed in absolute distances by about 0.05 Å, as compared to the bare systems, to cause the critical thickness to decrease from about 10 monolayers (ML) for the bare systems to about 8 ML for completely H covered Ni films. Calculations with statistically partial coverages with H and for a complete diffusion of H in the first Ni layer convincingly support this view.

11.2 Introduction

In general in thin magnetic films the orientation of the magnetization is either in-plane or perpendicular to the planes of atoms. The former is favored mostly by the shape anisotropy (magnetic dipole-dipole interaction), the latter by the so-called band energy contribution to the magnetocrystalline anisotropy (MAE). With increasing film thickness very often a shape anisotropy driven reorientation transition (RT) from perpendicular to in-plane is observed; the critical thickness typically is of the order of half a dozen monolayers. An exceptional case is a 'reverse RT', i.e., a RT from in-plane to perpendicular. Due an in-plane misfit strain of +2.6 % between Ni (lattice constant 3.52 Å) and Cu (3.61 Å) causing a uniform out-of-plane strain of -3.2 % for the Ni film [34] the most well-known example for this kind of behavior is the system Ni on Cu(001) [35]. Only very recently the influence of hydrogen on the direction of the spontaneous magnetization in Ni films on Cu(001) was discovered in the presence or absence of H in the atmosphere around the sample the magnetization seems to switch reversibly at about 8 ML Ni between the two types of

---

[1] The results of these calculation are published in an article [18]

orientation. For a bare Ni film on Cu(100) this RT occurs at a thickness of 10–11 ML [43]: a submonolayer coverage with H obviously shifts the RT to a lower thickness.

Because of this rather strange behavior and also since older experimental measurements most likely were carried out in the presence of a residual H atmosphere, in this paper the fully relativistic screened Korringa-Kohn-Rostoker method [47] is applied to describe the RT for H covered Ni films on Cu(100) films making use of the structure study [32] of this system in terms of the full potential linearized augmented plane wave method (FLAPW) [50]. It should be noted that each of these two theoretical methods has special features, none of them, however, is presently capable of providing completely satisfying simultaneous ab-initio answers to both lattice distortion **and** the critical thickness of the RT. Since the results of the FLAPW calculations were already published elsewhere [32], in here we concentrate on the main aspect of the problem, namely the critical thickness of the reorientation transition. It does seem necessary, however, to recall shortly some of the inherent methodological aspects of the two mentioned methods used in order to facilitate a correct assessment of respective theoretical results.

11.3 Methodological aspects

11.3.1 Shape approximations

Up-to-now only the FLAPW method [50] is capable to provide accurate enough ab-initio total energies suitable for predicting equilibrium geometrical structures, because no shape corrections for the potentials and the charge densities are assumed. The SKKR method on the contrary is restricted by the atomic sphere approximation (ASA) implying that total energies should not be used to perform geometrical mimizations; layer relaxations can therefore only be included parametrically [42], i.e., cannot be determined in an ab-initio like manner.

11.3.2 Magnetic moments

Since magnetic moments are per definition spherically averaged quantities within the FLAPW method they are confined to the so-called “muffin-tin” sphere, namely the radius of a sphere inscribed in a Wigner-Seitz cell, whereas in the SKKR approach they are defined with respect to the Wigner-Seitz radius, i.e., a radius of a sphere of the same volume as the Wigner-Seitz cell (ASA). Magnetic moments obtained within the FLAPW approach are therefore usually slightly smaller than those using the ASA.

11.3.3 Free standing thin films versus semi-infinite systems

By definition free standing films of the type $A_nB_mA_n$ as used in the FLAPW method are characterized by two surfaces (interfaces to vacuum). The Fermi energy therefore does not refer to a constant (This feature is due to the vacuum boundary conditions for the one-dimensional Poisson equation (along the surface normal)) that has to be solved in order to achieve charge selfconsistency for all m and n but is a function of the number of different atomic layers in the film, $\epsilon_F(n,m)$. If $\epsilon_F(A)$ and $\epsilon_F(B)$ denote the Fermi energies of the “bulk” systems A and B, then quite clearly

$$\lim_{n\to N}\epsilon_F(n,m)=\epsilon_F(A) \quad , \quad \lim_{m\to N}\epsilon_F(n,m)=\epsilon_F(B) \quad , \tag{11.1}$$

where N is a large enough integer number. This behavior has to be recalled when calculating properties as functions of n or m. Increasing for a given number m of Cu layers the number of Ni layers in films of the type H/Ni$_n$/Cu$_m$/Ni$_n$/H necessarily implies therefore that the Fermi energy is successively less Cu-like, i.e., refers less and less to those layers meant to serve as substrate.

In a semi-infinite system the Fermi energy is always that of the substrate. In systems such as fcc-Cu(100)/Cu$_m$/Ni$_n$/H there is only one surface. Usually m layers of the substrate material are used to take into account Friedel-like oscillations into the "bulk", matched on by means of surface Green's function techniques.

11.3.4 Relativistic levels

In FLAPW calculations a pseudo-relativistic ("Pauli-Schrödinger") version [36] of the FLAPW method is applied using a "second variation step" to include spin-orbit coupling. The fully relativistic spin-polarized SKKR approach [47] is based on the Kohn-Sham-Dirac Hamiltonian, i.e., relativistic corrections are taken into account to all orders of the speed of light.

11.4 Results

11.4.1 Computational details

In the following we only refer to results obtained by the screened Korringa-Kohn-Rostoker (SKKR-) method for layered systems. The effective potentials and effective exchange fields were determined selfconsistently within the local density approximation (LDA) [44] using a minimum of 45 k points in the ISBZ. In using the magnetic force theorem [21] the magnetic anisotropy energy (MAE) E_a,

$$E_a=\Delta E_b+\Delta E_{dd} \quad , \tag{11.2}$$

is given in terms of the so-called band energy contribution,

$$\Delta E_b=E_b(\|)-E_b(\perp) \quad , \tag{11.3}$$

and the corresponding difference in the magnetic dipole-dipole energy (shape anisotropy),

$$\Delta E_{dd}=E_{dd}(\|)-E_{dd}(\perp) \quad , \tag{11.4}$$

where $\|$ and $\perp$ denote uniform in-plane and perpendicular orientations of the magnetization, respectively, and $E(\|)$ and $E(\perp)$ refer to grand-potentials at T = 0. If c_α^p denotes the respective concentrations of the constituents A and B of an inhomogeneous binary substitutional alloy in layer p then in terms of the (inhomogeneous) CPA for layered systems [46] ΔE_b is given by

$$\Delta E_b=\sum_{p=1}^{N}\Delta E_b^p=\sum_{p=1}^{N}\sum_{\alpha=A,B}c_\alpha^p\Delta E_{b,\alpha}^p \quad , \tag{11.5}$$

$$E^p_{b,\alpha}(\hat{\mathbf{n}}) = \int_{\epsilon_b}^{\epsilon_F} n^p_\alpha(\epsilon;\hat{\mathbf{n}})(\epsilon - \epsilon_F)d\epsilon \quad , \tag{11.6}$$

where N is the total number of layers considered and the $n^p_\alpha(\epsilon;\hat{\mathbf{n}})$ are component and layer projected DOS corresponding to the (uniform) magnetic orientation $\hat{\mathbf{n}}$ of the magnetization. In eqn. (11.6) ϵ_b denotes the bottom of the valence band and ϵ_F is now the Fermi energy of the semi-infinite substrate.

All energy differences in Eq. (11.5) are evaluated via an integration in the upper half of the complex energy plane along a contour which starts at a real energy (ϵ_b) well below the valence band and ends at ϵ_F. For this type of calculations [47] a total of 990 $\mathbf{k}_{||}$ points in the ISBZ is used, which guarantees well converged results.

The shape anisotropy ΔE_{dd} in eqn. (11.3),

$$\Delta E_{dd} = E_{dd}(\|) - E_{dd}(\perp) \quad , \tag{11.7}$$

is calculated in this case directly in terms of the classical magnetic dipole-dipole interaction. Denoting for a chosen (uniform) orientation $\hat{\mathbf{n}}$ of the magnetization the magnetic moment in a cell centered around an atomic position $\mathbf{R}$ by $m_{\mathbf{R}}(\hat{\mathbf{n}})$ the (classical) magnetic dipole-dipole interaction energy is given (in atomic Rydberg units) by

$$E_{dd}(\hat{\mathbf{n}}) = \frac{1}{c^2} \sum_{\mathbf{R},\mathbf{R}';\mathbf{R}\neq\mathbf{R}'} \left\{ \frac{m_{\mathbf{R}}(\hat{\mathbf{n}}) \cdot m_{\mathbf{R}'}(\hat{\mathbf{n}})}{|\mathbf{R}-\mathbf{R}'|^3} - 3\frac{[m_{\mathbf{R}}(\hat{\mathbf{n}}) \cdot (\mathbf{R}-\mathbf{R}')]\,[m_{\mathbf{R}'}(\hat{\mathbf{n}}) \cdot (\mathbf{R}-\mathbf{R}')]}{|\mathbf{R}-\mathbf{R}'|^5} \right\} \quad . \tag{11.8}$$

This expression can be evaluated very efficiently by making use of the underlying two-dimensional translational symmetry; for further theoretical and computational details, in particular with respect to disordered systems, see [48].

All cases listed in Table 11.1 are investigated by taking into account uniform contractions [42] of the interlayer spacing (with respect to the lattice spacing of fcc Cu) in the Ni film and for the H layer [37]. Using the (inhomogeneous) coherent potential approximation [46] also the effect of diffusion of H into the first Ni layer and of incomplete H layers is considered such as, e.g., a statistically half-filled H layer ($c = 0.5$). In all these cases the thickness of the Ni film is varied from 1 to 12 layers. It should be noted that a contraction of 5.5% with respect to fcc Cu corresponds to about 3.5% with respect to fcc Ni. The maximum contraction of the H ML is limited to approximately 40% due to technical reasons in connection with the ASA implementation. By comparing the uncovered and the completely covered system it was found, e.g., that in qualitative agreement with results for Ni(100) [49], [5] the workfunction for the covered system is by about 1 eV larger than the uncovered one.

11.4.2 Magnetic moments

In Fig. 11.1 the magnetic moments are displayed for

$$Cu(100)|Ni(5.5\%)_n \text{ and } Cu(100)|Ni(5.5\%)_n|H(40\%) \text{ , n=6, 9 and 12.}$$

Table 11.1: Investigated systems using a semi-infinite substrate. The uniform contractions, x and y, are given in percent with respect to interlayer distance in fcc-Cu (substrate), the concentration is denoted by c

system	**x [%]**	**y [%]**	**c**
Cu(100)/Ni(x%)$_n$	$1.5 \le x \le 5.5$		
Cu(100)/Ni(x%)$_n$/H(y%)	$1.5 \le x \le 5.5$	$y \le 40$	
Cu(100)/Ni(x%)$_{n-1}$/(H$_c$Ni$_{1-c}$)(x%)	$1.5 \le x \le 5.5$		$0.2, 0.5$
Cu(100)/Ni(x%)$_n$/(H$_c$Vac$_{1-c}$)(y%)	$1.5 \le x \le 5.5$	$y \le 40$	$0.2, 0.5$

Table 11.2: Layer-resolved (spin-only) magnetic moments for a bare and a H covered Ni film on a semi-infinite Cu(100) substrate

layer	**Cu(100)/Ni$_6$**	**Cu(100)/Ni$_6$H**
	$[\mu_B]$	$[\mu_B]$
Ni$_1$	0.503	0.492
Ni$_2$	0.682	0.668
Ni$_3$	0.696	0.707
Ni$_4$	0.701	0.714
Ni$_5$	0.695	0.531
Ni$_6$	0.740	0.377

In this figure the first three layers correspond to Cu layers used as buffer to the semi-infinite substrate, the last few ones to vacuum layers. As can also be seen from Table 11.2 adsorbing H on Ni changes the magnetic moments in the top two Ni layers in a very characteristic manner that seems to be independent of the actual Ni film thickness. These results are in excellent agreement with the FLAPW calculation.

11.4.3 Magnetic anisotropy calculations

Bare and completely H covered systems

Inspecting the MAE in Fig. 11.2 it is evident that for bare Ni films on Cu(100) only a uniform contraction of about 2% (with respect to the interlayer spacing in fcc Cu) leads to a critical thickness for RT of about 10 ML Ni, whereas for the H covered films the experimentally proposed contraction of 5.5% yields a critical thickness of about 8 ML Ni. Obvious differences between the bare and the H covered systems can be read off from Fig. 11.2, since for ≤ 2 ML of Ni (in agreement with experiment in the case of H coverage the Ni film turns out to be non-magnetic (m $\approx 0\mu_B$, therefor also zero MAE).

Interdiffusion and partial coverage

In the top part of Fig. 11.3 the effect of diffusion of H into the first Ni layer, Cu(100)/Ni$_{n-1}$(Ni$_{1-c}$H$_c$), and cases of incomplete coverages of the Ni film with H, Cu(100)/Ni$_n$(Vac$_{1-c}$H$_c$), see also Ta-

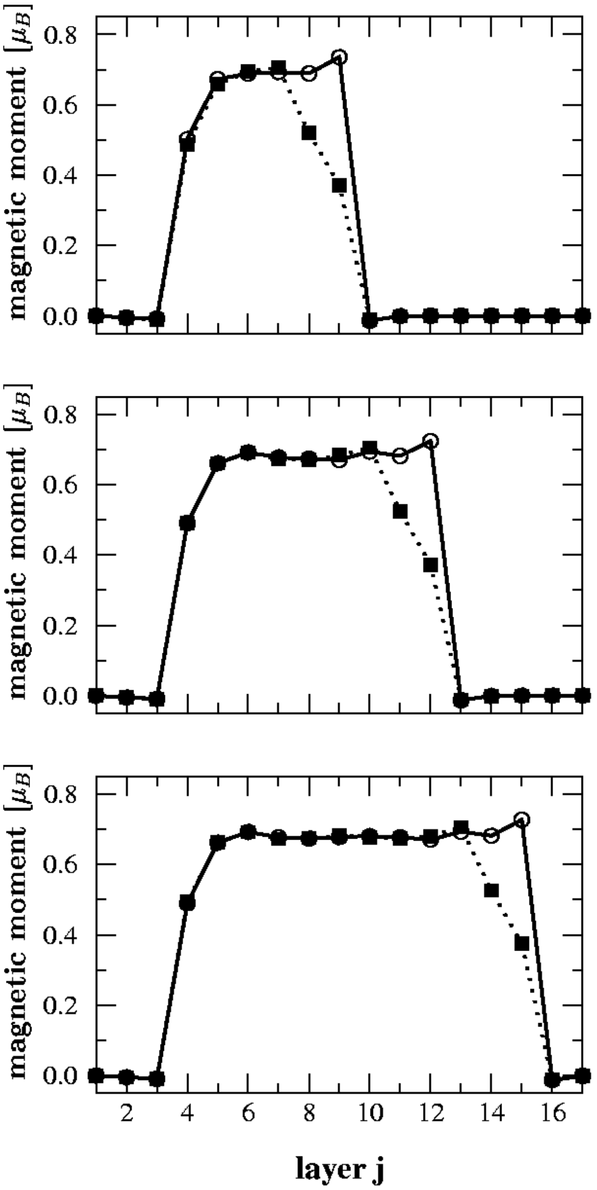

Figure 11.1: Layer-resolved magnetic moments in μ_B for uncovered (open circles) and H covered Ni films (squares) on Cu(100) of 6 (top), 9 (middle) and 12 (bottom) ML thickness.

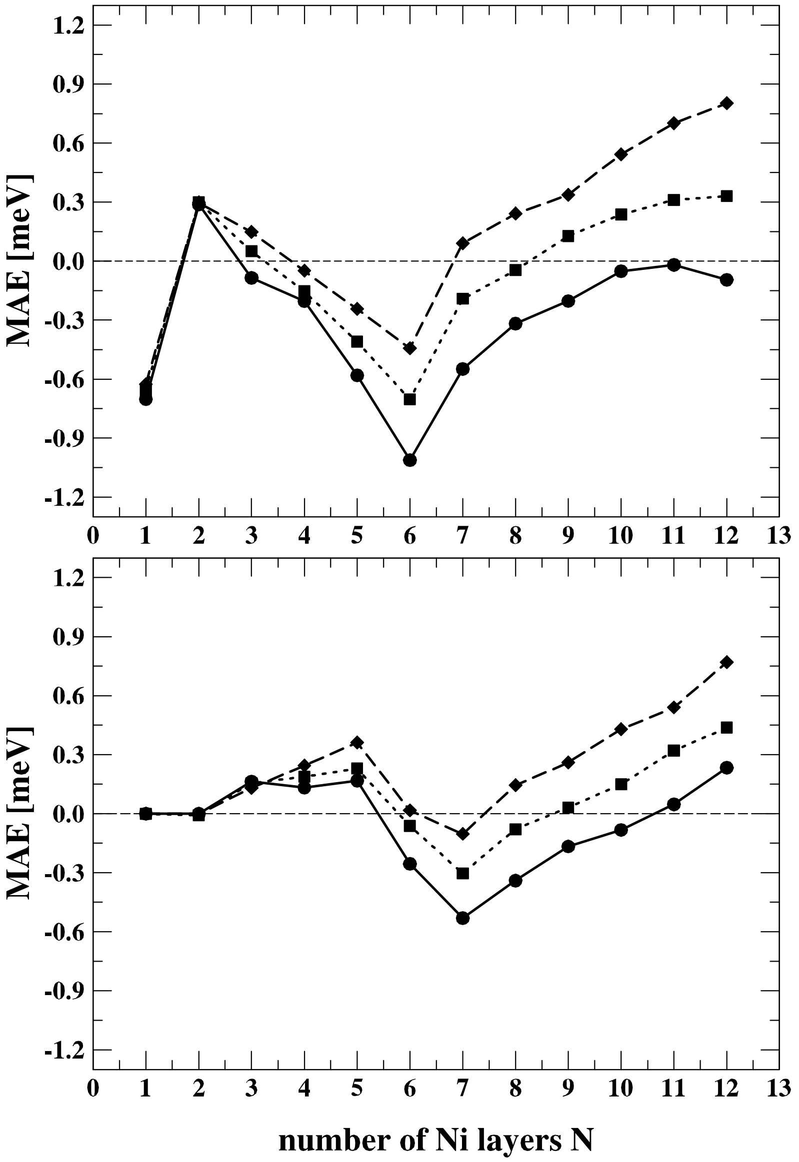

Figure 11.2: MAE for uncovered (top) and 1 ML H-covered (bottom) Ni films on Cu(100). The uniform contractions are given with respect to the interlayer spacing in fcc Cu (substrate). 1.5% (circles), 3.5% (squares),5.5% (diamonds)

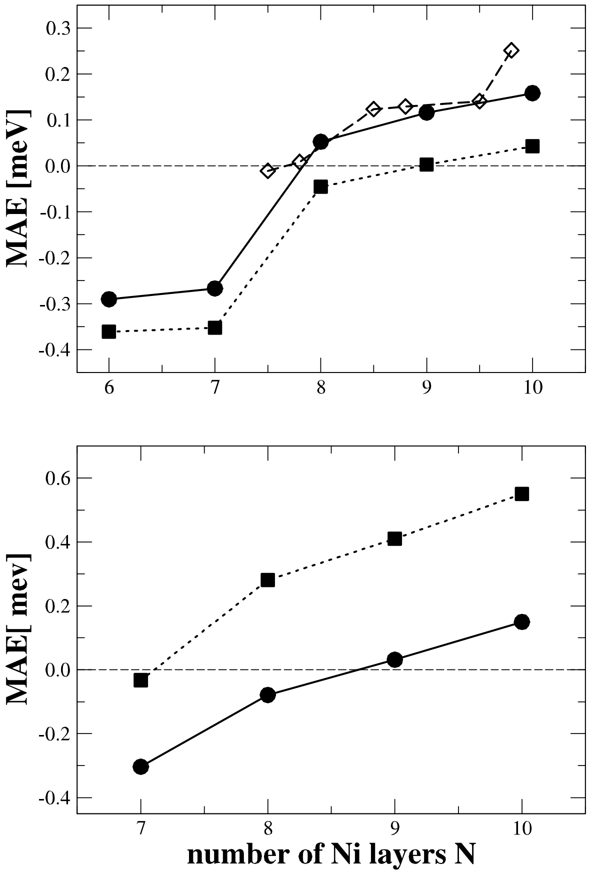

Figure 11.3: Effect of H diffusion into the first Ni layer and of incomplete H layers (top): MAE for $Cu(100)/Ni(5.5\%)_{n-1}/(H_cNi_{1-c})(5.5\%)$ (open diamonds), $Cu(100)/Ni(5.5\%)_n/(H_{0.2}Vac_{0.8})(5.5\%)$ (spheres) and $Cu(100)/Ni(5.5\%)_n/(H_{0.5}Vac_{0.5})(5.5\%)$ (squares). Effect of the interlayer distance profile (bottom): uniform contraction with 5.5% (squares), interlayer distances as given in Table 11.1.

ble 11.1, are shown. It should be noted that for these calculations the inhomogeneous coherent potential approximation (CPA) [46] is used; $Cu(100)/Ni_n(Vac_{1-c}H_c)$ refers to a statistical coverage of the Ni surface with c percent H. As can be seen at a given (uniform) contraction of the Ni interlayer distance both types of effects do not change significantly the critical thickness for the SR: it is mainly the contraction of the Ni interlayer spacing that determines the critical thickness. In all three cases shown a uniform contraction of 5.5% leads to a critical thickness of about 8 ML.

In the lower part of this figure the MAE corresponding to a uniform contraction of 5.5% is compared to a calculation using the interlayer distances as obtained from the FLAPW study (Table 1 of ref.[32]). As can be seen the assumption of a uniform contraction is quite good: both curves have very similar shapes; with the ab-initio determined interlayer distances the critical thickness for the RT occurs between 8 and 9 ML.

Table 11.3: Critical thickness for the reorientation transition

system	**contraction [%]**	**critical thickness [ML]**
Cu(100)/Ni$_n$	1.5	>11
	2.0	10 - 11
	2.5	9 - 10
	3.5	8
	5.5	6 - 7
Cu(100)/Ni$_n$H	1.5	11
	3.5	9
	5.5	7 - 8

Layer-resolved band energy contributions

In order to illustrate the difference between the bare and the H covered systems in Fig. 11.4 layer-resolved band energies (the sum over these values is the band energy) are displayed. Obviously as compared to the bare systems changes occur strongest at the surface but also throughout the whole Ni film: with adsorption of H (i) the strong (but in the two outermost layers alternating) contribution at the surface is substantially reduced and (ii) the contributions from the interior of the films are slightly decreased. One would like to apply the first feature for an easy explanation for the shift of the critical thickness: the reduced size of the surface contribution to the MAE would have caused this shift. However, since the contributions from the two outermost layers of the Ni film almost cancel each other the sum is almost unchanged by adsorption with H and the whole effect is more subtle.

Conclusion

In Table 11.3 finally the results of the calculated critical thicknesses are summarized with respect to a uniform contraction of the interlayer distance in the Ni film. This table suggests that in order to reproduce the experimentally observed critical thickness for the bare systems a contraction of about 2 - 2.5% applies, while for the H covered systems this contraction would amount to 5.0 - 5.5%. In the H covered systems the Ni films would then be by about 3% less contracted than in the bare systems: a very subtle effect indeed that most likely cannot be recorded experimentally in terms of LEED measurements, since in absolute values these 3% correspond to a change in the interlayer distance of only to about 0.05 Å. Since further experimental investigations are presently carried out, it remains to be seen whether covering Ni films on Cu(100) with hydrogen indeed reduces the critical thickness of the reorientation transition.

Acknowledgement

The authors would like to thank F. Maca for many useful discussions and for providing the FLAPW data. Financial support was provided by the Austrian Science Foundation (W004) and the Austrian Science Ministry (GZ 45.504) .

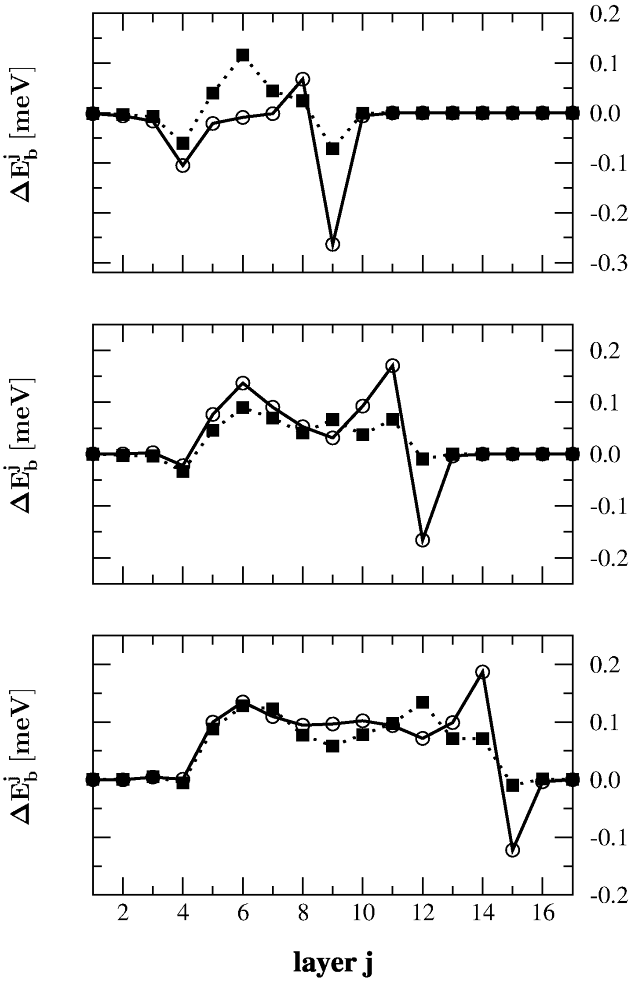

Figure 11.4: Layer-resolved band energy contributions for uncovered (open circles) and H covered Ni films (squares) on Cu(100) of 6 (top), 9 (middle) and 12 (bottom) ML thickness.

Appendix A

Appendix

A.1 The complex square function

If we take the complex function

$$f_0 \colon \left\{ \begin{array}{ccc} \mathbb{C} & \to & \mathbb{C} \\ z & \mapsto & z^2 \end{array} \right. \tag{A.1}$$

we have an analytic, surjective but not injective and therefore not bijective function. Our aim is to find a bijective form. There are always two principally different ways

- change of source set
- change of target set

A.1.1 Change of source set

If we take

$$\begin{array}{rcl} H^{I,+} & = & \{z \in \mathbb{C} : \operatorname{Im} z > 0\} \\ S^{R,+} & = & \mathbb{C} \setminus \mathbb{R}_0^+ \end{array}$$

and define the complex function

$$f_1 \colon \left\{ \begin{array}{ccc} H^{I,+} & \to & S^{R,+} \\ z & \mapsto & z^2 \end{array} \right. \tag{A.2}$$

we have an analytic, bijective function.

A.1.2 Change of target set

If we change the target set from $\mathbb{C}$ to the Riemann surface

$$R_2 = \left\{ \left(z, z^2\right) : z \in \mathbb{C} \right\}$$

and define the complex function

$$f_2 \colon \left\{ \begin{array}{ccc} \mathbb{C} & \to & R_2 \\ z & \mapsto & (z, z^2) \end{array} \right. \tag{A.3}$$

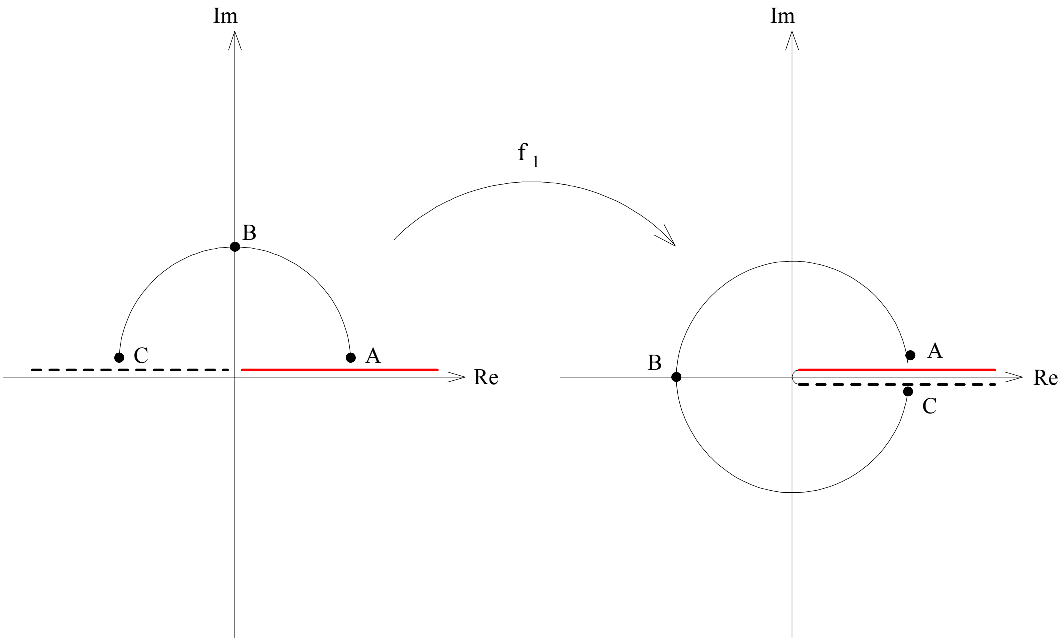

Figure A.1: The complex square function restricted to the upper halfplane.

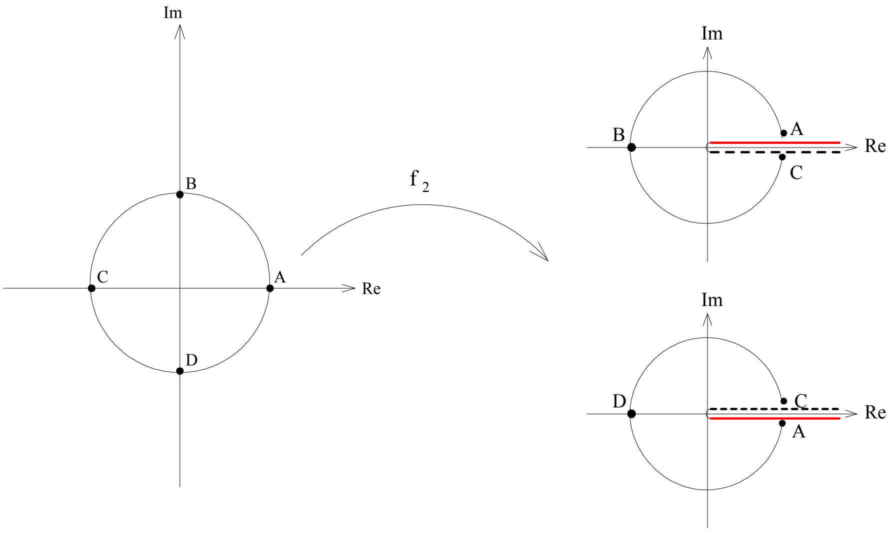

Figure A.2: Complex square function on the Riemann surface.

we have an analytic, bijective function.These construction can be viewed as if we glue 2 versions of the complex plane together, as shown in (A.2).

A.2 The Delta Function

The delta function of a variable x is commonly denoted as $\delta(x)$. It has the property of being zero for all values of x except at $x = 0$. There it is infinite in such a manner that its integral that contains the point $x = 0$ is equal to 1:

$$\int\limits_{-\infty}^{\infty} \delta(x)\,\mathrm{d}x = 1 \quad . \tag{A.4}$$

An important property of the delta function is that if it is multiplied by any continuous function $F(x)$ and the resulting product is integrated it results in

$$\int\limits_{-\infty}^{\infty} F(x)\,\delta(x-a)\,\mathrm{d}x = F(a) \quad . \tag{A.5}$$

$F(x)$ may be any kind of continuous function and can be a scalar, a vector, or a tensor. The usefulness of the delta function is not its value for a specific argument, but the evaluation of the product of a function with the delta function by an integral. In this sense the delta function is a generalized function.

The delta function can also be represented as a limit of an analytical function such as

$$\delta(x) = \lim_{L\to\infty} \frac{\sin(xL)}{\pi x} \quad , \tag{A.6}$$

where for $x = 0$, $\sin(xk)/\pi x = L/\pi$. This function has the same properties as the delta function. Using expression (A.6), the proof of the equation

$$(2\pi)^{-1} \int\limits_{-\infty}^{\infty} \mathrm{e}^{\mathrm{i}kx}\,\mathrm{d}k = \delta(x) \tag{A.7}$$

is simple:

$$(2\pi)^{-1} \int\limits_{-\infty}^{\infty} \mathrm{e}^{\mathrm{i}kx}\,\mathrm{d}k = \lim_{L\to\infty} (2\pi)^{-1} \int\limits_{-L}^{L} \mathrm{e}^{\mathrm{i}kx}\,\mathrm{d}k = \lim_{L\to\infty} \frac{\sin(xL)}{\pi x} = \delta(x) \quad . \tag{A.8}$$

The delta function can be extended to three dimensions where it is defined as:

$$\delta(\boldsymbol{r}) = \delta(x)\,\delta(y)\,\delta(z) = (2\pi)^{-3} \int \mathrm{e}^{\mathrm{i}\boldsymbol{k}\boldsymbol{r}}\mathrm{d}^3\boldsymbol{k} \tag{A.9}$$

As in the one dimensional case, when multiplied with a function and after integration the following relation results:

$$\int \delta(\boldsymbol{r})\,F(\boldsymbol{r})\,\mathrm{d}^3\boldsymbol{r} = F(0) \quad , \tag{A.10}$$

if $\boldsymbol{r}= 0$ is contained in the integration region. Finally there are some useful relations:

$$\delta(\boldsymbol{r}) = \frac{\delta(r)}{2\pi r^2}\,, \qquad \delta(\boldsymbol{r}' - \boldsymbol{r}) = \frac{2}{r^2}\,\delta(\boldsymbol{n}' - \boldsymbol{n})\,\delta(r' - r) \quad , \tag{A.11}$$

where $\boldsymbol{n}$ and $\boldsymbol{n}'$ are unit vectors in the direction of $\boldsymbol{r}$ and $\boldsymbol{r}'$.

A.3 The Green Function for Free Electrons

In this section the expressions for the free particle Green function in 3D will be derived in detail. The starting point is:

$$G^0(\boldsymbol{r}, \boldsymbol{r}'; E) = (2\pi)^{-3} \int \frac{\exp\left[\mathrm{i}\boldsymbol{q}(\boldsymbol{r} - \boldsymbol{r}')\right]}{k^2 - q^2}\, \mathrm{d}^3\boldsymbol{q} \quad . \tag{A.12}$$

Changing to spherical coordinates

$$\begin{aligned} \mathrm{d}^3\boldsymbol{q} &= q^2\,\mathrm{d}q\,\mathrm{d}\Omega \\ \mathrm{d}\Omega &= \sin\theta\,\mathrm{d}\theta\,\mathrm{d}\varphi \quad , \end{aligned}$$

with $0 \le q < \infty$, $0 \le \varphi \le 2\pi$, and $0 \le \theta \le \pi$, the integral transforms to

$$G^0(\boldsymbol{r}, \boldsymbol{r}'; E) = (2\pi)^{-3} \int_0^\infty \mathrm{d}q\, \frac{q^2}{k^2 - q^2} \int \mathrm{d}\Omega\, \exp(\mathrm{i}q|\boldsymbol{r} - \boldsymbol{r}'|\cos\theta) \quad , \tag{A.13}$$

where $\boldsymbol{q}{\cdot}\boldsymbol{r}= qr\cos\theta$ has been used. Next the integration over $\mathrm{d}\Omega$ is performed:

$$\begin{aligned} \int \mathrm{d}\Omega\, \exp(\mathrm{i}q|\boldsymbol{r} - \boldsymbol{r}'|\cos\theta) &= \int_0^{2\pi} \mathrm{d}\varphi \int_0^{\pi} \mathrm{d}\theta\, \sin\theta\, \exp(\mathrm{i}q|\boldsymbol{r} - \boldsymbol{r}'|\cos\theta) \\ &= (-2\pi)(\mathrm{i}q|\boldsymbol{r} - \boldsymbol{r}'|)^{-1} \left[\exp(-\mathrm{i}q|\boldsymbol{r} - \boldsymbol{r}'|) - \exp(\mathrm{i}q|\boldsymbol{r} - \boldsymbol{r}'|)\right] \end{aligned}$$

After substitution and rearrangement in (A.13), only the one dimensional radial integral is left:

$$\begin{aligned} G^0(\boldsymbol{r}, \boldsymbol{r}'; E) &= \frac{1}{4\pi^2\mathrm{i}|\boldsymbol{r} - \boldsymbol{r}'|} \int_0^\infty \frac{q\left[\exp(\mathrm{i}q|\boldsymbol{r} - \boldsymbol{r}'|) - \exp(-\mathrm{i}q|\boldsymbol{r} - \boldsymbol{r}'|)\right]}{k^2 - q^2}\, \mathrm{d}q & \text{(A.14)} \\ &= -\frac{1}{4\pi^2\mathrm{i}|\boldsymbol{r} - \boldsymbol{r}'|} \int_{-\infty}^{\infty} \frac{q\exp(\mathrm{i}q|\boldsymbol{r} - \boldsymbol{r}'|)}{q^2 - k^2}\, \mathrm{d}q \quad . & \text{(A.15)} \end{aligned}$$

The last expression contains a complex function of the variable q in the integral, which has two simple poles at $q = k$ and $q = -k$. For the evaluation of the integral a proper integration path in the upper half of the complex plane has to be chosen, which includes either one of the two poles. According to standard complex analysis an integral of the type (A.15) is evaluated as

$$\int_{-\infty}^{\infty} f(z)\,\mathrm{d}z = 2\pi\mathrm{i} \sum_{k=0}^{n} \mathrm{Res}_{z=z_k}\, f(z)\,, \quad \mathrm{Im}(z_k) > 0 \quad , \tag{A.16}$$

where z is a complex variable, z_k are the poles of $f(z)$, and $\mathrm{Res} f(z)$ refers to the residuum of the function $f(z)$, which can be evaluated from

$$\mathrm{Res}_{z=z_k} f(z) = \lim_{z \to z_k} (z - z_k) f(z) \quad . \tag{A.17}$$

With

$$\mathrm{Res}_{q=k} \left\{ \frac{q \exp(\mathrm{i}q|\boldsymbol{r} - \boldsymbol{r'}|)}{q^2 - k^2} \right\} = \frac{1}{2} \exp(\mathrm{i}k|\boldsymbol{r} - \boldsymbol{r'}|) \quad , \tag{A.18}$$

evaluation of the integral in (A.15) yields

$$G^0(\boldsymbol{r}, \boldsymbol{r'}; E) = -\frac{\exp(\mathrm{i}k|\boldsymbol{r} - \boldsymbol{r'}|)}{4\pi|\boldsymbol{r} - \boldsymbol{r'}|} \quad . \tag{A.19}$$

A.3.1 Partial Wave Expansion of the Free Particle Green Function

A commonly used description of the free particle Green's function is its expansion in terms of solutions of the free space Schrödinger equation and its partial wave components. We start off by rewriting equation (A.12)

$$G^0(\boldsymbol{r}, \boldsymbol{r'}; E) = (2\pi)^{-3} \int \exp(\mathrm{i}\boldsymbol{q}\boldsymbol{r}) \, \frac{1}{k^2 - q^2} \, \exp(-\mathrm{i}\boldsymbol{q}\boldsymbol{r'}) \, \mathrm{d}^3\boldsymbol{q} \quad . \tag{A.20}$$

Using the expansion (A.50), which is also known as Bauer's identity, we have

$$\begin{aligned} G^0(\boldsymbol{r}, \boldsymbol{r'}; E) &= (2\pi)^{-3} \int \mathrm{d}^3\boldsymbol{q} \left[\sum_L 4\pi \mathrm{i}^\ell \, j_\ell(qr) \, Y_L^*(\hat{\boldsymbol{q}}) \, Y_L(\hat{\boldsymbol{r}}) \right] \\ &\quad \times \frac{1}{k^2 - q^2} \left[\sum_{L'} 4\pi(-\mathrm{i}^{\ell'}) \, j_{\ell'}(qr') \, Y_{L'}^*(\hat{\boldsymbol{q}}) \, Y_{L'}(\hat{\boldsymbol{r}}') \right] \quad . \end{aligned} \tag{A.21}$$

Transformation to spherical coordinates and some rearrangement yields

$$\begin{aligned} G^0(\boldsymbol{r}, \boldsymbol{r'}; E) &= \frac{2}{\pi} \int_0^\infty \frac{q^2 \, \mathrm{d}q}{k^2 - q^2} \sum_{LL'} \mathrm{i}^\ell (-\mathrm{i}^{\ell'}) \, j_\ell(qr) j_{\ell'}(qr') \, Y_L(\hat{\boldsymbol{r}}) Y_{L'}^*(\hat{\boldsymbol{r}}') \\ &\quad \times \int \mathrm{d}\Omega \, Y_L(\hat{\boldsymbol{q}}) Y_{L'}^*(\hat{\boldsymbol{q}}) \quad . \end{aligned} \tag{A.22}$$

Now the orthogonality of the complex spherical harmonics can be used

$$\int \mathrm{d}\Omega \, Y_L(\hat{\boldsymbol{q}}) Y_{L'}^*(\hat{\boldsymbol{q}}) = \delta_{LL'} \quad , \tag{A.23}$$

and with $\mathrm{i}^\ell \cdot (-\mathrm{i}^\ell) = 1$, one can write

$$G^0(\boldsymbol{r}, \boldsymbol{r'}; E) = \frac{2}{\pi} \int_0^\infty \frac{q^2 \, \mathrm{d}q}{k^2 - q^2} \sum_L j_\ell(qr) j_\ell(qr') \, Y_L(\hat{\boldsymbol{r}}) Y_L^*(\hat{\boldsymbol{r}}') \quad . \tag{A.24}$$

Following from the fact that the integrand is even in q, this formula can be rewritten to yield the equation

$$G^0(\boldsymbol{r}, \boldsymbol{r'}; E) = \pi^{-1} \sum_L Y_L(\hat{\boldsymbol{r}})\, Y_L^*(\hat{\boldsymbol{r}}') \int\limits_{-\infty}^{\infty} \frac{j_\ell(qr)\, j_\ell(qr')}{k^2 - q^2}\, q^2 \mathrm{d}q \quad . \tag{A.25}$$

Hence we can define

$$G_\ell^0(r, r'; E) = \pi^{-1} \int\limits_{-\infty}^{\infty} \frac{j_\ell(qr)\, j_\ell(qr')}{k^2 - q^2}\, q^2 \mathrm{d}q \quad . \tag{A.26}$$

The evaluation of the integral has to be done by contour integration in the complex q plane. However, because the product $j_\ell(qr)\, j_\ell(qr')$ does not vanish along the semicircle in the upper half plane [Mertig] some care has to be taken. Following [15] for $r' > r$ the relation

$$j_\ell(qr') = \frac{1}{2}\left[h_\ell(qr') + h_\ell^*(qr')\right] \quad , \tag{A.27}$$

where $h_\ell(qr')$ is a spherical Hankel function of the first kind, helps out. After substitution in (A.25) the solutions to two integrals have to be found:

$$\mathrm{I}_1 = \frac{1}{2} \int\limits_{-\infty}^{\infty} \frac{q^2\, j_\ell(qr)\, h_\ell(qr')}{k^2 - q^2}\, \mathrm{d}q \quad , \tag{A.28}$$

$$\mathrm{I}_2 = \frac{1}{2} \int\limits_{-\infty}^{\infty} \frac{q^2\, j_\ell(qr)\, h_\ell^*(qr')}{k^2 - q^2}\, \mathrm{d}q \quad . \tag{A.29}$$

The integral I_1 can be solved by using the pole at $q = +k$ from

$$\begin{aligned}
\mathrm{I}_1 &= \tfrac{1}{2}\, 2\pi \mathrm{i}\, \mathrm{Res}_{q=+k} \left[\frac{q^2\, j_\ell(qr)\, h_\ell(qr')}{k^2 - q^2}\right] = && \text{(A.30)}\\
&= \pi \mathrm{i} \left[-\frac{1}{2}\, k\, j_\ell(kr)\, h_\ell(kr')\right] = && \text{(A.31)}\\
&= -\tfrac{1}{2}\, \mathrm{i}\pi k\, j_\ell(kr)\, h_\ell(kr')\,, \quad r' > r \quad . && \text{(A.32)}
\end{aligned}$$

The second integral can be evaluated by closing the contour in the lower half plane and thereby including the second pole $q = -k$. One then gets

$$\begin{aligned}
\mathrm{I}_2 &= \tfrac{1}{2}\, 2\pi \mathrm{i}\, \mathrm{Res}_{q=-k} \left[\frac{q^2\, j_\ell(qr)\, h_\ell^*(qr')}{k^2 - q^2}\right] = && \text{(A.33)}\\
&= -\tfrac{1}{2}\, \mathrm{i}\pi k\, j_\ell(-kr)\, h_\ell^*(-kr') \quad . && \text{(A.34)}
\end{aligned}$$

With the identities $j_\ell(-kr) = (-1)^{\ell+1} j_\ell(kr)$ and $h_\ell^*(-kr) = (-1)^\ell\, h_\ell(kr)$, I_2 finally yields a contribution identical to I_1:

$$\mathrm{I}_2 = -\tfrac{1}{2}\, \mathrm{i}\pi k\, j_\ell(kr)\, h_\ell(kr')\,, \quad r' > r \quad . \tag{A.35}$$

In total we have

$$\mathrm{I}_1 + \mathrm{I}_2 = -\mathrm{i}\pi k\, j_\ell(kr)\, h_\ell(kr')\,, \quad r' > r \quad . \tag{A.36}$$

The same procedure has to be used for $r > r'$ which gives the identical result, and in summary we can write

$$\mathrm{I}_1 + \mathrm{I}_2 = -\mathrm{i}\pi k\, j_\ell(kr_<)\, h_\ell(kr_>) \quad , \tag{A.37}$$

and therefore

$$G^0_\ell(r, r'; E) = -\mathrm{i}k\, j_\ell(kr_<)\, h_\ell(kr_>) \quad , \tag{A.38}$$

where $r_< := \min\{r, r'\}$ and $r_> := \max\{r, r'\}$. With this result the partial wave expansion of the free particle Green's function is given by

$$G^0(\boldsymbol{r}, \boldsymbol{r}'; E) = -\mathrm{i}k \sum_L j_\ell(kr_<)\, h_\ell(kr_>)\, Y^*_L(\hat{\boldsymbol{r}})\, Y_L(\hat{\boldsymbol{r}}') \quad , \tag{A.39}$$

and with the definitions:

$$\begin{aligned} j_L(k\boldsymbol{r}_<) &= j_\ell(kr_<)\, Y_L(\hat{\boldsymbol{r}}) &\text{(A.40)}\\ h_L(k\boldsymbol{r}_>) &= h_\ell(kr_>)\, Y_L(\hat{\boldsymbol{r}}) \quad , &\text{(A.41)}\end{aligned}$$

we can finally write

$$G^0(\boldsymbol{r}, \boldsymbol{r}'; E) = -\mathrm{i}k \sum_L j_L(k\boldsymbol{r}_<)\, h_L(k\boldsymbol{r}_>) \quad , \tag{A.42}$$

which is the partial wave expansion of the Green function.

A.4 Mathematical Relations for Madelung constants

Remark 4 *Condon-Shortly phase convention for spherical harmonics, defintion of $P_\ell^{|m|}$ differs from ([16]):*

$$Y_{\ell m}(\widehat{\mathbf{r}}) = i^{m+|m|}\sqrt{\frac{2\ell+1}{4\pi}\frac{(\ell-|m|)!}{(\ell+|m|)!}}P_\ell^{|m|}(\cos(\Theta))\exp(im\phi) \tag{A.43}$$

Lemma 5

$$\frac{1}{|\mathbf{r}-\mathbf{r}'|} = \sum_L \frac{4\pi}{2\ell+1}\frac{r^\ell}{(r')^{\ell+1}}Y^*_L(\widehat{\mathbf{r}})Y_L(\widehat{\mathbf{r}}') \qquad (r < r') \tag{A.44}$$

Lemma 6

$$\begin{aligned}\frac{1}{|\mathbf{r}-\mathbf{r}'|^{\ell+1}}Y_L(\widehat{\mathbf{r}-\mathbf{r}'}) = \sum_{L'}(-1)^\ell \frac{4\pi[2(\ell+\ell')-1]!!}{(2\ell-1)!!(2\ell'+1)!!}\mathcal{C}^{\ell'm'}_{\ell m,(\ell+\ell')(m'-m)}\times \\ \times\,\frac{r^{\ell'}}{(r')^{\ell+\ell'+1}}Y_{\ell'm'}(\widehat{\mathbf{r}})Y^*_{(\ell+\ell')(m'-m)}(\widehat{\mathbf{r}}') \qquad (r < r')\ ,\end{aligned} \tag{A.45}$$

with the Gaunt coefficients

$$\mathcal{C}^{L'}_{L,L''} = \int d\Omega Y_L(\Omega)Y^*_{L'}(\Omega)Y_{L''}(\Omega)\ . \tag{A.46}$$

Lemma 7

$$|\mathbf{r}-\mathbf{r}'|^{\ell}\, Y_L(\widehat{\mathbf{r}-\mathbf{r}'}) = \tag{A.47}$$

$$= \sum_{\ell',m'} \frac{4\pi(-1)^{\ell-\ell'}(2\ell+1)!!}{(2\ell'+1)!![2(\ell-\ell')+1]!!}\mathcal{C}^{(\ell-\ell'),(m+m')}_{\ell'm',\ell m}\, r^{\ell'}(r')^{(\ell-\ell')}Y^*_{\ell',m'}(\widehat{\mathbf{r}})Y_{(\ell-\ell'),(m+m')}(\widehat{\mathbf{r}}') \tag{A.48}$$

$$= \sum_{L',L''} \delta_{\ell,\ell'+\ell''}\delta_{m,m''-m'}\, r^{\ell'}Y^*_{L'}(\widehat{\mathbf{r}})\, \frac{4\pi(-1)^{\ell''}[2(\ell'+\ell'')+1]!!}{(2\ell'+1)!!(2\ell''+1)!!}\mathcal{C}^{\ell''m''}_{\ell'm',\ell m}\,(r')^{\ell''}Y_{L''}(\widehat{\mathbf{r}}') \tag{A.49}$$

Proof.

$$\exp(i\mathbf{k}\mathbf{r}) = 4\pi\sum_L i^{\ell}j_\ell(kr)Y_L(\widehat{\mathbf{k}})Y^*_L(\widehat{\mathbf{r}}) = 4\pi\sum_L i^{\ell}j_\ell(kr)Y^*_L(\widehat{\mathbf{k}})Y_L(\widehat{\mathbf{r}}) \tag{A.50}$$

$$\exp(i\mathbf{k}(\mathbf{r}-\mathbf{r}')) = 4\pi\sum_L i^{\ell}j_\ell(k\,|\mathbf{r}-\mathbf{r}'|)Y^*_L(\widehat{\mathbf{k}})Y_L(\widehat{\mathbf{r}-\mathbf{r}'}) \tag{A.51}$$

$$\exp(i\mathbf{k}\mathbf{r})\exp(-i\mathbf{k}\mathbf{r}') = (4\pi)^2\sum_{L',L''} i^{\ell'-\ell''}j_{\ell'}(kr)j_{\ell''}(kr')Y_{L'}(\widehat{\mathbf{k}})Y^*_{L''}(\widehat{\mathbf{k}})Y^*_{L'}(\widehat{\mathbf{r}})Y_{L''}(\widehat{\mathbf{r}}') \tag{A.52}$$

Thus,

$$j_\ell(k\,|\mathbf{r}-\mathbf{r}'|)Y_L(\widehat{\mathbf{r}-\mathbf{r}'}) = 4\pi\sum_{L',L''} i^{\ell'-\ell''-\ell}j_{\ell'}(kr)Y^*_{L'}(\widehat{\mathbf{r}})\mathcal{C}^{\ell''m''}_{\ell'm',\ell m}\,j_{\ell''}(kr')Y_{L''}(\widehat{\mathbf{r}}')\ . \tag{A.53}$$

Recalling that

$$\lim_{z\to 0} j_\ell(z) = \frac{z^\ell}{(2\ell+1)!!}\ , \tag{A.54}$$

yields

$$|\mathbf{r}-\mathbf{r}'|^{\ell}\, Y_L(\widehat{\mathbf{r}-\mathbf{r}'}) = \tag{A.55}$$

$$= \sum_{L',L''}\left[\lim_{k\to 0} k^{\ell'+\ell''-\ell}\right] r^{\ell'}Y^*_{L'}(\widehat{\mathbf{r}})\frac{4\pi i^{\ell'-\ell''-\ell}(2\ell+1)!!}{(2\ell'+1)!!(2\ell''+1)!!}\mathcal{C}^{\ell''m''}_{\ell'm',\ell m}\,(r')^{\ell''}Y_{L''}(\widehat{\mathbf{r}}') = \tag{A.56}$$

$$= \sum_{L',L''} \delta_{\ell,\ell'+\ell''}\delta_{m,m''-m'}\, r^{\ell'}Y^*_{L'}(\widehat{\mathbf{r}})\, \frac{4\pi(-1)^{\ell''}[2(\ell'+\ell'')+1]!!}{(2\ell'+1)!!(2\ell''+1)!!}\mathcal{C}^{\ell''m''}_{\ell'm',\ell m}\,(r')^{\ell''}Y_{L''}(\widehat{\mathbf{r}}')\ . \tag{A.57}$$

■

Remark 8

$$\Gamma(z+1) = z\Gamma(z) \tag{A.58}$$

$$\Gamma(1) = 1 \qquad \Gamma(n) = (n-1)\Gamma(n-1) = (n-1)! \tag{A.59}$$

$$\Gamma(\frac{1}{2}) = \sqrt{\pi} \qquad \Gamma(n+\frac{1}{2}) = \frac{2n-1}{2}\Gamma(n-\frac{1}{2}) = \sqrt{\pi}\frac{(2n-1)!!}{2^n} \tag{A.60}$$

$$\Gamma(\frac{1}{2}+\frac{1}{2}n)\Gamma(1+\frac{1}{2}n) = \frac{\sqrt{\pi}}{2^n}\Gamma\,(n+1) \tag{A.61}$$

Lemma 9

$$\frac{1}{A}=\frac{2}{\sqrt{\pi}}\int_0^\infty dx\exp(-A^2x^2)\qquad (A>0) \tag{A.62}$$

Lemma 10 *The following identity, stemming from the Poisson summation formula,*

$$\sum_n \exp(-\left|\mathbf{r}-\mathbf{T}_n\right|^2 x^2)=\frac{\pi^{d/2}}{Vx^d}\sum_j \exp(-\mathbf{G}_j^2/4x^2+i\mathbf{G}_j\mathbf{r})\ , \tag{A.63}$$

is valid for arbitrary dimension d. V is the volume of the d-dimensional unit cell in configurational space, while $\mathbf{T}_n$ *and* $\mathbf{G}_j$ *are vectors of the corresponding real and reciprocal lattices, respectively.*

Remark 11 Lemma 12 Proof. *For the Gaussian function* $u(\mathbf{r},t)=\frac{1}{(4\pi t)^{d/2}}e^{-\frac{r^2}{4t}}$ *it holds true*

$$\frac{\partial u(\mathbf{r},t)}{\partial t}-\Delta u(\mathbf{r},t)=0\ .$$

Namely,

$$\frac{\partial u(\mathbf{r},t)}{\partial t}=\frac{1}{4t^2\left(4\pi t\right)^{d/2}}\left(r^2-2td\right)e^{-\frac{r^2}{4t}}$$

and

$$\begin{aligned}
\frac{\partial f(r)}{\partial x_i}&=\frac{\partial r}{\partial x_i}\frac{df(r)}{dr}=\frac{x_i}{r}\frac{df(r)}{dr}\ ,\\
\frac{\partial^2 f(r)}{\partial x_i^2}&=\frac{1}{r}\frac{df(r)}{dr}+\frac{x_i^2}{r}\frac{d\left(\frac{1}{r}\frac{df(r)}{dr}\right)}{dr}=\frac{1}{r}\frac{df(r)}{dr}-\frac{x_i^2}{r^3}\frac{df(r)}{dr}+\frac{x_i^2}{r^2}\frac{d^2f(r)}{dr^2}\ ,\\
\Delta f(r)&=\sum_{i=1}^{d}\frac{\partial^2 f(r)}{\partial x_i^2}=\frac{d-1}{r}\frac{df(r)}{dr}+\frac{d^2f(r)}{dr^2}\ ,
\end{aligned}$$

therefore,

$$\Delta u(\mathbf{r},t)=\frac{1}{\left(4\pi t\right)^{d/2}}\left(-\frac{d-1}{r}\frac{r}{2t}-\frac{1}{2t}+\frac{r^2}{4t^2}\right)e^{-\frac{r^2}{4t}}=\frac{1}{4t^2\left(4\pi t\right)^{d/2}}\left(r^2-2td\right)e^{-\frac{r^2}{4t}}\ .$$

Let us define the function

$$U(\mathbf{r},t)=\frac{1}{\left(4\pi t\right)^{d/2}}\sum_n \exp\left(-\frac{\left(\mathbf{r}-\mathbf{T}_n\right)^2}{4t}\right)\ ,$$

for which the following properties are valid:

$$\begin{gathered}
U(\mathbf{r},t)=U(\mathbf{r}+\mathbf{T}_n,t)\quad \textit{for any } \mathbf{T}_n\ ,\\
\int d^d r U(\mathbf{r},t)=N\quad ,\quad \lim_{t\to 0}U(\mathbf{r},t)=\sum_n \delta\left(\mathbf{r}-\mathbf{T}_n\right)\ ,\\
\textit{and}\quad \frac{\partial U(\mathbf{r},t)}{\partial t}-\Delta U(\mathbf{r},t)=0\ .
\end{gathered}$$

Thus $U(\mathbf{r},t)$ can be written as

$$U(\mathbf{r},t)=\sum_j A_j\left(t\right)\exp\left(i\mathbf{G}_j\mathbf{r}\right)\ ,$$

where

$$\frac{\partial A_j(t)}{\partial t}-\mathbf{G}_j^2A_j(t)=0\implies A_j(t)=\frac{1}{V}\exp\left(-\mathbf{G}_j^2t\right)\ .$$

since the boundary condition $A_j(0)=1/V$ has to be fulfilled. Substituting $x^2=1/4t$ one gets

$$\sum_n\exp\left(-\left(\mathbf{r}-\mathbf{T}_n\right)^2x^2\right)=\frac{\pi^{d/2}}{x^dV}\sum_j\exp\left(-\mathbf{G}_j{}^2/4x^2+i\mathbf{G}_j\mathbf{r}\right)$$

which is the required formula for $\mathbf{k}=0$. Since

$$-\left(\mathbf{r}-\mathbf{T}_n\right)^2x^2-i\mathbf{k}\left(\mathbf{r}-\mathbf{T}_n\right)=-\left(\mathbf{r}-\mathbf{T}_n+i\mathbf{k}/2x^2\right)^2x^2-\mathbf{k}^2/4x^2$$

one can apply the above formula for $\mathbf{r}+i\mathbf{k}/2x^2$, which leads to

$$\begin{aligned}\sum_n\exp\left(-\left(\mathbf{r}-\mathbf{T}_n\right)^2x^2-i\mathbf{k}\left(\mathbf{r}-\mathbf{T}_n\right)\right)&=\frac{\pi^{d/2}}{x^dV}\exp\left(-\mathbf{k}^2/4x^2\right)\sum_j\exp\left(-\mathbf{G}_j{}^2/4x^2+i\mathbf{G}_j\mathbf{r}-\mathbf{G}_j\mathbf{k}/2x^2\right)\\&=\frac{\pi^{d/2}}{x^dV}\sum_j\exp\left(-\left(\mathbf{k}+\mathbf{G}_j\right)^2/4x^2+i\mathbf{G}_j\mathbf{r}\right)\ .\end{aligned}$$

QED! ■

Lemma 13 *([16], formula 3.381.3):*

$$\int_u^\infty x^{\nu-1}\exp(-\mu x)dx=\mu^{-\nu}\Gamma(\nu,\mu u)\qquad\left[u>0,Re\mu>0\right]. \tag{A.64}$$

Therefore,

$$\int_{|\mathbf{a}_{\mu\nu}-\mathbf{T}_n|/2\sigma}^\infty dx\,x^{2\ell}\exp(-x^2)= \tag{A.65}$$

$$=\frac{1}{2}\int_{|\mathbf{a}_{\mu\nu}-\mathbf{T}_n|^2/4\sigma^2}^\infty dy\,y^{\ell-\frac{1}{2}}\exp(-y)=\frac{1}{2}\Gamma(\ell+\frac{1}{2},\left|\mathbf{a}_{\mu\nu}-\mathbf{T}_n\right|^2/4\sigma^2)\ . \tag{A.66}$$

Remark 14 Lemma 15 *A few words about the error and incomplete Γ-functions:*

$$\mathrm{erf}\left(x\right)=\frac{2}{\sqrt{\pi}}\int_0^x e^{-t^2}dx \tag{A.67}$$

$$\mathrm{erfc}\left(x\right)=\frac{2}{\sqrt{\pi}}\int_x^\infty e^{-t^2}dx=1-\mathrm{erf}\left(x\right) \tag{A.68}$$

$$\mathrm{erf}\,(x) = \frac{2}{\sqrt{\pi}} \sum_{n=0}^{\infty} \frac{(-1)^n \; x^{2n+1}}{n! \; (2n+1)} = \frac{2}{\sqrt{\pi}} e^{-x^2} \sum_{n=0}^{\infty} \frac{2^n \, x^{2n+1}}{(2n+1)!!} \tag{A.69}$$

$$\gamma\,(a,x) = \int_0^x e^{-t}\, t^{a-1} dx \tag{A.70}$$

$$\Gamma\,(a,x) = \int_x^{\infty} e^{-t}\, t^{a-1} dx = \Gamma\,(a) - \gamma\,(a,x) \tag{A.71}$$

$$\gamma\left(\frac{1}{2}, x^2\right) = \sqrt{\pi}\,\mathrm{erf}\,(x) \;\;, \quad \Gamma\left(\frac{1}{2}, x^2\right) = \sqrt{\pi}\mathrm{erfc}\,(x) \tag{A.72}$$

$$\gamma(a+1,x) = a\gamma\,(a,x) - x^a e^{-x} \tag{A.73}$$

Lemma 16 *([16], formula 3.472.3):*

$$\int_0^{\infty} \exp\left(-\frac{a}{x^2} - \mu x^2\right) \frac{dx}{x^2} = \frac{1}{2}\sqrt{\frac{\pi}{a}} \exp(-2\sqrt{a\mu}) \qquad [Re\mu > 0, a > 0] \tag{A.74}$$

By choosing $a = \mathbf{G}_j^2/4$ *and* $\mu = z^2$ *yields*

$$\int_0^{\infty} dx \frac{1}{x^2} \exp(-z^2 x^2 - \mathbf{G}_j^2/4x^2) = \frac{\sqrt{\pi}}{G_j} \exp\left(-G_j\,|z|\right) \;, \tag{A.75}$$

which is valid also for $z = 0$.

Lemma 17 *([16], formula 3.461.5):*

$$\int_u^{\infty} \exp(-\mu x^2) \frac{dx}{x^2} = \frac{1}{u}\exp(-\mu u^2) - \sqrt{\mu\pi}\mathrm{erfc}(\sqrt{\mu}u) \qquad [|\arg\mu| < \frac{\pi}{2}, u > 0] \tag{A.76}$$

Proof.

$$\int_u^{\infty} \exp(-\mu x^2) \frac{1}{x^2} dx = -\int_u^{\infty} \exp(-\mu x^2) \frac{d}{dx}\left(\frac{1}{x}\right) dx = \tag{A.77}$$

$$= -\left[\exp(-\mu x^2)\frac{1}{x}\right]_u^{\infty} + \int_u^{\infty} \frac{d}{dx}\left\{\exp(-\mu x^2)\right\} \frac{1}{x} dx = \tag{A.78}$$

$$= \frac{1}{u}\exp(-\mu u^2) - 2\mu \int_u^{\infty} \exp(-\mu x^2) dx \tag{A.79}$$

By choosing $u = 1/2\sigma$ *and* $\mu = z^2$ *yields*

$$\int_{1/2\sigma}^{\infty} dx \frac{1}{x^2} \exp(-z^2 x^2) = 2\sigma \exp(-\frac{z^2}{4\sigma^2}) - 2z^2 \int_{1/2\sigma}^{\infty} \exp(-z^2 x^2) dx = \tag{A.80}$$

$$= 2\sigma \exp(-\frac{z^2}{4\sigma^2}) - |z|\,\sqrt{\pi}\mathrm{erfc}\left(\frac{|z|}{2\sigma}\right) \;. \tag{A.81}$$

■

Remark 18 *Recursive evaluation of the Integrals* $I_n(a,b)$ *where* $a,b>0$ *(namely* $a=G_j\sigma, b=|c_{pq\perp}|G_j/2$*, during the lattice summations the* G_j *become large)*

$$\underline{I_n(a,b) \equiv \int_{a^2}^{\infty} x^{-\frac{1}{2}-n} \exp\left(-\frac{b^2}{x}-x\right)\,dx} \qquad (a,b>0)$$

Integrating by parts yields

$$\left(n-\frac{1}{2}\right) I_n(a,b) = \frac{\exp\left(-\frac{b^2}{a^2}-a^2\right)}{a^{2n-1}} + b^2 I_{n+1}(a,b) - I_{n-1}(a,b)\ ,$$

from which the recursion relation

$$\underline{I_{n+2}(a,b) = \frac{1}{b^2}\left[\left(n+\frac{1}{2}\right) I_{n+1}(a,b) + I_n(a,b)\right] - \frac{\exp\left(-\frac{b^2}{a^2}-a^2\right)}{a^{2n+1}b^2}}\ , \tag{A.82}$$

can be obtained.

$$I_0(a,b) = \int_{a^2}^{\infty} x^{-\frac{1}{2}} \exp\left(-\frac{b^2}{x}-x\right)\,dx = 2\int_a^{\infty} \exp\left(-\frac{b^2}{y^2}-y^2\right)\,dy$$

According to ([16], formula 3.325), ([1] formula 7.4.3)

$$I_0(0,b) = 2\int_0^{\infty} \exp\left(-\frac{b^2}{y^2}-y^2\right)\,dy = \sqrt{\pi}\exp\left(-2b\right)$$

$$\begin{aligned}
\underline{I_0(a,b)} &= \sqrt{\pi}\exp\left(-2b\right) - 2\int_0^a \exp\left(-\frac{b^2}{y^2}-y^2\right)\,dy = \\
&= \sqrt{\pi}\exp\left(-2b\right) + \\
&- \int_0^a \left[\exp\left(2b\right)\exp\left(-(\frac{b}{y}+y)^2\right)(1-\frac{b}{y^2}) + \exp\left(-2b\right)\exp\left(-(\frac{b}{y}-y)^2\right)(1+\frac{b}{y^2})\right]\,dy = \\
&= \sqrt{\pi}\exp\left(-2b\right) + \frac{\sqrt{\pi}}{2}\left[\exp\left(2b\right)\left(1-\operatorname{erf}\left(\frac{b}{a}+a\right)\right) + \exp\left(-2b\right)\left(\operatorname{erf}\left(\frac{b}{a}-a\right)-1\right)\right] = \\
&= \underline{\frac{\sqrt{\pi}}{2}\left[\exp\left(-2b\right)\left(\operatorname{erf}\left(\frac{b}{a}-a\right)+1\right) - \exp\left(2b\right)\left(\operatorname{erf}\left(\frac{b}{a}+a\right)-1\right)\right]}
\end{aligned} \tag{A.83}$$

$$\begin{aligned}
\underline{I_1(a,b)} &= \int_{a^2}^{\infty} x^{-\frac{3}{2}} \exp\left(-\frac{b^2}{x}-x\right)\,dx = 2\int_a^{\infty} \frac{1}{y^2}\exp\left(-\frac{b^2}{y^2}-y^2\right)\,dy = \\
&= 2\int_0^{\frac{1}{a}} \exp\left(-b^2t^2-\frac{1}{t^2}\right)\,dt \\
&= |\textit{substitution } t \rightarrow bt \textit{ and above formula}| \\
&= \underline{\frac{\sqrt{\pi}}{2b}\left[\exp\left(-2b\right)\left(\operatorname{erf}\left(\frac{b}{a}-a\right)+1\right) + \exp\left(2b\right)\left(\operatorname{erf}\left(\frac{b}{a}+a\right)-1\right)\right]}
\end{aligned}$$

In the numerical evaluation one has the problem of multiplying the large term $\exp(2b)$ *with the small term* $(\mathrm{erf}(\frac{b}{a}+a)-1)$ *which leads to numerical problems, use inequality ([1] formula 7.1.13.) as help*

Proof. of eq. (6.140): ([16], formula *3.915.2):*

$$\int_0^{\pi} \exp(i\beta\cos(\phi))\cos(m\phi)d\phi = \pi\, i^m\, J_m(\beta) = \pi\, i^{-m}\, J_m(-\beta)\ ,$$

$$\int_0^{\pi} \exp(i\beta\cos(\phi+\pi))\cos(m(\phi+\pi))d\phi =$$

$$= (-1)^m \int_0^{\pi} \exp(-i\beta\cos(\phi))\cos(m\phi)d\phi = \pi\, i^{-m}\, J_m(-\beta)\ ,$$

$$\int_0^{2\pi} \exp(i\beta\cos(\phi))\cos(m\phi)d\phi = \int_0^{2\pi} \exp(i\beta\cos(\phi))\exp(-im\phi)d\phi = 2\pi\, i^m\, J_m(\beta)\ ,$$

$$\exp(im\phi_j)\int_0^{2\pi} \exp(i\beta\cos(\phi-\phi_j))\exp(-im\phi)d\phi =$$

$$= \int_0^{2\pi} \exp(i\beta\cos(\phi-\phi_j))\exp(-im(\phi-\phi_j))d\phi = 2\pi\, i^m\, J_m(\beta)\ .$$

■

Remark 19 *Because of the Taylor-expansion of the Bessel functions ([16], formula 8.440):*

$$J_\nu(z) = \sum_{k=0}^{\infty} \frac{(-1)^k}{k!\Gamma(\nu+k+1)}\left(\frac{z}{2}\right)^{2k+\nu}\ ,$$

one can write,

$$\begin{aligned} J_{|m|}(G_j r\sin(\Theta)) &= \sum_{k=0}^{\infty} \frac{(-1)^k}{k!(k+|m|)!}\left(\frac{G_j r\sin(\Theta)}{2}\right)^{2k+|m|} = \\ &= \sum_{k=0}^{\infty} \frac{(-1)^k}{2^{2k+|m|}k!(k+|m|)!} G_j^{2k+|m|}\sin^{2k+|m|}(\Theta)\, r^{2k+|m|} = \\ &= \sum_{k=|m|,|m|+2,\dots} \frac{(-1)^{\frac{k-|m|}{2}}}{2^k\left(\frac{k-|m|}{2}\right)!\left(\frac{k+|m|}{2}\right)!} G_j^k\sin^k(\Theta)\, r^k\ . \end{aligned} \tag{A.84}$$

Remark 20 *The binomial theorem implies*

$$\begin{aligned} \left(r^2\cos^2(\Theta) + 2rc_{pq\perp}\cos(\Theta)\right)^n &= \sum_{s=0}^{n}\binom{n}{s} r^{2s}\cos^{2s}(\Theta)2^{n-s}r^{n-s}c_{pq\perp}^{n-s}\cos^{n-s}(\Theta) = \\ &= \sum_{s=0}^{n}\binom{n}{s} 2^{n-s}c_{pq\perp}^{n-s}\cos^{n+s}(\Theta)\, r^{n+s} = \\ &= \sum_{s=n}^{2n}\binom{n}{s-n} 2^{2n-s}c_{pq\perp}^{2n-s}\cos^{s}(\Theta)\, r^{s}\ . \end{aligned} \tag{A.85}$$

Lemma 21 *([16], formula 7.132.5) (but other definition of* P_ℓ^m*):*

$$\int_0^1 dx\, x^s \left(1-x^2\right)^{\frac{|m|}{2}} P_\ell^{|m|}(x) = \tag{A.86}$$

$$= \frac{2^{-|m|-1}\Gamma(\frac{1}{2}+\frac{1}{2}s)\Gamma(1+\frac{1}{2}s)\Gamma(1+\ell+|m|)}{\Gamma(1+\ell-|m|)\Gamma(1+\frac{1}{2}s+\frac{1}{2}|m|-\frac{1}{2}\ell)\Gamma(\frac{3}{2}+\frac{1}{2}s+\frac{1}{2}|m|+\frac{1}{2}\ell)}\ . \tag{A.87}$$

Since the parity of $P_\ell^{|m|}(x)$ *is* $\ell+|m|$*, extending the range of the above integral to* $[-1,1]$*, will give a nonzero value only for even value of* $\ell+|m|+s$*. Therefore,* $1+\frac{1}{2}(s+|m|-\ell)$ *has always to be an integer number. As furthermore* $\frac{1}{\Gamma(z)}$ *has simple zeros at the points* $z=0,-1,-2,\ldots$*, the above integral is nonzero only for* $1+\frac{1}{2}(s+|m|-\ell)=1,2,\ldots \Rightarrow s=\ell-|m|\,,\ell-|m|+2,\ldots$

Remark 22 *(Easier from ([16], formula 7.126.1) From ([16], formula 8.922.1-2.) we learn that* z^n *can be expanded in terms of Legendre polynomials,*

$$z^n = \sum_{i=0}^{n} c_i^{(n)} P_i(z)\ , \tag{A.88}$$

and the expansion coefficients are

$$c_{2k}^{(2n)} = \frac{1}{2n+1}\delta_{k0} + (4k+1)\frac{2n(2n-2)\ldots(2n-2k+2)}{(2n+1)(2n+3)\ldots(2n+2k+1)}\left(1-\delta_{k0}\right) \quad \text{and} \quad c_{2k+1}^{(2n)} = 0\ , \tag{A.89}$$

$$c_{2k+1}^{(2n+1)} = \frac{3}{2n+3}\delta_{k0} + (4k+3)\frac{2n(2n-2)\ldots(2n-2k+2)}{(2n+3)(2n+5)\ldots(2n+2k+3)}\left(1-\delta_{k0}\right) \quad \text{and} \quad c_{2k}^{(2n)} = 0\ . \tag{A.90}$$

Because of the orthogonality of the Legendre polynomials,

$$\begin{aligned}\int_{-1}^{1} dx\, x^\ell P_\ell(x) = c_\ell^{(\ell)} &= \frac{2}{2\ell+1}\begin{cases} \delta_{\ell 0} + \frac{\ell(\ell-2)\ldots 4\cdot 2}{(\ell+1)(\ell+3)\ldots(2\ell-1)}(1-\delta_{\ell 0}) & \textit{if } \ell \textit{ is even} \\ \delta_{\ell 1} + \frac{(\ell-1)(\ell-3)\ldots 4\cdot 2}{(\ell+2)(\ell+4)\ldots(2\ell-1)}(1-\delta_{\ell 1}) & \textit{if } \ell \textit{ is odd} \end{cases} \\ &= 2\frac{\ell!}{(2\ell+1)!!} = \frac{\sqrt{\pi}\,\Gamma(\ell+1)}{2^\ell\Gamma(\ell+\frac{3}{2})}\ ,\end{aligned} \tag{A.91}$$

with the definitions $0! = 1! = (-1)!! = 1!! = 1$*. Examples:*

$$\begin{aligned}\int_{-1}^{1} dx\, P_0(x) &= \int_{-1}^{1} dx\ = 2 \\ \int_{-1}^{1} dx\, xP_1(x) &= \int_{-1}^{1} dx\, x^2 = \frac{2}{3} \\ \int_{-1}^{1} dx\, x^2P_2(x) &= \frac{1}{2}\int_{-1}^{1} dx\,(3x^4-x^2) = \frac{4}{15} \\ \int_{-1}^{1} dx\, x^3P_3(x) &= \frac{1}{2}\int_{-1}^{1} dx\,(5x^6-3x^4) = \frac{4}{35}\end{aligned}$$

Publications

1. R. Hammerling, C. Uiberacker, J. Zabloudil, P. Weinberger, L. Szunyogh and J. Kirschner,
   Magnetic anisotropy of thin films of Co on Cu(111),
   Phys. Rev. B **66**, 052402 (2002)
2. R. Hammerling, J. Zabloudil, and P. Weinberger, J. Lindner, E. Kosubek, R. Nünthel, and K. Baberschke,
   Interlayer exchange coupling and magnetic anisotropy in prototype trilayers: Ab initio theory versus experiment,
   Phys. Rev. B **68**, 092406 (2003)
3. R. Hammerling, J. Zabloudil, and S.Gallego,
   On the reorientation transition in Cu(111)/Ni/H,
   Phil. Mag. B 83, xxxx (2003)
4. P.Weinberger, J.Zabloudil, R.Hammerling, L.Szunyogh,T.L.Mochesky, and B.Heinrich,
   Role of interfaces in the magnetoresistance of Au/Fe/Au/Fe multilayers,
   Phys. Rev. B **67**, 054404-1 (2003)

Bibliography

[1] Abramowitz and Stegun. "Handbook of Mathematical Functions, With Formulas, Graphs, and Mathematical Tables". Dover Pubns, London (1974).

[2] K. Baberschke, M. Donath, and W. Nolting. "K. Baberschke in Bandferromagnetism". Springer-Verlag, Berlin (2001).

[3] P. Bruno. *Phys. Rev. B* **52**, 411 (1995).

[4] J. Camarero, J. J. de Miguel, A. Hernando, and R. Miranda. *J. Appl. Phys.* **89**, 7150 (2001).

[5] K. Christmann, O. Schober, G. Ertl, and M. Neumann. *J. Chem. Phys.* **60**, 4528 (1974).

[6] A. S. Dawydow. "Quantenmechanik". Johann Ambrosius Barth, Leipzig; Berlin; Heidelberg (1992).

[7] J. de la Figuera, J. E. Prieto, C. Ocal, and R. Miranda. *Phys. Rev. B* **47**, 13043 (1993).

[8] E.M.Lifshitz. *Zh.Eksp.Teor.Fiz.* **29**, 94 (1955).

[9] P. P. Ewald. *Ann. Phys.* **64**, 253 (1921).

[10] E.Zaremba and W. Kohn. Van der waals interaction between an atom and a solid surface. *Phys. Rev. B* **13**(6), 2270 (1976).

[11] M. Farle. *Rep. Prog. Phys.* **61**, 755 (1998).

[12] M. Farle, B. Mirwald-Schulz, A. N. Anisimov, W. Platow, and K. Baberschke. *Phys. Rev. B* **55**, 3708 (1997).

[13] J. Fassbender, R. Allenspach, and U. Drig. *Surface Science* **383**, L742 (1997).

[14] J. S. Faulkner. Multiple-scattering calculations in two dimensions. *Phys. Rev. B* **38**, 1686 (1988).

[15] A. Gonis. "Green Functions for Ordered and Disordered Systems". Elsevier Science Publishers B.V., New York (1992).

[16] Gradshteyn and Ryzhik. "Table of Integrals, Series, and Products". Academic Press; 6th edition, New York (2000).

[17] R. Hammerling, C. Uiberacker, J. Zabloudil, P. Weinberger, L. Szunyogh, and J. Kirschner. Magnetic anisotropy of thin films of co on cu(111). *Phys. Rev. B* **66**, 052402 (2002).

[18] R. Hammerling, J. Zabloudil, and S.Gallego. On the reorientation transition in cu(111)/ni/h. *Phil. Mag. B* **83**, xx (2003).

[19] R. Hammerling, J. Zabloudil, P. Weinberger, J. Lindner, E. Kosubek, R. Nnthel, and K. Baberschke. Interlayer exchange coupling and magnetic anisotropy in prototype trilayers: Ab initio theory versus experiment. *Phys. Rev. B* **68**, 092406 (2003).

[20] H.C.Herper, P.Weinberger, L.Szunyogh, and C.Sommers. Multiple scatttering theory in condensed materials. *Phys. Rev. B* **66**, 064426 (2002).

[21] H. J. F. Jansen. *Phys. Rev. B* **59**, 4699 (1999).

[22] H. Jenniches, M. Klaua, H. Hche, and J. Kirschner. *Appl. Phys. Lett.* **69**, 3339 (1996).

[23] K. Kambe. *Z. Naturforschung* **22a**, 322 (1967).

[24] W. Kohn, Y. Meir, and D.E. Makarov. Van der waals energies in density functional theory. *Phys. Rev. Lett.* **80**(19), 4153 (1998).

[25] W. Kohn and N. Rostoker. Solution of the Schrödinger equation in periodic lattices with an application to metallic lithium. *Phys. Rev.* **94**, 1111 (1954).

[26] W. Kohn and L. J. Sham. Self-consistent equations including exchange and correlation effects. *Phys. Rev.* **140**(4A), 1133 (1965).

[27] J. Lindner and K. Baberschke. *J. Magn. Magn. Mater.* **240**, 220 (2002).

[28] J. Lindner and K. Baberschke. *J. Phys. Cond. Matter* **15**, S465,R193 (2003).

[29] J. Lindner, Z. Kollonitsch, E. Kosubek, M. Farle, and K. Baberschke. *Phys. Rev. B* **63**, 094413 (2001).

[30] J. Lindner, P. Poulopoulos, R. Nnthel, E. Kosubek, H. Wende, and K. Baberschke. *Surface Science* **523**, L65 (2003).

[31] J. Lindner, C. Rdt, E. Kosubek, P. Poulopoulos, K. Baberschke, P. Blomquist, R. Wppling, and D. L. Mills. *Phys. Rev. Lett.* **88**, 167206 (2002).

[32] F. Maca, A. B. Shick, J. Redinger, R. Podloucky, and P. Weinberger. *Czech. J. of Physics* **53**, 33 (2003).

[33] A. Ney, A. Scherz, P. Poulopoulos, K. Lenz, H. Wende, K. Baberschke, F. Wilhelm, and N. B. Brookes. *Solid State Commun.* **65**, 024411 (2002).

[34] W. Platow, U. Bovensiepen, P. Poulopoulos, M. Farle, K. Baberschke, L. Hammer, S. Walter, S. Mller, and K. Heinz. *Phys. Rev. B* **59**, 12641 (1999).

[35] B. Schulz and K. Baberschke. *Phys. Rev. B* **50**, 13467 (1994).

[36] A. B. Shick, D. L. Novikov, and A. J. Freeman. *Phys. Rev. B* **60**, 6277 (1999).

[37] I. Stensgaard and F. Jakobsen. *Phys. Rev. Lett.* **54**, 711 (1985).

[38] M. D. Stiles. *Phys. Rev. B* **48**, 7238 (1993).

[39] L. Szunyogh, B. Újfalussy, C. Blaas, U. Pustogowa, C. Sommers, and P. Weinberger. Oscillatory behavior of the magnetic anisotropy energy in cu(100)/Co$_n$ multilayer systems. *Phys. Rev. B* **56**, 14036 (1997).

[40] L. Szunyogh, B. Újfalussy, and P. Weinberger. Magnetic anisotropy of iron multilayers on Au(001): first-principles calculations in terms of the fully relativistic spin-polarized screened KKR method. *Phys. Rev. B* **51**, 9552 (1995).

[41] B. P. Tonner, Z.-L. Han, and J. Zhang. *Phys. Rev. B* **47**, 9723 (1993).

[42] C. Uiberacker, J. Zabloudil, P. Weinberger, L. Szunyogh, and C. Sommers. *Phys. Rev. Lett.* **82**, 1289 (1999).

[43] R. Vollmer, Th. Gutjahr-Lser, J. Kirschner, S. van Dijken, and B. Poelsema. *Phys. Rev. B* **60**, 6277 (1999).

[44] S. H. Vosko, L. Wink, and M. Nusair. *Can. J. Phys.* **58**, 1200 (1980).

[45] Yang Wang, G. M. Stocks, and J. S. Faulkner. General method for evaluating shape truncation fucntions of Voronoi polyhedra. *Phys. Rev. B* **49**, 5028 (1994).

[46] P. Weinberger, P. M. Levy, J. Banhart, L. Szunyogh, and B. jfalussy. *J. Phys. Cond. Matter* **8**, 7677 (1996).

[47] P. Weinberger and L. Szunyogh. *Comp. Mat. Sci.* **17**, 414 (2000).

[48] P. Weinberger, L. Szunyogh, and I. Turek. *Int. J. Quantum Chem.* **63**, 165 (1996).

[49] M. Weinert and J. W. Davenport. *Phys. Rev. Lett.* **54**, 1547 (1985).

[50] E. Wimmer, H. Krakauer, and A.J. Freeman. *Phys. Rev. B* **56**, R14259 (1997).

[51] M. Zheng, J. Shen, J. Barthel, P. Ohresser, Ch. V. Mohan, and J. Kirschner. *J. Phys. Cond. Matter* **12**, 783 (2000).

[52] M. Zheng, J. Shen, Ch. V. Mohan, P. Ohresser, J. Barthel, and J. Kirschner. *Appl. Phys. Lett.* **74**, 425 (1999).

[53] L. Zhong, M. Kim, X. Wang, and A. J. Freeman. *Phys. Rev. B* **53**, 9770 (1996).

Acknowledgements

My acknowledgement goes to my supervisor Prof. Dr. Peter Weinberger for his guidance and permanent encouragement during the course of this work. Many thanks also to Dr. Laszlo Szunyogh for his cooperation on various aspects of the theoretical part of the thesis and for many clarifying discussions, further the interesting stay in Budapest.

I had the pleasure to work at the University of California Santa Barbara with Prof. Dr. W.Kohn. This visit has been a great source of inspiration and opened a new part of the world for me thanks to Prof. Dr. W.Kohn.

Furthermore I want to thank my main cooperator Dr. J.Zabloudil for excellent and encouraging working atmosphere when we have shared a room at the CMS. Thanks also to Prof. Dr. P. Mohn, Prof. Dr. J. Redinger, Prof. Dr. R. Dirl, Prof. Dr. P. Kasperkovitz for their help on various physical and mathematical problems. The 'reduced dimensional examples' in this thesis are dedicated to Prof. Dr. P. Kasperkovitz, who initiated my interest in this useful way of approaching physical problems.

My gratitude goes to the members of the CMS. Many thanks to E. Mössler for her help on all organizational matters. Thanks to R. Zucca for proofreading the thesis and C. Franchini, S. Khmelevskiy for vital discussions about another very complex matter, namely football. Not to forget to mention Dr. F. Maca, Dr. V. Drchal, Dr. J. Kudrnovsky, Dr. S. Gallego, Dr. A. Vernes, Dr. I. Turek, Dr. L. Udvardi, and Prof. Dr. J. Keller.

My greatest thanks goes to my family and friends for their loving support, patience and understanding during the preparation of this work.

This work would have not been possible without the financial support of the Center for Computational Materials Science (CMS) and the Science College of the FWF (Project number: W004).

Appendix B

Curriculum Vitae

B.1 Personal data:

name:	Robert-Matthias Hammerling
address:	Institut fuer Allgemeine Physik, Technische Universitaet Wien, Getreidemarkt 9/134, A-1060 Vienna, Austria
born:	June 2, 1975 in Vienna, Austria
nationality:	Austrian
marital status:	unmarried, no children
languages:	German, English, (Spanish)

B.2 Basic Education:

1981-1985	elementary school in Vienna
Sep 1985 – Jun 1993	grammar-school in Vienna

B.3 Studies:

B.3.1 Undergraduate studies:

Oct 1993 - Jun 2000	Technical Physics at the Technische Universitaet Wien, Austria
Nov 1995	1.Diplompruefung
since Apr 1999	Institut fuer Technische Elektrochemie, TU Wien, Austria in the group “Theoretical Metallurgy” supervisor Univ.-Prof. Dr. Peter Weinberger
May 1999 – Jun 2000	diploma thesis “Magnetic Anisotropy of Cobalt on Cu(111)”, supervisor Univ.-Prof. Dr. Rainer Dirl, Institut fuer Theoretische Physik, Univ.-Prof. Dr. Peter Weinberger, Institut fuer Technische Elektrochemie
Jun 2000	diploma degree
Mar 1998 - Jul 1998	Studyassistent in “Quantum Mechanics” at the Institut fuer Theoretische Physik
Jul 1999 - Oct 1999	experimental work in the field of surface science, Institut fuer Allgemeine Physik, TU Wien supervisor Univ.-Prof. Dr. Peter Varga,
Oct 1999 - Jan 2000	Studyassistent in “Classical Electrodynamics and Relativity” at the Institut fuer Theoretische Physik

B.3.2 Postgraduate studies:

since Jul 2000	doctoral study of Technical Sciences-physics, member of the Science College at CMS supervisor Univ.-Prof. Dr. Peter Weinberger, Institut fuer Allgemeine Physik
Sept 2000 – Feb 2001	Stay at UCSB, University of California Santa Barbara, CA,USA supervisor Prof. Walter Kohn, work on ’dispersion interaction’
March 2002 – Jul 2002	Studyassistent in “Quantum Mechanics” at the Institut fuer Theoretische Physik
December 2002	Stay at Technical University of Budapest, Hungary supervisor Prof. Laszlo Szunyogh, work on ’Madelung potential’

B.4 Other working experiences:

Jul 1998 – Feb 1999	working in software development for mobile phones, GSM, PSE Programm und Systementwicklung Siemens AG, Austria